School of Pharmacy and Biomedical Sciences

Adipose Loss and Metabolic Disease Due to Seipin Deficiency: Systemic Versus Tissue Specific Effects

Ahlima Roumane

0000-0001-6831-4426

This thesis is presented for the collaborative Degree of

Doctor of Philosophy
of
Curtin University and University of Aberdeen

December 2021

DECLARATION

I, Ahlima Roumane, hereby declare that this thesis has been composed by myself. All the work in this thesis has been carried out by myself as part of a collaborative doctoral programme at both the University of Aberdeen (Aberdeen, Scotland) and Curtin University (Perth, Australia). Any assistance has been fully acknowledged. All quotations have also been distinguished by quotation marks and the sources of information specifically acknowledged. To the best of my knowledge and belief, this thesis contains no material previously published by any other person except where due acknowledgement has been made. This thesis has not been accepted or submitted for any previous application for a higher degree.

Ahlima Roumane

20 December 2021

Table of Contents

SUMMARY

Disruption of the BSCL2 gene, which encodes the protein seipin, causes congenital generalised lipodystrophy type 2 (CGL2), the most severe form of lipodystrophy. Affected individuals almost entirely lack adipose tissue stores which results in ectopic fat accumulation in other tissues. This typically leads to severe metabolic complications including insulin resistance and type 2 diabetes. While seipin has been shown to play crucial roles in adipogenesis and lipid droplet biogenesis, it is not clear which of these functions are responsible for causing the severe adipose tissue loss in patients with *BSCL2* mutations. Given the fact that seipin is expressed in several other tissues, it may also exert cell-autonomous effects in non-adipose tissues relevant to the pathogenesis of CGL2. Using *in vivo* and *in vitro* models, the work in this thesis aimed to understand the molecular mechanisms *via* which *BSCL2* disruption causes metabolic disease in CGL2.

The results presented here provide evidence of a conserved role of seipin in regulating lipolysis in adipocytes. While seipin does not appear to have a critical role in macrophage function, preliminary data presented here strongly suggest it may be involved in the regulation of insulin secretion in pancreatic β-cells. This work also reveals a potential interaction between seipin and glucagon-like peptide 1 receptor (GLP-1R) which may underlie the dramatic pancreatic islet expansion observed in our pre-clinical model of CGL2. The work in this thesis also demonstrates the therapeutic potential of liraglutide, a GLP-1R agonist, to treat metabolic disease in CGL2 patients.

Overall, the studies presented in this thesis indicate that seipin may have significant roles in non-adipose tissues. Their contribution to the metabolic phenotype observed in seipin knockout mice and CGL2 patients remains to be assessed. However, this could permit the identification of novel therapeutic targets for the treatment of CGL2.

ABBREVIATIONS

A

AC	· Adenylate cyclase
ACC	· Acetyl CoA carboxylase
ADP	· Adenosine diphosphate
AGPAT	· 1-acylglycerol-3-phosphate-O-acyltransferase
AldoA	· Aldolase A
ALT	· Alanine aminotransferase
AMPK	· AMP-activated protein kinase
ANOVA	· Analysis of variance
aP2	· Adipocyte protein 2
ApoE	· Apolipoprotein E
ASPA	· Animals Scientific Procedures Act
AST	· Aspartate aminotransferase
ATF6β	· Activating transcription factor 6 β
ATGL	· Adipose triglyceride lipase
ATP	· Adenosine triphosphate
AUC	· Area under the curve

B

BAT	· Brown adipose tissue
BCA	· Bicinchoninic acid
BHI	· Brain heart infusion
BMDM	· Bone marrow-derived macrophages
BMP	· Bone morphogenetic protein
BSA	· Bovine serum albumin

BSCL	· Berardinelli-Seip congenital lipodystrophy
Bscl2(fl/fl)	· Bscl2 floxed mice
Bscl2-/-	· Bscl2 knockout mice

C

C/EBP	· CCAAT/enhancer binding protein
cAMP	· Cyclic adenosine monophosphate
CAV1	· Caveolin 1
CCL2	· CC motif chemokine ligand 2
CD68	· Cluster of differentiation 68
cDNA	· Complementary deoxyribonucleic acid
CFU	· Colony forming units
CGL	· Congenital generalised lipodystrophy
CNX	· Calnexin
CTRL	· Control

D

DAB	· 3, 3 -diaminobenzidine
DAG	· Diacylglycerol
DAPI	· 4′,6-diamidino-2-phenylindole
DGAT2	· Acyl-CoA diacylglycerol acyltransferase 2
DMSO	· Dimethylsulfoxide
DNA	· Deoxyribonucleic acid
DNL	· *De novo* lipogenesis
DPP-4	· Dipeptidyl peptidase-4

E

ECL	· Enhanced chemiluminescence
EDTA	· Ethylenediaminetetraacetic acid
EGFR	· Epidermal growth factor receptor
ELISA	· Enzyme-linked immunosorbent assay
Epac2	· Exchange protein directly activated by cAMP 2
ER	· Endoplasmic reticulum

F

FABP4	· Fatty acid binding protein 4
FBS	· Fetal bovine serum
FDA	· Food and drug administration
FFA	· Free fatty acid
FPLD	· Familial partial lipodystrophy

G

G3P	· Glycerol 3-phosphate
GCK	· Glucokinase
GDP	· Guanosine diphosphate
GH	· Growth hormone
GIP	· Gastric inhibitory polypeptide
GLP-1	· Glucagon-like peptide 1
GLP1-R	· Glucagon-like peptide 1 receptor
GLUT	· Glucose transporter
GPAT	· Glycerol-3 phosphate acyltransferase
GPCR	· G-protein coupled receptor
GPI	· Glucose-6-phosphate isomerase

GRP78	· Glucose-regulated protein 78
GRPP	· Glicentin-related polypeptide
GSIS	· Glucose-stimulated insulin secretion
GTP	· Guanosine triphosphate
GTT	· Glucose tolerance test
gWAT	· gonadal white adipose tissue

H

H&E	· Hematoxylin and eosin
HBS	· Hepes-buffered saline
HBSS	· Hank's balanced salt solution
HEK	· Human embryonic kidney
HOMA-IR	· Homeostatic model assessment of insulin resistance
HRP	· Horseradish peroxydase
HSL	· Hormone sensitive lipase

I

i.p.	· Intraperitoneal
IBMX	· 3-isobutyl-1-methylxanthine
IHC	· Immunohistochemistry
IL	· Interleukin
INSR	· Insulin receptor
IP	· Immunoprecipitation
IP-1	· Intervening peptide-1
IRS	· Insulin-receptor substrate
ITT	· Insulin tolerance test
iWAT	· inguinal white adipose tissue

K

KRBH   · Krebs-Ringer Bicarbonate Hepes

L

LAMP-1   · Lysosome-associated membrane protein-1

LD   · Lipid droplet

LdhA   · Lactate dehydrogenase A

LDS   · Lithium Dodecyl Sulphate

LKB1   · Liver kinase B1

LPA   · Lysophosphatidic acid

LPL   · Lipoprotein lipase

LPS   · Lipopolysaccharide

LysM-B2KO   · Myeloid-specific Bscl2 knockout mice

M

MAPK   · Mitogen activated protein kinase

MCP1   · Monocyte chemoattractant protein 1

M-CSF   · Macrophage colony stimulating factor

MEF   · Mouse embryonic fibroblast

MG   · Monoacylglycerol

MGAT   · Monoacylglycerol acyltransferase

MGL   · Monoacylglycerol lipase

MOI   · Multiplicity of infection

MPGF   · Major proglucagon fragment

mRNA   · Messenger ribonucleic acid

MSC   · Mesenchymal stem cell

MYTH   · Membrane-based split ubiquitin yeast two-hybrid

N

n.d.	· Non detectable
NADH	· Nicotinamide adenine dinucleotide hydrogen
NCS	· Newborn Calf Serum
NEAA	· Non-essential amino acid
NTS	· Nucleus tractus solitarius

O

ORO	· Oil red O

P

P/S	· Penicillin/streptomycin
PA	· Palmitic acid
PAP	· Phosphatidic acid phosphatase
PBS	· Phosphate buffered saline
PC1/3	· Prohormone convertase 1/3
PCR	· Polymerase chain reaction
PDE3B	· Phosphodiesterase 3B
Pfkp	· Phosphofructokinase platelet
PKA	· Protein kinase A
PLIN	· Perilipin
PPARγ	· Peroxisome proliferator-activated receptor γ
PTRF	· Polymerase 1 and transcript release factor
PVDF	· Polyvinylidene fluoride

Q

qPCR	· Quantative polymerase chain reaction
qRT-PCR	· Quantative reverse transcription polymerase chain reaction
QUICKI	· Quantitative insulin sensitivity check index

R

RIPA	· Radioimmunoprecipitation assay
RNA	· Ribonucleic acid
RPM	· Rotation per minute
RT	· Room temperature
rWAT	· Retroperitoneal white adipose tissue

S

S.D.	· Standard deviation
SDS	· Sodium dodecyl sulfate
SDS-PAGE	· Sodium dodecyl sulfate-polyacrylamide gel electrophoresis
SE	· Sterol ester
SEM	· Standard error to the mean
SGBS	· Simpson Golabi Behmel Syndrome
shRNA	· Short hairpin ribonucleic acid
siRNA	· Short interfering ribonucleic acid
SKO	· Seipin knockout mice
SLC2A2	· Solute Carrier Family 2 member 2
SREBP1	· Sterol regulatory element binding protein 1
SUR1	· Sulfonylurea receptor 1
SVC	· Stromal vascular cell
SVF	· Stromal vascular fraction

T

T2D	· Type 2 diabetes
TAG	· Triacylglycerol
TBS	· Tris-buffered saline
TBST	· Tris-buffered saline tween
TCA	· Tricarboxylic acid
TGF	· Transforming growth factor
TLR	· Toll-like receptor
TNF	· Tumour necrosis factor

U

UCP1	· Uncoupling protein 1

V

VDCC	· Voltage dependent calcium channel
VLDL	· Very-low-density lipoprotein

W

WAT	· White adipose tissue
WT	· Wild-type

Z

ZF	· Zucker fatty

ACKNOWLEDGEMENTS

First and foremost, I would like to thank my supervisors, Dr Justin Rochford and Professor Philip Newsholme for their unwavering support and guidance throughout my PhD. I am very grateful to Dr Justin Rochford for allowing me to stay in his lab during the pandemic, when I could not go back to Australia. He has been a tremendous help over the last three years, and I could not have hoped for a better mentor. Thank you for the valuable insights and opportunities you have provided to me. I will forever be grateful for this.

I would also like to acknowledge the Aberdeen-Curtin Alliance for providing the funding and resources that allowed me to conduct this collaborative project at Curtin University (Perth, Australia) and at the University of Aberdeen (Aberdeen, Scotland).

I would like to thank both former and current members of the Rochford and Newsholme research groups. It is their help and friendship that have made my PhD journey and life in the UK and Australia an amazing experience. For all the fun and distractions we had in the lab and in social settings, I am deeply grateful to Dr George D. Mcilroy, Ms Nadine Sommer and Dr Alasdair T.S. Leeson-Payne. A huge thank you goes to George who has helped me from the start until the very end. Without his insightful comments, encouragement and support, this journey would not have been possible. I really hope that my French lessons have paid off and that you can order more than just a beer now! A special mention to Nadine who has been my bubble for the last two years. I feel very fortunate to count you as my friend and look forward to our new adventures. Alasdair, thank you for your friendship and support throughout the years, which kept me very motivated. It was really nice to still have you around. I would also like to take the opportunity to thank everyone in the lab 4.035 who have made the Rowett a great place to work.

I would like to thank my family and friends for the unconditional love and support they have given me throughout my studies. Anne-Laurie and Camille, I am grateful for those skype nights which made the lockdown(s) almost pleasant.

Finally, special thanks to Jimmy for putting up with me all these years. I am very lucky to have you by my side and cannot wait to see where the future will take us.

CHAPTER 1
1. INTRODUCTION

1.1. Adipose tissue

Adipose tissue plays a key role in maintaining a healthy state, most critically by providing a safe, systemic store for lipids in the body. However, adipose tissue is also an important endocrine organ with complex functions. It can be viewed as a gatekeeper of energy homeostasis whose disruption may, therefore, cause several severe health disorders.

1.1.1.   Adipose tissue composition

Adipose tissue is principally comprised of adipocytes, highly specialised cells with the capacity to safely and flexibly store significant quantities of lipid within highly regulated lipid droplets (1). However, adipose tissue also contains a heterogenous population of cell types that all contribute to its function including pre-adipocytes, nerve cells, precursor cells, immune cells, endothelial cells and fibroblasts (**Figure 1.1**). These non-adipocyte cell types are usually referred to as the stromal vascular fraction (SVF) of adipose tissue (1,2). By producing and secreting hormones and cytokines, cells in the SVF exert paracrine effects on adjacent adipocytes and therefore participate actively to the overall state of adipose tissue (See section 1.1.5.4).
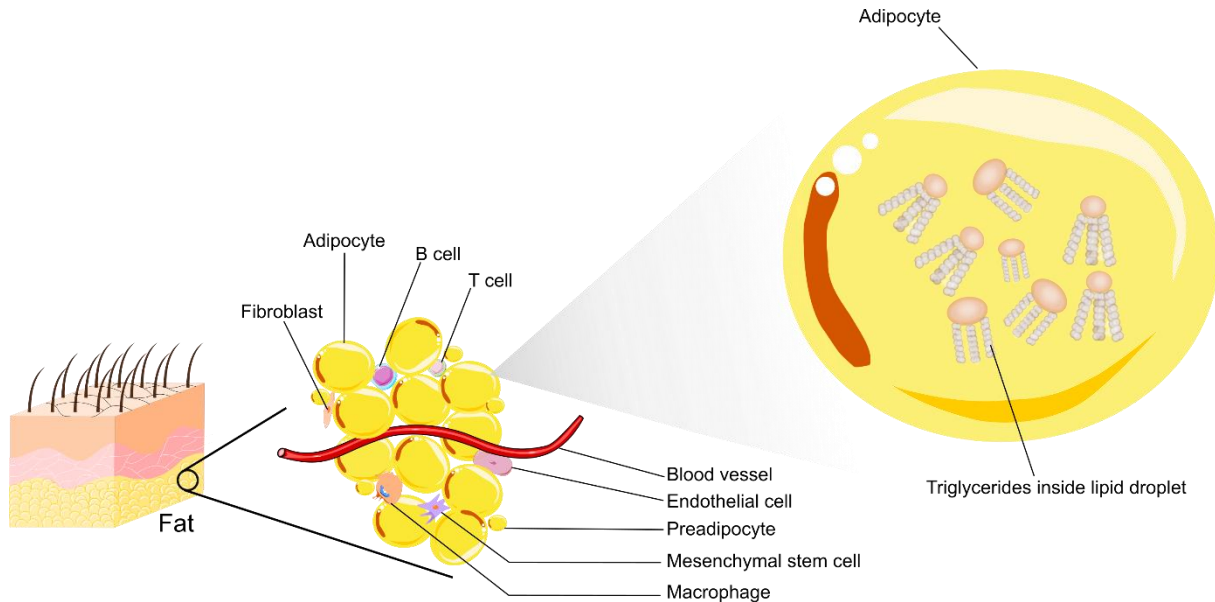
Figure 1.1: Adipose tissue composition*. Adipose tissue is a loose connective tissue of which adipocytes are the main cellular component. In addition to adipocytes, adipose tissue comprises a stromal vascular fraction consisting of precursor cells (mesenchymal stem cells) and immune cells mostly.*

1.1.2.   Adipose tissue heterogeneity

Histologically, adipose tissue can principally be classified into three different types ; white adipose tissue (WAT), brown adipose tissue (BAT) and beige/brite adipose tissue ; whose origin, composition, function and location differ in the body (3).

White adipose tissue constitutes the primary site for energy storage in the body and is thought to contribute to more than 95% of adipose tissue in humans (3). WAT develops in the early stages of life and continues throughout life. In adults, adipocyte number is constant despite a rapid turnover (4). Phenotypically, WAT adipocytes are characterized by a single large lipid droplet occupying the vast majority of the cytoplasm. As a result, WAT adipocytes typically have a large spherical shape of variable size, and other organelles (Golgi apparatus, endoplasmic reticulum, mitochondria) are restricted to the periphery of the cell. This organisation perfectly accommodates WAT's primary function of storing lipids (See section 1.1.5.1).

Brown fat is especially abundant in hibernating mammals and has been extensively described in rodents. Highly present in newborns and infants, BAT is nonetheless present in adult humans where it accounts for 1 to 2% of adipose tissue mass (3,5). BAT is easily distinguishable from WAT because of its small multilocular lipid droplets and the abundance of mitochondria. As the main site for non-shivering thermogenesis, BAT dissipates energy in the form of heat. This process will be further described in section 1.1.5.3.

In contrast to WAT and BAT, brite adipose cells are difficult to quantify precisely. They refer to a cluster of adipocytes resembling BAT cells within WAT depots (Brown in white = Brite). As an intermediate state between WAT and BAT cells, brite adipocytes; also known as beige adipocytes; contain multilocular lipid droplets and numerous mitochondria giving it thermogenic properties. Despite this resemblance with BAT adipocytes, brite adipocytes arise from different precursors and do not express thermogenic genes under basal conditions but only upon stimulation (6,7).

A summary of morphological differences between WAT, BAT and beige adipocytes is depicted in **Error! Reference source not found.**.

WAT

BAT

lipid droplet
mitochondria

Beige/Brite
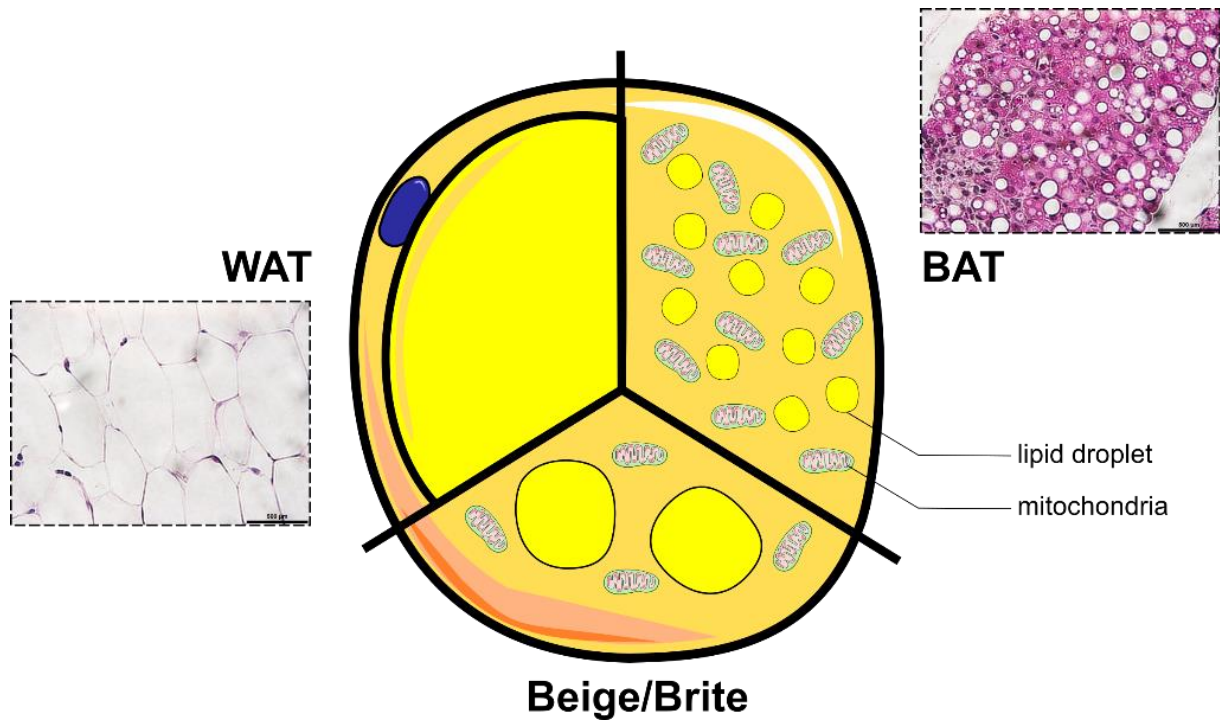
Figure 1.2: Morphological characteristics of white, brown, and beige adipocytes. *In dashed boxes, hematoxylin and eosin staining shows phenotypical changes between fat depots. Bars denote 500 μm. WAT: white adipose tissue; BAT: brown adipose tissue.*

1.1.3.   Adipose tissue location / distribution

Besides the morphological differences described above, WAT, BAT and brite cells are also typically found in defined anatomical locations and display variable functions (see section 1.1.5). WAT, for example, is generally further divided into visceral and subcutaneous depots (1). As implied by the name, subcutaneous depots are found under the skin while visceral depots are located in deeper regions of the abdominal cavity, where it surrounds internal organs. WAT is also found in orbits, palms and soles where it offers mechanical support (8). Long seen as a typical WAT, bone marrow adipose tissue has been proven to be distinct from WAT not only for its location but also its features and function. Given its role in haematopoiesis and the immune system, this depot could be worth studying in the context of the higher rate of infections observed in congenital generalised lipodystrophy type 2 patients (see section 1.2.2.4).

In the foetus and the newborn, BAT is distributed among the interscapular region, around blood vessels and around the kidneys and heart. It is also found in the neck, shoulder (supraclavicular/interscapular) and thoracic vertebrae regions in adults (9–11).

In healthy individuals, adipose tissue is usually limited principally to those defined locations. However, in certain conditions including obesity and lipodystrophy, WAT can accumulate ectopically in regions that may predispose to complications (see section 1.1.6). Accumulation of fat, mainly the visceral adipose tissue, is commonly associated with insulin resistance, type 2 diabetes and cardiovascular risks (12–14).

1.1.4.   Adipocyte differentiation

Due to the structural complexity of adipose tissue, knowledge of the processes and mechanisms controlling adipocyte differentiation mostly comes from *in vitro* studies performed on preadipocyte cell lines such as the murine 3T3-L1 and C3H10T1/2 cells and human Simpson Golabi Behmel Syndrome (SGBS) cells (15).

Adipocytes are believed to originate from pluripotent mesenchymal stem cells (MSCs) in the mesoderm. Depending on the environmental cues and stimuli, MSCs can give rise to several different tissues including adipocytes, chondrocytes, osteoblasts and myocytes (16). The commitment of a pluripotent stem cell into the adipocyte lineage involves both positive and negative factors whose balance dictates its fate. Members of the transforming growth factor (TGF) family including bone morphogenetic proteins (BMP) 2 and 4, and members of the Wnt family have been shown to regulate MSC fate towards the adipocyte lineage. By modulating several elements of the cytoskeleton, BMP2 and BMP4 more specifically play a critical role in the early phase of adipogenesis by allowing the transition from a fibroblastic shape to a more spherical shape typical of adipocytes (16–18).

To become mature, lipid laden adipocytes, preadipocytes cells must undergo key processes involving multiple co-ordinated transcriptional events. Early stages of the differentiation process are marked by the transient induction of several members of the CAAT/enhancer-binding protein (C/EBP) family (20). C/EBPβ and C/EBPδ appear first in the adipogenic transcription cascade (21). They lead to the induction of C/EBPα, sterol regulatory element binding protein 1 (SREBP1) and peroxisome proliferator-activated receptor γ (PPARγ) (22,23). PPARγ, a member of the nuclear receptor superfamily, is considered the master regulator of

adipogenesis (24,25). Its absence or dysfunction can lead to lipodystrophy in mice and humans highlighting its crucial role in adipogenesis, maintenance of the differentiated state and regulation of key adipocyte processes (26–29). As such, PPARγ agonists such as rosiglitazone are routinely added to preadipocyte cultures to enhance their differentiation. SREBP1 and more specifically SREBP1c is a lipogenic transcription factor and PPARγ target gene that controls the expression of multiple genes regulating the generation of lipids (30). PPARγ regulates a wide array of other genes involved in insulin sensitivity, lipogenesis, and lipolysis. Some of those targets include the glucose transporter GLUT4, fatty acid binding protein 4 (FABP4), perilipins and lipoprotein lipase (LPL) to name just a few. Those downstream effectors are usually considered as characteristic of mature adipocytes (31).

A summary of key transcriptional events that govern adipocyte differentiation is depicted in

Figure 1.*3*.
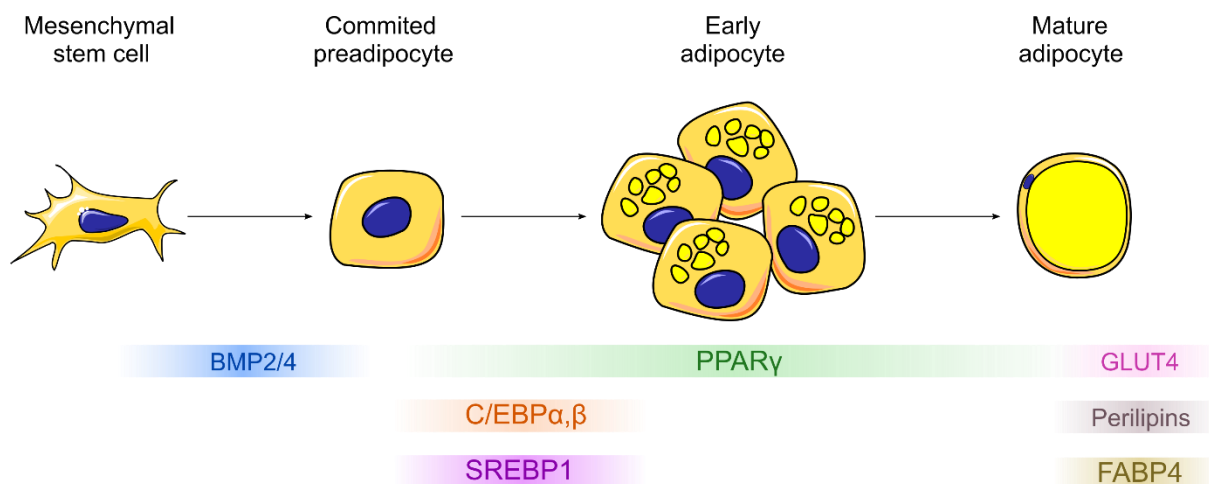
Figure 1.3: Transcriptional regulation of adipocyte formation. Adipogenesis describes the process by which a mesenchymal stem cell gives rise to a mature adipocyte following sequential transcriptional events. BMP: bone morphogenetic proteins; PPARγ: peroxisome proliferator-activated receptor γ; C/EBP: CAAT/enhancer-binding protein; SREBP1: sterol regulatory element binding protein 1; GLUT4: glucose transporter 4; FABP4: fatty acid binding protein 4.

Different developmental origins of adipocytes could explain adipose tissue depots heterogeneity and might influence fat patterning in certain lipodystrophies (see section 1.2).

1.1.5.   Adipose tissue function

The appreciation of a fully functional white adipocyte is often assessed through the presence of an unilocular lipid droplet (LD). Although virtually every cells in the body can have lipid droplets, those organelles are usually found in the cytoplasm of cells specialized for the intracellular storage of lipids such as adipocytes and hepatocytes (32). Occasionally, lipid droplets have been found in the nucleus (33). A significant amount of detailed molecular knowledge of lipid droplet biology comes from studies in drosophila and yeast where it was shown that LDs are involved in endoplasmic reticulum (ER) stress, protein degradation and pathogen infection (34–38). Most importantly, in the case of adipocytes, LDs are highly efficient at storing lipids and by sequestering lipids systemically, protecting other tissues from lipotoxicity.

1.1.5.1.   Energy storage - Lipogenesis

Lipid droplets share a common organisation structured around a neutral core containing triacylglycerols (TAGs) and sterol esters (SE), surrounded by a phospholipid monolayer (amphipathic lipids) and proteins (**Figure 1.4**). TAGs and SE are used for energy demand and membrane and steroid synthesis (39). The surrounding proteins can be classified into structural proteins (perilipin family members), lipid-synthesis enzymes (acetyl coenzyme A (CoA) carboxylase (ACC), acyl-CoA synthetase, acyl-CoA diacylglycerol acyltransferase 2 (DGAT2)), lipases (adipose tissue triacylglycerol lipase (ATGL)) and membrane-trafficking proteins (Rab5, Rab18 and ARF1) (40,41).
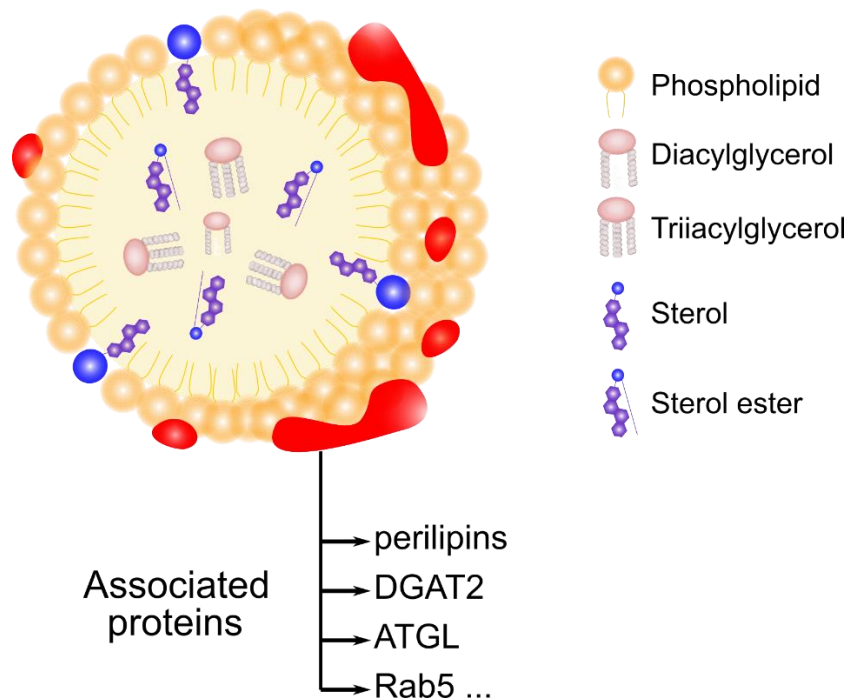
Figure 1.4: Lipid droplet composition. *LD consists of a hydrophobic core containing di-/tri-acylglycerols and sterol esters. LD associated proteins are anchored in the phospholipid monolayer. DGAT2: diacylglycerol acyltransferase 2; ATGL: adipose triglyceride lipase. Based on Guo et al. 2009 (42).*

Lipid droplets are formed *de novo* from the ER where enzymes for neutral lipid synthesis are localised (43). The most common pathway for the generation of triacylglycerols is the glycerolipid synthesis pathway, also called the Kennedy pathway, which is catalysed by glycerol-3 phosphate acyltransferase (GPAT) and 1-acylglycerol-3-phosphate O-acyltransferase (AGPAT) enzymes. Although less frequent, the monoacylglycerol pathway is also observed in enterocytes and adipocytes and involves monoacylglycerol acyltransferase (MGAT) enzymes. Both pathways utilise DGAT enzymes to catalyse the final stage of TAG synthesis (44).

Once formed in the ER, neutral lipids accumulate between leaflets of the ER bilayer, distorting the membrane and leading to the formation of a lens shape. Above a certain size, lipid droplets start budding from the ER to form a roundly shaped lipid droplet (44). This step is regulated by many proteins including seipin, a protein whose disruption causes generalised loss of adipose tissue in humans, and which is the focus of the work presented in this thesis (see section 1.2.3). Seipin protein has been shown to stabilise ER-LD contacts and facilitate transfer of lipids and proteins within the two organelles (45). To respond to cell energy demand, lipid droplets can expand their size within a range of 0,4 µm to 100 µm (46). This growth can be explained by the

transfer of lipids from the ER to the LD, transport of lipids or by the fusion of smaller lipid droplets (36) (***Figure 1.5***).

1.1.5.2.   Lipolysis

To respond to an increase in cell energy demand or when carbohydrates reserves are depleted (such as during fasting), free fatty acids (FFAs) can be mobilized by other tissues, particularly adipose tissue, through the process of lipolysis. This catabolic process releases into the circulation non esterified fatty acids and glycerol, from the hydrolysis of TAG, that become directly available for take up by other cells (47). In adipocytes, this is the result of the sequential actions of three lipases: adipose triglyceride lipase (ATGL), hormone-sensitive lipase (HSL) and monoacylglycerol lipase (MGL) as depicted in ***Figure 1.5***. These FFAs and glycerol can be oxidised within the adipocyte or used by other tissues such as the liver for hepatic gluconeogenesis (see section 1.3.5.2). The lipolytic process is regulated at several levels by the sympathetic nervous system, hormones including insulin, growth factors and adipokines (47–49).
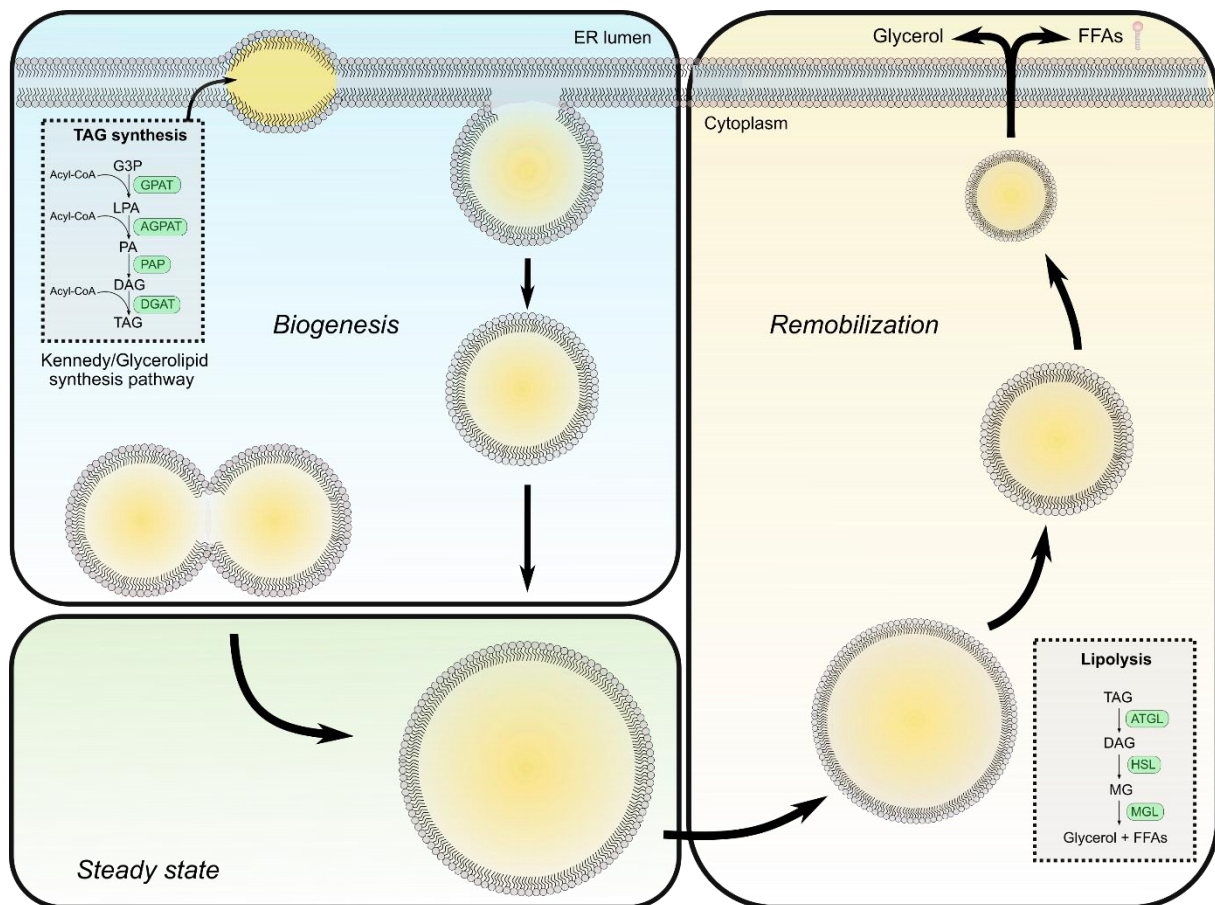
Figure 1.5 : Lipid droplet dynamics. *Lipid droplets emerge from the endoplasmic reticulum (ER) where triacylglycerol (TAG) synthesis occurs. Large lipid droplets are generated following a growth phase or from the fusion of smaller lipid droplets. Free fatty acids (FFAs) can then be remobilised from the lipid droplet through the lipolytic process to supply peripheral tissues. See the main text for details. GPAT: Glycerol-3 phosphate acyltransferase; AGPAT: Acylglycerolphosphate acyltransferase; PAP: Phosphatidic acid phosphatase; DGAT: Diacylglycerol acyltransferase; ATGL: Adipose triglyceride lipase; HSL: Hormone-sensitive lipase; MGL: Monoacylglycerol lipase; G3P: Glycerol-3-phosphate; LPA: Lysophosphatidic acid; DAG: Diacylglycerol; MG: Monoacylglycerols; FFAs: Free fatty acids. Based on Abdou et al. 2017 (50).*

1.1.5.3.   Non shivering thermogenesis

As seen in the previous section (1.1.5.2), the lipolytic process culminates into the production of FFAs and glycerol. Within the adipocyte, FFAs are converted to fatty acyl-CoA esters and transported to the mitochondria where they can undergo β-oxidation to generate acetyl-CoA (51). Mitochondria is also the site of oxidative phosphorylation, a process in which electrons are transported across the inner mitochondrial membrane to generate a proton gradient to be used for adenosine triphosphate (ATP) production as a source of energy for the cells (52). In

BAT, this gradient is not used to drive ATP synthesis but is instead used to generate heat. This occurs due to the presence of the uncoupling protein 1 (UCP1) located in the inner mitochondrial membrane of brown adipocytes. UCP1 allows the free passage of protons across the membrane allowing the dissipation of this proton gradient thereby forming a futile cycle which generates heat instead producing ATP. The close proximity of BAT to blood vessels facilitates the transfer of the heat throughout the body. Thermogenesis can be stimulated by β-adrenergic agonists which upregulate UCP1 expression (53,54). This sympathetic stimulation has long been investigated for the treatment of obesity as it offers potential means to increase basal energy expenditure and so facilitating weight loss (55).

1.1.5.4. Endocrine functions

In addition to its role in storing lipids and thermogenesis, adipose tissue also secretes a variety of factors, collectively known as adipokines, that act as autocrine, paracrine and endocrine molecules (56). These adipokines modulate multiple processes including appetite, insulin sensitivity and immune responses (57). The two best-studied and arguably most important regulatory hormones secreted by adipose tissue are leptin and adiponectin.

Leptin and the leptin receptor were first identified in the spontaneous *ob/ob* mouse model of obesity and obese diabetic *db/db* mice, respectively (58,59). Leptin plasma levels were found to strongly correlate with body fat mass (60). Leptin regulates appetite by decreasing food intake and increasing energy expenditure through its receptors in the hypothalamus (61). Independently to its action on brain and the central nervous system, leptin also regulates glucose and lipid metabolism via leptin receptors on pancreatic β-cells and hepatocytes (62). Additional roles in immunity, bone metabolism and angiogenesis have also been attributed to leptin (63–65). Adiponectin is another adipokine highly abundant in the circulation. Unlike leptin, adiponectin levels are inversely correlated to body fat mass (66). Adiponectin has been shown to exert anti-hyperglycaemic, anti-inflammatory and insulin-sensitizing effects through its actions most notably on liver and skeletal muscle (67).

Along with lipids, leptin and adiponectin, adipose tissue also secretes a broad range of inflammatory cytokines and hormones that contribute to physiological and pathological processes (56).

1.1.6.　　Importance of functional adipose tissue

The ability of adipose tissue to store and release lipids along with its role as an endocrine organ place this tissue as a key player of energy homeostasis and metabolism. Its critical roles are probably best understood and most widely studied in the context of obesity given the prevalence of human disease associated with unhealthy weight gain in the population.

Obesity results from an imbalance between nutrient intake and energy expenditure and is commonly associated with a sedentary lifestyle (68). However, obesity etiology is far more complex and involves multiple factors including genetic and environmental influences (69). To accommodate excess caloric intake, adipocytes accumulate lipids and increase in size (hypertrophy) and number (hyperplasia) (70). However, with excessive expansion, the adipose tissue becomes less vascularized creating a hypoxic environment often associated with fibrosis (71,72). Adipose tissue expansion considerably alters the secretion of adipokines and cytokines including tumour necrosis factor α (TNFα) and interleukin 6 (IL-6) (73). Together with an infiltration of immune cells most notably macrophages, elevated levels of cytokines contribute to a chronic state of low-grade inflammation in the tissue (74,75). The adipose tissue progressively becomes non-functional and less responsive to external stimuli (76). Insulin for example is no longer able to suppress lipolysis in adipocytes (77). This inflammatory state not only affects adipose tissue but also impacts other tissues. When adipocytes are unable to further expand their mass and number, the adipose tissue reaches its capacity for safely storing lipids. As a result, lipids spill over into the circulation and are deposited in other organs, that are not specialized for the storage of lipids. Common features of obesity such as insulin resistance, type 2 diabetes and hepatic steatosis are strongly associated with this lipotoxicity (78). Interestingly, these metabolic disturbances are also observed in other disorders affecting lipid storage including lipodystrophies, in which there may be a primary defect of adipose development or function that restricts adipose storage capacity. As a result, lipodystrophies probably most clearly demonstrate the critical importance of functional adipose tissue in human health (see section 1.2).

1.2. Lipodystrophies

Lipodystrophies refer to a heterogenous group of disorders characterised by a selective lack of adipose tissue, adipose redistribution and/or primary adipose dysfunction (79,80). They are commonly classified according to their aetiology (inherited or acquired) and the extent of adipose tissue loss (partial or generalised) (81). The work presented in this thesis will focus particularly on one category, congenital generalised lipodystrophies.

1.2.1.   Congenital generalised lipodystrophy

Congenital generalised lipodystrophy (CGL), also known as Berardinelli-Seip syndrome or Berardinelli-Seip Congenital Lipodystrophy (BSCL), refers to a rare autosomal recessive disorder characterised by a near complete lack of adipose tissue from birth or early childhood (82–85). To date, there have been around 500 cases reported in the world (86). Clinical signs associated with CGL include acanthosis nigricans, muscular appearance, hyperandrogenism and hepatomegaly (84,85,87,88). Because of the paucity of adipose tissue in CGL patients and, thus, lack of functional triglycerides stores, lipids remain in the bloodstream or are deposited in ectopic sites such as the liver contributing to the hypertriglyceridemia and hepatic steatosis, respectively (89). Similarly, dramatically reduced fat mass also results in low levels of circulating adipokines including leptin and adiponectin (90). This typically leads to metabolic complications including insulin resistance and type 2 diabetes (91).

To date, four genetic loci have been linked to CGL. Mutations affecting 1-acylglycerol-3-phosphate O-acyltransferase 2 (*AGPAT2*) (88,92,93), Berardinelli-Seip Congenital Lipodystrophy type 2 (*BSCL2*) (85), caveolin-1 (*CAV1*) (94) and polymerase 1 and transcript release factor (*PTRF*) (95) are responsible for CGL1, CGL2, CGL3 and CGL4, respectively. These CGLs are all characterised by a lack of fat although the extent of adipose tissue loss and related metabolic complications differ depending on the underlying genetic cause. Distinct characteristic features help clinicians distinguish between the four different CGL types. Mutations in *AGPAT2* and *BSCL2* account for more than 95% of the reported cases (96). CGL3 and CGL4 types are less frequently encountered (**Figure 1.*6*.6**). Generally, the amount of adipose tissue correlates with the severity of the disease. The next sections will focus on CGL2, the most severe form of CGL.
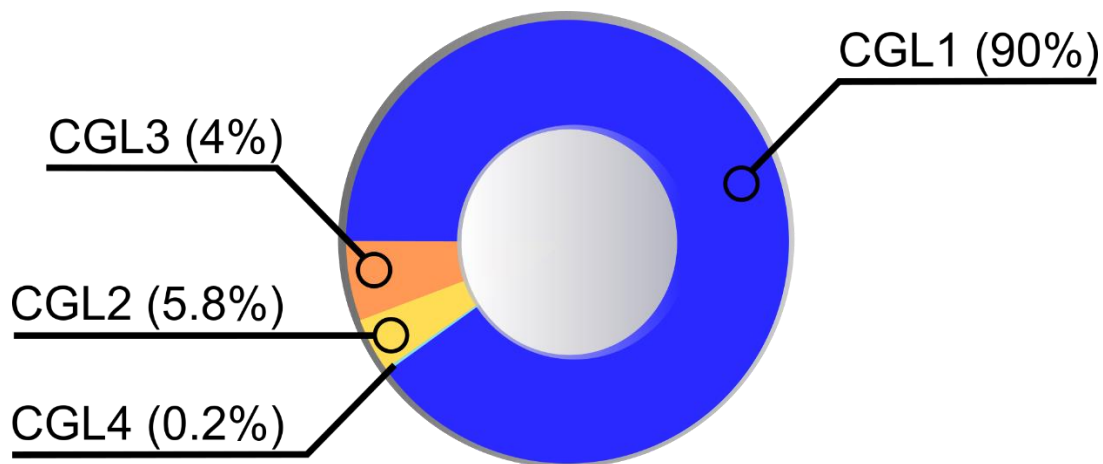
Figure 1.6 : Prevalence of CGL types among the population.

1.2.2. Congenital generalised lipodystrophy type 2

1.2.2.1. Genetic cause and clinical features

Congenital generalised lipodystrophy type 2 (CGL2) is caused by mutations in the BSCL2 gene, located on the chromosome 11q13 and which encodes a protein named seipin (85,97). Individuals affected by CGL2 present with a near complete loss of adipose tissue, with both mechanical and metabolically active fat depots being virtually absent (**Figure *1.71.7***) (87,98). A moderate intellectual impairment has also been reported in CGL2 patients (89,96). Paucity of adipose tissue in CGL2 results in extremely low levels of leptin and considerably reduced levels of adiponectin (99). Muscle hypertrophy, hypertriglyceridemia and hepatic steatosis are common features of affected individuals (100). Severe insulin resistance that may develop into diabetes is typically observed from a young age similarly to obese patients (101).
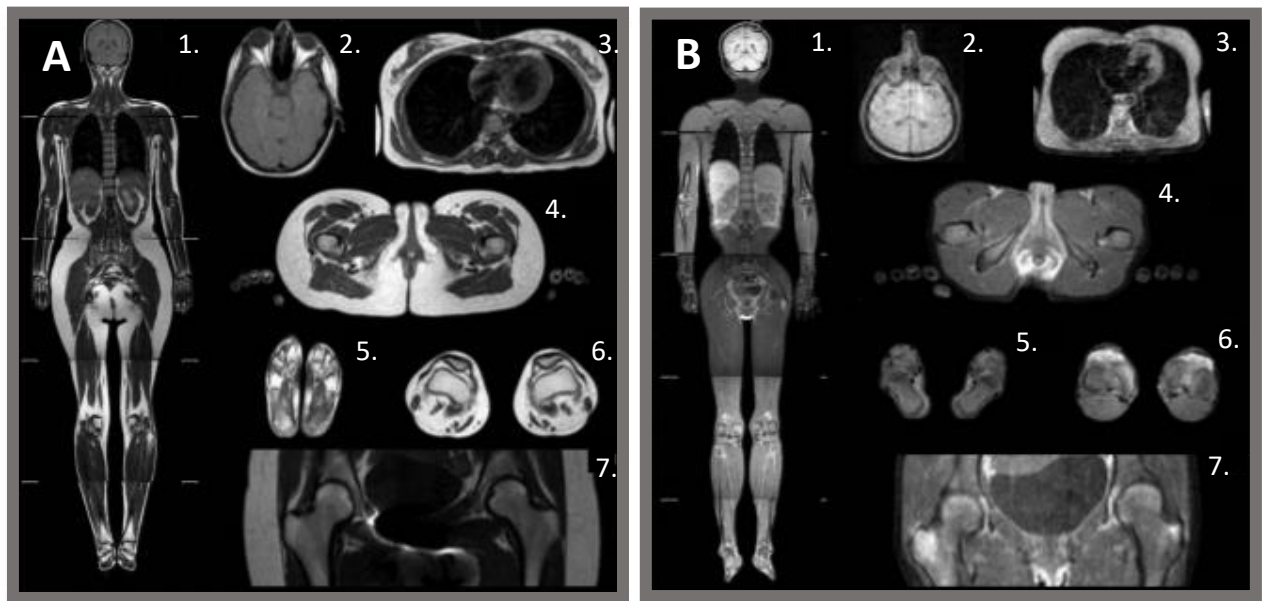
***Figure 1.7** : **Adipose tissue distribution in a patient with CGL2**. (**A**) a 28-year-old healthy woman. (**B**) a 25-year-old female patient with CGL2. (1. Whole body, coronal T1-weighted imaging; 2. Orbital fat and scalp, axial T1-weighted imaging; 3. Breasts, axial T1-weighted imaging; 4. External genital region and palms, axial T1-weighted imaging; 5. Soles, axial T1-weighted imaging; 6. Patellar region, axial T1-weighted imaging; 7. Hip region, coronal T1-weighted imaging.) Adapted from Altay et al. 2017.*

As yet, no cure has been found for lipodystrophies and the loss of adipose tissue cannot be reversed. Current therapies include the management of the symptoms and of the complications associated with this condition. Early diagnosis and management are the key to improved quality of life.

1.2.2.2.   Dietary approaches to treat CGL2

Effective management of CGL2 and more broadly lipodystrophy syndromes rely on a strict control of diet. Reducing fat intake, mainly triglycerides, help to prevent ectopic fat storage. Combined with caloric restrictions, a low-fat diet improved hyperglycaemia and hyperlipidaemia (102). A combination of statins, fibrates and long-chain omega-3 fatty acids may be considered to avoid complications of severe hypertriglyceridemia (103,104). Guidelines recommend a balanced diet consisting of 50-60% carbohydrates, 20-30% fat and 20% protein (103,105). However, due to leptin deficiency, patients suffering from CGL2 are typically hyperphagic which renders this strict diet difficult to follow (106).

1.2.2.3.   Clinical management of insulin resistance and diabetes in CGL2

Consequences of insulin resistance in CGL2 including hyperglycaemia are to some extent circumvented by the use of insulin-sensitising agents such as metformin (102,103,107). Metformin has been widely used for the treatment of type 2 diabetes where its glucose-lowering capacities are well-described (108). The mode of action of metformin is primarily based on the inhibition of hepatic gluconeogenesis through liver kinase B1 (LKB1) and adenosine monophosphate-activated protein kinase (AMPK) signalling (109). Metformin also promotes glucose uptake and utilisation in peripheral tissues such as the muscle, delays intestinal glucose absorption and stimulates glycogen synthesis (110). As the disease progresses, insulin requirements increase and some patients require high daily doses of exogenous insulin in addition to metformin (107,111). Insulin glargine, a long-acting insulin, is usually prescribed. Along with maintaining glycaemic control, insulin injections have been proven to ameliorate acanthosis nigricans in a CGL2 patient (111,112). However, the long-lasting effect of insulin glargine requires the formation of a precipitate in subcutaneous fat (113). Because of the lack of subcutaneous adipose tissue, the slow absorption of insulin cannot occur in CGL2 patients which makes them more prone to hypoglycaemia episodes (103,114). Concentrated insulin such as U-300 and U-500 may be more suitable (111,115,116). Preclinical studies suggest a beneficial role of thiazolidinediones in the treatment of congenital generalised lipodystrophy (117,118). Although no dedicated human clinical trials have been performed, pioglitazone has been used to treat some CGL2 patients but with varying success (119–121). Other hypoglycaemic agents such as glucagon-like-peptide 1 receptor agonists have not been studied in congenital generalised lipodystrophies.

As mentioned before, patients with CGL2 exhibit extremely low levels of circulating leptin hormone (101). Metreleptin, a recombinant human methionyl leptin analogue, was approved in Japan in 2013 followed by US Food and Drug Administration (FDA) approval in 2014 as a first-line treatment for generalised lipodystrophies (122). Although being granted an orphan drug designation in Europe since 2012, metreleptin only gained commercial approval by the European Commission in 2018 for the treatment of various forms of lipodystrophies. To date, it is the only drug specifically approved for the treatment of metabolic complications in patients with lipodystrophy in adjunct to a controlled diet (107,123,124). Daily metreleptin injections significantly reduce appetite which consequently is reflected by a decrease in food intake and weight loss most likely to contribute to metabolic improvements (107,125–129). Metreleptin

appears to be the most successful strategy for managing hypertriglyceridemia and diabetes in CGL2 patients (92,125,126,130,131). Twice-daily injections of metreleptin markedly improved fasting glucose and triglycerides levels after just one week of treatment (126). Leptin therapy also has a beneficial effect in hepatic steatosis by reducing hepatic triglycerides content and increasing insulin sensitivity resulting in an apparent reduction of hepatomegaly. This is consistent with a decrease in alanine aminotransferase (ALT) and aspartate aminotransferase (AST) liver enzymes levels (132–134). Importantly, beneficial effects of metreleptin were sustained throughout the therapy. As a consequence, leptin-replacement therapy often abolishes or strongly reduces the need for oral hypoglycemic agents and insulin (126,135). In some rare CGL2 cases, resistance to leptin-replacement therapy was associated with the development of neutralising antibodies (136,137).

1.2.2.4.   Causes of death

The CGL caused by BSCL2 mutations is characterised by a higher incidence of premature death and a higher mortality rate than that observed in any other CGL types (89,138). A study of CGL2 patients conducted in Rio Grande do Norte in Brazil, a region with a high prevalence of CGL2 cases, evaluated lifespan and causes of morbidity of patients with CGL2 over a 20-year period (86). None of the patients were using leptin replacement therapy but only standard medications to manage their diabetes, hypertension, and dyslipidaemia. Therefore, this study closely reflected the natural history of the disease. The authors found that life expectancy is considerably reduced by more than thirty years in patients with CGL2 condition with death occurring around 27 years of age. The authors identified three significant causes of deaths in those patients. About one third of patients died as a result of liver disease or its consequences including hepatic failure or gastrointestinal bleeding secondary to cirrhosis. This finding was consistent with the severe hepatic steatosis observed in those patients. Interestingly, infection caused the death of another third of these patients. Pneumonia accounted for most of the deaths in this group followed by respiratory failure and bacterial skin infection that evolved in septic arthritis. Remaining patients died of diabetes complications including renal failure, myocardial infarction, and acute pancreatitis (**Figure *1.8*1.8**). While deaths resulting from liver disease and complications of diabetes were expected, the high incidence of deaths caused by infections is not easily explained. This study in Brazil was not the only report of higher infection rates among CGL2 patients. In 1986, Rheuban *et al.* have documented a patient with generalised lipodystrophy who died as a result of peritonitis and septicemia (139). In 2002, Van Maldergem

et al. reported pneumonia and sepsis as causes of deaths in 28,5% of their CGL2 patients (89). In 2016, Gupta *et al.* observed that respiratory infection was the most frequent cause of deaths among CGL patients, regardless of the type (140). In 2018, Hsu et *al.* also reported a death related to pneumonia in their cohort of children suffering from CGL2 (119). These isolated observations made by independent groups have all pointed to the recurrence of infections as a cause of morbidity among CGL patients and more specifically CGL2 patients. Further analyses are needed to determine what predisposes CGL2 affected individuals to higher rates of infection.
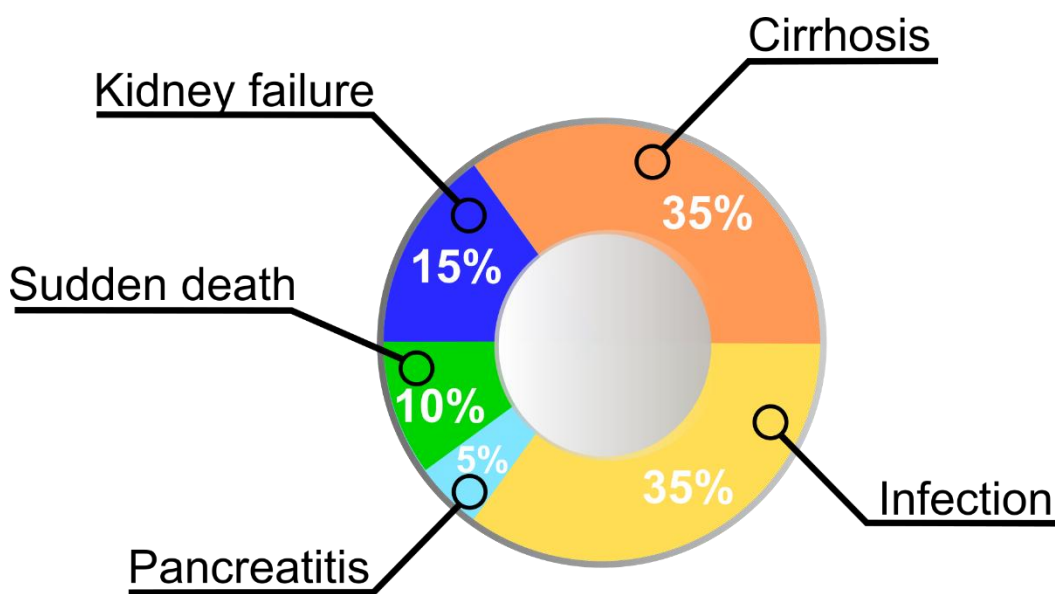
Figure 1.8 : Major causes of deaths in CGL2 patients.

1.2.3. Seipin protein

In 2001, Magré *et al.* first identified *BSCL2* gene as a causative gene for Berardinelli-Seip Congenital Lipodystrophy type 2 (85). Twenty years later, its functions are still not fully understood.

The *BSCL2* gene (OMIM #606158) encodes a 398 or 462 amino acid protein referred to as the short and long form of seipin, respectively (141). In humans, the *BSCL2* gene was found to be highly expressed in testis and brain (85,141,142). Most other tissues displayed detectable levels of *BSCL2* mRNA with a high expression in the pancreas and a lower expression in adipose tissue (85,141). Mouse Bscl2 tissue distribution mirrored the human pattern with a strong

expression in the testes. However, unlike humans, murine Bscl2 was detected at low levels in the brain but was highly expressed in adipose tissue (141,143).

Seipin protein is located in the membrane of the endoplasmic reticulum (ER) (142). Topological mapping studies have demonstrated that seipin protein comprises an ER luminal loop (residues 117-294) between two transmembrane domains (94-117, 294-316) with both N- and C-termini facing the cytoplasm (*Figure 1.9*) (144). Cryogenic electron microscopy revealed that human seipin is an undecamer, forming a ring-like structure in the ER. Several types of CGL2-causing mutations have been identified in the *BSCL2* gene including nonsense, missense, deletions, insertions and splice site mutations (85,96,145,146). The majority of them resulted in a frameshift and truncated version of the protein most likely leading to a complete loss or severe disruption of *BSCL2* function. In addition to causing lipodystrophy, mutations in *BSCL2* are also involved in motor neuropathy although it might be mechanistically different (142,147). Dominant gain-of-function in the N-glycosylation site of seipin leads to the accumulation of mutant proteins in the ER resulting in ER stress which causes the neurological disorders collectively known as seipinopathies (148).
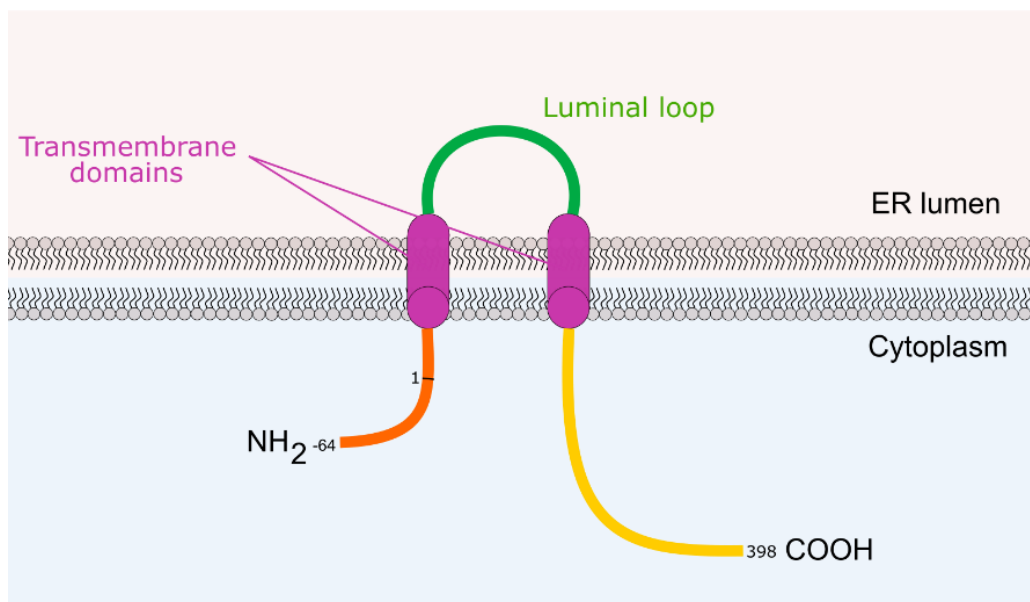
Figure 1.9 : Schematic diagram of seipin structure. *Seipin protein is composed of two transmembrane domains, an ER luminal loop and cytosolic N- and C-termini. Seipin protein was originally predicted to be a 398-amino acid protein but another initiation site, 64 bases upstream of the original site, can also encode a protein of 462 amino acids.*

Despite considerable progress into seipin structure, no consensus motif or similarity to other known proteins that could predict its function have been identified. The strong expression of seipin in brain and testes strongly suggests its involvement in neuronal and reproductive systems but will not be discussed in this thesis. However, germ-line specific deletion of seipin in mice resulted in male infertility and highlights a role of seipin in spermatogenesis (149). Similarly, lack of seipin specifically in neurons leads to affective disorders in male mice (150).

1.2.3.1. The role of seipin in adipogenesis

As the main manifestation of lipodystrophy is adipose tissue loss, it is not surprising that several studies have examined the role of seipin in adipogenesis. An involvement of seipin in this process was initially suggested by the observation that *Bscl2* mRNA expression levels increase during hormone-induced adipocyte differentiation in murine 3T3-L1 preadipocytes and C3H10T1/2 multipotent stem cells (143,151). The same studies also observed that the initial induction of the key adipogenic markers PPARγ, C/EBP-α, C/EBP-β and C/EBP-δ was not dramatically affected by inhibiting seipin expression by transfecting cells with short hairpin RNAs (shRNAs) targeting the Bscl2 gene. Similarly, seipin deficiency had no effect on bone morphogenetic protein 4 (BMP4) – induced preadipocyte commitment of C3H10T1/2 cells (151). These observations were further supported by Chen *et al.* and Prieur *et al.* in mouse embryonic fibroblasts (MEF) and stromal vascular cells (SVC) isolated from Bscl2$^{-/-}$ mice (117,152). Isolated MEF and SVC were successfully able to initiate adipocyte differentiation and form lipid droplets (LDs) in the absence of seipin. However, after four days of differentiation, those cells failed to maintain the differentiation process and displayed supersized LDs. By day 8, the majority of the cells were depleted of intracellular LDs. This was associated with a considerable decrease in PPARγ, C/EBP-α and downstream transcriptional targets Plin1 and aP2 gene expression from day 6 onwards. Similar defects in adipogenesis were observed during the late stages of differentiation in knockdown experiments using 3T3-L1 and C3H10T1/2 cells (143,151). The failure of terminal differentiation in MEF and SVC was associated with an increased basal cAMP/PKA-mediated lipolysis (117,152). All this together indicates that seipin loss is not detrimental to the early-phase differentiation process but crucial for the maturation of adipocytes.

1.2.3.2.   Seipin's role in LD formation

The seipin protein is not evenly distributed within the ER membrane but forms defined and dynamic foci. During LD biogenesis, seipin foci have been shown to travel through the ER membrane until they get stalled at a nascent LD, supporting a role in LD formation (153–155). Consistent with its localisation at ER/LDs junctions, disruption of seipin or its orthologue results in severe defects in LD morphology and in several model organisms. In *Saccharomyces cerevisiae*, the absence of the seipin orthologue Sei1 (previously named Fld1p) resulted in a few significantly enlarged LDs whose diameter exceeded 0.5 µm and many small irregularly shaped LDs that appear to be clustered alongside the ER (154,155). Similar defects of heterogenous LDs were observed in seipin deficient *Drosophila melanogaster*, *Caenorhabditis elegans* and *Arabidopsis thaliana* (153,156,157). Numerous small and aggregated droplets were also apparent in lymphoblastoid cell lines and a fibroblast cell line derived from subjects with CGL2 (155,158). Common alterations in LD phenotype in yeast, fly, plant, and mammalian cells demonstrate a conserved role of seipin in LD biogenesis across species. However, the molecular mechanisms by which seipin exerts this function are not fully understood. Several studies suggest that seipin might modulate triglycerides and phospholipids biosynthesis through its interaction with lipogenic enzymes including glycerol-3-phosphate acyltransferase (GPAT), AGPAT2 and lipin (158–164). Other studies have assigned a more structural function to seipin. Although seipin amino acid sequence is poorly conserved between species, a similar organisation with two transmembrane domains and a luminal loop is shared (144,165,166). This topology has led several researchers to propose another model in which seipin would play a more structural role by stabilising the contact sites between the ER and the LD and regulating lipid transfer between these two organelles (45,153,167,168). Those two models are not mutually exclusive and additional studies are required to fully understand the role of seipin in LD biogenesis.

1.2.3.3.   The functions of seipin in mature adipocytes

As seen in section 1.2.3.1, seipin disruption affects the process of adipocyte differentiation. However, whether seipin regulates mature adipocytes, independently of its function(s) in adipogenesis and LD biogenesis is unclear. Chen *et al.* have examined this by selectively deleting *Bscl2* in mature adipocytes using the tamoxifen-inducible adiponectin promoter driven Cre-LoxP system (169). The authors observed that *Bscl2* disruption causes a progressive fat

loss in mice with an overall 40 % reduction of adiposity 12 weeks after tamoxifen administration. Histological analysis of adipose tissue revealed morphological changes with an increased quantity of both small and large adipocytes. When fed a high fat diet, mice lacking *Bscl2* in adipocytes gained less weight but were still susceptible to hepatic steatosis and insulin resistance. The authors demonstrate that loss of *Bscl2* in adults adipocytes promotes fatty acid oxidation, cAMP/PKA-mediated lipolysis and browning that most likely contribute to the fat loss and protection from diet-induced obesity (169). Using an alternative cell based doxycycline-inducible model, Dollet *et al.* observed that loss of seipin in 3T3-L1 adipocytes results in a progressive loss of mature adipocytes and an increase in caspase-3 activity and p38 MAPK phosphorylation associated with apoptotic cell death (170). Altogether, these studies strongly suggest that seipin is important for the maintenance of mature adipocytes. Whether this function is mechanistically linked to seipin's role in adipogenesis, and LD biogenesis remains unclear. Similarly, it is not yet evident which of these actions or effects of seipin are directly involved in causing the severe adipose tissue loss in patients with *BSCL2* mutations nor precisely how this occurs.

1.3. Pancreatic regulation of glucose homeostasis

As described above, dysfunction of adipose tissue plays a key role in the development of impaired glucose regulation due to the development of insulin resistance as a result of lipotoxicity. However, typically appropriate glucose regulation can initially be maintained by increasing the secretion of insulin from the pancreas to compensate for insulin resistance. The development of overt type 2 diabetes subsequently occurs once this compensatory mechanism is no longer sufficient or fails. A significant component of the work in this thesis characterises how these compensatory mechanisms may operate in lipodystrophy and so the pancreas is discussed in further derail below.

1.3.1.   Anatomy and location of the pancreas

The pancreas is an elongated retroperitoneal glandular organ located in the abdominal cavity. It is commonly divided into three parts: the head, the body and the tail, as depicted in ***Figure 1.10.*10**. The head corresponds to the wider part of the pancreas and is connected to the

duodenum *via* the pancreatic duct. The narrow-end portion of the pancreas, corresponding to the tail, extends near the hilum of the spleen (171).
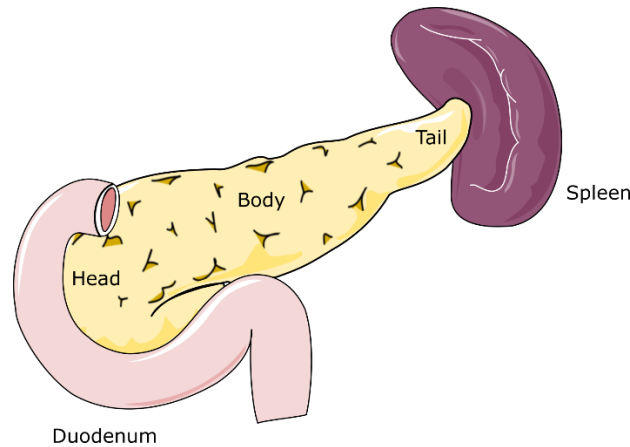
Figure 1.10 : Parts of the pancreas. The pancreas is located in the abdomen between the duodenum and the spleen.

1.3.2.   Structure and function

The pancreas is essentially compartmentalised into two structures, which have defined functions. Normal functioning of the pancreas relies on different cell types distributed across the tissue within those compartments.

1.3.2.1.   The exocrine pancreas

The exocrine portion of the pancreas accounts for approximately 95% of the total pancreatic mass (172). It is composed of acinar and ductal epithelial cells arranged in grape-like structures (*Figure 1.11*). Each acinar gland is connected by small, intercalated ducts joining larger ducts which culminate in the main pancreatic duct called the duct of Wirsung. As part of the gastrointestinal system, the main function of the exocrine pancreas is the synthesis, the storage, and the secretion of digestive enzymes. Pancreatic enzymes are secreted in their inactive form into the lumen of the acini and transported to the intestinal lumen through that duct system. The main pancreatic duct extends from the tail to the head of the pancreas, collecting and channelling pancreatic secretions to the duodenum where it joins the common bile duct to form the hepatopancreatic Ampulla of Vater. Together with the bile secreted by the gallbladder, pancreatic secretions subsequently activated inside the duodenum actively participate to the digestion process. Among others, these include the chymotrypsin, the amylase and the

pancreatic lipase responsible for the breakdown of proteins, carbohydrates and triglycerides, respectively (171–173).
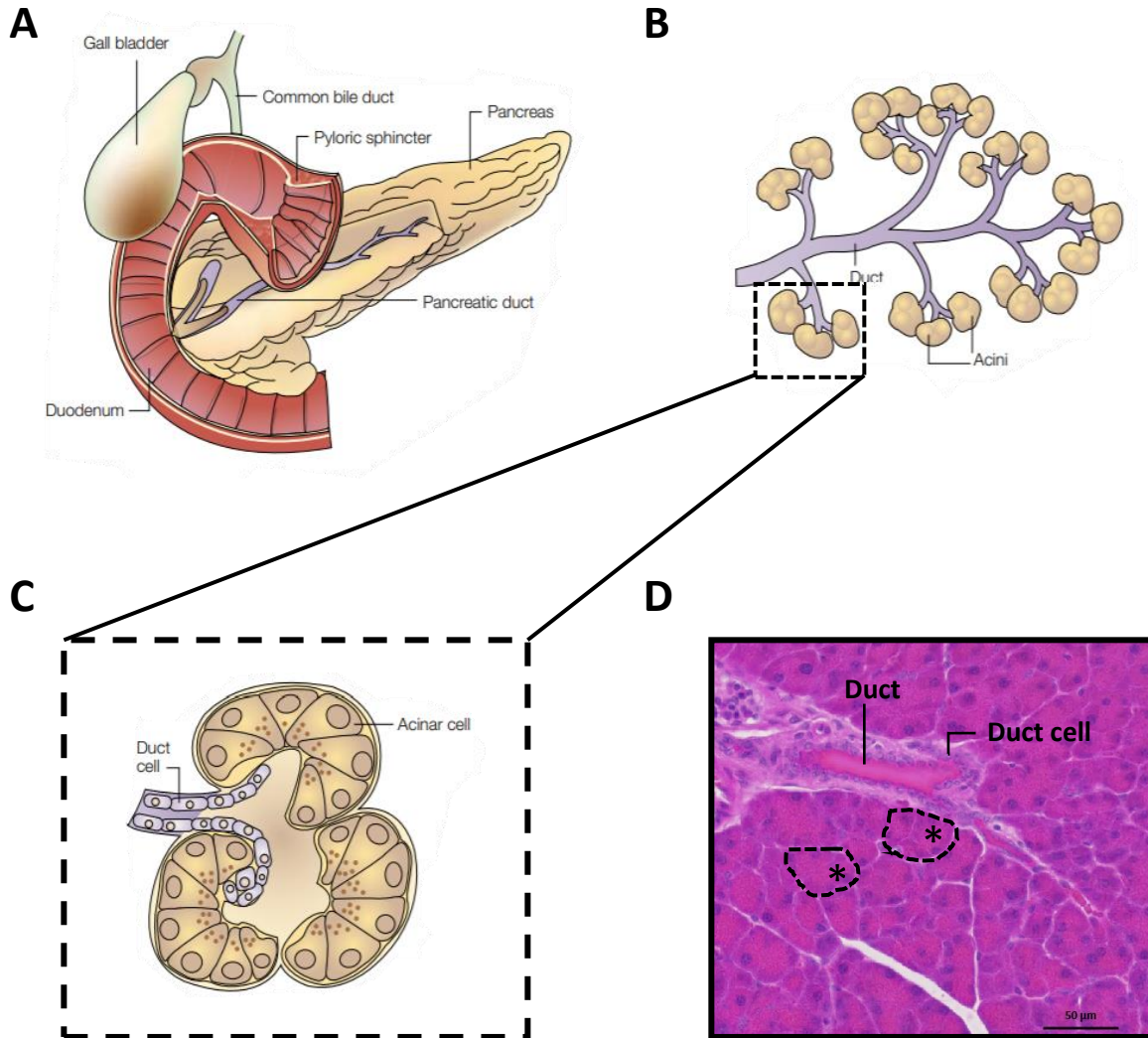
***Figure 1.11** : **Anatomy of the exocrine pancreas**. (**A**) Schematic representation of the pancreas. (**B**) Duct system of the exocrine pancreas. (**C**) Schematic representation of a single acinus. (**D**) Hematoxylin and eosin staining of mouse pancreatic tissue. * Indicates acini. Bar denotes 50 µm. (**A/B/C**: Adapted from Bardeesy et al. 2012)*

1.3.2.2. Endocrine pancreas

Contrary to the exocrine pancreas, the endocrine portion of the pancreas only represents between 1 and 2 % of the total pancreatic mass. Notwithstanding these low proportions, the endocrine pancreas plays considerable roles in glucose homeostasis and, more broadly, normal functioning of the body. This function is performed by the islets of Langerhans, named after Paul Langerhans, who discovered this structure in 1869, but are usually referred to simply as pancreatic islets. Pancreatic islets are dispersed throughout the pancreas among the acinar lobules. Islet size and shape can vary greatly, reflecting the adaptation to the surrounding environment. They comprise several endocrine cell types including β-cells, α-cells, δ-cells and γ or PP cells releasing insulin, glucagon, somatostatin and pancreatic polypeptide, respectively (174). A fifth cell type, the ε-cells, are present to a lesser extent and produce the hormone ghrelin (175). Each of these hormones is directly secreted into the bloodstream where they have distinct properties but act together along with surrounding tissues to maintain blood glucose levels within the physiological range of 4-6 mM (176).

Islet composition and structure differ between species (177,178). In humans, β-cells are the most prevalent endocrine cell type within the pancreatic islet (~55 %), followed by α-cells (~30 %), δ-cells (~10 %) and some PP cells which appear to be randomly distributed throughout the islet (179). In contrast, rodents islets are structurally organised with β-cells (~60-80 %), primarily located in the core and α and δ-cells restricted to the periphery of the islet (180,181) (**Figure 1.12**).

A

50 µm

B

Sympathetic
fibres

Parasympathetic
fibres

HUMAN   Blood vessels   **RODENT**

β-cell   α-cell   δ-cell
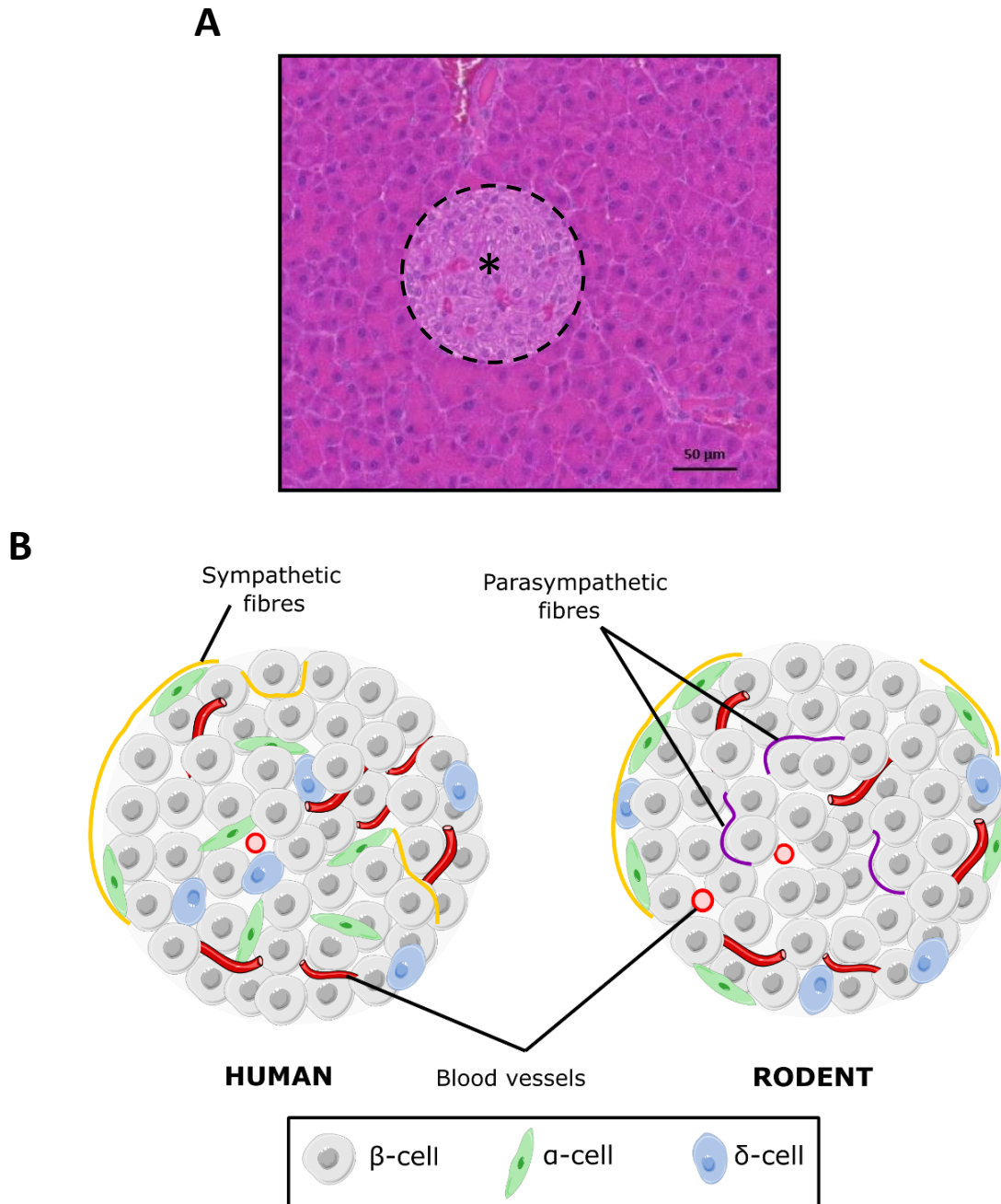
*Figure 1.12 : The endocrine pancreas. (A) Hematoxylin and eosin staining of mouse pancreatic tissue. * Indicates islet. Bar denotes 50 µm. (B) Schematic comparison of human and rodent islets. Note that α and δ-cells are randomly spread across human islets while they are segregated to the periphery of the islet in rodents.*

1.3.3.   Glucose homeostasis

Plasma glucose levels are constantly maintained between a narrow range of 4-6 mM despite wide variations in the supply of glucose from the gut in response to diet. This is achieved through a tight balance between glucose release and glucose removal from the circulation (182). In the fed state, circulating glucose originates from the diet through intestinal absorption (183). In these conditions, glucose uptake by the liver, muscle and adipose tissue is enhanced while glucose production from the liver is reduced (184,185). On the other hand, when exogenous glucose supplies are limited, such as during fasting, plasma glucose concentrations are maintained by glucose production from the liver through gluconeogenesis and glycogenolysis (183). A strict control between glucose absorption in the intestine, glucose production in the liver and glucose uptake by peripheral tissues (including adipose tissue) dictates the overall capacity of the organism to adapt to glucose fluctuations. This complex adaptation requires many glucoregulatory hormones, incretins and neurotransmitters and involves several tissues. Among them, insulin produced by β-cells in the pancreatic islets stands as the master regulator of glucose metabolism, for its direct capacity to lower blood glucose levels. The following sections describe in further detail the roles of insulin and GLP-1 incretin hormone in the regulation of glucose homeostasis.

1.3.3.1.   Insulin secretory pathway

Glucose-stimulated insulin secretion features a rapid, robust but transient first phase followed by a slower second phase which is sustained until euglycemia is restored (186). This biphasic pattern is believed to reflect distinct mechanisms within the β-cell machinery and is achieved through the combination of triggering and amplifying pathways (**Figure *1.13*1.13, A**).

1.3.3.1.1.   Triggering pathway - canonical pathway

β-cells can sense a wide variety of nutrients including glucose, amino acids (187,188) and fatty acids (189) and respond accordingly with appropriate insulin secretion (190). As a potent secretagogue, glucose is the primary stimulatory signal for insulin secretion (190). Rather than activating specific receptors, glucose is metabolised within the cell to generate metabolic signals that stimulate insulin secretion (191,192). Glucose uptake is mediated by specific glucose transporters (GLUT) on the plasma membrane which facilitates the diffusion of glucose across the β-cell plasma membrane (193). In rodent pancreatic β-cells, GLUT2 (also known as Solute Carrier Family 2 member 2; SLC2A2) is predominantly and constitutively expressed

and its disruption impairs glucose uptake and glucose-stimulated insulin secretion in mice (194). GLUT2 is a facilitative transporter with a relatively high Km and coupled to high expression levels in the cell, this means that a rise in circulating glucose levels rapidly leads to a corresponding elevation of intracellular glucose in β-cells. Once inside the β-cell, glucose is rapidly phosphorylated to glucose-6-phosphate by glucokinase (GCK), also known as hexokinase IV, and enters the glycolytic pathway. This primary step is viewed as the rate-limiting step of glucose-stimulated insulin secretion with the glucokinase enzyme adjusting the flux through glycolysis (195–197). The end-product of glycolysis, pyruvate, is converted to acetyl CoA in the mitochondria where it enters the tricarboxylic acid (TCA) cycle, leading to the generation of NADH and $FADH_2$ (198). These are further oxidised in the mitochondrial respiratory chain (also known as the electron transport chain) to produce adenosine triphosphate (ATP). This leads to a rise in ATP/ADP ratio within the first minute of β-cell stimulation with glucose. The resulting ATP binds and inhibits ATP-sensitive potassium channel (K_{ATP}) which consists of the pore-forming $K_{IR}6.2$ and the regulatory sulfonylurea receptor 1 (SUR1) subunits (199–202). The closure of K_{ATP} channels prevents the potassium from exiting the cell causing the depolarisation of the plasma membrane of the β-cell and the opening of voltage-gated Ca^{2+} channel (203). The influx of Ca^{2+} into β-cells increases the concentration of cytosolic Ca^{2+} and this is sensed by calcium-binding proteins that then activate the exocytic machinery. This triggers the release of insulin from a readily releasable pool of insulin-containing secretory granules (**Figure *1.13*1.13, B**) (204–206). This triggering pathway, also known as K_{ATP} dependent pathway, is rapid and robust and usually occurs within the first ten minutes after glucose stimulation (186,207,208).

1.3.3.1.2. Amplifying pathways

Evidence for another glucose stimulated pathway came from the observation that glucose can stimulate insulin secretion in a K_{ATP}-independent manner in rodents and human islets (209,210), perfused rat pancreas (211) and pancreatic β-cell lines (212). This second pathway, known as the K_{ATP}-independent pathway, is also referred to as the amplifying pathway (213–215). Glucose-stimulated insulin secretion is augmented by the amplifying pathways, but these cannot occur without the initial triggering pathway. Amplifying pathways include metabolic amplification pathways that require metabolic signals issued from β-cell glucose metabolism and amplification pathways activated by neurohormonal amplifiers such as glucagon-like peptide 1 (GLP-1) (199,215–217). Metabolites that have been identified to mediate positively

or negatively the amplification of insulin secretion include ATP/ADP (218–220), GTP/GDP ratios (221,222) and glutamate (223) (*Figure 1.13*, **B**).
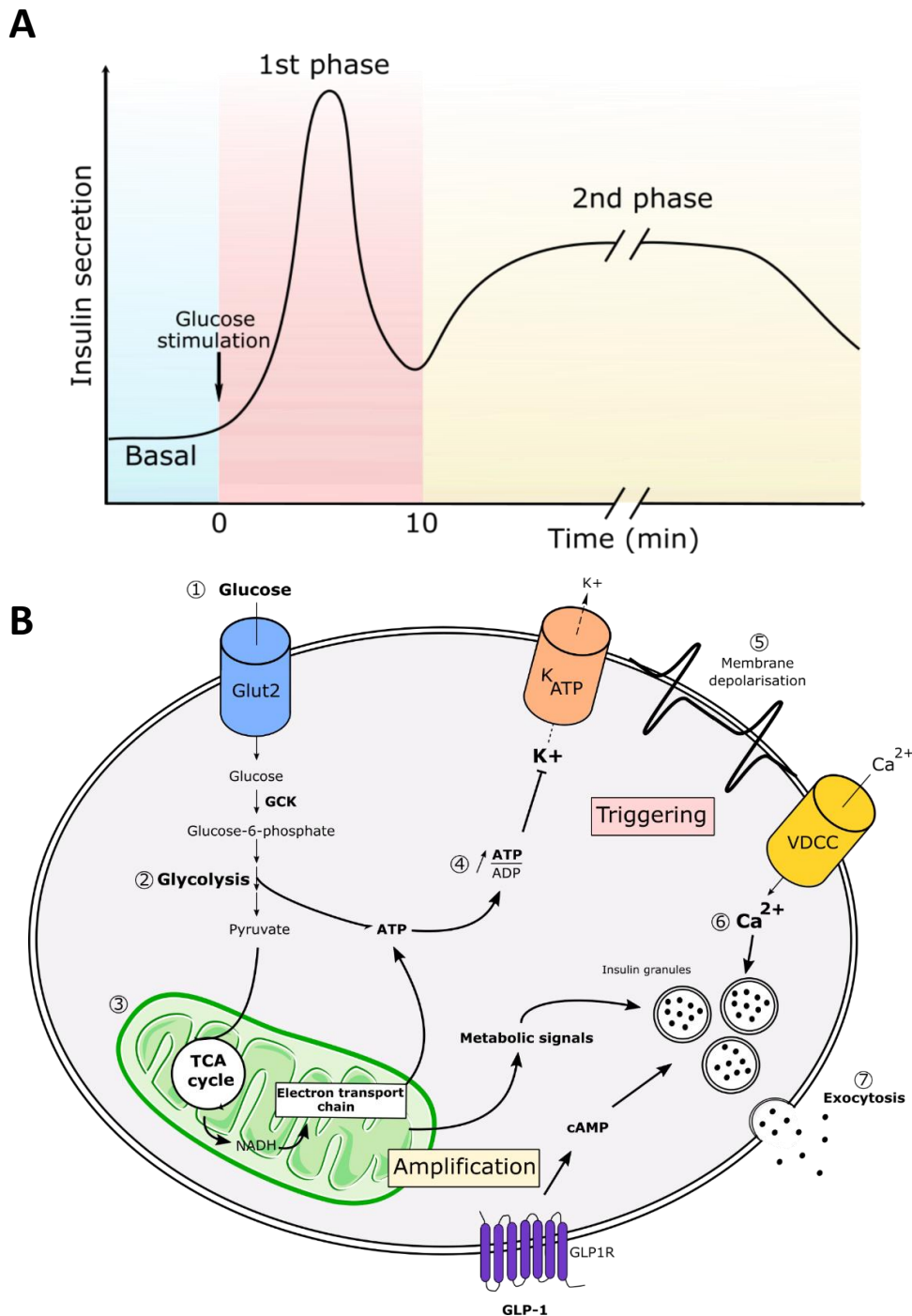
***Figure 1.13** : **Key mechanisms of insulin secretion in pancreatic β-cells**. (**A**) Schematic representation of glucose-stimulated biphasic insulin secretion in pancreatic β-cells. (**B**) Overview of glucose-stimulated insulin secretion pathways in pancreatic β-cells. Glut2: Glucose transporter 2; GCK: Glucokinase; TCA: tricarboxylic acid cycle; NADH: Nicotinamide adenine dinucleotide hydrogen; ATP/ADP: Adenosine triphosphate/Adenosine diphosphate; VDCC: Voltage dependent calcium channel; cAMP: cyclic adenosine monophosphate; GLP-1: Glucagon-like peptide 1; GLP1R: GLP-1 receptor.*

1.3.4. Regulation of insulin release

Only a fraction of the total insulin content of the β-cell is released during glucose-stimulated insulin secretion (186). This suggests that the tight control of glucose homeostasis relies more on the regulation of insulin release than on the regulation of insulin biosynthesis. In section 1.3.3.1.1, glucose, amino acids and free fatty acids have been shown to promote insulin secretion from pancreatic β-cells, but additional factors can also influence the release of insulin.

1.3.4.1. Counterregulatory hormones

The tight control of glucose levels by insulin is balanced by the counterregulatory hormones glucagon, somatostatin, pancreatic polypeptide, catecholamines, cortisol and growth hormone (GH). Those hormones have opposing actions on glycaemia by raising glucose levels to prevent hypoglycaemia. As plasma glucose concentrations progressively decrease, insulin secretion from the pancreatic β-cells is first reduced, limiting the glucose utilisation by other tissues and favouring glucose production (224). If plasma glucose levels continue to drop, counterregulatory hormones are secreted, among which glucagon, adrenaline, cortisol and the growth hormone are the best characterised (225,226). Glucagon is released from pancreatic α-cells and increases hepatic glucose production by stimulating glycogenolysis and gluconeogenesis (227). Adrenaline is secreted from the adrenal medulla and increases hepatic glucose production via β-2 adrenergic receptors on the liver by directly mobilising gluconeogenic substrates such as alanine and lactate from the muscle and glycerol from the adipose tissue (228,229). Prolonged hypoglycaemia will trigger the secretion of growth hormone and cortisol (225,230). In contrast to the acute effects of glucagon and adrenaline on glucose regulation, growth hormone and cortisol stimulate lipolysis in adipose tissue and hepatic ketogenesis and gluconeogenesis over a longer period of time (231,232). Collectively, these redundant glucose counterregulatory responses ensure the maintenance of blood glucose levels within the narrow physiological range of 4-6 mM and prevent the occurrence of hypoglycaemia.

1.3.4.2. Incretin hormones

The insulin response to oral glucose is considerably greater than following an equivalent intravenous glucose administration. This phenomenon has been described as the "incretin effect" and led to the discovery of intestinal hormones known as incretins that potentiate insulin

secretion (233). It is believed that the incretin effect accounts for 60 % of the insulin secretion following an oral glucose load (234). To date, the two best characterised incretins are the glucose-dependent insulinotropic polypeptide or gastric inhibitory polypeptide (GIP) and GLP-1 (235,236). In the following sections, the mechanisms of GLP-1 actions will be reviewed.

1.3.4.3.   GLP-1 synthesis and secretion

GLP-1 is mainly synthetised by enteroendocrine L cells of the small and large intestine from posttranslational processing of the proglucagon gene by prohormone convertase 1/3 (PC1/3) (237). It is also produced in the central nervous system and to a lower extent in α-pancreatic cells (238–241). In addition to GLP-1, processing of the proglucagon gene by different prohormone convertase leads to the synthesis of glucagon, glicentin, oxyntomodulin, glicentin-related polypeptide (GRPP) and GLP-2 depending on the tissue (*Figure 1.14*). GLP-1 is secreted into the circulation within minutes after nutrient ingestion including carbohydrates (242), proteins (243) and lipids (244) suggesting that both neural and endocrine factors are responsible for its secretion from intestinal cells. Native GLP-1 is rapidly degraded in the circulation by dipeptidyl peptidase 4 (DPP-4) resulting in a short half-life of less than two minutes (245,246). To overcome this, analogues of GLP-1 that are resistant to DPP-4-mediated degradation are being studied as a potential treatment for type 2 diabetes (247).
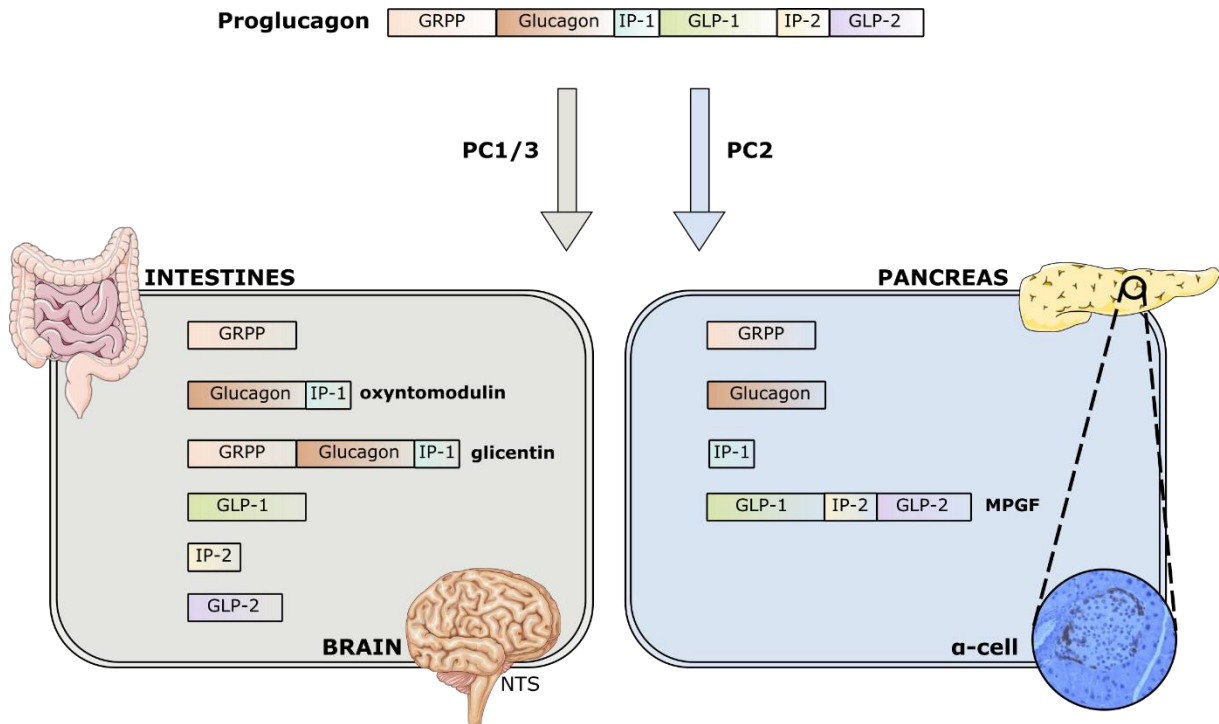
Figure 1.14 *: **Schematic representation of tissue-specific processing of proglucagon**. GRPP: glicentin-related polypeptide; IP-1: intervening peptide-1; IP-2: intervening peptide-2; GLP-1: Glucagon-like peptide-1; GLP-2: Glucagon-like peptide-2 ; PC1/3: prohormone convertase 1/3; PC2: prohormone convertase 2; MPGF: major proglucagon fragment; NTS: nucleus tractus solitarius.*

1.3.4.4.   GLP-1 actions

Mechanistically, GLP-1 exerts its effects through binding to GLP-1 receptor (GLP-1R) (248). GLP-1R is a B class guanine nucleotide-binding protein (G-protein) coupled receptor (GPCR) and is abundantly expressed in pancreatic β-cells and the central nervous system. There is also a strong body of evidence detecting its presence in extrapancreatic tissues including liver, heart, kidney and lung (249–253). Upon binding to GLP-1R found on the β-cells, GLP-1 activates adenylyl cyclase (AC) through the stimulatory protein G_S and leads to cAMP accumulation in the cell (254). This triggers the activation of cAMP-dependent second messengers including protein kinase A (PKA) and exchange protein directly activated by cAMP 2 (Epac2) (255). By modulating the closure of K_{ATP} channels, PKA and Epac2 activities potentiate the depolarisation of the plasma membrane and facilitate the opening of voltage-gated Ca^{2+} channels (256,257). Together, they promote Ca^{2+}-dependent exocytosis of insulin-containing granules therefore potentiating glucose-stimulated insulin release (see section 1.3.3.1.2). In addition to the acute stimulation of insulin secretion, GLP-1 can also modulate the expression

of regulatory genes including *Insulin* itself via cAMP response elements present on the promoter regions (258–260). GLP-1 has also been shown to promote β-cell proliferation through the transactivation of the epidermal growth factor receptor (EGFR) while inhibiting β-cell apoptosis resulting in the expansion of β-cell mass (261–265). GLP-1 exerts glucose-lowering properties also by inhibiting glucagon release as shown in mice and humans (266–270). Others actions of GLP-1 include delayed gastric emptying and increase in satiety that most likely contribute to the reduction in body weight observed in subjects receiving GLP-1R analogues (271–275).

1.3.5.   Insulin actions

Insulin exerts its effects by binding to a glycoprotein insulin receptor (INSR) on the surface of target tissues including the liver, muscle and adipose tissue (276). INSR is a receptor tyrosine kinase and is composed of two extracellular α subunits ; which bind insulin ; and two β subunits embedded in the plasma membrane (277). Binding of insulin to the α subunits induces a conformational change in the β subunits which allows the trans-autophosphorylation of tyrosine residues within β subunits thereby activating the catalytic activity of the receptor (278–280). Activated INSR then recruits phosphotyrosine-binding scaffold proteins which activate downstream intracellular targets (281). Those include mitogenic (MAPK pathway) and metabolic signals (PI3K/AKT signalling pathway). Among INSR substrates, insulin-receptor substrate (IRS) family is probably the best characterised and plays a key role in engaging downstream signalling molecules to modulate intracellular signalling events that drive the many effects of insulin (282–284).

1.3.5.1.   Carbohydrate metabolism

Insulin, along with other pancreatic hormones, are first secreted into the portal vein before entering the systemic circulation, exposing the liver to high concentrations of insulin, two to three times greater than that in the bloodstream (285). Similarly, because of their absorption into the hepatic portal vein, most of the ingested nutrients are first processed in the liver making it a major player of glucose homeostasis. After a meal, around 33 % of the glucose is immediately taken up by the liver where it is stored in the form of glycogen (286). Increased insulin concentrations following digestion and absorption of nutrients directly stimulate glycogen formation from glucose by activating several enzymes involved in this pathway

including glucokinase, phosphofructokinase and glycogen synthase (287–290). Together with glucose, insulin also inhibits liver glycogen phosphorylase activity with the net effect of promoting glycogen synthesis (291–293). When nutrient become scarce, such as in the fasted state, insulin levels decrease and the liver starts producing and releasing glucose into the bloodstream through two processes : glycogenolysis and gluconeogenesis (294). These processes are inhibited by insulin but are also regulated by counterregulatory hormones including glucagon (295) (see section 1.3.4.1).

Facilitated diffusion of extracellular glucose into hepatocytes through GLUT2 glucose transporters does not require the presence of insulin. In many other tissues including the muscle and adipose tissue, glucose entry is responsive to stimulation with insulin. In these tissues, binding of insulin to INSR stimulates the translocation of insulin-responsive GLUT4 transporters from intracellular pools to the myocyte and the adipocyte plasma membrane therefore enabling glucose uptake in these cells (296,297). When insulin levels decrease, GLUT4 transporters are no longer required at the plasma membrane and are recycled back into GLUT4 containing vesicles within the cytoplasm (298).

1.3.5.2.   Lipid metabolism

As discussed above, insulin stimulates glycogen synthesis in the liver. However, when carbohydrates are abundant, the liver becomes saturated with glycogen and any additional glucose taken up by hepatocytes is converted into fatty acids, a process known as *de novo* lipogenesis (DNL) (299). Insulin stimulates free fatty acids synthesis from glucose mainly through transcriptional regulation of several genes involved in DNL (300,301). Within the hepatocyte, fatty acids are esterified to glycerol-3-phosphate to generate triglycerides. These neutral lipids will be either stored in the liver in lipid droplets or exported to tissues as very-low-density protein (VLDL) particles (302). The overall effect of insulin is thus to promote lipid storage in the hepatocyte and indirectly reduce the supply of fatty acids for oxidation by other tissues.

As mentioned in section 1.3.5.1, insulin facilitates glucose entry into adipocytes where it can be used to synthesise glycerol. Along with the fatty acids derived from the liver, glycerol is then used to form triglyceride within the adipocyte. Moreover, insulin potently suppresses lipolysis in adipocytes by restraining the activity of adipose triglyceride lipase (ATGL) and hormone sensitive lipase (HSL) through mechanisms involving cAMP, protein kinase A (PKA) and phosphodiesterase 3B (PDE3B), whilst also upregulating lipoprotein lipase (LPL) to

enhance delivery of new substrates for triglyceride synthesis in the cell (303,304). Through these mechanisms, insulin indirectly promotes the accumulation of fat in adipose tissue.

The main systemic effects of insulin in controlling glycaemia and lipid storage are summarised in *Figure 1.15*.
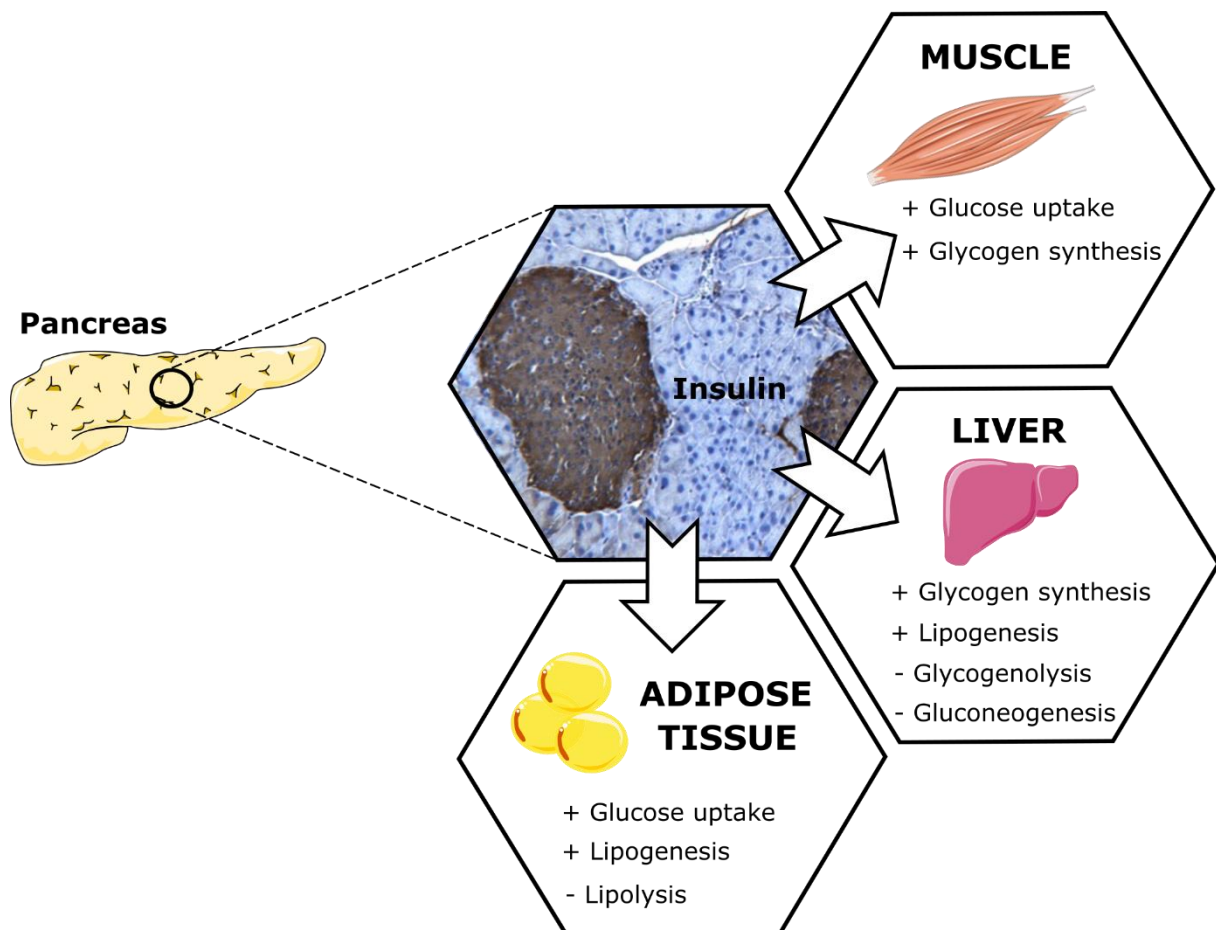
Figure 1.15 : Summary of insulin actions on glucose and fatty acid metabolism in adipose tissue, liver, and muscle.

1.3.6.   Insulin resistance

Insulin resistance is defined as an impaired response of target tissues - mainly liver, muscle, and adipose tissue – to insulin stimulation. In other terms, insulin resistance is observed when the organism is unable to mount an adequate glucose-lowering effect in response to normal insulin levels (305). It is commonly associated with obesity and type 2 diabetes, but other conditions are also linked to insulin resistance including lipodystrophies (see section 1.2).

1.3.6.1.   Causes of insulin resistance

The molecular mechanisms underlying insulin resistance are not fully elucidated but appear to involve both genetic and environmental factors (306). As discussed in section 1.3.5.1, insulin is responsible for glucose entry into adipocytes and myocytes. Any defects in insulin signalling transduction will therefore result in hyperglycaemia due to the inability of these cells to take up glucose (300). Similarly, any impairment of glucose production, glycogen synthesis and lipolysis is likely to contribute to insulin resistance (307,308). While the exact pathophysiology of insulin resistance is unclear, ectopic lipid accumulation in the liver and the muscle is believed to be involved in the development of insulin resistance as well as the impairment of β-cell function (309). In addition to this so-called lipotoxicity, nutrient oversupply in general, endoplasmic reticulum stress, reactive oxygen species, mitochondrial dysfunction, inflammation and adipokines have all been suggested to impair carbohydrate and lipid metabolism and decrease insulin sensitivity in target tissues (310).

1.3.6.2.   Compensatory mechanisms

Pancreatic islets can adapt to physiological and pathophysiological conditions by modulating their function and mass to maintain glucose homeostasis (181,311,312). As highlighted earlier, to meet the increased insulin requirements, most insulin-resistant individuals are able to increase β-cell insulin secretion and thus compensate for insulin resistance. This compensatory hyperinsulinemia is achieved by a transient increase in insulin production that may or may not be associated with a change in islet mass (313). Pancreatic islet compensation and expansion of β-cell mass is well illustrated in the leptin receptor-deficient Zucker fatty (ZF) rats, which offer an accurate model of genetic obesity (314). Diet-induced obese rodent strains also model this adaptative response well, with a striking increase in β-cell number and size (315,316). In addition to those structural changes, β-cells are also able to adjust their metabolism to accommodate the changes in insulin demand (317). These functional adaptations can occur at all stages in the stimulus-secretion coupling from the initial nutrient sensing to the exocytosis of insulin granules (see section 1.3.3.1.1). This is achieved in part by alterations of the activity of key metabolic enzymes through transcriptional events, allosteric regulation and post-translational modifications (217,317–322). Upregulation of several glycolytic enzymes including the low-affinity enzyme glucokinase has been observed in several animal models of successful β-cell adaptation (318,320,322). Studies in ZF rats also showed an increased flux through pyruvate carboxylase and malate-pyruvate shuttle in compensating islets, providing

metabolic coupling factors for the amplifying pathways of GSIS (317). Similarly, excess lipid supply, as observed in obesity, also contributes to the potentiation of GSIS through the production of metabolic coupling factors (317). Collectively, these structural and functional adaptations, by modulating the insulin secretory response to nutrient, allow the organism to effectively cope with the increased insulin demand and prevent fasting hyperglycaemia in insulin-resistant states. As a consequence, insulin-resistant states are not necessarily associated with glucose intolerance, even under conditions of severe insulin resistance. The signals that drive the β-cell compensatory response are not completely understood but a dominant role for an increased β-cell workload, and more specifically glucose, has been proposed (323).

1.3.6.3.   Type 2 diabetes mellitus (T2D)

As detailed above, most insulin-resistant individuals are able to compensate for insulin resistance and do not initially develop diabetes. The failure of this adaptative response to maintain euglycemia is thought to be a key determinant in the onset of diabetes (324–326). In T2D, continuous insulin demand exceeds the β-cell insulin secretory capacity which ultimately fails to appropriately compensate for impairments in insulin action (327). Chronic exposure to glucose and lipids is also believed to eventually impair insulin secretion leading to β-cell dysfunction and/or cell death. Sustained production of insulin results in endoplasmic reticulum (ER) stress, oxidative stress, reactive oxygen species and inflammation which impede β-cell function and promote apoptotic pathways (328–333). Thus, defects in both target tissues and β-cells are required for the development of T2D (334). As a consequence, diabetes is generally characterised by a persistent hyperglycaemia in the fasted state concomitant with a decrease in insulin levels (335).

The capacity of β-cells to mount a compensatory response to insulin resistance is clearly important in order to prevent progression to T2D. This pancreatic β-cell plasticity is well-described in obesity, a critical risk factor for T2D. The majority of obese people are insulin-resistant but are not diabetic due to their ability to effectively increase their insulin secretory capacity. Only a subset of those individuals, in whom β-cell compensation is inadequate, will develop diabetes (336). Identifying the mechanisms involved in the transition toward decompensation is crucial in improving our understanding of the progression of T2D. Novel therapeutic targets aimed at maintaining β-cell compensation while preserving β-cell integrity appear as attractive approaches for the long-term management of insulin resistance.

1.4. Thesis rationale and aims

1.4.1. Rationale of thesis

Mutations in the *BSCL2* gene, which encodes the protein seipin, cause CGL2, the most severe form of lipodystrophy (85). The functions of seipin are still not fully understood but a role of seipin in both adipogenesis and lipid droplet biogenesis has been examined in significant detail (152,164). Despite this, it is not clear which of these actions are directly involved in causing the severe adipose tissue loss in patients with *BSCL2* mutations. Furthermore, seipin is expressed in several non-adipose tissues, which implies that it might have important unexplored role in these tissues.

The overall aim of this thesis was to examine the effects of seipin loss in human adipocytes, which was not studied before, but also to investigate potential functions in non-adipose tissues. In particular, the work aimed to evaluate if any non-adipose functions of seipin may contribute to the metabolic phenotype observed in seipin knockout mice. In doing so, the work may elucidate further the molecular mechanisms *via* which *BSCL2* disruption causes metabolic disease and, ultimately, identify novel therapies that may be of benefit to affected individuals with CGL2.

1.4.2. Aims of thesis

This thesis aimed to address the following:

1) The role of seipin in human adipocyte function

❖ Characterise adipocyte differentiation in human Simpson Golabi Behmel Syndrome (SGBS) preadipocyte cell line.

❖ Examine the effects of seipin disruption on the processes of adipogenesis and lipolysis in SGBS preadipocytes.

❖ Compare the effects of seipin disruption in SGBS cells to the effects observed in immortalised mouse cell lines and in murine stromal vascular cells.

2) The role of seipin in the regulation of macrophage function

❖ Investigate the physiological consequences of *Bscl2* ablation specifically within the myeloid cell lineage *in vivo* in LysM-B2KO mice.

❖ Investigate the inflammatory response of seipin-deficient bone marrow-derived macrophages (BMDMs) to lipopolysaccharides (LPS) and saturated fatty acids *in vitro*.

❖ Evaluate the ability of seipin knockout macrophages to phagocytose and eliminate *Staphylococcus aureus in vitro*.

3) The pancreatic islet adaptation to adipose insufficiency in seipin knockout mice

❖ Characterise the progression of the metabolic disease in seipin knockout mice *in vivo*.

❖ Evaluate the adaptation of pancreatic islets to insulin resistance in seipin knockout mice.

❖ Evaluate the contribution of sexual dimorphism to the phenotype observed in SKO mice.

4) The role of seipin in pancreatic β cells

❖ Determine whether the loss of seipin specifically influences the insulin secretion.

❖ Evaluate the potential interaction between seipin and GLP-1R and their contribution to the islet hyperplasia observed in seipin knockout mice.

❖ Investigate the therapeutic potential of the GLP-1R agonist liraglutide to treat metabolic disease in seipin knockout mice.

CHAPTER 2

2. MATERIAL AND METHODS

2.1. Animal studies

2.1.1.   Ethics statement

Housing, handling and all regulated procedures conducted on animals used in this thesis have been approved by the University of Aberdeen Ethics Review Board and UK Home Office and performed under project licence P1ECEB2B6 and personal licence I76FBAA81. The use of animals strictly followed the Animals Scientific Procedures Act 1986 (ASPA) legislation.

2.1.2.   LysM-B2KO mice

$Bscl2^{(fl/fl)}$ mice were generated as previously described (337). To generate myeloid-specific $Bscl2$ knockout mice (LysM-B2KO mice), $Bscl2^{(fl/fl)}$ mice were crossed with heterozygous $Bscl2^{(fl/wt)}$ mice expressing Cre recombinase under the control of the endogenous Lyz2 promoter. LysM-B2KO littermates that were $Bscl2^{(fl/wt)}$ were used as controls (CTRL).

2.1.3.   SKO mice

Global seipin knockout (SKO) mice were generated using cell permeable TAT-Cre recombinase using similar methods to those previously described (338). TAT is a cell-penetrating peptide derived from the transactivator of transcription (TAT) of human immunodeficiency virus. Briefly, superovulated C57BL/6J female mice were mated with $Bscl2^{(fl/fl)}$ male mice. Fertilised $Bscl2^{(fl/wt)}$ one-cell embryos were collected, washed with Dulbecco's Modified Eagle's Medium high glucose (DMEM, Sigma-Aldrich, #D5671) then incubated *ex vivo* with 3 μM TAT-CRE Recombinase (Sigma-Aldrich, #SCR508) for 2 hours at 37°C. Embryos were then re-implanted into surrogate female dams. Pups were screened by polymerase chain reaction (PCR) (***Figure 2.1***). The colony was maintained by intercrosses.
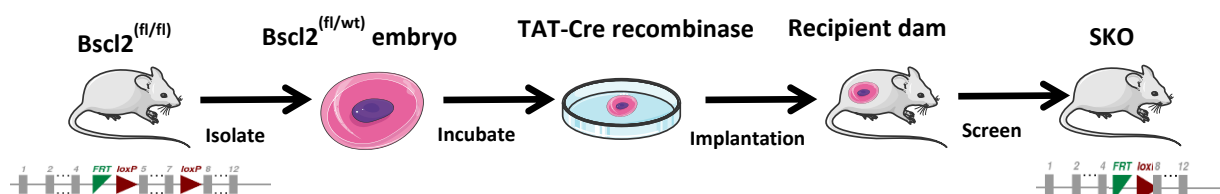
Figure 2.1: Strategy for the generation of seipin knockout (SKO) mice.

2.1.4.   Housing conditions

Experiments involved both male and female mice, WT and SKO mice, group-housed by gender at 20-24°C, 45-65% humidity and exposed to a 12-hour light/12-hour dark period in a specific pathogen free facility. For experiments involving treatments, control and treated mice were mixed in the same cage. Body weights were monitored weekly. Unless stated otherwise, mice had *ad libitum* access to water and food consisting of a standard rodent chow diet (Special Diets Services, #CRM (P) 801722).

2.1.5.   Procedures

2.1.5.1.   Body composition analysis

Whole body fat and lean mass were measured by quantitative nuclear resonance using an EchoMRI^{TM}-500 body composition analyser (Zinsser Analytic GmbH) and normalised to body weight. Briefly, live and unanaesthetised mice were restrained and placed in a plastic holder then inserted into the analyser. Mice were subjected to 3 scans and the average was used for analysis.

2.1.5.2.   *In vivo* lipopolysaccharides challenge

At 32 weeks of age, LysM-B2KO mice were placed into clean cages and food withheld for 2 hours. Mice were then injected with 1 mg/kg of lipopolysaccharides (LPS, Sigma #L8274) by intraperitoneal injection (i.p.) and food withheld for a further 3 hours. Mice were maintained at standard housing temperatures. Five hours after LPS injections, mice were killed as described in section 2.1.5.5.

2.1.5.3.   Glucose and insulin tolerance tests

Prior to tolerance tests, mice were placed into clean cages and food withheld for 5 hours. Mice were weighed and basal glucose levels were determined by glucometer readings (AlphaTrak® II, Zoetisus, Parsippany-Troy Hills, NJ, USA) from tail punctures. The experiment was initiated with an i.p. bolus of 2 mg/g D-glucose (Sigma, #G8270) for a glucose tolerance test (GTT) or 0.75 unit/kg of human insulin (Actrapid 100 IU/mL, Novo Nordisk) for insulin tolerance test (ITT). Blood glucose levels were then measured over time at 15, 30, 60, and 120 minutes with

the glucometer. Mice had *ad libitum* access to water throughout the experiment and were monitored closely for any adverse effects.

2.1.5.4. Serum biochemical parameters

After 5 hours of fasting, blood was collected from cardiac punctures performed by Dr. George D. Mcilroy under the personal licence I913DE295. Collected blood was placed in serum separator tubes (SST Amber tubes, BDMicrotainer^{TM}, #365979) and tubes inverted to activate the clotting. After 30 minutes at room temperature (RT), samples were centrifuged at +4 °C for 10 minutes at 12,000 x g. The upper phase *i.e.* the serum was collected, snap frozen in liquid nitrogen and stored at -70 °C for further measurements. IL6, TNFα, IL10 and MCP1 measurements were performed at the Core Biochemical Assay Laboratory (CBAL, Cambridge, UK). Following manufacturer's protocol, glucose levels were determined using the Glucose Colorimetric Assay Kit (Cayman Chemical, Ann Arbor, MI, USA). Serum triglyceride contents were determined using the Triglyceride Liquid Assay (Sentinel Diagnostics) following manufacturer's instructions. Serum insulin levels were measured using a mouse insulin enzyme linked immunosorbent assay (ELISA) kit (Mercodia, Uppsala, Sweden). Quantitative insulin sensitivity check index (QUICKI) was calculated from fasting glucose (mg/dL) and insulin (µU/mL) values as previously described (339). QUICKI = 1/ [log (I_0) + log (G_0)], where I_0 is fasting insulin and G_0 is fasting glucose. QUICKI is a dimensionless index without units. Homeostatic model assessment of insulin resistance (HOMA-IR) was calculated from fasting glucose (mmol/L) and insulin (µU/mL) values as previously described (340). HOMA-IR = (G_0*I_0)/22,5; where I_0 is fasting insulin and G_0 is fasting glucose.

2.1.5.5. Tissue collection

In strict accordance with Schedule 1 of the ASPA 1986, mice were killed by exposure to a rising concentration of carbon dioxide followed by cervical dislocation. Appropriate measures were implemented to minimise pain, suffering and distress experienced by the mice. Tissues of interest were collected and either snap-frozen in liquid nitrogen or fixed in 10% neutral buffered formalin (Sigma-Aldrich, #HT501128) for molecular analysis and histology, respectively. In some cases, organs were weighed before fixation or freezing.

2.2. Mouse tissue isolation and culture

2.2.1. Pancreatic islets isolation

2.2.1.1. Collagenase administration and pancreas removal

Rapidly after death, the abdominal cavity was completely opened to expose the liver and intestines. Intestines were pulled out and set outside the body while the lobes of the liver were held back against the diaphragm. After locating the gall bladder and the common bile duct, the ampulla of Vater was clamped with hemostatic forceps to block the bile pathway to the duodenum. Using a 2 mL syringe mounted with a 25-gauge needle, 1 mg/mL type XI collagenase solution (Sigma, #C7657) was slowly injected through the common bile duct into the pancreas. Fully distended pancreas was then detached from the surrounding tissues and placed into a 50 mL Falcon conical tube containing collagenase solution. If dissecting more than one mouse, several pancreata of the same genotype were pooled in the same tube. Pancreata could be left in this state for up to 1 hour before proceeding to the next step.

2.2.1.2. Pancreas digestion

Tubes containing pancreata and collagenase solution were placed at 37 °C on an orbital shaker. After 10 minutes, 25 mL of RPMI 1640 medium (ThermoFisher, #10379144); supplemented with 10 % *v/v* foetal bovine serum (FBS, Gibco, #10270-106) and 1 % *v/v* penicillin/streptomycin (P/S, Gibco, #15140-122); were added and tubes hand-shaked vigorously for 10 seconds to disrupt the pancreas (approximately 3 shakes/sec). After a centrifugation at 1,400 RPM for 1 minute at + 4 °C, supernatants were discarded, and pellets resuspended in 25 mL of RPMI medium. This centrifugation and resuspension steps were repeated twice.

2.2.1.3. Islets isolation

Homogenous suspensions were filtered through a 425 μm diameter wire mesh into new 50 mL Falcon tubes. Islets were pelleted by centrifugation at 1,500 RPM for 2 minutes and supernatants discarded. All centrifugation steps were performed at + 4 °C. Tubes were inverted on a piece of tissue paper and inside walls of the tube wiped with tissue to remove any trace of liquid. Islets were then resuspended in 15 mL of Histopaque-1077 (Sigma, #10771) in a new 50 mL tube. 10 mL of RPMI medium were carefully poured on top of the Histopaque, very

slowly down the walls, to preserve two distinct layers. After a centrifugation at 3,500 RPM for 25 minutes with slow acceleration and no braking, the two layers should be easily distinguishable. Islets were recovered from the histopaque/medium interface using a plastic Pasteur pipette and transferred into a new tube (see *Figure 2*).
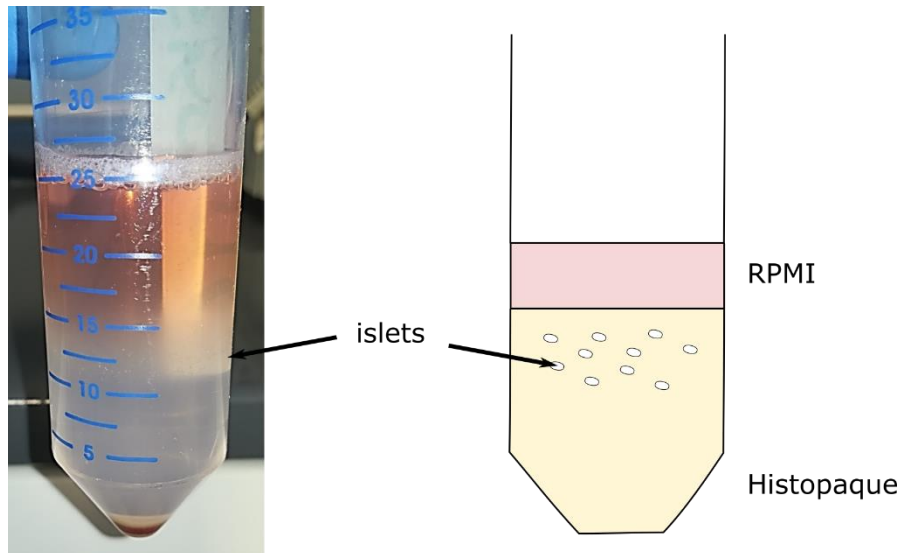
Figure 2.2: Isolation of mouse pancreatic islets using Histopaque.

2.2.1.4.   Islets purification

Islets were washed with 30 mL medium and centrifuged for 2 minutes at 1,500 RPM. Islets were then resuspended in fresh RPMI medium, transferred into 90 mm bacterial petri dishes, and incubated overnight at 37 °C, 5 % CO_2. The following day, islets were hand-picked under a stereomicroscope (Leica S6D) and transferred into a new Petri dish. Islets were allowed to recover for 16 hours before further experiment.

2.2.1.5.   Static glucose-stimulated insulin secretion (GSIS) on isolated islets

15 isolated islets were collected using a P10 pipette and transferred into a 1,5 mL Eppendorf tube. Islets were first pre-incubated for 1 hour at 37 °C in Krebs-Ringer Bicarbonate Hepes (KRBH) buffer containing 128.8 mM NaCl, 4.8 mM KCl, 1.2 mM KH_2PO_4, 1.2 mM $MgSO_4$, 2.5 mM $CaCl_2$, 5 mM $NaHCO_3$, 10 mM HEPES, 0.1 % BSA (pH 7.4) supplemented with 2,5 mM glucose. After another hour of pre-incubation period, islets were incubated in KRBH buffer

with 2,5 mM glucose (low glucose condition) or 25 mM glucose (high glucose condition) for 60 minutes at 37 °C, 5 % CO_2, with or without 10 nM exendin-4 (Tocris, #1933). Lids were kept open throughout the incubations. After each incubation, tubes were briefly centrifuged at 1,000 RPM for 1 min to pellet the islets and collect the supernatants. At the end of the experiments, islets were lysed in acid ethanol (1.5 % *v/v* HCl in 95 % *v/v* ethanol) to determine the total insulin content. Secreted insulin and total insulin were stored at -70 °C until insulin measurements with a mouse ELISA insulin kit (Mercodia, Uppsala, Sweden). Each condition was analysed in triplicate.

2.2.2.   Stromal vascular fraction (SVF) isolation

2.2.2.1.   Adipose tissue digestion

Immediately after death, inguinal white adipose tissue (iWAT) was removed from the mice and placed in phosphate-buffered saline (PBS, Sigma, #P4417). All subsequent steps were performed under a tissue culture hood. Resected tissue was quickly dried out on tissue paper and transferred to a Petri dish. The tissue was enzymatically digested with collagenase D (#11088858001, Roche Diagnostics GmbH, Mannheim, Germany) and minced into small pieces using scissors and forceps. The resulting mixture was transferred to a 50 mL Falcon tube and incubated for 1 hour at 37 °C with constant agitation.

2.2.2.2.   SVF isolation

Enzymatic activity of collagenase was neutralised by the addition of growth medium consisting of DMEM High glucose supplemented with + 1 % *v/v* P/S, 1 % *v/v* sodium pyruvate (Sigma-Aldrich, #S8636), 2 % *v/v* glutamine (Sigma-Aldrich, #G7513) and 10 % *v/v* FBS. The suspension was centrifuged at 700 x g for 10 minutes. Upper phase corresponding to the adipocyte layer and supernatant were discarded. The brown pellet, containing the SVF cells, was resuspended in a suitable volume of medium before being filtered through a 70 μm cell strainer (Sigma-Aldrich, #Z742103). Cells were finally pelleted by centrifugation, resuspended in fresh medium, and plated onto 10 cm diameter tissue culture dishes. SVF cells were cultured at 37 °C, 5 % CO_2 in a humidified incubator for up to 3 passages.

2.2.2.3. Differentiation into adipocytic lineage

Confluent SVF cells were incubated in adipogenic medium consisting of growth medium supplemented with 1 μM dexamethasone (Sigma-Aldrich, #D4902), 0.5 mM 3-isobutyl-1-methylxanthine (IBMX, Sigma-Aldrich, #I5879) and 1 μM insulin (Sigma-Aldrich, #I9278). After 2 days, cells were maintained in growth medium with insulin only. Medium was changed every 2 to 3 days until cells were fully differentiated. In some cases, rosiglitazone was also added to the adipogenic medium at a concentration of 2 μM (Cayman Chemical, #71740).

2.2.3. Bone marrow-derived macrophages (BMDMs) isolation and growth

2.2.3.1. Preparation of L929 conditioned media

L929, a murine fibroblast cell line, was used in the culture of BMDM as a source of macrophage colony stimulating factor (M-CSF). L929 (Strain L, Clone 929) cells were kindly provided by Professor Mirela Delibegovic. L929 conditioned media was generated by culturing L929 cells in T175 cm^2 flasks for 7 days without disturbance. After that period, medium was collected, filtered through a 0,45 μm filter and stored at -20 °C for downstream applications in macrophages culture.

2.2.3.2. Mice dissection

After cervical dislocation, Achilles's tendons were cut, and skin and muscles removed from hind legs to expose the femur and the tibia. Legs were dislocated at the hip joint; leaving knee and ankle joints intact; and bones placed in ice-cold DMEM High glucose supplemented with 1 % *v/v* P/S. Cleaned bones were transported on ice to primary tissue culture hood.

2.2.3.3. Bone marrow cell isolation

Legs were briefly sprayed with 70 % ethanol and remaining soft tissues were removed from the bones, where possible, using forceps and scissors. To disconnect the femur from the tibia, bones were gently twisted at the knee joint. Using scissors, both ends of each bone were cut, allowing the insertion of a syringe with 21G needle, filled with PBS and 1 % *v/v* P/S. Bone marrow was flushed out on top a cell strainer into a 50 mL Falcon tube. Flushing was repeated as many

times as needed until the release of bone marrow plugs. After gently disrupting the plugs, bone marrow suspension was centrifuged at RT for 5 minutes at 1,200 RPM. To remove erythrocytes from the preparation, pellet was resuspended in 2 mL of Red Blood Lysing Buffer (Sigma-Aldrich, Roche-11814389001) and incubated for 10 minutes at RT. Lysis was stopped with the addition of 10 mL of PBS and centrifugation at 1,200 RPM for 5 minutes.

2.2.3.4. Macrophages maturation

Cells were resuspended in 5 mL BMDM growth medium consisting of DMEM High Glucose L-Glutamine medium, 10 % *v/v* FBS, 20 % *v/v* L929 conditioned media (see section 2.2.3.1), 100 u/mL penicillin, 100 mg/mL streptomycin, 1x Non Essential Amino Acid (NEAA, Sigma-Aldrich, #M7145), 1 mM sodium pyruvate and 0.25 mM β-mercaptoethanol (Sigma, #M3148). Using a haemocytometer chamber (Neubauer), cells were counted and plated at a density of 5 x 10^6 cells per 10 cm Petri dish in 10 mL growth medium. Cells were cultured at 37 °C, 5 % CO_2. On day 1 after isolation, 10 mL of growth medium were added to the dish bringing the total volume of media to 20 mL. On day 4, medium was replenished by removing half of the medium and replacing it with fresh complete medium. After 7 days of differentiation, mature macrophages were assessed for functionality.

2.2.3.5. BMDMs stimulation

After 7 days in culture, BMDMs were detached with trypsin, seeded in six-well plates, and stimulated for 4 hours with growth medium containing 100 ng/mL LPS to activate M1 polarisation. PBS was used as vehicle control.

2.2.3.6. BMDMs bacterial infection

2.2.3.6.1. Bacterial preparation

Staphylococcus aureus SH1000 mCherry was kindly provided by Professor Simon Foster, Krebs Institute, University of Sheffield, UK. *S. aureus* was cultured overnight at 37 °C in Luria-Bertani (LB) broth (Melford, #L24041) in a bacterial incubator shaker. The next morning,

overnight culture was diluted and incubated at 37 °C for approximately 2 hours until the optical density at 600 nm (OD600) had reached 0,6. OD600 of 1 corresponds to 1.5×10^9 CFU/mL.

2.2.3.6.2. Phagocytosis and gentamicin-protection assay

One day before the assay, BMDMs were seeded at a density of 50 000 cells/well in 24-well plates on glass coverslips (VWR, #631-0149). The next morning, bacteria was added to the well in Hank's Balanced Salt Solution (HBSS, Gibco, #14025-092) at a multiplicity of infection (MOI) of 5 for 1 hour at 37 °C, 5 % CO_2 in a humidified incubator. One-hour post-infection (p.i.), cells were washed with PBS and incubated for 30 minutes with BMDM growth medium supplemented with 100 µg/mL gentamicin (ThermoFisher Scientific UK, #BP918) to remove any extracellular bacteria. Gentamicin has a high bactericidal effect on *S. aureus* but a poor penetration inside mammalian cells. Infected BMDMs were then washed with PBS and maintained in growth medium supplemented with 5 µg/mL gentamicin. At indicated times, cells were washed in PBS and either fixed in 10 % formalin for immunofluorescence (see section *2.8.1*) or lysed in 0.1 % Triton X-100 (Sigma-Aldrich, #T8787) for serial dilutions and plating onto Brain Heart Infusion (BHI) agar plates. After an overnight incubation at 37 °C, colonies were counted to determine the colony-forming unit (CFU) *i.e* the number of viable intracellular *S. aureus* within BMDMs.

2.2.3.7. BMDMs lipid treatment

Palmitic acid (PA) was prepared as a 500 mM solution in 100 % ethanol (Sigma, #P0500). The preparation was heated to 70°C until obtention of a clear solution.

10 % BSA-DMEM solution was prepared by dissolving BSA powder (Melford, #A30075-100) in DMEM high glucose supplemented with 10 % FBS, 1 % NEAA and 1 % sodium pyruvate. The mixture was heated to 37 °C until full dissolution.

500 mM of palmitic acid solution was added to the 10 % BSA-DMEM preparation to make a 5 mM palmitic acid solution. PA-BSA was incubated at 37 °C for one hour. The molar ratio of PA to BSA is 3,3:1. The vehicle control was prepared by adding 100 % ethanol to 10 % BSA-DMEM. PA-BSA and the vehicle control were stored at -20 °C and thawed in a 37 °C water bath before each experiment.

49

The day before the experiment, BMDMs were seeded at a density of 50 000 cells/well in 24-well plates. The next day, media was replaced and changed with growth medium containing 200 μM palmitic acid solution conjugated to BSA or the vehicle control. Cells were collected 18 hours later for RNA extraction (see section 2.6.1).

2.3. DNA constructs

2.3.1. Transformation of bacteria

Following manufacturer's protocol, NEB 10-beta competent *Escherichia coli* cells (New England Biolabs, #C3019I) were transformed with exogenous plasmid DNA constructs listed in **Table 2.1**. Briefly, 25 μL of competent cells were thawed on ice. Between 1 pg and 100 ng of plasmid DNA were added to the mixture and incubated on ice for approximately 30 minutes. The mixture was subsequently immersed in a 42 °C water bath for exactly 30 seconds to allow entry of the exogenous DNA into the bacteria and followed by a 5 minute-incubation on ice. 300 μL of room temperature NEB 10-beta Stable Outgrowth medium (New England BioLabs, #B9035S) were added to the mixture and placed at 37 °C with gentle rotation to allow recovery of the cells and expression of antibiotic resistance. A fraction of the mixture was plated onto pre-warmed Luria-Bertani (LB) agar plates containing 100 μg/mL ampicillin and incubated overnight at 37 °C. Single colonies were ready to be picked the following day and grown into 5 mL of LB medium with ampicillin. After an overnight incubation at 37 °C, one mL of the culture was grown into 100 mL LB medium overnight to perform maxiprep the next day (see following section *2.3.2*).

Table 2.1: DNA constructs used in this thesis.

Target	Construct	Backbone
Empty vector	pcDNA3.1 myc/His	pcDNA3.1
	pCMV3xFlag	pCMV
Seipin	hBSCL2-long myc/His	pcDNA3.1
	Ito-hBSCL2-WT	pcDNA3.1/V5His or pCS2-Myc
	Ito- hBSCL2-ΔNT	pcDNA3.1/V5His or pCS2-Myc
	Ito- hBSCL2-ΔCT	pcDNA3.1/V5His or pCS2-Myc
	Ito- hBSCL2-ΔTm1	pcDNA3.1/V5His or pCS2-Myc
	Ito- hBSCL2-ΔTm2	pcDNA3.1/V5His or pCS2-Myc
	Ito- hBSCL2-Δloop	pcDNA3.1/V5His or pCS2-Myc
GLP1R	hGLP1R-Flag/Halo	pSP

HALO-GLP1R construct was a generous gift from Professor David J. Hodson, Institute of Biomedical Research, University of Birmingham, UK. Ito plasmids were kindly provided by Associate Professor Daisuke Ito (Keio University, Japan).

2.3.2.   Maxiprep

DNA extraction and purification of plasmid DNA from *Escherichia coli* bacteria were performed using a QIAGEN Plasmid Maxi Kit (Qiagen, #12163). Steps included harvesting, lysis of bacteria then purification of plasmid DNA. Overnight bacterial cultures were first pelleted at 6,000 x g for 15 minutes at +4 °C. Bacterial pellet was completely resuspended in chilled resuspension buffer P1 containing RNase I solution and LyseBlue reagent. Bacteria was then lysed with the addition of lysis buffer P2 and a short incubation at room temperature. The solution turning blue was an indicator of an efficient lysis. Lysis was then stopped with the addition of pre-chilled neutralisation buffer P3. The mixture was centrifuged at high speed (≥

20,000 x g) for 30 minutes at +4 °C and the resulting supernatant centrifuged for another 15 minutes. Clear supernatant was applied onto a QIAGEN-tip 500 previously equilibrated with equilibration buffer QBT and allowed to enter the resin by gravity flow. QIAGEN-tip was washed twice with washing buffer QC then DNA eluted with elution buffer QF into a clean vessel. Room-temperature isopropanol was added to the eluate to precipitate the DNA. After a centrifugation at $\geq$ 15,000 x g for 30 minutes at +4 °C, supernatant was discarded, and DNA pellet washed carefully with room-temperature 70 % ethanol. After another centrifugation at $\geq$ 15,000 x g for 10 minutes at +4 °C, supernatant was discarded, and DNA pellet air-dried. Finally, DNA pellet was resuspended in a suitable volume of Tris-EDTA buffer, quantified on a Nanodrop (Thermo Fisher Scientific, #ND-1000 Spectrophotometer) then stored at -20 °C for future transfections.

2.4. Cell culture

2.4.1. General considerations

All cells were maintained at 37 °C, 5 % CO_2 in a humidified incubator. Cell lines were routinely maintained in tissues culture treated T75 polystyrene flasks while primary cultures were grown in 90 mm diameter petri dishes. When ready to be split, cells were washed with PBS to remove any trace of medium that might inhibit enzymatic activity of the trypsin in the following step. Cells were detached with Trypsin-EDTA solution (Sigma-Aldrich, #T3924) at 37 °C for 5 minutes. Trypsin was then neutralised with growth medium containing serum and cells centrifuged at RT for 3 min at 300 x g. Cell pellets were resuspended in a suitable volume of growth medium, counted if necessary, using a haemocytometer, and plated accordingly in a new tissue culture vessel. When needed for cryopreservation, cell pellets were resuspended in regular growth medium supplemented with 10 % *v/v* dimethyl sulfoxide (DMSO, Sigma, #D8418), placed for one night in an isopropanol-filled container at -70 °C then finally transferred into liquid nitrogen for long-term conservation.

## 2.4.2.	Growth and maintenance

### 2.4.2.1.	A mouse preadipocyte cell line: 3T3-L1

3T3-L1 cells were purchased from ZenBio (USA) and used at passage between 15 and 40. Cells were grown in DMEM High Glucose supplemented with 10 % *v/v* Newborn Calf Serum (NCS, Sigma-Aldrich, #N4762), 2 % *v/v* L-Glutamine, 1 % *v/v* sodium pyruvate, 1 % *v/v* NEAA and 1 % *v/v* P/S. For maintenance purposes, cells were never grown to confluency in order to preserve differentiation capacity of the cells.

Differentiation was initiated 48 hours after 3T3-L1 cells became confluent by incubation with 3T3-L1 differentiation media (DMEM High Glucose, 10 % *v/v* FBS, 2 % *v/v* L-Glutamine, 1 % *v/v* sodium pyruvate, 1 % *v/v* NEAA and 1 % *v/v* P/S) supplemented with 1 µM insulin, 1 µM dexamethasone and 0.5 mM IBMX during the first two days of differentiation (DAY 0 – DAY 2). From day 2 to day 4, cells were cultured in 3T3-L1 differentiation media supplemented with 1 µM insulin only. From day 4 onwards, cells were grown in 3T3-L1 media without any supplement and medium was changed regularly. Cells were usually considered fully differentiated by day 12. In some cases, 1 µM rosiglitazone were added to the differentiation media the first 2 days to help the differentiation process.

### 2.4.2.2.	A human preadipocyte cell line: Simpson Golabi Behmel Syndrome (SGBS) cells

SGBS cells were kindly provided by Professor Martin Wabitsch (Department of Pediatric Endocrinology and Diabetology, University of Ulm, Germany) and cultured following previously described methods (341). Cells were grown and maintained in DMEM/F12 medium (Gibco, #31330-038) supplemented with 10 % *v/v* FBS and 1 % *v/v* P/S. For maintenance purposes, cells were never grown to confluency in order to preserve differentiation capacity of the cells.

Differentiation was initiated on confluent SGBS cells by incubation with SGBS differentiation media (DMEM/F12 + 1 % *v/v* P/S) supplemented with 25 nM dexamethasone, 0.5 mM IBMX, 0.1 µM cortisol (Sigma-Aldrich, #H-0888), 0.01 mg/mL transferrin (Sigma-Aldrich, #T-2252), 0.2 nM 3,2',5-Triiodo-L-thyronine (T3, Sigma-Aldrich, #T-6397) and 20 nM insulin during the first 4 days of differentiation (DAY 0 – DAY 4). From day 4 onwards, cells were cultured in

SGBS differentiation media supplemented with 0,1 μM cortisol, 0,01 mg/mL transferrin, 0,2 nM T3 and 20 nM insulin. Medium was changed every 4 days and cells usually considered fully differentiated by day 12. In some cases, 2 μM rosiglitazone were added to the differentiation media the first 4 days to help the differentiation process.

2.4.2.3.   HEK 293

Commercially available HEK 293 cells were cultured in DMEM high glucose supplemented with 10 % *v/v* heat-inactivated FBS, 2 % *v/v* L-Glutamine, 1 % *v/v* sodium pyruvate and 1 % *v/v* P/S.

2.4.2.4.   INS-1 pancreatic β cells

Rat INS-1 cells were a generous gift from Professor Kevin Docherty. INS-1 cells were grown in RPMI L-glutamine medium supplemented with 10 % *v/v* FBS, 1 % *v/v* P/S, 1 % *v/v* sodium pyruvate and 50 μM β-mercaptoethanol.

2.4.2.5.   Min6 pancreatic β cells

Mouse Min6 cells were a generous gift from Professor Kevin Docherty. Min6 cells were cultured in DMEM high glucose medium supplemented with 10 % *v/v* FBS, 2 % *v/v* L-glutamine, 1 % *v/v* sodium pyruvate, 1 % *v/v* P/S and 50 μM β-mercaptoethanol.

2.5. Assays

2.5.1.   Lipolysis assay

Lipolysis assays were performed on fully differentiated SGBS and SVF cells seeded on 24-well plates. On the day of the assay, cells were washed with PBS then incubated with Opti-MEM (Gibco, #10149832) for 2 hours. After this incubation, cells were washed twice with KRBH consisting of 118.5 mM NaCl, 4.75 mM KCl, 1.92 mM $CaCl_2$, 1.19 mM KH_2PO_4, 1.19 mM $MgSO_4$. $(H_2O)_7$, 25 mM $NaHCO_3$, 10 mM HEPES, and 6 mM Glucose (Sigma, #G8270), pH 7.4. Basal lipolysis was measured by incubating cells with KRBH buffer supplemented with 4 % *w/v* BSA and 6 μM Triacsin C (Enzo Life Sciences, #BML-EI218-0100). Stimulated

lipolysis was initiated with KRBH buffer supplemented with 4 % *w/v* BSA, 6 μM Triacsin C and 1 μM isoproterenol (Sigma, #I6379). DMSO was used as a vehicle for unstimulated wells. A sample of the media was collected at specified time points to measure the glycerol released into the incubation media using the Triglyceride Liquid Kit (Sentinel Diagnostics, #17628). At the end of the experiment, cells were lysed as in section 2.7.1 and protein quantified to normalise glycerol levels to protein content.

2.5.2. Static glucose-stimulated insulin secretion (GSIS)

GSIS assay was performed on Min6, and INS-1 cells plated onto 12-well plates. On the day of the experiment, cells were washed with PBS and incubated for 2 hours with KRBH consisting of: 128.8 mM NaCl, 4.8 mM KCl, 1.2 mM KH_2PO_4, 1.2 mM $MgSO_4$, 2.5 mM $CaCl_2$, 5 mM $NaHCO_3$, 10 mM HEPES and 0.1 % BSA (pH 7.4). Cells were then incubated with KRBH buffer supplemented with 2.5 mM glucose with or without 10 nM exendin-4 at 37 °C, 5 % CO_2 (low glucose condition). After 1 hour, medium was collected and stored at -70 °C until insulin assay. Cells were then incubated with 25 mM glucose with or without 10 nM exendin-4 (high glucose condition). After another hour, medium was collected, and cells lysed as in section 2.7.1 to normalise insulin release to total insulin content. Insulin levels were determined using commercially available mouse or rat ELISA insulin kit (Mercodia, Uppsala, Sweden).

2.5.3. Transient transfections for overexpression

2.5.3.1. Calcium-phosphate method

HEK 293 cells were seeded in tissue culture plates or 10 cm dishes at a confluency of 70 %. Cells were left overnight to adhere and were transfected the next morning. Two hours before transfection, medium was replaced with fresh media. Transfections mixes were prepared as showed in **Table 2**. Briefly, plasmid DNA was mixed with 1X HEPES-buffered saline (HBS; 21 mM HEPES, 137 mM NaCl, 5 mM KCl, 0.7 mM Na_2HPO_4, 5.5 mM dextrose, pH 7.1) in a tube then 2.5 M calcium chloride ($CaCl_2$) was added to the mixture and tubes inverted a few times. After a 20 minutes incubation at room temperature, mixtures were added to the cells, in a dropwise manner. After gently rocking the plates back and forth, cells were put back in a humidified incubator at 37 °C, 5 % CO_2. The next morning, cell culture media was replaced with fresh medium and cells typically harvested 48 hours after transfection.

Table 2.2: Calcium phosphate mediated transfection.

Culture plates or dishes	Transfection medium (mL)	DNA/well (μg)	1X HBS/well (μL)	2,5 M CaCl₂/well (μL)
100 mm	8	15	500	30
6-well	2	2	86	5,1
12-well	1	1	36	2,1

2.5.3.2. Lipofectamine LTX & PLUS Reagent method

3T3-L1, Ins1 and Min6 cells were transfected using the Lipofectamine LTX & PLUS Reagent following the manufacturer's protocol (Invitrogen, #15338). Briefly, Lipofectamine LTX Reagent provided was diluted in Opti-MEM medium. DNA purified in section 2.3.2 was diluted in Opti-MEM with PLUS reagent. Diluted DNA was then mixed with diluted Lipofectamine LTX Reagent and incubated at room temperature for 5 minutes. DNA-lipid complexes were finally added to the adherent cells in a dropwise manner and incubated at 37 °C. Unless otherwise stated, cells were harvested or analysed 48 hours post-transfection. Details of the transfection procedure according to cell culture plates format are given in the **Table 2.3** below.

Table 2.3: Lipofectamine LTX reagent mediated transfection.

Culture plates	Transfection medium (μL)	DNA per well (ng)	PLUS Reagent per well (μL)	Lipofectamine LTX Reagent per well (μL)	DNA-lipid complex (μL)
6-well	2000	2000	2,5	9	250
12-well	1000	1000	1	4	100
24-well	500	500	0,5	2	50

2.5.4.   Transient transfections for knockdown

Short interfering RNA (siRNA)-mediated knockdown were performed using Lipofectamine RNAiMAX Transfection Reagent (ThermoFisher SCIENTIFIC, #13778075) and Silencer Select siRNA (ThermoFisher Scientific) to transiently knockdown gene expression in cell cultures. Briefly, cells were seeded in tissue culture plates so that they will be around 60-80 % confluency at the time of transfection. Firstly, Lipofectamine RNAiMAX Reagent was diluted in Opti-MEM medium. In parallel, siRNA was also diluted in Opti-MEM medium. Diluted siRNA was added to the diluted Lipofectamine RNAiMAX Reagent and incubated at room temperature for 5 minutes. siRNA-lipid complexes were finally added to the tissue culture plates, in a dropwise manner, and incubated at 37 °C. At mRNA level, optimal knockdown was achieved 48 hours after the transfection. Transfection reagents amounts and siRNAs used in this thesis are listed in the **Table 2.4** and **Table 2.5**, respectively.

Table 2.4: RNAiMAX-mediated siRNA transfection.

Culture plates	Transfection medium (µL)	[siRNA]/well (nM)	Lipofectamine RNAiMAX Reagent/well (µL)	siRNA-lipid complex (µL)
6-well	1000	10	2	200
12-well	500	10	1	100
24-well	500	10	1	100

Table 2.5 : List of siRNAs used in this thesis.

Target	Species	Assay ID
Negative control	-	Cat. N° 4390846
Bscl2	Mouse	s66846
		s66847
		s66848
Bscl2	Human	s25557
Agpat2	Human	s223130

2.6. Molecular biology

2.6.1.   RNA extraction

Total RNA was extracted and purified from cell cultures and mouse tissues using the RNeasy Mini Kit (Qiagen, #74106) following manufacturer's instructions. Briefly, cells were first lysed in 350 µL RLT buffer and an equal amount of 70 % ethanol was added to the sample to promote selective binding of the RNA onto the column. When extracting RNA from mouse tissues, 700 µL of RLT buffer was used for the lysis and the volume of 70 % ethanol in the following step was scaled up accordingly. Tissue was disrupted and homogenised by rapid agitation with 1 mm diameter zirconia beads (BioSpec Products, #11079110zx) using the Precellys-Bertin homogeniser (Bertin Technologies, USA).

The mixture was then applied onto a RNeasy Mini spin column placed on a collection tube and centrifuged for 1 minute. RNA bound to the membrane and the flowthrough was discarded. After two washes with washing buffer RW1 and another two washes with buffer RPE, 1 minute each, the membrane was dried out and RNA eluted in a suitable volume of Tris-EDTA buffer (Fisher Scientific, #BP2473-100). All centrifugation steps were performed at 17,000 x g at room temperature. RNA quantity and quality was finally assessed on a Nanodrop.

2.6.2.   Reverse transcription

Any residual genomic DNA present in the RNA sample prepared in section 2.6.1. was removed using the Amplification Grade DNase I kit (Sigma-Aldrich, #AMPD1) following manufacturer's instructions. Briefly, DNAse I treatment was performed at 37 °C for 10 minutes then heat-inactivated at 70 °C for 10 minutes after addition of the Stop solution (final volume = 11 µL).

Following DNase I treatment, 14 µL of the mixes in **Table 2.6** were added to the 11 µL of RNA preparations to perform the reverse transcription using M-MLV reverse transcriptase at 37 °C for 1 hour in a thermal cycler (Biorad). All reagents were purchased from Promega. A "No Reverse Transcriptase" (NRT) control, containing all the reagents listed above but the reverse transcriptase, was also included in the analysis to detect any residual DNA from the RNA preparations. After the complementary DNA (cDNA) synthesis, 5 µL of each sample were pooled to create a standard. 10-fold serial dilutions were used to generate a standard curve that

will be used to estimate primers efficiency during the quantitative polymerase chain reaction (PCR). cDNA was generally diluted 1:5 with DEPC-treated water (Invitrogen, #46-2224) before continuing with qPCR analysis. If not used immediately, cDNA was stored at -70 °C.

Table 2.6 : cDNA synthesis.

Reagent	Promega reference	Volume/reaction (µL)
M-MLV 5X Reaction Buffer	#M531A	5
10 mM dNTPs	#U151B	0,75
100 µg/mL Random Primers	#C118A	1
M-MLV Reverse Transcriptase	#M170B	0,5
H2O	-	6,75
DNAse-treated RNA sample	-	11
Total	-	**25 µL**

2.6.3. Quantitative real-time PCR (qRT-PCR)

qRT-PCR was performed using commercially available master mixes, Power SYBR Green PCR Master Mix (Thermo Fisher Scientific, #4367659) and TaqMan Universal PCR Master Mix (Thermo Fisher Scientific, #4304437). PCR master mixes already contain buffer, DNA polymerase and dNTPs. qRT-PCR mixes were prepared by adding primers or probe and water to the master mixes just as stated in **Table 2.7** and **Table 2.8** and dispensing 5 µL of those, using an automated pipette, into a 384-well hard-shell PCR plate (BIO-RAD, #HSP3805).

Table 2.7 : SYBR Green method.

Reagent	Volume/reaction (µL)
Power SYBR Green PCR Master Mix	3,5
10 µM Primers (Forward+Reverse)	0,15
H_2O	1,35
Total	**5 µL**

Table 2.8 : TaqMan method.

Reagent	Volume/reaction (µL)
TaqMan Universal PCR Master Mix	3,5
TaqMan probe	0,08
H2O	1,42
Total	**5 µL**

2 µL of diluted cDNA samples, standards or controls were then added to the wells and run in duplicate. Controls included NRT control mentioned before and a "No Template Control" (NTC) where water replaces cDNA sample. Plates were sealed with optical adhesive covers (Life Technologies, #4360954) and centrifuged for 1 minute at 1,000 x g.

qRT-PCR was carried out on CFX384 Real-time Thermal Cycler (BIO-RAD, #C1000[TM] Touch Thermal Cycler) using the following settings (**Figure 2..3**).
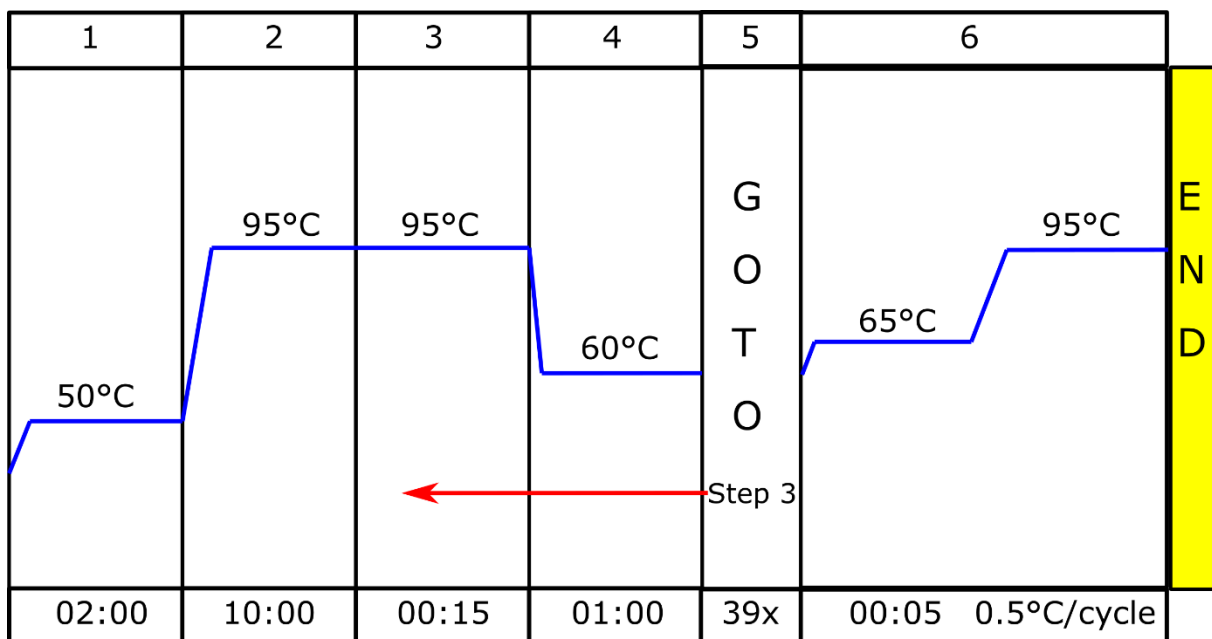
*Figure 2.3: **Quantitative real time polymerase chain reaction settings**. Lid temperature was maintained at 105 °C throughout the cycles.*

2.6.4.   qRT-PCR analysis

2.6.4.1.   Overview

SYBR Green is a DNA-binding dye that incorporates into double-stranded DNA (dsDNA) at each cycle, in a non-specific manner. When bound to dsDNA, SYBR Green emits fluorescence that can be detected by the thermocycler. Similarly, TaqMan probes are labelled with a fluorophore FAM (carboxyfluorescein) at the 5' end and a quencher at the 3' end. In this state, fluorescence is quenched by the proximity between the reporter and the quencher. During the PCR, the probe binds to the target sequence and the 5'-exonuclease activity of Taq polymerase cut off the reporter resulting in the emission of fluorescence. In both SYBR Green and TaqMan-based assays, the fluorescence emitted during the amplification reaction is directly proportional to the amount of amplified product and will be used for quantitative analysis.

CFX Maestro software generated amplification plots just like the one in **Figure 4**. X-axis corresponds to the PCR cycle number while the fluorescence is shown on the y-axis. Fluorescence is initially undetected during the first cycles but eventually, enough PCR products accumulate to yield a detectable fluorescent signal. The threshold cycle, denoted as CT, corresponds to the PCR cycle number at which this detection occurs. When a large quantity of template is present at the beginning of the reaction, few amplifications cycles will be needed to bring the fluorescence signal above the detectable threshold and the CT value will be low. Inversely, if the reaction starts with a small amount of template, more copies *i.e.* more cycles will be required to detect fluorescence signal, leading to a high CT value. As a result, Ct values are inversely correlated with the initial amount of template present in the reaction.
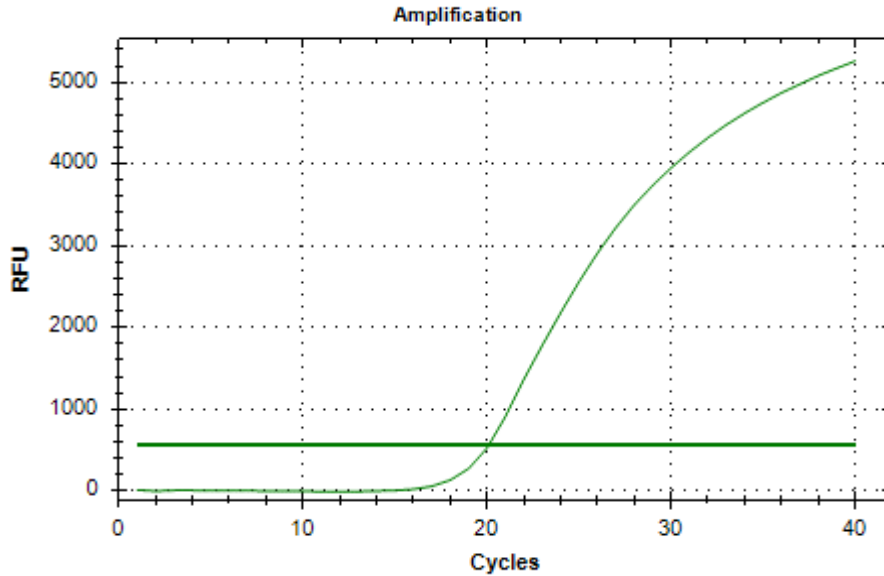
Figure 2.4: ***Amplification plot***. *Green horizontal line denotes the threshold line above which the fluorescence signal is detectable.*

2.6.4.2.　　Contamination products

NRT and NTC were used as internal controls and should not show any amplification product. In certain cases where thermocycler could detect fluorescence in NRT and NTC samples, PCR was repeated.

2.6.4.3.　　Primer efficiency

By plotting the log of the starting quantity against the Ct values calculated during the amplification of the 10-fold dilutions template, a standard curve can be generated (**Figure 5**). From the linear regression equation, Pearson's correlation coefficient (r) and slope can be estimated. A r value > 0,99 is an indicator of a good standard curve. Primer efficiency (E) is calculated from the slope using the following equation: $E = 10^{-1/slope}$.

Assuming that the quantity of PCR product doubles at each cycle, a reaction efficiency of 2 should be expected bringing the slope value to -3,32.
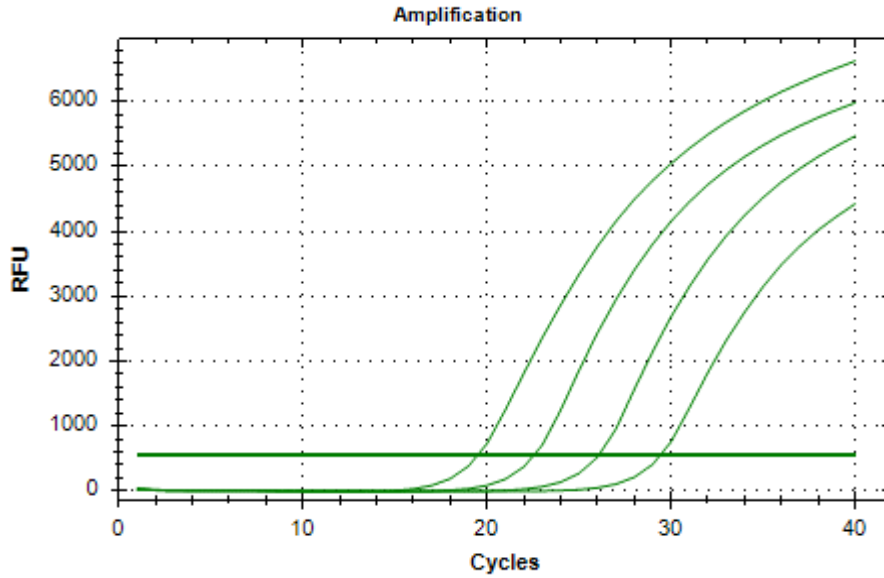
Figure 2.5: Standard curve amplification plots. A standard curve was generated using a 10-fold dilution of a sample on a CFX384 Real-time Thermal Cycler.

2.6.4.4.   Melt-curve analysis

When using SYBR Green-based PCR, a melt curve analysis was performed to assess the specificity of the reaction. The melt curve was generated at the end of the PCR by slowly increasing the temperature while monitoring the decrease in fluorescent signal at each step. A single peak at the amplicon's melting temperature, reflecting the amplification of a single product, should be observed (**Figure 2.66**). On the contrary, several peaks would denote the presence of multiple products or primer-dimers.
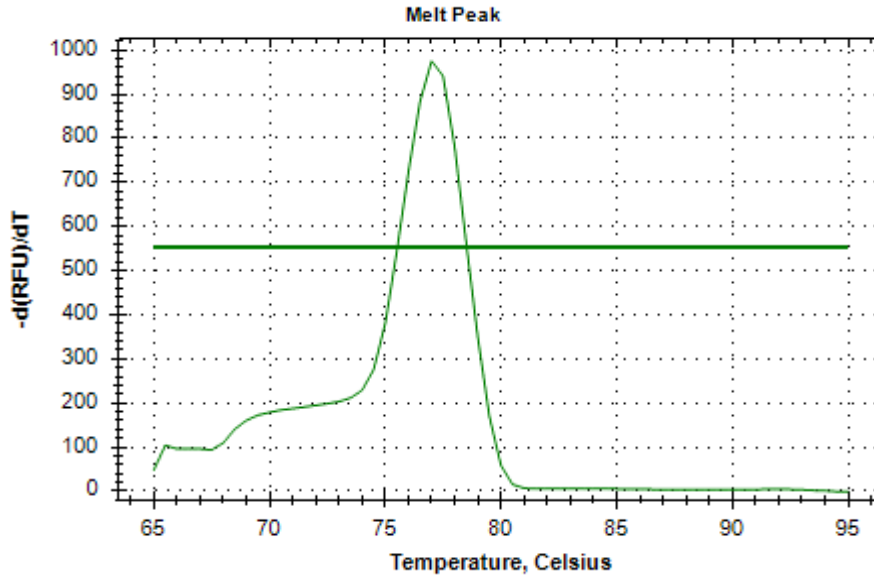
Figure 2.6*: **Melt curve analysis**. A melt curve was generated from amplification products of SYBR Green-based assays by plotting the negative first derivative of the change in fluorescence against the temperature.*

2.6.4.5.   Relative quantification

Relative expression of target gene in WT vs SKO cells or untreated vs untreated samples was determined by calculating the expression level *i.e.* CT values of both the target and reference genes. Geometric mean of *Nono*, *Hprt* and *Ywhaz* and in some rare cases, 18s only were used as reference genes for normalisation using the PfaffI method (342) :

$$Normalised\ expression\ ratio = \frac{\left(E_{target}\right)^{\Delta C_T, target(untreated-treated)}}{\left(E_{ref}\right)^{\Delta C_T, ref(untreated-treated)}}$$

Where: $\qquad \Delta C_T, target(untreated - treated) = C_T(target, untreated) - C_T(target, treated)$

And: $\Delta C_T, ref(untreated - treated) = C_T(ref, untreated) - C_T(ref, treated)$

2.6.5. List of primers

TaqMan probes were purchased from ThermoFisher and are listed in **Table 2.9**.

Table 2.9: List of TaqMan probes used in this thesis.

Gene	Species	Assay ID
18S	Mouse	Mm03928990_g1
Bscl2	Mouse	Mm01230976_m1
BSCL2	Human	Hs00369057_m1
PPARγ	Human/mouse	Mm01184322_m1

Primers for SYBR Green-based assays were designed with Primer Bank (Massachusetts General Hospital, Harvard Medical School, The Center for Computational and Integrative Biology). Self-complementarity and secondary structures were checked with Oligo Calculator (Northwestern University). 0,025 µmole of primers were then purchased from Sigma-Aldrich, desalted and in lyophilised form. **Table 2.10** provides all the sequences for the genes of interest used in this thesis.

Table 2.10: List of primers used in SYBR Green-based assays.

Gene	Forward primer (5'- 3')	Reverse primer (3'- 5')
hADIPONECTIN	TGCTGGGAGCTGTTCTACTG	TACTCCGGTTTCACCGATG
hAGPAT2	GCCGAGTTCTACGCCAAGG	CGAACCAGCCGATGATGCT
mAgpat2	CAGCCAGGTTCTACGCCAAG	TGATGCTCATGTTATCCACGGT
AldoA	AGAACACCGAGGAGAACAG	TTAATGCCCACAACACCAC
haP2/FABP4	ACTGGGCCAGGAATTTGACG	CTCGTGGAAGTGACGCCTT
maP2/Fabp4	CAAACTGGGCGTGGAATTCG	ACCAGCTTGTCACCATCTCG
Atgl	CAACGCCACTCACATCTACG	ATGCACAGGACCCAGGAAC
hC/EBPβ	CTTCAGCCCGTACCTGGAG	GGAGAGGAAGTCGTGGTGC
hC/EBPγ	ACTCCAGGGGTGAACGGAA	CATGGGCGAACTCTTTTTGCT
mC/ebpα	CAAGAACAGCAACGAGTAC	GTCACTGGTCAACTCCAGCAC
Glp-1R	ACGGTGTCCCTCTCAGAGAC	ATCAAAGGTCCGGTTGCAGAA
Glucokinase	TGAGCCGGATGCAGAAGGA	GCAACATCTTTACACTGGCCT
Glut2	TTCCAGTTCGGCTATGACATCG	CTGGTGTGACTGTAAGTGGGG
hGLUT4	TGGGCGGCATGATTTCCTC	GCCAGGACATTGTTGACCAG
mGlut4	ACTCATTCTTGGACGGTTCCT	CACCCCGAAGATGAGTGGG
Gpi	TCAAGCTGCGCGAACTTTTTG	GGTTCTTGGAGTAGTCCACCAG
Grp78	AGAAACTCCGGCGTGAGGTAGA	TTTCTGGACAGGCTTCATGGTAG
Hif1α	ACCTTCATCGGAAACTCCAAAG	CTGTTAGGCTGGGAAAAGTTAGG
Hprt	GTTAAGCAGTACAGCCCCAAA	AGGGCATATCCAACAACAAACTT
Hsl	ACGCTACACAAAGGCTGCTT	TCGTTGCGTTTGTAGTGCTC
Il-1α	GCACCTTACACCTACCAGAGT	AAACTTCTGCCTGACGAGCTT
Il-1ꞵ	GCAACTGTTCCTGAACTCAACT	ATCTTTTGGGGTCCGTCAACT
Il-6	TAGTCCTTCCTACCCCAATTTCC	TTGGTCCTTAGCCACTCCTTC
Il-10	GCTCTTACTGACTGGCATGAG	CGCAGCTCTAGGAGCATGTG
iNos	GGAGTGACGGCAAACATGACT	TAGCCAGCGTACCGGATGA
Insulin	GCTTCTTCTACACACCCATGTC	AGCACTGATCTACAATGCCAC
LdhA	TGTCTCCAGCAAAGACTACTGT	GACTGTACTTGACAATGTTGGGA
Mcp1	TTAAAAACCTGGATCGGAACCAA	GCATTAGCTTCAGATTTACGGGT
Nono	GCCAGAATGAAGGCTTGACTAT	TATCAGGGGGAAGATTGCCCA
hPLIN1	TGTGCAATGCCTATGAGAAGG	AGGGCGGGGATCTTTTCCT
hPLIN2	ATGGCATCCGTTGCAGTTGAT	GGAACATGAGGTCATACGTGGAG
hPLIN3	TATGCCTCCACCAAGGAGAG	ATTCGCTGGCTGATGCAATCT
hPLIN4	GGAGCTGCAACCTTCGGAAA	GGACCACTCCCTTAGCCAC
hPLIN5	AAGGCCCTGAAGTGGGTTC	GCATGTGGTCTATCAGCTCCA
mPLIN1	CACTCTCTGGCCATGTGGAT	AGAGGCTGCCAGGTTGTG
Pfkp	GGGACCATCATCGGTAGTGC	GTCCGCTCCACTCCTTTCG
Psck1	CTTTCGCCTTCTTTTGCGTTT	TCCGCCGCCCATTCATTAAC
hSREBP1c	GCATGGACGGGTACATCTT	ACAGTGACTTCCCTGGCCT
Tnfα	CCCTCACACTCAGATCATCTTCT	GCTACGACGTGGGCTACAG
Yhwaz	GAAAAGTTCTTGATCCCCAATGC	TGTGACTGGTCCACAATTCCTT

66

2.7. Protein analysis

2.7.1. Protein extraction and quantification

Cultured cells were first washed with PBS then lysed in Radio Immuno Precipitation Assay buffer (RIPA : 50 mM Tris-HCl pH 6.8 ; 150 mM NaCl ; 1 mM Ethylenediaminetetraacetic acid (EDTA, Sigma-Aldrich, #E5134) ; 0,1 % (*w/v*) Sodium Dodecyl Sulphate (SDS, Sigma-Aldrich, #L3771) ; 1 % (*v/v*) Triton X-100 (Sigma-Aldrich, #T8787) ; 0,5 % (*w/v*) sodium deoxycholate (Sigma-Aldrich, #D6750)) supplemented with cOmplete protease inhibitor cocktail (Roche**,** #11836153001), 50 mM of sodium fluoride (NaF, Sigma-Aldrich, #S7920) and 1 mM sodium orthovanadate (Na_3VO_4, Sigma-Aldrich, #S6508). When extracting proteins from cell cultures, a cell scraper was commonly used. Cell lysates were incubated on ice for 20 minutes before being centrifuged at 17,000 x g for 10 minutes at +4 °C. Supernatants were collected and kept at -70 °C if not used immediately. The protein concentration was determined with a Pierce Bicinchoninic Acid (BCA) Protein Assay Kit (Thermo Fisher Scientific, #23227) following manufacturer's instructions. Absorbance was measured at 562 nm using μQuant spectrophotometer (Bio-Tek Instruments).

2.7.2. Immunoprecipitation

Forty-eight hours after transfection for overexpression (see section 2.5.3.1), HEK 93 cells plated in 10 cm diameter dishes were briefly washed in ice-cold PBS then harvested using a cell scraper into 500 μL of immunoprecipitation (IP) lysis buffer. IP lysis buffer contained 50 mM Tris Base pH 6.8, 150 mM NaCl, 1 mM EDTA and 1 % *v/v* Triton X-100 (incomplete buffer). Phosphatase inhibitors cocktails were freshly added to the buffer before collection of the cells (Sigma-Aldrich, #P5726, #P0044 used at 1:100 and 1:250, respectively). Collected cells were kept on ice at all times. Cells were sonicated at a medium intensity using the MSE Soniprep 150 (Sanyo, UK) for two pulses of 30 seconds each with a pause of 5 seconds in between. Samples were incubated for at least 20 minutes on ice then centrifuged at 17,000 x g for 15 minutes at +4 °C. Supernatants were transferred into a fresh tube and protein quantified as described above. Between 500 μg and 1 mg of protein lysates were incubated with 30 μL anti-FLAG (Sigma, #A2220) or anti-MYC (Santa Cruz, #sc-40 AC) antibodies conjugated to agarose beads for 2 hours at +4 °C and under gentle rotation. Following a centrifugation at 8,200 x g for 30 seconds or 5,000 RPM for 1 min for anti-FLAG or anti-MYC agarose beads,

respectively, supernatants were discarded, and beads washed 3 times with incomplete IP lysis buffer. All excess lysis buffer was removed after the final wash. FLAG-tagged proteins were eluted from the agarose beads by the addition of 200 ng/µL 3x FLAG peptide (Sigma-Aldrich, #F4799) in Tris-buffered Saline (TBS, 50 mM Tris-HCl pH 7.4, 150 mM NaCl) and incubation at +4 °C for 30 minutes under gentle rotation. FLAG samples were then centrifuged, and supernatants saved into a new tube. MYC-tagged proteins were eluted by adding NuPAGE Lithium Dodecyl Sulphate (LDS) Sample Buffer (Thermo Fisher Scientific, #NP0007) containing 5 % β-mercaptoethanol directly onto the beads. Elutions were stored at -70 °C if not used immediately.

2.7.3.   Western Blot

Western blot analysis was performed using standard methods. Cell lysates were denatured in NuPAGE LDS Sample Buffer containing 5 % β-mercaptoethanol. Unless stated otherwise, samples were not heated before loading onto agarose gels to avoid protein aggregation. Around 20 µg of proteins were separated by SDS-polyacrylamide gel electrophoresis using precast NuPAGE 4-12 % Bis-Tris Gels (Invitrogen, #NP0322BOX). Protein ladder was run in parallel of the samples to evaluate molecular weight. Samples and protein ladder were ran at 80 V for the first 20 minutes then at 100 V in NuPAGE MOPS SDS Running Buffer (Invitrogen, #NP0001) until nice protein separation.

After migration, proteins were blotted onto 0,45 µm polyvinylidene fluoride (PVDF) membranes (Merck, #ISEQ00010) using the Trans-Blot Turbo Transfer System (BIO-RAD) and the semi-dry protocol. Briefly, methanol-activated membrane and the gel were placed in the transfer system cassette between filter papers (Thermo Fisher Scientific, #88615) humidified with transfer buffer consisting of 48 mM Tris base, 39 mM Glycine and 20 % *v/v* methanol. Once the transfer pack was assembled, the cassette was placed in the Trans-Blot instrument and run at 25 V constant for 30 minutes.

To prevent non-specific binding of the antibodies, unspecific sites were blocked by incubation with 5 % *w/v* non-fat dry milk in Tris-Buffered Saline-Tween (TBST-T; 10 mM Tris pH 8, 150 mM NaCl, 0.5 % Tween-20) at room temperature. Membranes were then incubated overnight at +4 °C with primary antibodies and under gentle agitation. Membranes were subsequently washed three times in TBS-T then incubated with horseradish peroxidase-conjugated anti-rabbit (Cell Signaling, #7074S) or anti-mouse (Cell Signaling, #7076S) secondary antibodies

for 1 hour at RT. Antibodies references and dilutions used in this thesis figure in the **Table 2.19** below.

Table 2.19: List of the antibodies and conditions used in this thesis for western blot.

Target	Manufacturer	Reference	Dilution
Acc	Cell Signaling	#3676	1/1000
Agpat2	Cell Signaling	#14937	1/1000
aP2/FABP4	Cell Signaling	#3544	1/1000
Atgl	Cell Signaling	#2138	1/1000
β-actin	R&D Systems	#MAB8929	1/5000
Calnexin	Abcam	#ab75801	1/2000
Flag	Sigma	#F1804	1/1000
Hsl	Cell Signaling	#4107	1/1000
Myc	Cell Signaling	#2272	1/1000
Perilipin 1	Cell Signaling	#9349S	1/1000
Pparγ	Cell Signaling	#2430	1/1000
Seipin	Cell Signaling	#23846	1/1000

Blots were developed using the Enhanced Chemiluminescence (ECL) system using Luminata Crescendo Western HRP Substrate (Merck, #WBLUR0500) and the iBright FL1000 imager (Thermo Fisher Scientific). Analysis of the blots were performed using ImageJ software (NIH, Version 1.52a) (343).

2.8. Imaging

2.8.1. Immunofluorescence

Cells were seeded onto 13 mm round glass coverslips (VWR, #631-0149) previously washed in methanol and sterilised under UV-light for 20 minutes. When ready to analyse, cells were washed with PBS then fixed for 10 minutes at RT with 10 % neutral buffered formalin (Sigma-Aldrich, #HT501128). Cells were then washed in ice-cold PBS and stored in PBS at +4 °C if not used immediately. If pursuing with staining, cells were first permeabilised with 0,2 % Triton X-100 in PBS for 10 minutes at RT. Following 3 washes with PBS, cells were blocked in 3 % *w/v* BSA in PBS for 1 hour at RT in a humid chamber. Cells were then incubated overnight with the primary antibody diluted in 3 % BSA/PBS at +4 °C in a humid chamber. The next day, cells were washed 3 times with PBS and incubated with Alexa Fluor secondary antibody also diluted in 3 % BSA/PBS for 1 hour at RT in the dark. After 3 washes with PBS, cells were incubated with 1 µg/mL DAPI in PBS (Thermo Fisher Scientific, #15823959) for 10 minutes at RT to counterstain nuclei. After a final wash with PBS, coverslips were mounted onto Superfrost *PLUS* glass slides (Thermo Fisher Scientific, #J1800AMNZ) using Prolong Gold Antifade Mountant (Invitrogen, #P36930). Immunofluorescence images were acquired on Zeiss LSM880 confocal microscope (Carl Zeiss) and analysed using Zeiss ZEN Lite software (blue edition).

Table 2.12 described antibodies and dilution used for immunofluorescence staining.

Table 2.12: List of the antibodies used in this thesis for immunofluorescence.

Target	Manufacturer	Reference	Dilution
FLAG	Sigma	#F1804	1/500
LAMP-1	Developmental Studies Hybridoma Bank (DSHB)	#1D4B	1/500
Myc	Cell Signaling	#2272	1/500
Perilipin 1	Cell Signaling	#9349S	1/500

2.8.2. Histology

2.8.2.1. Fixation and embedding

To preserve cellular and molecular structures, tissues collected from mice were immersed in a suitable volume of 10 % *v/v* neutral buffered formalin. After 48 hours, PBS was substituted for formalin and samples stored at +4 °C. Due to the hydrophobic property of paraffin wax, tissues were dehydrated before infiltration with wax using standard methods. Briefly, resected organs were placed in tissue processing cassettes and dipped in increasing concentrations of ethanol. Paraffin and ethanol being immiscible, a third solvent was used as an intermediate. This was achieved by dipping the cassettes in several changes of xylene and chloroform. Tissues were immersed in molten paraffin and maintained at 60 °C for hours to allow complete infiltration of the wax into the tissue. All the above steps, from dehydration to infiltration with liquid paraffin, were carried out on an automated tissue processor at the Microscopy and Histology Core Facility (Institute of Medical Sciences, Aberdeen). **Table 2.13** describes in detail the program followed by the automat.

Table 2.13: Automatic tissue processor program for histology.

STEP	Time
70 % Ethanol	2 hours
95 % Ethanol	2 hours
100 % Ethanol	3 hours
100 % Ethanol	3 hours
100 % Ethanol	3 hours
Chloroform/Xylene 1 :1	2 hours
Chloroform/Xylene 1 :1	2 hours
Chloroform/Xylene 1 :1	2 hours
Wax	1 hour
Wax	2 hours

Once infiltration was completed, tissue was removed from the cassette and placed in an appropriate mould with liquid paraffin according to its size. Moulds-containing tissues were

transferred to a cooling plate to allow paraffin's solidification. Particular attention was paid to tissue orientation as its positioning directly determines the plane of the section.

2.8.2.2.　Sectioning

Unless otherwise stated, paraffin-embedded organs were sectioned into 10 µm thick slices using a microtome (Leica, #RM2125RT). Sections were placed in a 37 °C water bath to smooth the tissue and eliminate any wrinkles. Floating sections were then directly picked up from the water bath on Superfrost *PLUS* glass slides (Thermo Fisher Scientific, #J1800AMNZ) and dried overnight in a 56 °C oven.

2.8.2.3.　Immunohistochemistry (IHC)

To detect the presence of a specific protein within a tissue, immunohistochemistry methods were used. When interested in cellular and tissue structures visualisation, basic colorations or special staining were performed.

2.8.2.3.1.　Deparaffinisation

To remove paraffin from the tissue sections, slides were immerged in different baths of xylene then rehydrated through a series of passages in decreasing concentrations of ethanol (**Table 2.14**).

Table 2.14: Deparaffinisation and rehydration steps for histology.

STEP	Time
Xylene	5 min
Xylene	5 min
Xylene/100 % Ethanol 1 :1	3 min
100 % Ethanol	3 min
100 % Ethanol	3 min
95 % Ethanol	3 min
70 % Ethanol	3 min
50 % Ethanol	3 min
Water	5 min

2.8.2.3.2. Heat-induced epitope retrieval (HIER)

Fixative such as formalin creates methylene bridges that hide antigenic sites. To unmask antigenic epitopes, slides were placed in a metal rack containing 10 mM Sodium Citrate Buffer (Sigma, #C8532) with 0.05 % *v/v* Tween-20 pH 6 and heated in an autoclave at a temperature near boiling point. Slides were left only 3 minutes at 126 °C then cooled down under running tap water.

2.8.2.3.3. Endogenous peroxidases quenching and blocking

When using horseradish peroxidase (HRP) conjugated secondary antibodies, it is necessary to block endogenous peroxidase activity that may otherwise interfere with antigen detection by generating non-specific background staining. This was achieved by submerging the slides in 3 % *v/v* hydrogen peroxide (Sigma, #H1009) diluted in methanol for 15 minutes. Similarly, to prevent non-specific binding of the antibody to the tissue, slides were incubated for 1 hour at RT in blocking buffer consisting of 3 % *v/v* BSA in TBS-T.

2.8.2.3.4. Immunostaining

Following blocking, sections were incubated overnight at +4 °C in a humid chamber with primary antibodies directed against proteins of interest. Antibodies used for immunochemistry were diluted in blocking buffer and are listed in **Table 2.15**. A "no primary antibody" control, incubated in blocking buffer only at this stage, was always included in the analysis. The next day, all sections (including controls) were washed with TBS-T and incubated for 1 hour at RT with HRP-conjugated or Alexa-Fluor secondary antibodies if using chromogenic or fluorescent detection systems, respectively. Following manufacturer's instructions, 3,3'-diaminobenzidine (DAB, Vector Laboratories, #SK-4100) was used as a substrate for chromogenic detection and produced a brown precipitate in presence of peroxidase enzyme.

Table 2.15: List of the antibodies used in this thesis for immunohistochemistry.

Target	Manufacturer	Reference	Dilution
CD68	Invitrogen	#MA5-13324	1/100
Insulin	Cell Signaling	#8138	1/500
Glucagon	Cell Signaling	#8233P	1/100
Glut2	Abcam	#ab111117	1/250
Ki67	Abcam	#ab16667	1/100
Somatostatin	Santa Cruz	#sc-13099	1/250

2.8.2.3.5. Nuclear counterstaining

To gain insight into overall tissue architecture, DAB colorations were counterstained with Gill's Hematoxylin (Sigma, #GHS232). The duration of this step depends on the tissue origin but varied between 1 to 5 minutes. Sections were subsequently dehydrated in ethanol, clarified in xylene and coverslipped with mounting medium (Leica, #14046430011). Sections were observed under a standard brightfield microscope (Leica DMR).

For fluorescence IHC, nuclei were stained for 10 minutes with 1 μg/mL 4', 6-diamidino-2-phenylindole (DAPI, Thermo Fisher Scientific, #15823959). Sections were washed with PBS then mounted with Prolong Gold Diamond Antifade mounting medium (Invitrogen, #P36930). Immunofluorescence images were acquired on Zeiss LSM880 confocal microscope (Carl Zeiss) and analysed using Zeiss ZEN Lite software (blue edition).

2.8.2.4. Basic colorations

2.8.2.4.1. Hematoxylin & Eosin (H&E) staining

H&E staining was routinely used to assess cellular and tissue morphology. Hematoxylin-stained nuclear components in blue while eosin-stained cytoplasmic components such as collagen and fibres in pink. The following table (**Table 2.16**) provides details of the H&E protocol for paraffin-embedded sections.

Table 2.16: H&E protocol for paraffin-embedded tissues.

STEP	Time
56 °C Oven	Overnight
Xylene 1	15 min
Xylene 2	15 min
100 % Ethanol	2 min
70 % Ethanol	2 min
Running tap water	2 min
Gill's Hematoxylin	5 min
Tap Water	2 min
2 % Acid Alcohol	3 dips
Tap Water	1 min
Saturated Lithium Carbonate	1 min
Tap Water	1 min
Eosin	2 min
Tap Water	20 sec
70 % Ethanol	rinse
100 % Ethanol	rinse
Xylene 1	3 dips
Xylene 2	2 min
Xylene 3	2 min
Coverslipping	Coverslip

The 2 % *v/v* acid alcohol solution was prepared by diluting 2 mL of concentrated HCl into 100 mL of 70 % ethanol. Saturated lithium carbonated solution was prepared by dissolving 1,54 grams of lithium carbonate (Sigma, #L4283) into 100 mL of distilled H_2O (dH_2O).

2.8.2.4.2. Oil Red O (ORO) staining

Due to the use of xylene during slides preparation, staining of lipids using ORO staining was not suitable for paraffin-embedded sections and performed on frozen sections instead. Frozen tissues were covered with cryo-embedding media (Optimal Cutting Temperature OCT compound, TAAB Laboratories Equipment Ltd, #O023) and sectioned into 10 µm thickness

slices using a cryotome (Leica, #CM1950). Tissue sections were placed onto Superfrost glass slides and air dried at least 30 minutes before pursuing with ORO staining. Sections were fixed for 10 minutes in 10 % *v/v* neutral buffered formalin then rinsed with tap water. After a quick passage in 60 % isopropanol, sections were stained for 10 minutes with filtered ORO working solution prepared from 0.5 % *w/v* ORO stock solution (Sigma, #O0625) as described in **Table 2.17**. Slides were rinsed in 60 % isopropanol then water then counterstained with Gill's Hematoxylin for 2 minutes. After several washes with water, slides were coverslipped using Leica mounting medium and visualised under brightfield microscope.

Table 2.17: Preparation of Oil Red O solution for lipid staining.

0,5 % Oil Red O stock solution		Oil Red O working solution	
Reagent	**Amount**	**Reagent**	**Amount**
Oil Red O powder	0,5 grams	0,5 % Oil Red O stock solution	6 parts
Isopropanol	100 mL	dH2O	4 parts

2.9. Statistical analyses and illustrations

All the data in this thesis are presented as mean ± SEM (standard error of the mean). The n value mentioned in the figure's legend refers to the number of mice or biological replicates analysed during the study. When variables were normally distributed and homoscedasticity (equality of variances) confirmed, an unpaired t-test was used to compare the means of two independent groups. If not, non-parametric Mann-Whitney-Wilcoxon test was employed. If comparing more than two independent groups on one single variable, a one-way analysis of variance (ANOVA) with Tukey *post-hoc* test was used. A p-value < 0.05 was considered as statistically significant and denoted with a single asterisk (*). P values < 0.01, 0.001, 0.0001 were represented with **, *** and ****, respectively.

Statistical analysis and graphs presented in this study were generated using GraphPad Prism (GraphPad Software, version 8.3.0 for Windows, San Diego, California, USA). Unless stated otherwise, illustrations presented in this thesis were made by myself using Inkscape software.

CHAPTER 3

3. Effects of seipin loss on adipogenesis and lipolysis in a human preadipocyte cell line

3.1. Introduction

Patients with loss-of-function mutations in the Berardinelli-Seip congenital lipodystrophy type 2 (*BSCL2)* gene, which encodes the protein seipin, suffer from congenital generalised lipodystrophy type 2 (CGL2) and display a near total lack of adipose tissue (85,98). This is believed to result from a defect in adipogenesis associated with a failure in maintaining mature adipocytes. While a role of seipin has been reported in both adipogenesis, lipid droplet biology and lipolysis, the underlying molecular mechanisms are poorly understood (143,151,152,169,344). *In vitro* studies of seipin have mainly relied on murine primary cell cultures or preadipocyte cell lines including 3T3-L1 (143,151).

In terms of clinical relevance, greater benefits could emerge from the use of a human cell line. In 2001, Wabitsch *et al.* first reported the use of the Simpson Golabi Behmel Syndrome (SGBS) preadipocyte cell line (345). These cells were derived from the stromal vascular fraction (SVF) of subcutaneous adipose tissue of a diseased infant with SGBS, a X-linked congenital overgrowth syndrome (346). They are highly proliferative and retained capacity for adipogenic differentiation *in vitro* providing an important source of human preadipocytes.

In addition, finding an antibody that specifically recognises the murine seipin protein has been challenging for us and others (152) and this has limited our ability to study endogenous protein in mouse derived cells and tissue samples. In contrast, a monoclonal antibody developed by Cell Signaling TECHNOLOGY® has proven highly effective in detecting human seipin protein (347). Thus, the use of human adipocytes has the added technical benefit of allowing detection of endogenous seipin in our samples.

This chapter examines the relevance of the SGBS cell line for the study of CGL2 in humans. In addition, the effects of seipin loss on lipolysis are examined in this cell line. Previous studies have shown that terminal adipocyte differentiation of mouse embryonic fibroblasts (MEF) and stromal vascular cells (SVC) isolated from $Bscl2^{-/-}$ mice failed because of an increase of basal lipolysis in these cells (117,152). However, this effect is not evident in 3T3-L1 and C3H10T1/2 murine preadipocyte cell lines when seipin expression is inhibited. In these cells, loss of seipin inhibits adipogenic gene expression (143,151). Seipin disruption in SGBS cells has previously been reported in a high throughput study of cellular morphology following adipose gene disruption using CRISPR/Cas9 (348). This revealed a direct interaction of seipin with the key lipolytic regulator perilipin 1 but did not directly assess the effects of seipin loss on adipocyte

lipolysis. Experiments presented in this chapter were designed to elucidate whether the effects of seipin loss in SGBS cells were similar to studies in murine models and whether seipin might directly influence lipolysis in adipocytes. To this end, SGBS cells were first differentiated using standard protocols and characterised with respect to their morphology, gene, and protein expression. Using small interfering RNA (siRNA), seipin expression was inhibited in SGBS preadipocytes and the processes of differentiation and lipolysis were examined in these cells. A key aim was also to determine whether SGBS cells could provide a valuable tool in which to investigate the roles of seipin in adipogenesis and lipolysis and potentially testing novel therapeutics.

3.2. Results

3.2.1. Differentiation of SGBS cells into adipocytes

Whilst murine 3T3-L1 is a well-established preadipocytes cell line that has greatly contributed to our knowledge on adipogenesis, this model has several limitations when it comes to its applicability to human diseases (349). In an attempt to find a model that more closely resembles the human condition, Simpson Golabi Behmel Syndrome (SGBS) cells were used here. SGBS cells are a human preadipocyte cell line which displays fibroblast-like features in the undifferentiated state (***Figure 3.1, A***). SGBS preadipocytes were efficiently differentiated in culture upon exposure to a defined mixture of dexamethasone, methylisobuthylxantine, cortisol, transferrin, triiodothyronine and insulin, following a specific procedure nicely described in (341). After 12 days of culture, lipid droplets were clearly visible in differentiated SGBS cells (***Figure 3.1, B***). The addition of rosiglitazone, a peroxisome proliferator-activated receptor γ (PPARγ) agonist, during the first four days of the differentiation process markedly enhanced the differentiation process with almost all SGBS preadipocytes accumulating lipid droplets by day 12 (***Figure 3.1, C***).
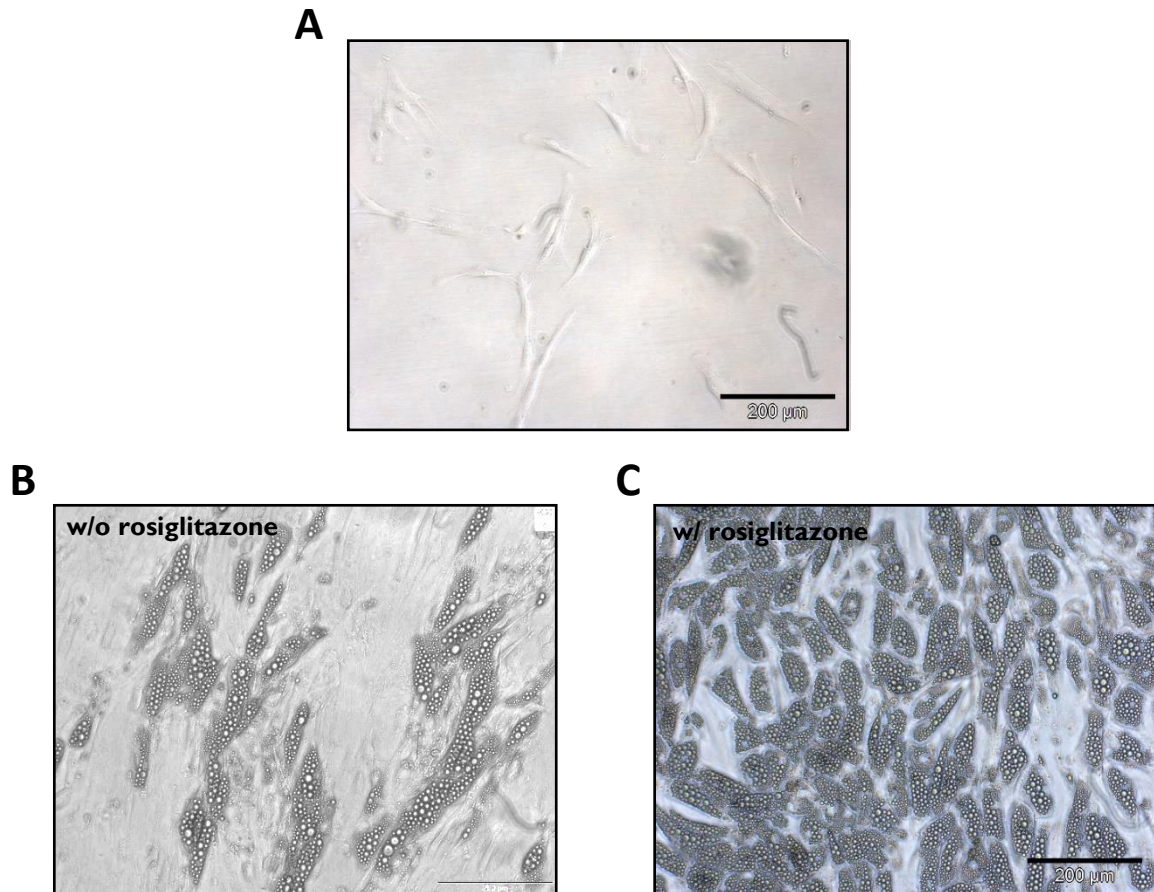
*Figure 3.1: **Morphological changes in differentiating SGBS cells**. Representative brightfield images of undifferentiated SGBS cells (**A**), SGBS cells differentiated in the absence of the PPARγ agonist rosiglitazone (**B**) and SGBS cells differentiated in the presence of 2 µM rosiglitazone (**C**) after 12 days of differentiation in culture. Bars denote 200 µm.*

3.2.2.　Transcriptional regulation of adipogenesis in SGBS cells

The transcriptional cascade that drives adipogenic differentiation has been extensively studied and is well documented (350). To get a comprehensive understanding of this process in seipin-deficient cells, I first needed to characterise it in native SGBS cells. This was achieved by determining the gene expression profile of key transcription factors known to regulate adipogenesis using quantitative reverse transcription polymerase chain reaction (qRT-PCR). To ensure optimal conditions, cells were differentiated in the presence of rosiglitazone and collected at different time points up to 12 days. Adipogenesis was initiated by the activation of CCAAT/enhancer-binding protein (C/EBP) family members including *C/EBPβ* and *C/EBPγ*

(**Figure 3.2, A/B**). Their transient expression between day 0 and day 4 indicated their participation in the early stages of differentiation rather than terminal differentiation (**Figure 3.2, A/B**). Sterol regulatory element-binding protein 1c (*SREBP1c*) was also induced early in the differentiation process and its transcription level incrementally increased as cells acquired mature adipocyte features (**Figure 3.2, C**). Those early adipogenic factors are believed to, in turn, induce the expression of other transcription factors, the most important of which is PPARγ (351,352). *PPARγ* expression was detected at low levels at day 0 and rapidly increased over the course of the differentiation (**Figure 3.2, D**).
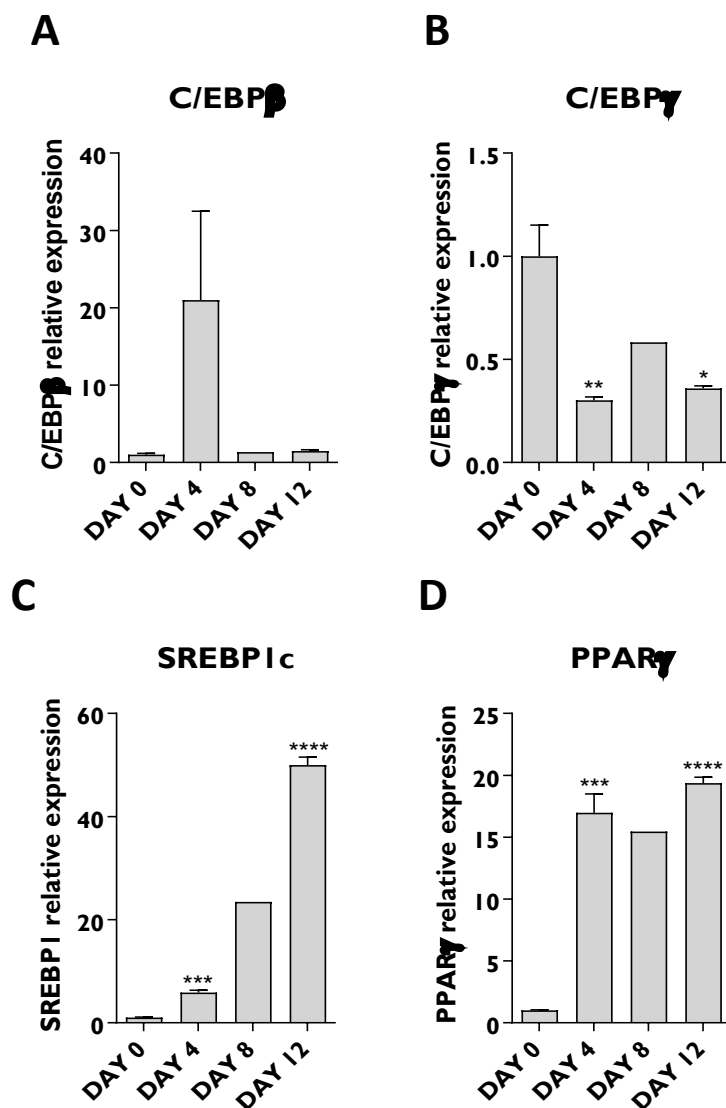
Figure 3.2: **Time-course transcriptional control of adipogenesis in SGBS cells**. *mRNA relative expression of C/EBPβ (**A**), C/EBPγ (**B**), SREBP1c (**C**) and PPARγ (**D**) in SGBS cells differentiated for 12 days in the presence of 2 μM rosiglitazone. Gene expression was normalised to Hprt reference gene (number of experimental replicates: n=3). Data are expressed as mean ± SEM. Student's t-test: *p<0.05, **p<0.01, ***p<0.001, ****p<0.0001 when compared to day 0 samples.*

The key transcription factors mentioned just above regulate, in turn, the expression of other genes involved in lipogenesis, lipolysis and insulin sensitivity including adipocyte protein 2, *aP2* (also known as fatty-acid binding protein 4, *FABP4*), glucose transporter 4 (*GLUT4*), perilipin 1 (*PLIN1*), 1-Acylglycerol-3-Phosphate O-Acyltransferase 2 (*AGPAT2*), *BSCL2* and ADIPONECTIN (353,354). This was evidenced by the presence of regulatory elements and binding sites for PPARγ and C/EBP family members in the promoter regions of their target genes (31,355,356). *aP2*, *ADIPONECTIN*, *PLIN1* and *GLUT4* were not expressed as detectable levels at day 0 (***Figure 3.3, A-D***). However, their mRNA expression steadily increased over the course of the differentiation of SGBS cells (***Figure 3.3, A-D***). *AGPAT2* was detected only at low levels at day 0 but similarly to other genes, its expression progressively increased as cells develop into mature adipocytes reaching a 50-fold increase at day 12 (***Figure 3.3, E***). *BSCL2* expression was induced early on in the adipogenic process and was maintained at equivalent levels from day 4 onwards (***Figure 3.3, F***).

Next, the protein levels of those target genes were measured to determine if they reflect their transcript levels (***Figure 3.3, G***). PPARγ and aP2/FABP4 were detected at a protein level from day 8 onwards. Adipose triglyceride lipase (ATGL) and hormone-sensitive lipase (HSL) are the two major lipases involved in lipolysis in adipocytes (357–359). Their protein levels were not detected in the early stages of differentiation in SGBS cells and acetyl-CoA carboxylase (ACC), involved in lipogenesis, followed the same expression pattern (***Figure 3.3, G***). AGPAT2 and BSCL2 protein levels were in accordance with mRNA levels. AGPAT2 protein expression steadily increased over time. BSCL2 expression was also induced by the adipogenic cocktail with day 8 and day 12 protein lysates exhibiting equivalent seipin levels. Collectively, these data demonstrate how SGBS cells successfully acquired characteristics of lipid laden adipocytes over the course of their differentiation. They also expressed clearly detectable levels of *BSCL2* mRNA and seipin protein, making them a useful model for studying the role of seipin in human adipocyte biology.
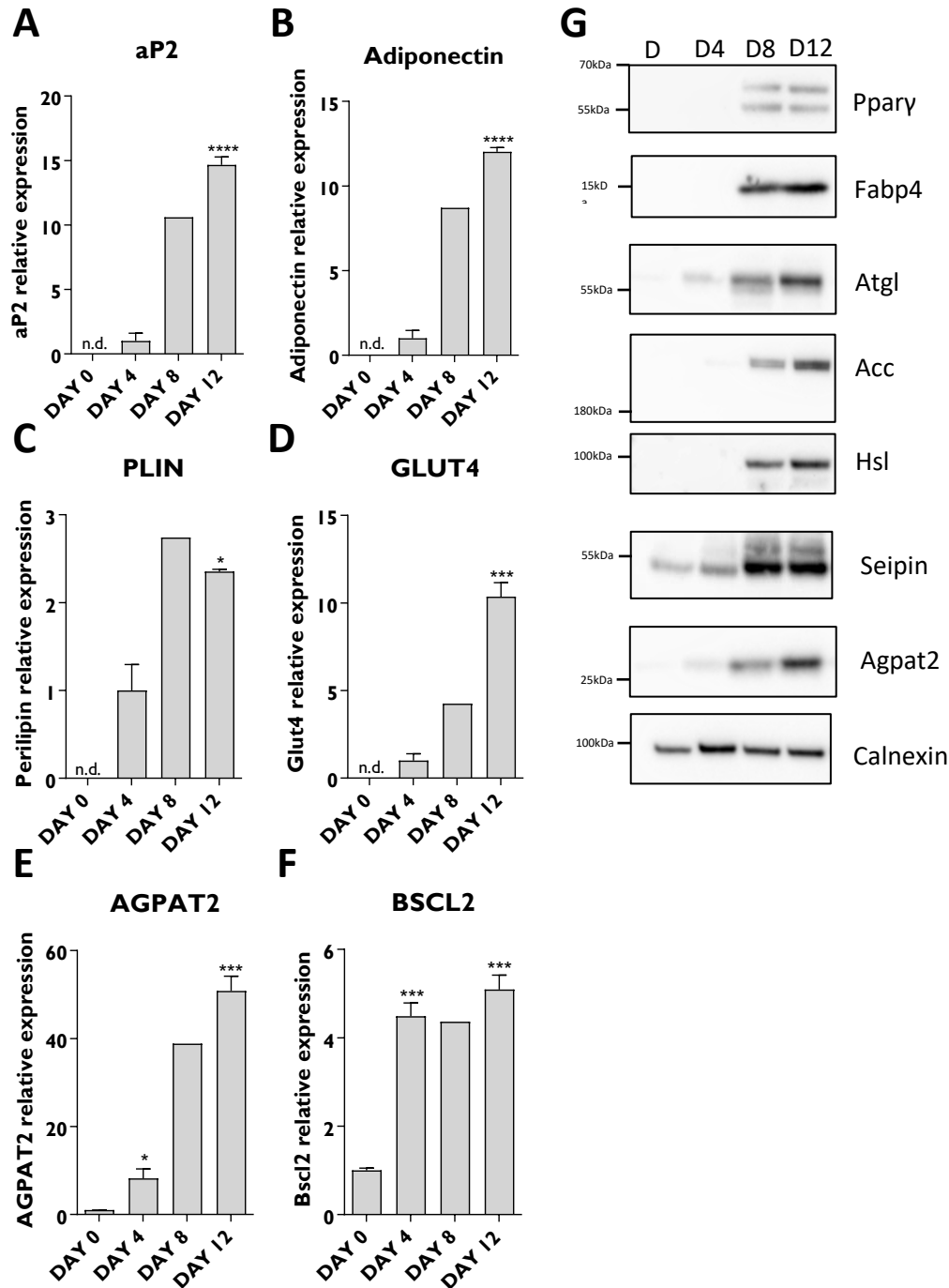
Figure 3.3: **Adipogenic differentiation of SGBS cells in the presence of the PPARγ agonist rosiglitazone.** *SGBS cells were differentiated in the presence of 2 μM rosiglitazone and collected at day O, day 4, day 8 and day 12. mRNA relative expression of aP2/FABP4 (**A**), adiponectin (**B**), perilipin/PLIN (**C**), Glut4 (**D**), Agpat2 (**E**) and Bscl2 (**F**). Gene expression was normalised to Hprt reference gene (n=3). n.d. non detectable. Data are expressed as mean ± SEM. Student's t-test: *p<0.05, ***p<0.001, ****p<0.0001 when compared to day 0 samples or day 4 if day 0 n.d. (**G**) Protein lysates were separated by SDS-PAGE and immunoblotted with Pparγ, aP2/Fabp4, Atgl, Acc, Hsl, Seipin and Agpat2 antibodies. Calnexin was used as a loading control. Presented blots are representative of three independent experiments (n=3).*

3.2.3. Effect of seipin loss on SGBS preadipocytes differentiation

As seen in section 3.2.2, BSCL2/seipin is induced early on during the adipogenesis process. As a consequence, and in an attempt to target seipin expression before its induction, SGBS cells were transfected both two days prior to and at day 0 of the differentiation with a siRNA directed against BSCL2. After 12 days in culture in the presence of rosiglitazone, SGBS differentiated adipocytes were analysed morphologically and at protein levels. A representative blot is shown in ***Figure 3.4, A***. Quantification of each protein relative to calnexin control is shown in ***Figure 3.4, B-H***. siRNA treatment efficiently decreased seipin expression with no apparent protein after 12 days of differentiation (***Figure 3.4, A/B***). Control cells and seipin knockdown cells had equivalent expression of AGPAT2, aP2/FABP4 and HSL at day 12 (***Figure 3.4, C-E***). ACC was modestly but statistically more elevated in seipin-deficient SGBS cells (***Figure 3.4, F***). I observed a 2-fold increase in ATGL protein expression in seipin knockdown cells when compared to controls (***Figure 3.4, G***). Finally, a slight increase in PLIN1 protein level was observed in knocked-down cells upon rosiglitazone treatment although this was not significant (***Figure 3.4, H***). Altogether, control and seipin-depleted SGBS adipocytes displayed equivalent levels of adipogenic protein expression. This suggests that seipin is not needed for the differentiation of SGBS preadipocytes, at least in the presence of the PPARγ agonist rosiglitazone.
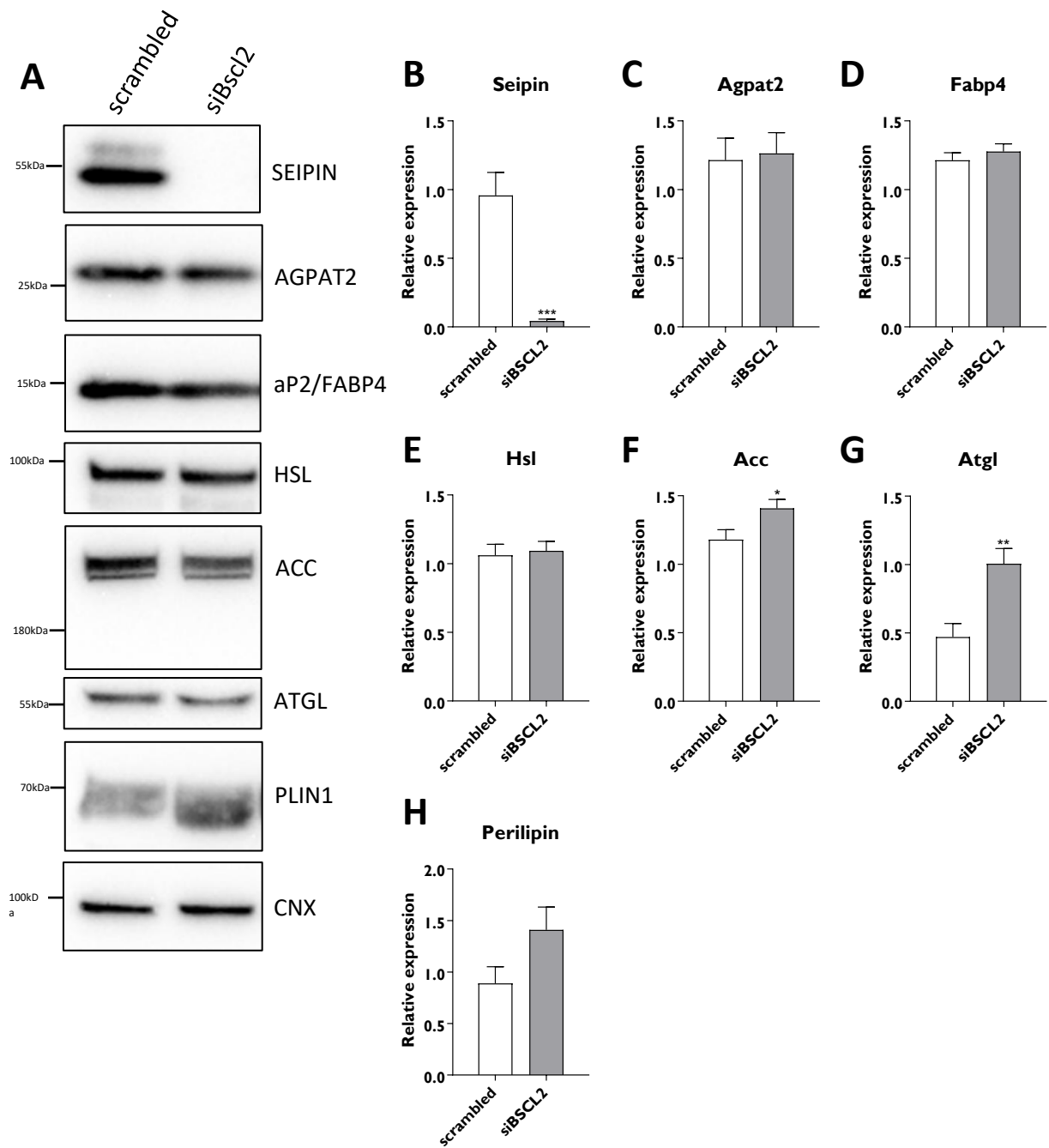
Figure 3.4: Adipogenic differentiation of seipin-deficient SGBS cells in the presence of the PPARγ agonist rosiglitazone. *SGBS cells were transfected with a control siRNA (scrambled) or a siRNA targeting Bscl2 (siBscl2) two days prior and at day 0 of differentiation. Differentiated adipocytes were examined after 12 days of differentiation in the presence of 2 μM rosiglitazone. Protein lysates were separated by SDS-PAGE and immunoblotted with Seipin, 1-acylglycerol-3-phosphate O-acyltransferase 2 (Agpat2), fatty acid binding protein 4 (Fabp4), hormone-sensitive lipase (Hsl), acetyl-CoA carboxylase (Acc), adipose triglyceride lipase (Atgl) and Perilipin-1 antibodies. Calnexin (CNX) was used as a loading control. (**A**) Representative blot of seven independent experiments (n=7). (**B-H**) Quantification of protein levels compared to calnexin control. Data are expressed as mean ± SEM (number of experimental replicates: n=7). Student's t-test: *p<0.05, **p<0.01, ***p<0.001.*

85

Light microscopy morphological examination of differentiated adipocytes provided important information regarding lipid droplets size. Both control and seipin knockdown cells displayed numerous lipid droplets after 12 days of differentiation (***Figure 3.5, A/B***). However, siRNA-mediated knockdown of *BSCL2* induced the appearance of multiple larger lipid droplets in mature adipocytes (***Figure 3.5, B***). This phenotype was similar to observations made by others in murine embryonic fibroblasts isolated from Bscl2$^{-/-}$ mice (117) and was not observed in 3T3L1 or C3H10T1/2 cells (*personal communication*). Interestingly, this phenotype was not observed in SGBS cells in which I had used siRNA to knockdown expression of AGPAT2, a seipin-binding protein whose disruption also causes another type of congenital generalised lipodystrophy (88,162) (***Figure 3.5, C***). As shown in ***Figure 3.5, D***, AGPAT2 and seipin protein levels are essentially undetectable in SGBS cells transfected with the corresponding siRNAs.
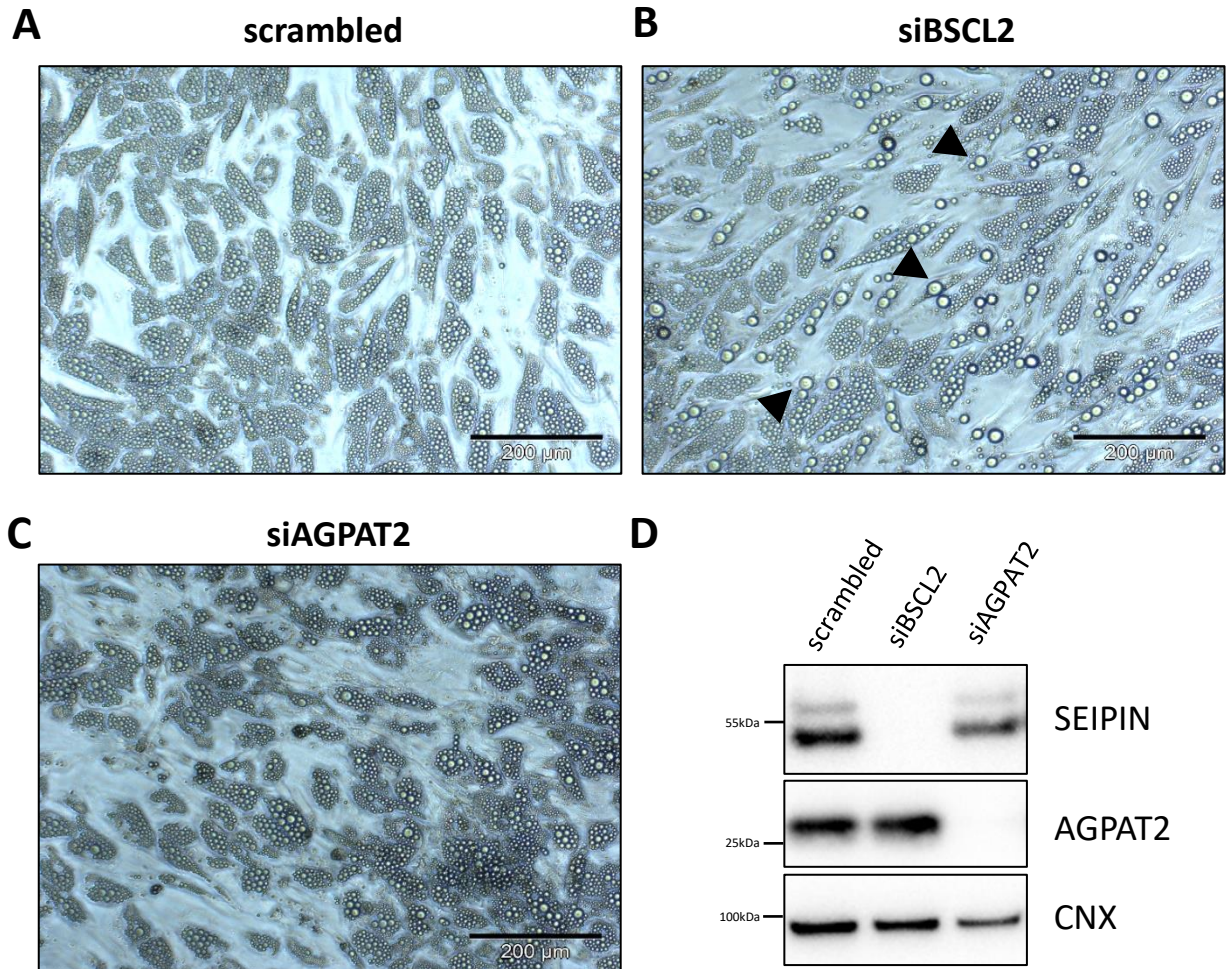
Figure 3.5: Knockdown of seipin in SGBS cells leads to enlarged lipid droplets in the presence of the PPARγ agonist rosiglitazone*. Representative brightfield images of control (**A**) seipin knockdown (siBSCL2) (**B**) and AGPAT2 knockdown (siAGPAT2) SGBS cells (**C**) 12 days after differentiation in the presence of 2 µm rosiglitazone. Bars denote 200 µm. Black arrowheads indicate supersized lipid droplets. (**D**) Protein lysates were separated by SDS-PAGE and immunoblotted with Seipin and AGPAT2 antibodies. Calnexin (CNX) was used as a loading control. Presented blots are representative of seven independent experiments (n=7).*

Although LDs were readily visible by light microscopy, the aberrant LD morphology of seipin-deficient adipocytes was further confirmed using immunofluorescence microscopy. Fully differentiated adipocytes were fixed and stained with an anti-perilipin 1 antibody, the most abundant LD-associated protein in adipocytes, and LipidTOX dye to detect neutral lipid droplets. Confocal microscopy imaging revealed that PLIN1 was evenly distributed around LDs in both control and seipin knockdown cells (***Figure 3.6, A/B***). In accordance with light microscopy observations, seipin-deficient adipocytes harbour remarkably large spherical LDs compared to control cells with some LDs reaching more than 30 µm in diameter (***Figure 3.6, B***).

A scrambled **B** siBSCL2

DAPI

PLIN

LipidTOX

Merge

CTRL-
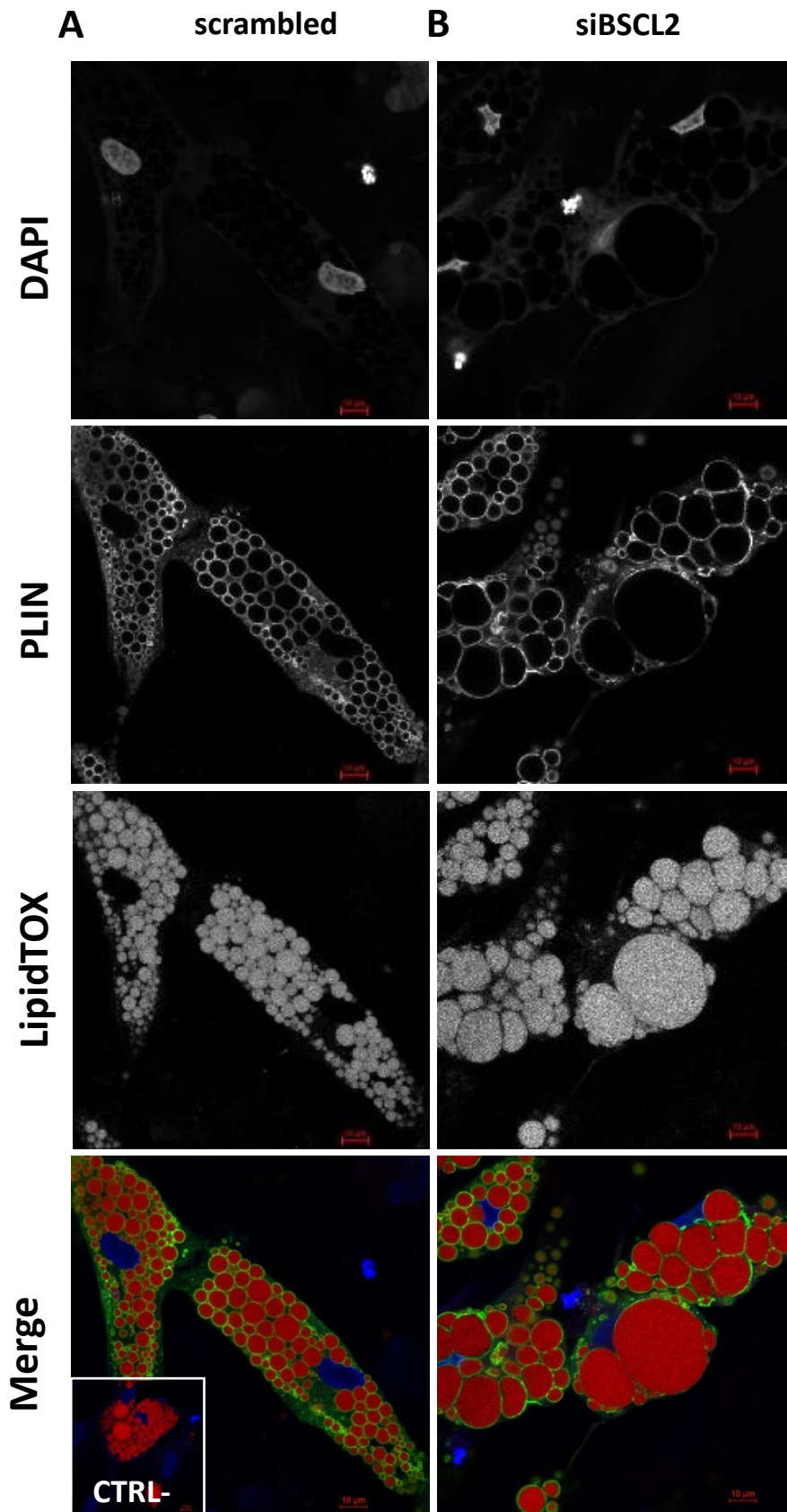
Figure 3.6: Seipin deficiency alters LD morphology in SGBS cells differentiated in the presence of the PPARγ agonist rosiglitazone. Fully differentiated control (A) or seipin-deficient (siBSCL2) (B) SGBS cells were fixed with formalin and stained for perilipin 1 (PLIN) and neutral lipids with LipidTOX. DAPI nuclei, PLIN and lipid staining are shown in blue, green, and red, respectively. Scale bars denote 10 μm. Negative control (CTRL-) was stained with LipidTOX, DAPI and the secondary antibody used for PLIN1 antibody recognition.

Previous studies reported lower levels of Pparγ, aP2 and Adiponectin in mature adipocytes originating from Bscl2$^{-/-}$ murine embryonic fibroblasts (117). The authors also showed that this impairment could partially be restored by rosiglitazone treatment (117). As a potent enhancer of adipogenesis, it is possible that the use of rosiglitazone might have masked any effect of seipin loss on adipocyte differentiation in our SGBS model. To evaluate this hypothesis, SGBS cells were also differentiated in the absence of rosiglitazone and the expression of adipocyte marker genes were examined.

In the absence of rosiglitazone, BSCL2 mRNA expression was decreased by 70 % in seipin knockdown cells when compared to control cells at the start of the differentiation process. This reduction in BSCL2 expression was maintained throughout the experiment (***Figure 3.7, A***). AGPAT2, PLIN1, PPARγ and ADIPONECTIN expression was induced to the same extent in native and seipin-deficient mature adipocytes (***Figure 3.7, B/E***). Only aP2 mRNA expression was significantly reduced in seipin-deficient mature adipocytes at day 12 (***Figure 3.7, F***). Collectively, although there were modest differences in the expression of some adipogenic markers when not using rosiglitazone, it would appear that seipin is not an essential requirement for the differentiation of SGBS cells.
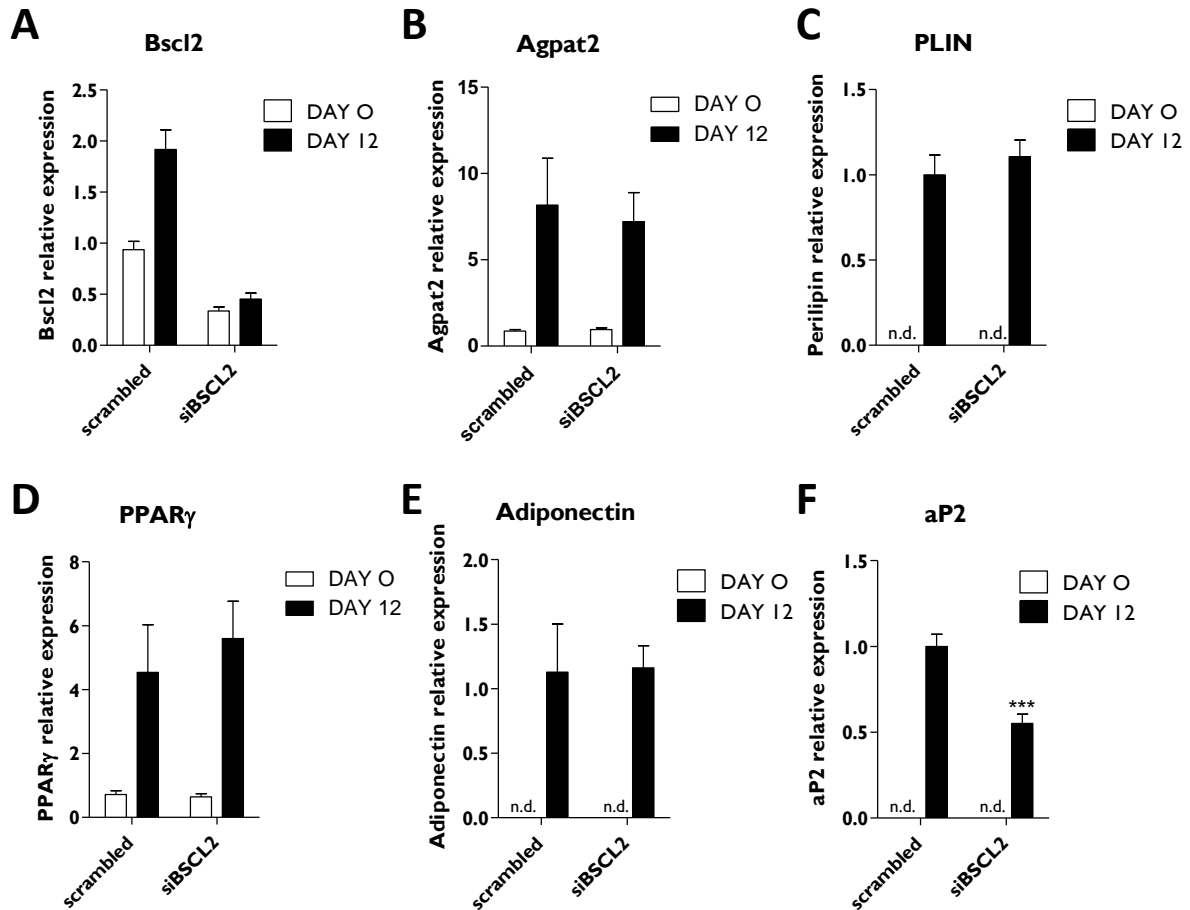
Figure 3.7: Adipogenic differentiation of seipin-deficient SGBS cells in the absence of the PPARγ agonist rosiglitazone. *mRNA relative expression of BSCL2 (**A**), AGPAT2 (**B**), PLIN1 (**C**), PPARγ (**D**), ADIPONECTIN (**E**) and aP2 (**F**) in control (scrambled) and seipin knockdown (siBSCL2) SGBS cells. Gene expression was normalised to Hprt reference gene (number of experimental replicates: n=8). Data are expressed as mean ± SEM, n.d. non detectable, One-way ANOVA: ***p<0.001.*

3.2.4.   Adipocyte differentiation comparison between SGBS and stromal vascular cells

Previous work from our lab has shown a failure of adipocyte differentiation in murine cell lines lacking seipin (143). Others have also reported adipogenesis defects in murine embryonic fibroblasts (MEF) and stromal vascular cells (SVC) isolated from seipin-null (SKO) mice (152). I first sought to examine whether those observations could be replicated *in vitro* on primary cells harvested from our own SKO mice. To this end, SVCs were isolated from subcutaneous adipose tissue of WT and SKO mice and differentiated to adipocytes in culture in the absence or presence of rosiglitazone. After 6 days in culture, lipid accumulation was assessed to estimate

the degree of differentiation of these cells. In the absence of rosiglitazone, differentiation was decreased in SKO SVCs when compared to WT SVCs (*Figure 3.8, A*). The addition of rosiglitazone in the adipogenic medium overcame this defect with WT and SKO SVCs displaying equivalent lipid accumulation (*Figure 3.8, B*). By day 6 of differentiation, some SKO SVCs exhibited large lipid droplets when compared to controls although this was less striking than was previously observed in SGBS cells (*Figure 3.8, B*).
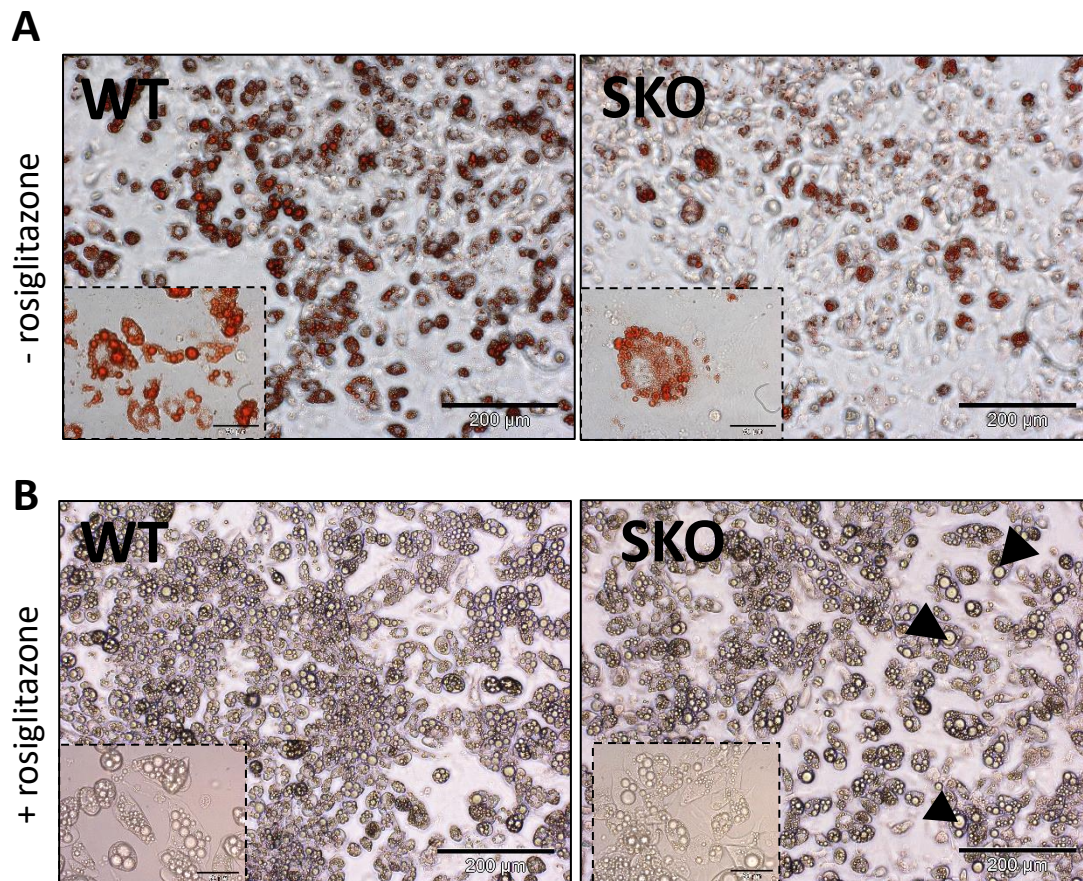
Figure 3.8: Lipid accumulation differs between WT and SKO SVCs depending on the presence of rosiglitazone. (A) Representative brightfield images of Oil Red O staining in SVCs isolated from wild-type (WT) and seipin-null (SKO) mice and differentiated to adipocytes in culture in the absence of rosiglitazone. (B) Representative brightfield images of WT and SKO SVCs differentiated to adipocytes in the presence of 2 μm rosiglitazone. Bars denote 200 μm.

Comparison of adipogenic gene expression profiles revealed notable differences between WT and SKO SVCs. As expected, *Bscl2* expression was totally absent in SKO SVCs (*Figure 3.9, A*). Interestingly, several adipogenic markers were significantly reduced in SKO SVCs when compared to WT controls in the absence of rosiglitazone. *Agpat2* expression was reduced in SKO SVCs, but it was overcome by the addition of rosiglitazone (*Figure 3.9, B*). *PPARγ*

expression was only modestly reduced in SKO SVCs, in both the absence and presence of rosiglitazone (***Figure 3.9, C***). No significant changes were observed in *aP2*, *Plin1* and *C/ebpβ* levels between WT and SKO SVCs (***Figure 3.9, D-F***). Similar to *Agpat2*, C/ebpα, *Glut4*, *Atgl* and *Hsl* expression was significantly impaired in SKO SVCs in the absence of rosiglitazone, but this was rescued by the addition of the PPARγ agonist.

Collectively, these data demonstrate that adipocyte differentiation and lipid accumulation are impaired in murine SKO SVCs in the absence of rosiglitazone. This contrasts with what was observed previously in seipin-deficient human SGBS cells.
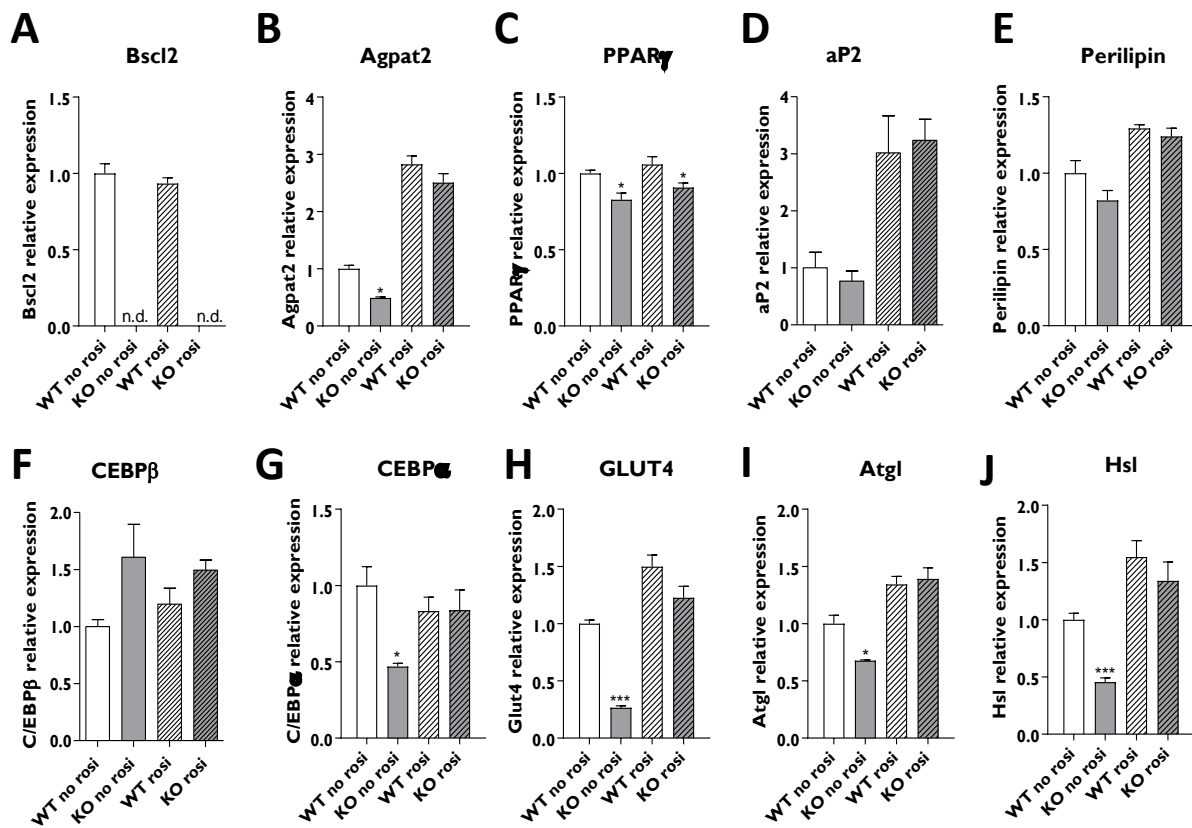
Figure 3.9: Effects of rosiglitazone on the adipogenic differentiation of WT and SKO SVCs. *SVCs isolated from wild-type (WT) and seipin-null (SKO) mice were differentiated in culture in the absence (no rosi) or the presence (rosi) of 2 μm rosiglitazone. Differentiated adipocytes were examined after 6 days of differentiation. mRNA relative expression of Bscl2 (**A**), acyltransferase 2 (Agpat2) (**B**), peroxisome proliferator-activated receptor γ (Pparγ) (**C**), adipocyte protein 2 (aP2) (**D**), perilipin 1 (**E**), CCAAT/enhancer binding protein β (C/ebpβ) (**F**), CCAAT/enhancer binding protein α (C/ebpα) (**G**), glucose transporter 4 (GLUT4) (**H**), adipose triglyceride lipase (Atgl) (**I**) and hormone-sensitive lipase (Hsl)(**J**). Gene expression was normalised to the geometric mean of Hprt, Nono and Yhwaz reference genes (number of experimental replicates: n=4v6). n.d. non detectable. Data are expressed as mean ± SEM. One-way ANOVA: *p<0.05, ***p<0.001.*

3.2.5.   Lipolysis

Previous reports have shown that seipin inhibition can alter lipolysis in seipin knockout mice (SKO) (169), MEFs and SVCs (152). To remove any bias from a defect in adipogenesis introduced by seipin loss and to solely focus on the examination of seipin's role in lipolysis process, SVCs were differentiated in the presence of rosiglitazone to maximally promote adipocyte differentiation. Lipolysis assays were then performed on mature adipocytes at day 6. Glycerol released into the culture media over a period of six hours was determined as a measure of the rate of lipolysis. In the absence of external stimuli, basal lipolysis was significantly elevated in SKO SVCs compared to WT SVCs (***Figure 3.10, A***). When lipolysis was stimulated with the β-adrenergic agonist isoproterenol, the rate of lipolysis was much higher only in the WT SVCs but relatively unaffected in SKO SVCs. As a result, there was no significant difference in the lipolytic rate in WT *versus* SKO SVCs under these conditions (***Figure 3.10, B***).
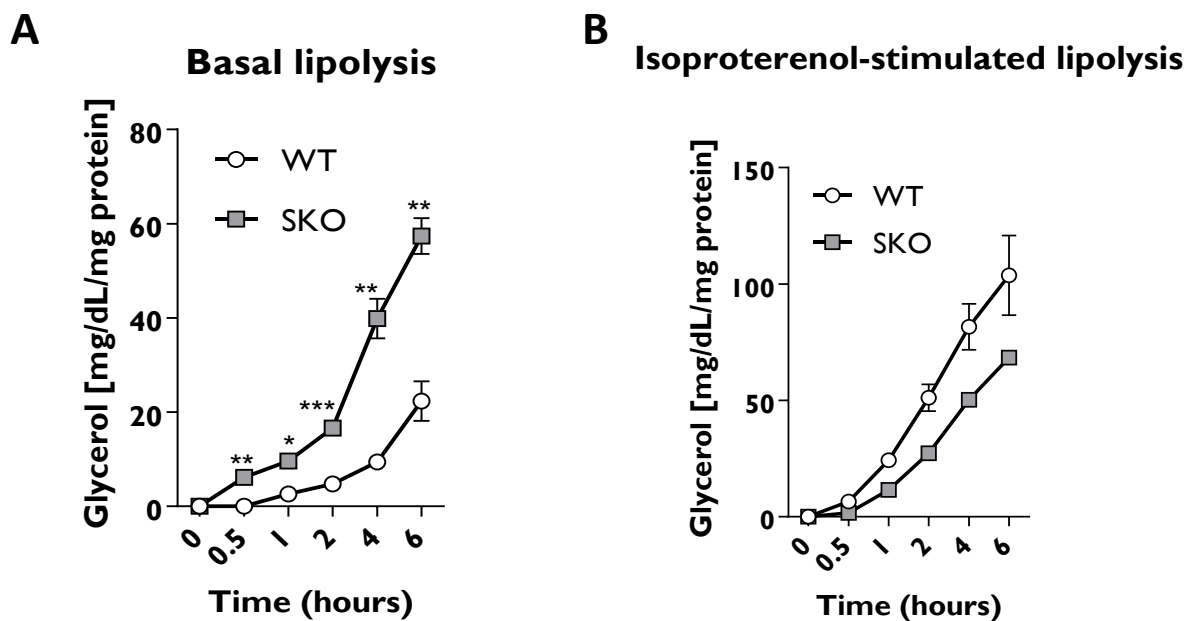
Figure 3.10: Increased basal lipolysis in adipocytes derived from SKO stromal vascular cells (SVC). SVCs were isolated from wild-type (WT) and seipin-null (SKO) mice. Lipolysis assays were performed on mature adipocytes after 6 days of differentiation with 2 μm rosiglitazone. (A) Basal lipolysis, (B) 1 μM isoproterenol-stimulated lipolysis (number of experimental replicates: n=3). Glycerol content was normalised to cellular protein content. Presented graphs are representative of three independent experiments. Data are expressed as mean ± SEM. One-way ANOVA: *p<0.05, **p<0.01, ***p<0.001.

These results are consistent with observations previously published by others (152). I finally chose to examine the effect of seipin deficiency on lipolysis in our human SGBS cell line. SGBS cells were transfected both two days prior and at day 0 of the differentiation with an siRNA directed against BSCL2 and differentiated in the presence of rosiglitazone. Lipolysis assays were performed on mature adipocytes at day 12. Inhibition of seipin significantly increased the basal rate of lipolysis by 4-fold, measured as the amount of glycerol released into the incubation media after four hours (***Figure 3.11, A***). In contrast, when control and seipin knockdown SGBS cells were stimulated with isoproterenol, lipolysis was more robustly stimulated in control cells. As a result, no difference in the rate of lipolysis was observed between control and seipin knockdown cells in the stimulated state (***Figure 3.11, B***).
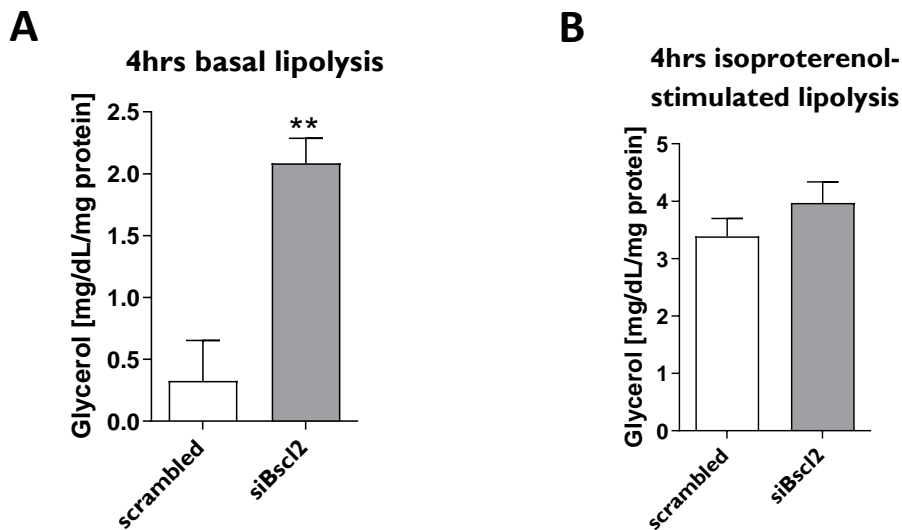
Figure 3.11: Increased basal but not stimulated lipolysis in SGBS adipocytes following seipin inhibition. *SGBS cells were transfected with a control siRNA (scrambled) or a siRNA targeting BSCL2 (siBSCL2) two days prior and at day 0 of differentiation. Lipolysis assays were performed on mature adipocytes after 12 days of differentiation with rosiglitazone. (**A**) Basal lipolysis. (**B**) 1 μM isoproterenol-stimulated lipolysis (number of experimental replicates: n=4). Glycerol content was normalised to cellular protein content. Presented graphs are representative of three independent experiments. Data are expressed as mean ± SEM. Student's t-test: **p<0.01.*

Chen *et al.* have shown that the enhanced basal lipolysis observed in differentiating Bscl2^{-/-} MEFs was associated with an upregulation of perilipin 2 (Plin2) protein (152). Given this report and the striking large LD phenotype I have observed in our seipin-deficient SGBS cells, I chose to examine the mRNA levels of members of the perilipin family in these cells. *PLIN1* transcripts were expressed at similar levels in control and seipin-deficient SGBS cells (***Figure 3.12, A***).

Interestingly, a statistically significant increase in *PLIN2* mRNA expression was observed in seipin knocked-down SGBS cells when compared to controls (***Figure 3.12, B***). This upregulation was not observed in AGPAT2 knockdown SGBS cells (***Figure 3.12, B***). In the absence of seipin, the expression of the other perilipins (PLIN3-5) was reduced (***Figure 3.12, C-E***) although this was only statistically significant for *PLIN4* mRNA levels (***Figure 3.12, D***).
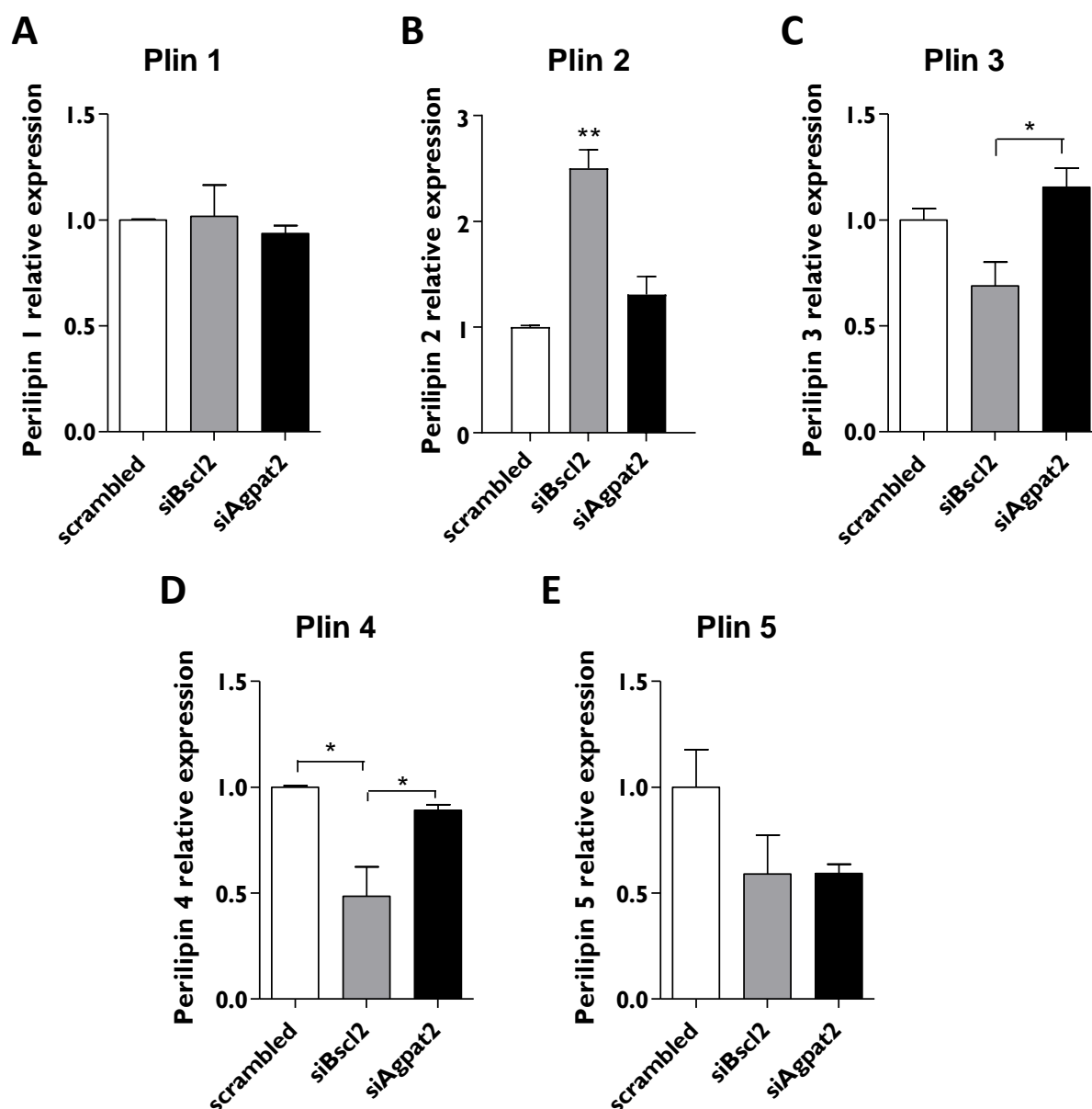
Figure 3.12: Perilipin 2 expression is increased in differentiated seipin knocked-down SGBS cells. *SGBS cells were transfected with a control siRNA (scrambled), a siRNA targeting BSCL2 (siBSCL2) or a siRNA targeting AGPAT2 (AGPAT2) two days prior and at day 0 of differentiation. Adipocytes were examined after 12 days of differentiation in the presence of 2 μM rosiglitazone. mRNA relative expression of perilipin 1 (Plin1) (**A**), perilipin 2 (Plin2) (**B**), perilipin 3 (Plin3) (**C**), perilipin 4 (Plin4) (**D**) and perilipin 5 (Plin5) (**E**). Gene expression was normalised to Hprt reference gene (number of experimental replicates: n=5). Data are expressed as mean ± SEM. One-way ANOVA: *p<0.05, **p<0.01.*

Collectively, our data demonstrate that seipin loss increases the rate of basal lipolysis in SGBS cells. A similar phenomenon could be observed in differentiated SVF cells isolated from our seipin knockout mice, consistent with previous work by others. Increased lipolysis was associated with an increase in *PLIN2* and reduction in PLIN4 mRNA expression. Altogether, the SGBS cell line may offer a useful model in which to examine how seipin may influence adipocyte lipolysis (117,152).

3.3. Discussion

BSCL2 was identified as the causative gene for congenital generalised lipodystrophy type 2 two decades ago however, most studies examining the role of the BSCL2 gene product seipin in adipocytes have relied on murine models (85). Although the murine 3T3-L1 preadipocyte cell line is well established and the most frequently used cellular model of white adipocytes, the use of a human *in vitro* model may be of greater relevance in CGL2 disease. In this chapter, I aimed to compare the effects of seipin loss in the SGBS cell line to previous studies performed on murine cells.

During adipocyte differentiation, SGBS cells exhibited a gene expression pattern similar to the one observed in 3T3-L1 cells (350). Others studies reported that SGBS cells closely resemble human primary subcutaneous adipocytes and human primary omental adipocytes in terms of their morphology and the induction of adipocyte-specific genes (360,361). Altogether, these studies supported the use of the SGBS cell line for the study of human adipocyte biology.

The results presented in this chapter are broadly consistent with studies performed in Bscl2$^{-/-}$ MEFs and SVCs. After 12 days of differentiation, abnormally large lipid droplets were observed in SGBS adipocytes lacking seipin. In addition to Bscl2$^{-/-}$ MEFs, this phenotype was also noted in yeast lacking the seipin orthologue Sei1 (154). I found that the aberrant LD morphology in seipin-deficient SGBS adipocytes was associated with an enhanced basal lipolysis rate in these cells. This increased lipolysis was associated with the upregulation of *PLIN2* mRNA. The levels of PLIN2 protein have not been measured in this chapter but will be examined in the future as proteasome degradation plays a major role in PLIN regulation (362). Collectively, our findings are consistent with the observations of Chen *et al.* in regard to the effects of seipin deficiency on lipolysis (152). To the best of our knowledge, our study is the first report of seipin loss consequences on lipolysis in a human adipocyte cell line.

A recent study conducted by our lab and others also found that large lipid droplets were observed when *BSCL2* was ablated from SGBS cells using the CRISPR/CAS9 system (348). However, lipolysis was not investigated in that study. Here, similar defects in LD morphology were observed when Bscl2 expression was silenced with siRNA. Efficient knockdowns of *BSCL2* and also *AGPAT2* were achieved in SGBS cells and maintained for 12 days in culture. This high transfection efficiency further highlights the potential of SGBS cell line as an effective model for the study of CGL. However, one limitation of this chapter is that only one siRNA was used to silence BSCL2 expression in SGBS cells. It will be valuable to confirm these findings with other siRNA targeted against BSCL2 although the consistency with the study cited above using CRISPR/Cas9 makes it unlikely that these are off-target effects.

In the present work, seipin loss did not significantly impair the adipocyte differentiation of SGBS cells regardless of whether they are incubated with the PPARγ agonist rosiglitazone. These results contrast with other published reports from our lab and others using murine preadipocyte cells. Chen *et al.* observed a reduction in the expression of key adipogenic markers when differentiating Bscl2 knockdown 3T3-L1 cells with a standard hormonal cocktail (151). In that same study, addition of the PPARγ agonist pioglitazone to the adipogenic medium rescues this process. In this chapter, I was surprised to observe equivalent adipocyte differentiation of BSCL2 knockdown and control SGBS cells, whether a PPARγ agonist was included in the medium. The discrepancies between the observations of Chen *et al.* and the data obtained in our study may be explained by species selective differences however, the duration of the differentiation process may also be relevant. In this chapter, SGBS cells were considered mature adipocytes after 12 days of incubation with adipogenic medium. While not unilocular, almost all cells exhibited lipid droplets after 12 days when using rosiglitazone. I chose to keep that same time when differentiating cells without rosiglitazone even though both control and BSCL2 knockdown cells had accumulated less lipid droplets (*i.e.* were less differentiated than with rosiglitazone). This is confirmed by the mRNA levels of PPARγ in these cells when compared to levels in rosiglitazone-treated SGBS cells (***Figure 3.2 versus Figure 3.7***). Hence, SGBS cells differentiated in a rosiglitazone-free adipogenic medium may be at an earlier stage of adipogenesis after 12 days but might exhibit clear differences in adipogenic markers at a later time point. If this is the case, our findings would be consistent with previous reports indicating that Bscl2 is not essential for the early stages of differentiation in murine cells but becomes critical as the adipocytes mature (143,151). Therefore, extending the length of the differentiation process in some of our experiments could be valuable in determining whether or

not adipogenesis in BSCL2 deficient SGBS cells would eventually fail. Similarly, a more detailed time course of adipocyte differentiation in the absence of rosiglitazone would be beneficial to clearly identify specific stages of differentiation and any defect in seipin deficient SGBS cells.

Another possible explanation for not observing major defect in adipogenesis upon seipin loss in our model could arise from the brown characteristics of SGBS adipocytes. Although SGBS cells are widely used as a representative model of white preadipocytes, several reports have noted a gene expression signature with features of brown adipocytes in these cells. Guennoun *et al.* have observed a transient expression of BAT markers such as the uncoupling protein 1 (Ucp1) at day 14 of differentiation (363). This was supported by the work of Yeo *et al.* work who also detected UCP1 mRNA and protein expression in SGBS adipocytes (364). Altogether, despite the white adipose tissue origin of SGBS cells, it would appear that these cells can nevertheless shift towards a brown/beige phenotype. Given that seipin is not required for brown adipogenesis (365), it is possible that adipocyte differentiation occurred in seipin-deficient SGBS cells by engaging pathways of brown adipogenesis.

In summary, this present work highlights the relevance of the SGBS cell line for the study of CGL2 and more broadly human adipocyte biology. For the first time, the data presented in this chapter directly compares the effects of seipin loss observed in both human and murine preadipocyte cell models undergoing adipogenesis and in mature adipocytes. As seipin loss did not significantly affect adipogenesis in SGBS cells, they may be of limited value in examining seipin's role in this process but should encourage subsequent studies to determine whether human adipocyte differentiation absolutely requires seipin. Regardless, the data presented do strongly support the use of this cellular model for future molecular studies to define the functions of seipin in lipid droplet regulation and lipolysis in human adipocytes.

CHAPTER 4

4. Effect of myeloid Bscl2 deficiency on the immune response in congenital generalised lipodystrophy

4.1. Introduction

The state of Rio Grande do Norte in Brazil has one of the highest rates of BSCL prevalence in the world due to a founder effect. A recent study has examined death certificates and medical records of BSCL2 patients from this region, in order to evaluate the life expectancy and cause of death (86). The authors identified that twenty BSCL patients had died between 1997 and 2017 and that premature death decreased the patient's lifespan by more than thirty years. One third of these patients died as a result of liver disease and its complications, which is not unexpected due to the severe metabolic dysfunction that arises due to generalised lipodystrophy in this condition (See Chapter 5). However, this study also revealed that one third of these patients had died as a result of infectious diseases.

In 2014, Liu et al. have reported an infiltration of macrophages and inflammation in adipose tissue of adipose-specific seipin knockout mice (366). I have also shown the presence of macrophages in the pancreatic islets of our older SKO mice (see Chapter 5). Pathogen phagocytosis by macrophages and progression and maturation of pathogen-containing phagosomes, a crucial event for destruction of the pathogen, occurs in parallel with formation of lipid droplets. Seipin has been shown to play important, evolutionarily conserved roles in lipid droplet biogenesis and dynamics in multiple cell types and species from yeast to man (367). Within immune cells, lipid droplets synthesize and store inflammatory mediators and are considered structural markers of inflammation (368). Interaction of lipid droplets with pathogen-containing phagosomes has increasingly been reported in response to infections and may contribute to destruction or survival of the microorganisms within host cells (369). Via altering lipid droplet function, seipin could play an important role in the capacity of macrophages to respond appropriately to infections. To test this hypothesis, we ablated *Bscl2* specifically within the myeloid cell lineage (monocytes, mature macrophages and granulocytes) using the LysM Cre mouse line and characterised the innate immune response in this novel mouse model. In addition, I confirmed our findings in bone marrow derived macrophages isolated from a global seipin knockout mouse model.

4.2. Results

4.2.1. Disruption of *Bscl2* in the myeloid lineage does not cause lipodystrophy or metabolic dysfunction

In order to investigate the role of seipin deficiency in macrophages function, I used a previously described mouse model generated from Bscl2[tm1a(EUCOMM)Hmgu] ES cells in which exons 5-7 of the *Bscl2* gene are flanked by LoxP sites (***Figure 4.1, A***) (337). Bscl2[(fl/fl)] mice were crossed with Bscl2[(fl/wt)] mice expressing Cre recombinase under the control of the endogenous Lyz2 promoter (***Figure 4.1, B***) to generate myeloid-specific *Bscl2* knockout mice (LysM-B2 KO mice). Analysis of multiple tissues including gonadal white adipose tissue (gWAT), brown adipose tissue (BAT), liver, spleen, and bone-marrow-derived macrophages (BMDM) revealed that *Bscl2* mRNA levels were readily detectable in BMDM from control mice and similar to the level observed in gWAT (***Figure 4.1, C***). qPCR analysis showed that Bscl2 mRNA expression was significantly reduced in BMDM from LysM-B2KO mice while remaining unaltered in BAT, liver, and spleen. A significant increase in Bscl2 mRNA expression was however observed in gWAT from LysM-B2KO mice (***Figure 4.1, C***).
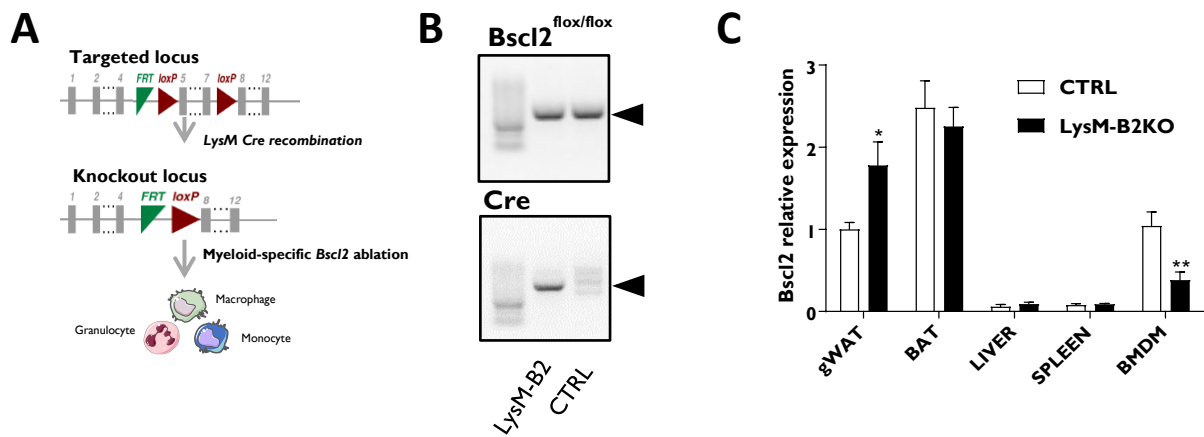
Figure 4.1: ***Generation of LysM-B2KO mice*** (***A***) *Targeting strategy for the conditional disruption of the Bscl2 gene in the myeloid lineage. (**B**) Genotyping analysis by PCR of control (CTRL) and LysM-B2KO mice. (**C**) Bscl2 mRNA expression across different tissues and bone marrow derived macrophages (BMDM) of control (CTRL) and LysM-B2KO male and female mice relative to 18S gene (n=6). Data are presented as mean ± SEM, *p<0.05, **p<0.01.*

The characterisation of male and female LysM-B2KO mice revealed no significant differences in body weight when compared to littermate controls (***Figure 4.2, A/B***). Similarly, echo-MRI analysis revealed that LysM-B2KO and control mice were not significantly different regarding fat mass (***Figure 4.2, C/D***) and lean mass (***Figure 4.2, E/F***) percentages up to 32 weeks of age. The glucose tolerance tests performed in 24-week-old mice showed no signs of glucose intolerance from both male (***Figure 4.2, G***) and female (***Figure 4.2, H***) LysM-B2KO mice. Overall, these findings revealed that specific disruption of *Bscl2* in the myeloid lineage does not lead to clinical features commonly observed in CGL2 patients and global *Bscl2* knockout mice. Therefore, by not displaying any metabolic disorders, this mouse model will allow us to study the direct effect of *Bscl2* disruption in the myeloid lineage.
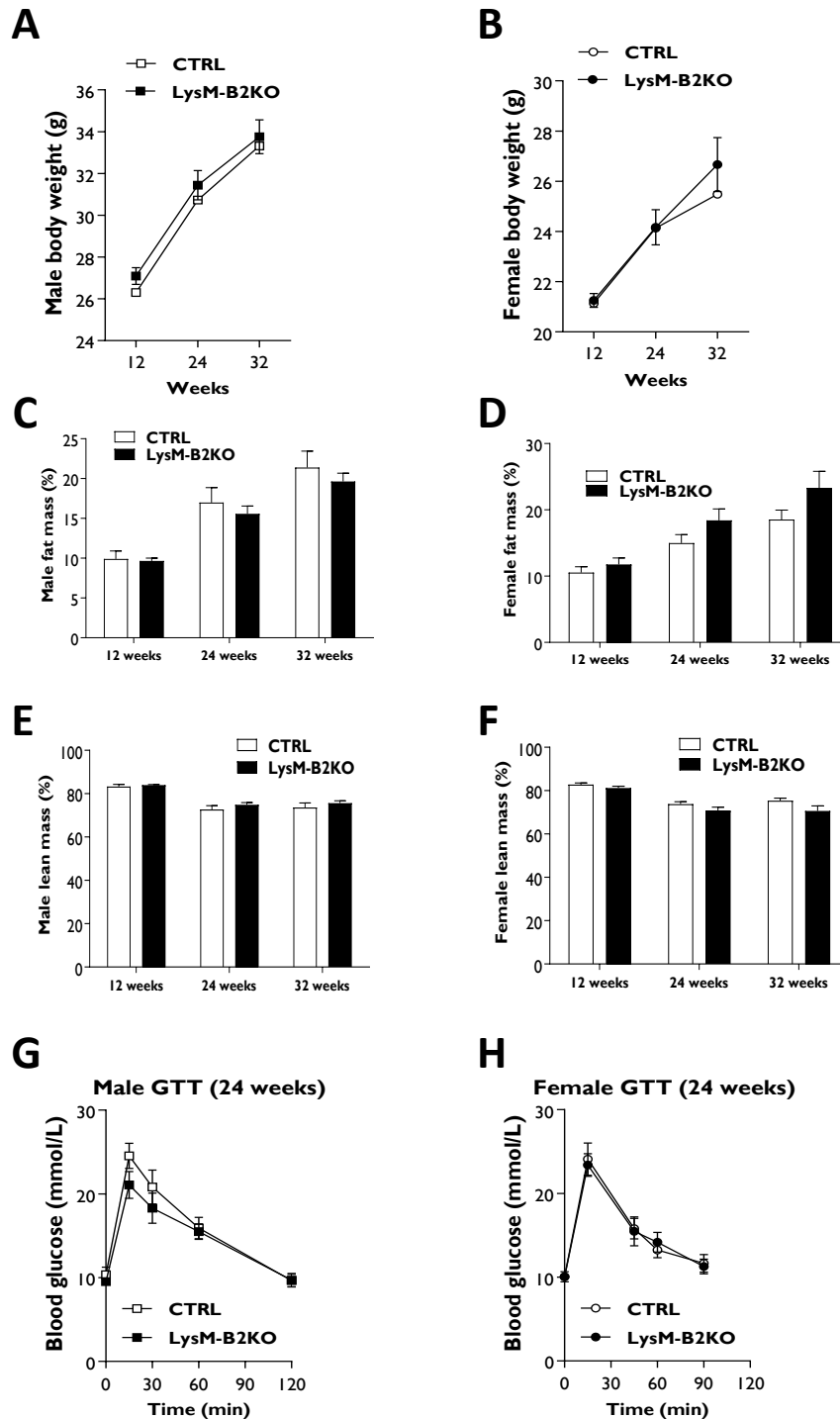
Figure 4.2*: **Characterisation of LysM-B2KO mice.** Male and female body weight (**A-B**), male and female fat mass (**C-D**), male and female lean mass (**E-F**) and male and female glucose tolerance (**G-H**) of control (CTRL) and LysM-B2KO mice at 12, 24 or 32 weeks of age as indicated (female n=6-7, male n=7-10). Data are presented as mean ± SEM. Two-way ANOVA with Bonferroni post-hoc test.*

I acknowledge Dr. George D. Mcilroy for performing the echo-MRI imaging and the glucose tolerance tests in LysM-B2KO mice.

4.2.2. Investigating lipopolysaccharide-mediated inflammatory response in LysM-B2KO mice

To assess whether *Bscl2* deficiency plays a role in the inflammatory response to Toll-like receptor 4 (TLR4) activation, LysM-B2KO mice were injected with a sub-lethal dose of lipopolysaccharide (LPS, 1 mg/kg), and their response to the endotoxin was analysed. LPS is the main wall component of Gram-negative bacteria and TLR4 ligand.

To gain insights into consequences of seipin loss on inflammatory response, I performed a serum analysis and examined several parameters. The serum triglyceride levels were unaffected by LPS injections and were equivalent in control and LysM-B2KO mice (***Figure 4.3, A/B***).
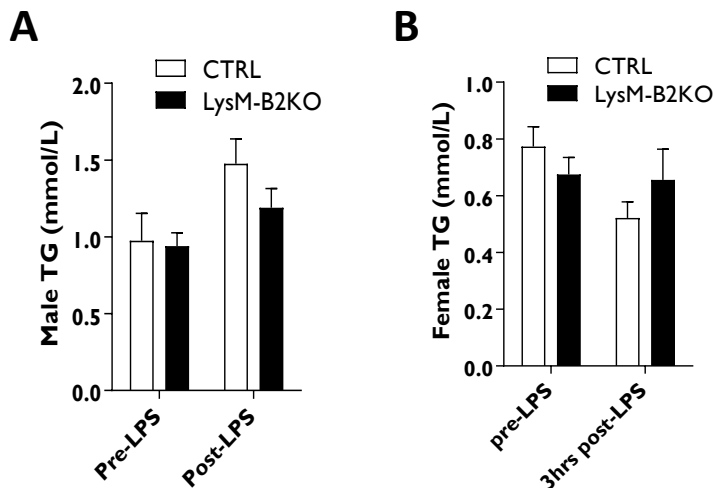
Figure 4.3: Lipopolysaccharides-mediated inflammatory response in LysM-B2KO mice. Analysis of serum triglycerides of male (A) and female (B) control (CTRL) and LysM-B2KO mice fasted for five hours and subjected to LPS treatment. (Female n=6-7, male n=7-10). Data are presented as mean ± SEM, *p<0.05. Abbreviations: TG, triglycerides.

Serum insulin levels were similar in control and LysM-B2KO mice, regardless of LPS administration. Quantitative insulin sensitivity check index (QUICKI) revealed that LysM-B2KO mice were not insulin-resistant when compared to littermate controls following the *in vivo* LPS challenge (***Table 4.1***).

Table 4.10 : *Insulin and quantitative insulin sensitivity check index (QUICKI) analysis of serum in control (CTRL) and LysM-B2KO mice fasted for five hours and subjected to 1 mg/kg LPS for three hours (female n=5-7, male n=7-10). Data are presented as mean ± SEM.*

	Genotype	Male		Female	
		Pre-LPS	Post-LPS	Pre-LPS	Post-LPS
Insulin (µg/L)	CTRL	0.28 ± 0.15	1.75 ± 1.51	0.16 ± 0.03	0.21 ± 0.07
	LysM-B2KO	0.34 ± 0.13	0.99 ± 0.46	0.18 ± 0.11	0.39 ± 0.08
QUICKI	CTRL	0.34 ± 0.03	0.30 ± 0.04	0.36 ± 0.02	0.39 ± 0.04
	LysM-B2KO	0.33 ± 0.02	0.33 ± 0.02	0.37 ± 0.03	0.38 ± 0.02

TLRs present on the surface on macrophages can sense LPS and trigger the synthesis of inflammatory cytokines in order to eliminate the pathogen (370). Levels of both pro- and anti-inflammatory cytokines - known to be secreted after a LPS challenge - were measured in this chapter. LysM-B2KO mice displayed decreased levels of serum TNF-α when compared to controls, although this was not significant (***Table 4.2***). Circulating IL-10 levels showed greater fluctuations among males and females following LPS injection, without being significant (***Table 4.2***). IL-6 and MCP1 levels were considerably elevated following LPS administration and could not be accurately quantified (***Table 4.2***). Taken together, our data indicate that LysM-B2KO mice responded to *in vivo* LPS challenge in a similar manner as their littermate counterparts.

Table 4.11 : *Cytokine multiplex analysis of serum in LysM-B2KO mice fasted for five hours and subjected to 1mg/kg LPS for three hours (female n=5-7, male n=7-10). Data are presented as mean ± SEM, *p<0.05. #Out-of-range values.*

	Genotype	Male	Female
IL-10 (pg/mL)	CTRL	453.91 ± 104.65	561.13 ± 113.92
	LysM-B2	404.87 ± 114.11	865.17 ± 408.16
TNF-α (pg/mL)	CTRL	390.78 ± 68.26	394.17 ± 387.63
	LysM-B2	313.94 ± 97.05	200.21 ± 107.88
IL-6 (pg/mL)	CTRL	>15500[#]	>15500[#]
	LysM-B2	14509[#]	13600[#]
MCP-1 (pg/mL)	CTRL	>1350[#]	>1350[#]
	LysM-B2	>1350[#]	>1350[#]

4.2.3.   Evaluation of cytokine gene expression in the spleen from LysM-B2KO mice

Besides its roles in haematopoiesis and clearing erythrocytes, the spleen participates actively in the immune system (371). To elucidate whether circulating cytokine levels correlate with splenic mRNA levels, mRNA expression of several cytokines was evaluated in the spleen of LysM-B2KO mice using qPCR. mRNA expression levels of proinflammatory cytokines including *Tnf-α*, *Il-6*, *Il-1β* and *Il-1α* were equivalent in male and female mice, regardless of the genotype (***Figure 4.4, A-D***). A significant increase in anti-inflammatory *Il-10* mRNA levels was observed in the spleen from LysM-B2KO male mice (***Figure 4.4, E***) but not from female mice (***Figure 4.4, F***).
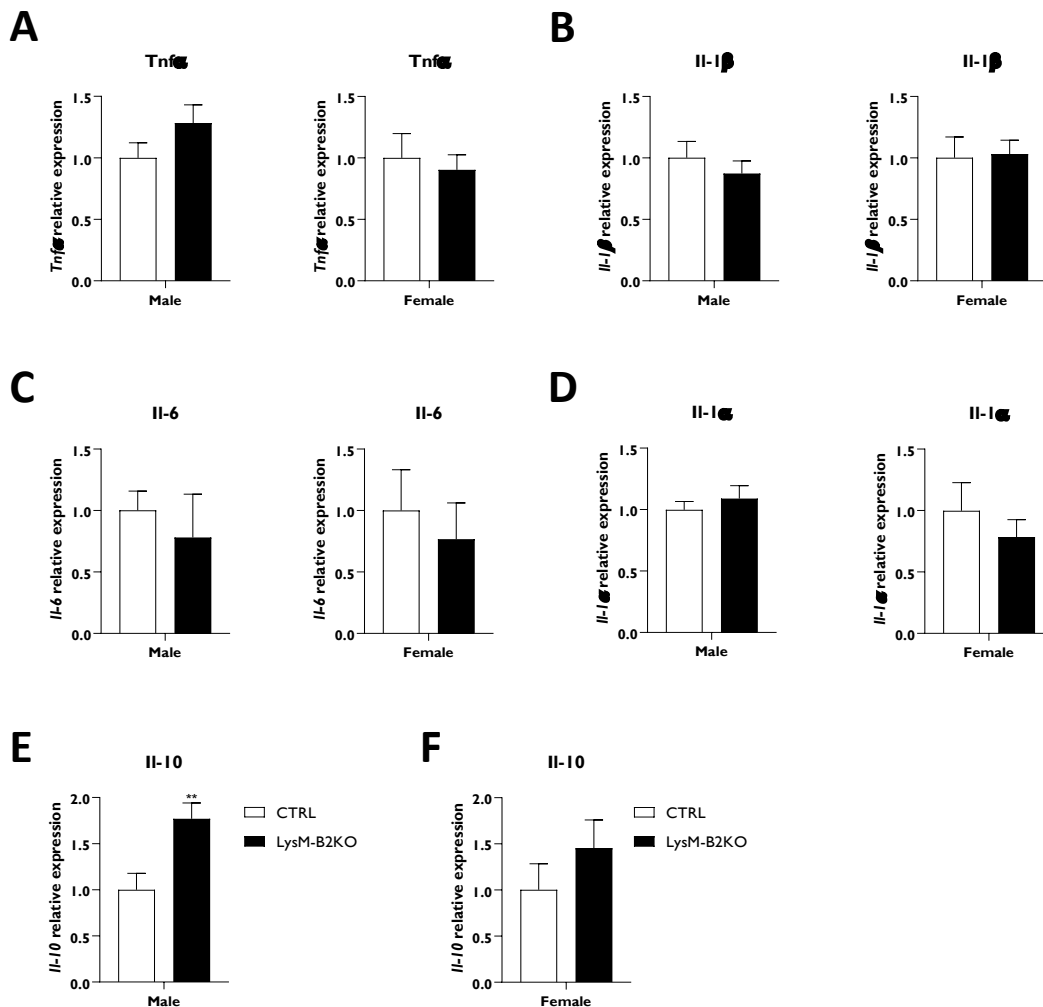
Figure 4.4*: **Cytokine genes expression in the spleen of control and LysM-B2KO mice.** mRNA levels of Tnfα (**A**), Il-1β (**B**), Il-6 (**C**), Il-1α (**D**) and Il-10 (**E/F**) from the spleen of male and female control (CTRL) and LysM-B2KO mice (female n=6-7, male n=7-10). Gene expression was normalised to three reference genes (Nono, Yhwaz and Hprt). Data are presented as mean ± SEM, **p<0.01.*

4.2.4. LysM-B2KO macrophages acute inflammatory response to LPS

To further investigate the role of *Bscl2* in the inflammatory process, BMDM were isolated from male and female control and LysM-B2KO mice. As expected, both male and female LysM-B2KO mice exhibited reduced Bscl2 mRNA expression. *Bscl2* deletion efficiency in BMDMs was estimated at around 48 % and 78 % in male and female LysM-B2KO mice, respectively (***Figure 4.5, A/B***). However, no change in the expression of proinflammatory (*Tnfα*, *Il-6*, *Il-1β*) or anti-inflammatory cytokines (*Il-10*) was observed in the seipin-deficient cells (***Figure 4.5, A/B***).
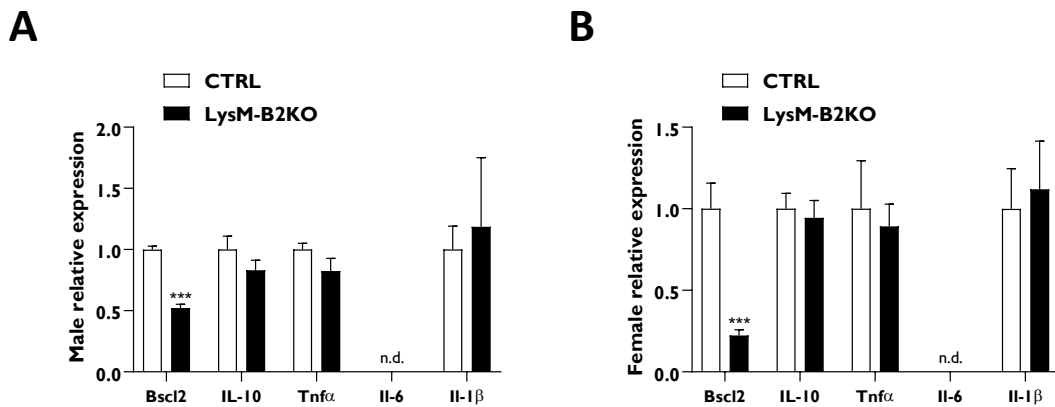
Figure 4.5*: **Bone-marrow derived macrophages of control and LysM-B2KO mice.** Basal mRNA levels of cytokines in BMDM isolated from male (**A**) and female (**B**) control (CTRL) and LysM-B2KO mice (female n=5-7, male n=7-10). Gene expression was normalised to three reference genes (Nono, Yhwaz and Hprt). Data are presented as mean ± SEM, ***p<0.001.*

BMDM from female LysM-B2KO mice exhibited a more robust reduction in Bscl2 mRNA than corresponding males. Therefore, I focussed on BMDM from female control and LysM-B2KO mice and examined the effect of stimulation with 50 or 100 ng/mL LPS for four hours. Interestingly, *Bscl2* mRNA expression was significantly reduced upon stimulation with LPS, even at the lower dose (***Figure 4.6, A***). CD68 and F4/80, as frequently used murine macrophages markers, were examined to characterise LysM-B2KO BMDM. CD68 mRNA expression was not induced upon exposure to LPS but was equivalent between control and LysM-B2KO mice (***Figure 4.6, B***). F4/80 expression was increased by the stimulation with LPS, at both 50 and 100 ng/mL doses but did not differ between genotypes (***Figure 4.6, C***).
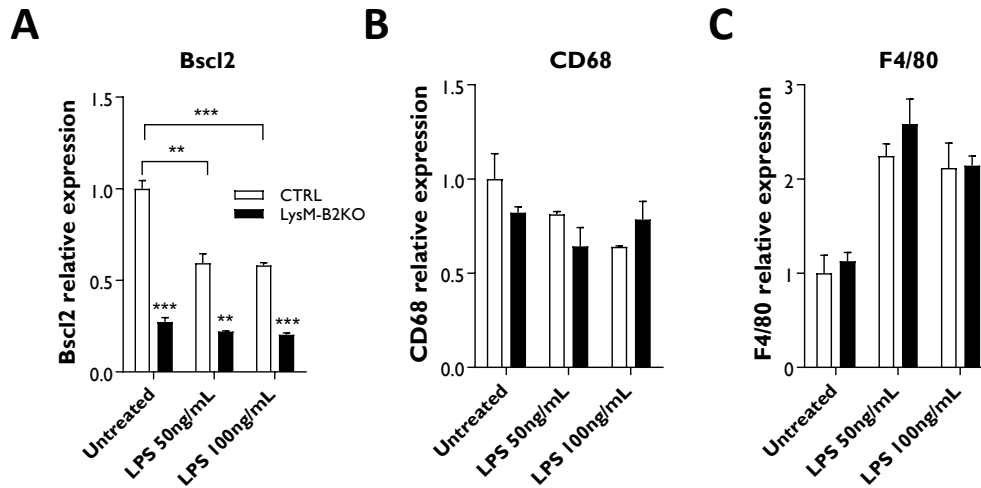
Figure 4.6*: **Lipopolysaccharides-mediated inflammatory response in bone-marrow derived macrophages of female LysM-B2KO mice.** mRNA relative expression of Bscl2 (**A**), CD68 (**B**) and F4/80 (**C**) of female BMDM treated with 50 ng/mL or 100 ng/mL LPS for four hours (n=3). Gene expression was normalised to three reference genes (Nono, Yhwaz and Hprt). Data are presented as mean ± SEM, **p<0.01, ***p<0.001.*

Similarly, the induction of *Mcp1*, *iNos*, *Tnfα*, *Il-6*, *Il-1α*, *Il-1β* and *Il-10* was unchanged by the loss of seipin in LysM-B2KO BMDM from female mice (***Figure 4.7, A-F***), although the induction of *Il-1α* was modestly but significantly greater (***Figure 4.7, G***). Collectively, these results did not identify *Bscl2* as a critical regulator in macrophage function during LPS-induced inflammatory response.
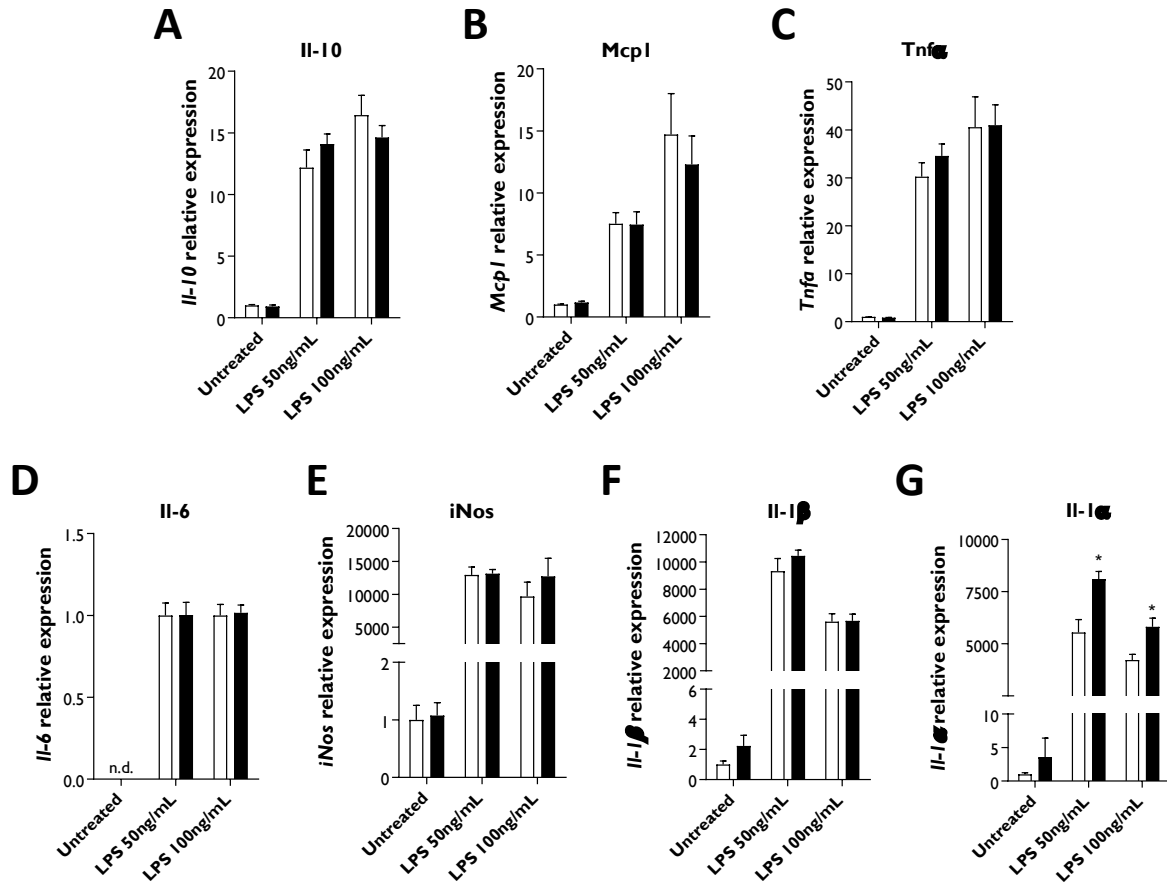
Figure 4.7*: **Lipopolysaccharides-mediated inflammatory response in bone-marrow derived macrophages of LysM-B2KO mice.** mRNA relative expression of Il-10 (**A**), Mcp1 (**B**), Tnfα (**C**), Il-6 (**D**), iNos (**E**), Il-1β (**F**) and Il-1α (**G**) of female BMDM treated with 50 ng/mL or 100 ng/mL LPS for four hours (n=3-6). Gene expression was normalised to three reference genes (Nono, Yhwaz and Hprt). Data are presented as mean ± SEM, *p<0.05.*

## 4.2.5. Seipin knockout macrophages acute inflammatory response to LPS

BMDM isolated from LysM-B2KO mice show significantly reduced but still clearly detectable levels of *Bscl2* expression (***Figure 4.5, A/B***). While this might be due to the presence of non-macrophages cells that do not express the LysMCre promoter, it can also arise from an incomplete LysMCre-mediated recombination, a phenomenon reported before (372). Due to the unavailability of efficient murine antibodies for western blots, I was unable to accurately determine the resulting seipin protein levels. To rule out the possibility that *Bscl2* effects were not being observed due to the remaining expression of *Bscl2* in LysM-B2KO macrophages, I next examined the innate immune response in macrophages isolated from global Bscl2

knockout (SKO) mice to evaluate the effect of a complete Bscl2 deletion in this cell type. These mice were generated as shown schematically in the methods section (see 2.1.3). The *Bscl2* expression was decreased by more than 98 % in female SKO BMDM when compared to control BMDM (***Figure 4.8, A***). However, similar to observations in LysM-B2KO mice, the basal and LPS-induced expression of pro and anti-inflammatory cytokines was not significantly different between the control and SKO BMDM (***Figure 4.8, B-H***).

Figure 4.8*: **Lipopolysaccharides-mediated inflammatory response in female bone-marrow derived macrophages of wild-type and SKO mice.** mRNA relative expression of Bscl2 (**A**), Tnfα (**B**), Il-6 (**C**), Il-1β (**D**), Mcp1 (**E**), Il-10 (**F**), iNos (**G**) and Il-1α (**H**) of female BMDM treated with 100 ng/mL LPS for four hours. BMDMs were isolated from wild-type (WT) and seipin-null (SKO) mice (n=3). Gene expression was normalised to three reference genes (Nono, Yhwaz and Hprt). Data are presented as mean ± SEM, **p<0.01, ****p<0.0001, n.d. not detected.*

Additionally, although *Bscl2* expression was not detectable in BMDM from male SKO mice (***Figure 4.9, A***), LPS-mediated production of *Tnf-α*, *Il-6*, *Il-1β*, *Mcp-1*, *Il-10*, *iNos* and *Il-1α* cytokines was not altered in SKO BMDM when compared to controls (***Figure 4.9, B-H***). Taken together, these results clearly demonstrate that similarly to observations in BMDM

isolated from LysM-B2KO mice, Bscl2 is not required for cytokine production during an inflammatory challenge with LPS in SKO BMDM.
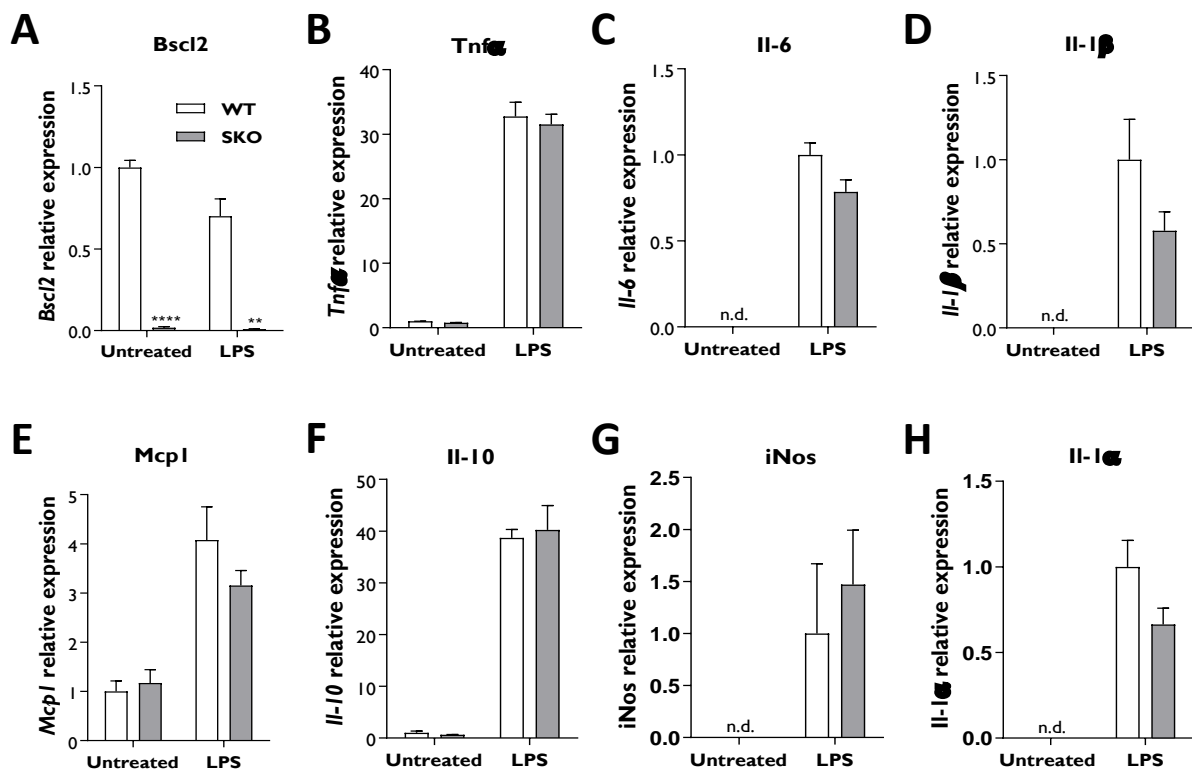

Figure 4.9*: **Lipopolysaccharides-mediated inflammatory response in male bone-marrow derived macrophages of wild-type and SKO mice.** mRNA relative expression of Bscl2 (**A**), Tnfα (**B**), Il-6 (**C**), Il-1β (**D**), Mcp1 (**E**), Il-10 (**F**), iNos (**G**) and Il-1α (**H**) of male BMDM treated with 100 ng/mL LPS for four hours. BMDMs were isolated from wild-type (WT) and seipin-null (SKO) mice (n=3). Gene expression was normalised to three reference genes (Nono, Yhwaz and Hprt). Data are presented as mean ± SEM, n.d. not detected.*

4.2.6. The effect of palmitic acid on inflammatory response in SKO BMDM

Although not observed in the SKO mouse model, hypertriglyceridemia is commonly associated with CGL2 in humans (84). It has been previously shown that fatty acids can activate TLR4, the LPS receptor, and trigger proinflammatory pathways that drive inflammation (373). To investigate whether the high incidence of infections in CGL2 patients could be explained by the activation of proinflammatory pathways by circulating levels of fatty acids, I sought to examine SKO macrophages response to exposure to a saturated fatty acid. To that end, macrophages were cultured for 18 hours with 100 μM palmitic acid and the mRNA expression levels of several cytokines were evaluated. As expected, palmitic acid induced the expression

of ER stress genes; glucose-regulated protein 78 (GRP78) and activating transcription factor (ATF6β); but to a similar extent in control and SKO macrophages, in both males (***Figure 4.10, A/B***) or females (***Figure 4.10, C/D***).
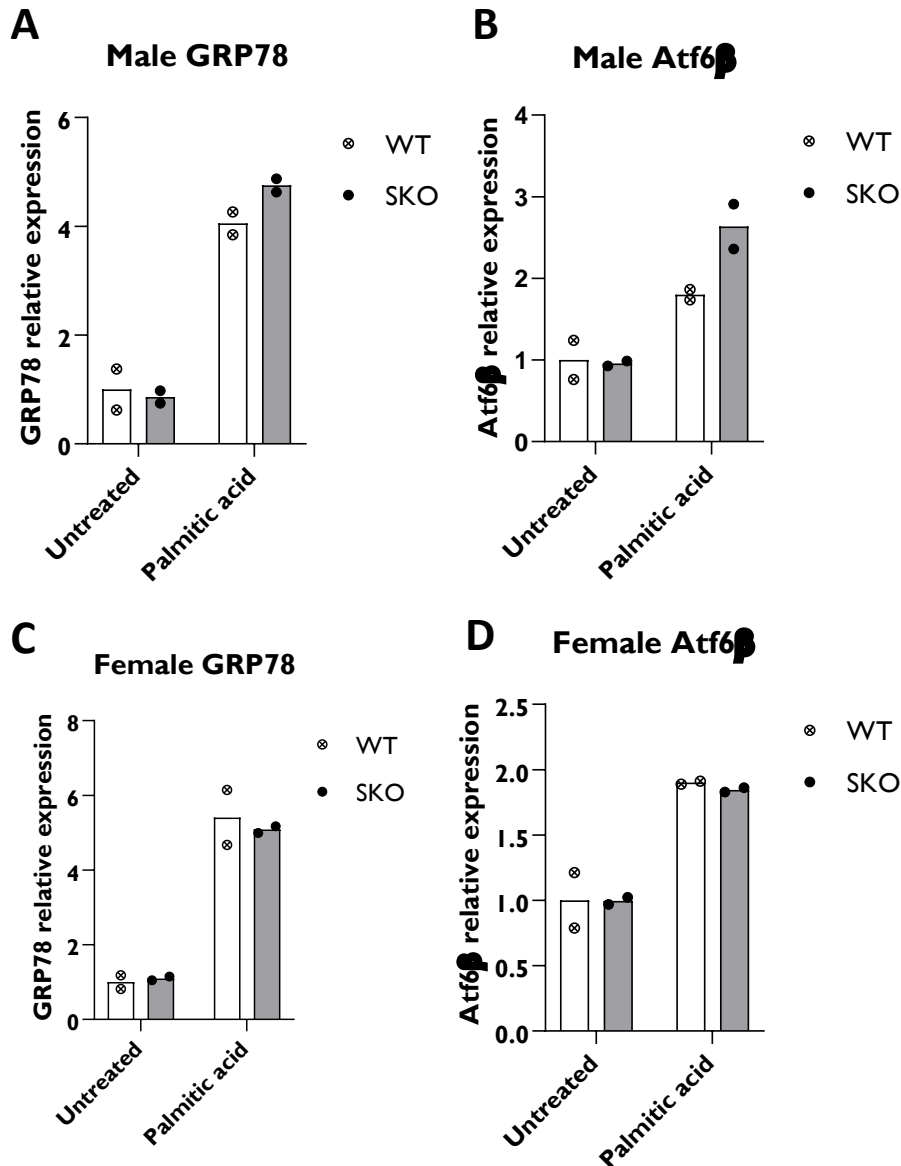
Figure 4.10: Palmitic acid induces ER stress in bone-marrow derived macrophages. *mRNA relative expression of GRP78 in male (**A**) and female (**C**) and Atf6β in male (**B**) and female (**D**) BMDM treated for 18 hours with 100 μM palmitic acid. BMDMs were isolated from wild-type (WT) and seipin-null (SKO) mice (n=2). Gene expression was normalised to three reference genes (Nono, Yhwaz and Hprt). Data are presented as scatter plots with mean.*

The induction of *Tnfα* by palmitic acid was modestly lower in male SKO BMDMs (***Figure 4.11, A***). Il-6 expression followed the same pattern (***Figure 4.11, B***). There was a trend toward

an augmentation of Il-10 expression in SKO BMDMs when compared to controls (***Figure 4.11, C***). Interestingly, *Mcp-1* mRNA expression was enhanced in male SKO macrophages when compared to palmitic acid-treated controls (***Figure 4.11, D***). I acknowledge that a low n number was used for these experiments so all these data should be taken as pilot, indicative.
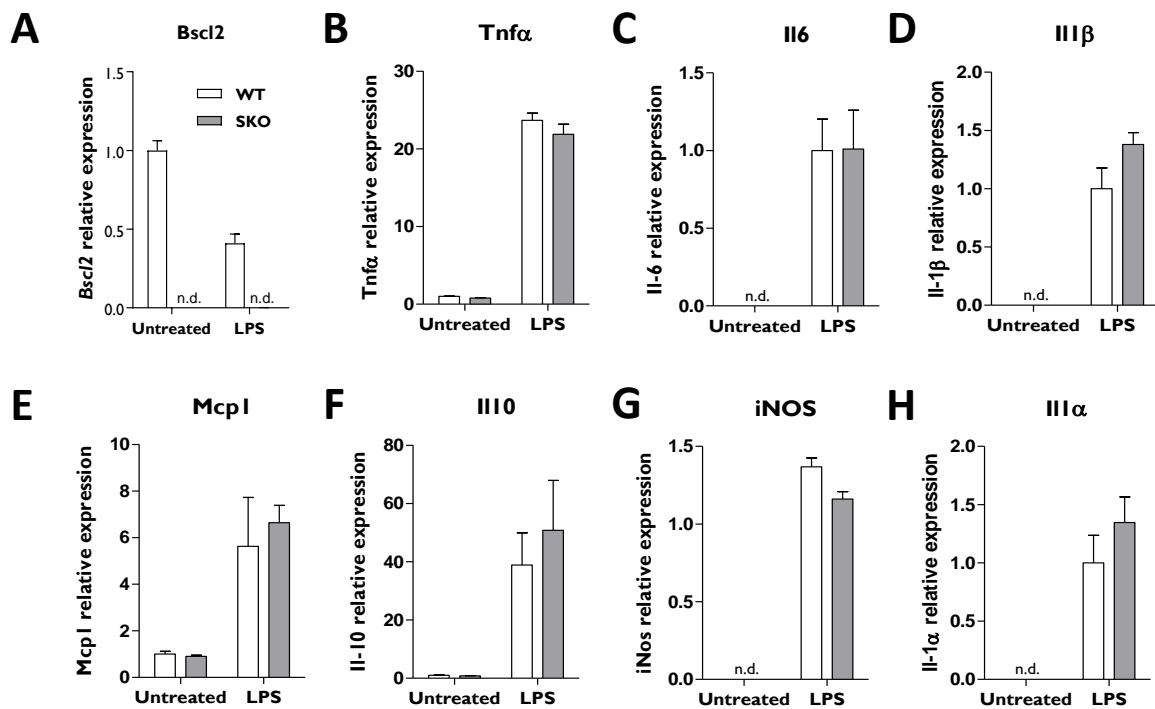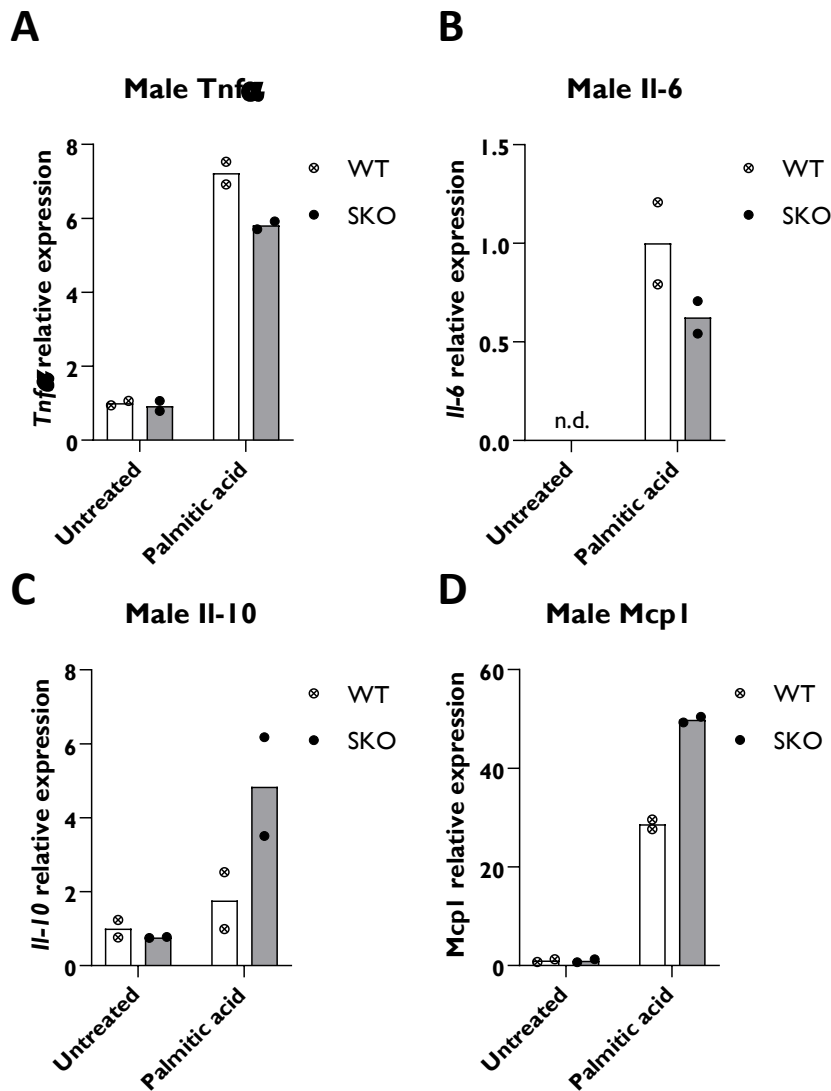

Figure 4.11*: **Palmitic acid-mediated inflammatory response in male bone-marrow derived macrophages from wild-type and SKO mice.** mRNA relative expression of Tnfα (**A**), Il-6 (**B**), Il-10 (**C**) and Mcp1 (**D**) of male BMDM treated for 18 hours with 100 μM palmitic acid. BMDMs were isolated from wild-type (WT) and seipin-null (SKO) mice (n=2). Gene expression was normalised to three reference genes (Nono, Yhwaz and Hprt). Data are presented as scatter plots with mean, n.d. not detected.*

Tnfα induction was equivalent in female macrophages, with no effect of the genotype (***Figure 4.12, A***). Although clearly activated upon exposure with palmitic acid, *Il-6* mRNA expression

was induced to a lesser extent in female SKO macrophages in comparison with controls (***Figure 4.12, B***). *Il-10* expression followed the same pattern as *Il-6* (***Figure 4.12, C***). Similar to observations made in male SKO BMDM, *Mcp-1* expression was greatly increased in female treated SKO BMDMs when compared to controls (***Figure 4.12, D***).
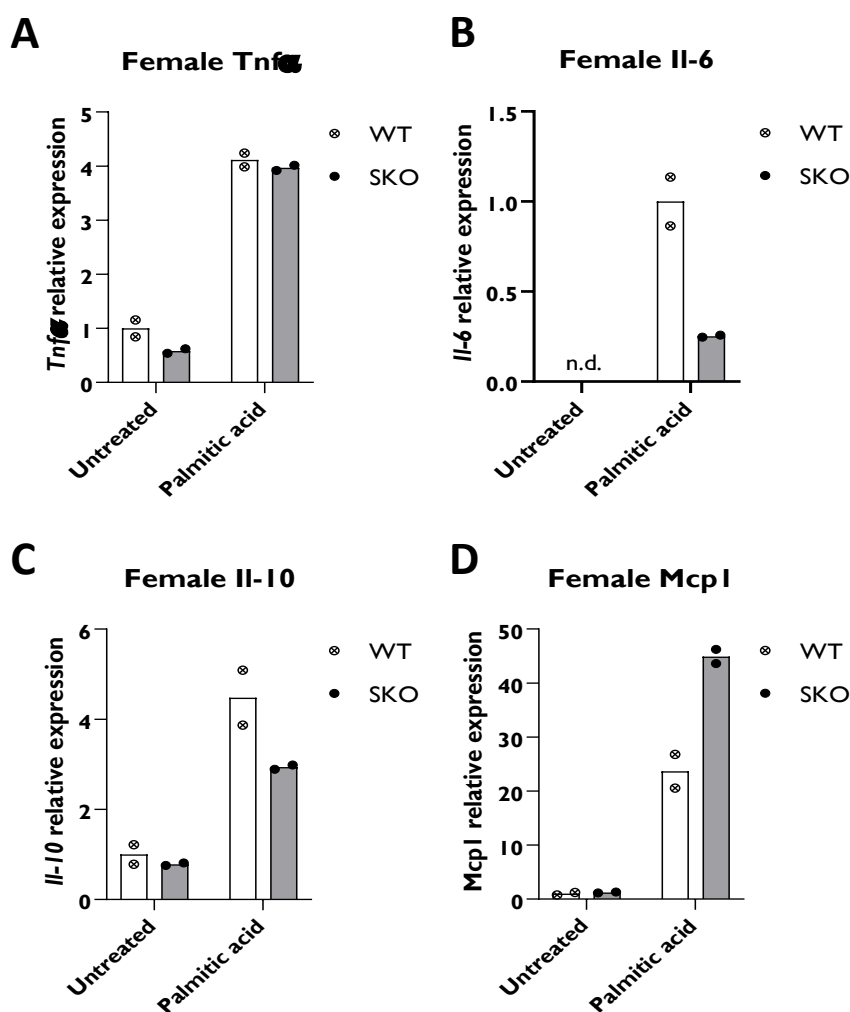

***Figure 4.12**: **Palmitic acid -mediated inflammatory response in female bone-marrow derived macrophages from wild-type and SKO mice.** mRNA relative expression of Tnfα (**A**), Il-6 (**B**), Il-10 (**C**) and Mcp1 (**D**) of female BMDM treated for 18 hours with 100 μM palmitic acid. BMDMs were isolated from wild-type (WT) and seipin-null (SKO) mice (n=2). Gene expression was normalised to three reference genes (Nono, Yhwaz and Hprt). Data are presented as scatter plots with mean, n.d. non detected.*

Collectively, if appropriately powered, this study could reveal that seipin influences the inflammatory response activated by saturated fatty acids in macrophages. However, the increase in *Mcp-1* expression upon exposure to palmitic acid, which was apparent in both male and female, might also suggest that seipin-deficient cells may have a better ability to recruit macrophages to the site of inflammation, potentially exacerbating the inflammation.

4.2.7. Staphylococcus aureus uptake and clearance in SKO macrophages

To limit proliferation and dissemination of pathogens, phagocytes such as macrophages engulf the pathogen into sub-compartments in the cell. After internalization into phagosomes, pathogens are trafficked to lysosomes where they will be enzymatically degraded while generating antigens for the activation of the adaptative immune system. *Staphylococcus aureus* is a commensal gram-positive bacterium but can become an opportunistic pathogen that often causes a wide variety of infections (374). To compare the ability of macrophages to phagocytose a common bacterial pathogen, control and SKO BMDM were infected with *Staphylococcus aureus* SH1000 strain expressing mCherry. 1.5h post-infection, bacteria were internalised into macrophages and found in lysosome-associated membrane protein-1 (LAMP-1) positive vacuoles (***Figure 4.13, A***). Sixty to seventy percent of intracellular *S. aureus* were found to colocalise with LAMP-1 vacuoles in both control and SKO macrophages (***Figure 4.13, B***). This reveals that SKO macrophages can efficiently engulf bacteria and that *S. aureus* trafficking into SKO macrophages follows the classical endocytic pathway.
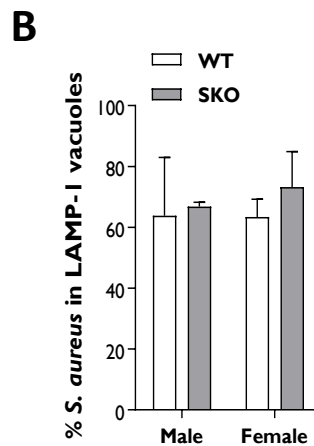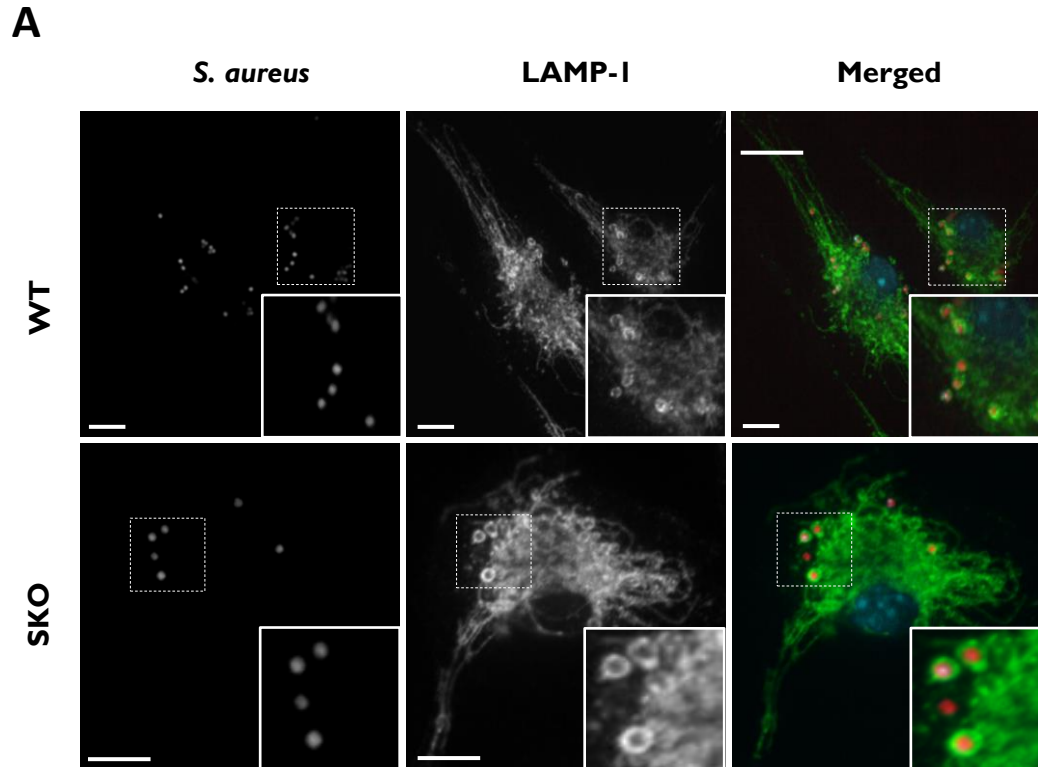
Figure 4.13*: **Staphylococcus aureus uptake in bone marrow derived macrophages from wild-type and SKO mice.** (**A**) Representative confocal micrographs of the LAMP-1 distribution in BMDM infected with S. aureus-mCherry. (Wild-type: WT, seipin-null: SKO). Dotted boxes indicate selected regions magnified in the white boxes. Bars denote 14 μm. (**B**) Quantification of the LAMP-1 association with S. aureus-mCherry (n=6). Data are presented as mean ± SEM.*

To determine whether SKO macrophages could efficiently kill *S. aureus* once internalized, I next examined the intracellular fate of bacteria using a gentamicin protection assay. I found that the number of viable bacteria within both control and SKO macrophages rapidly decreased after internalization. *S. aureus* did not persist in the cell as control and SKO macrophages efficiently clear *S. aureus* from the cell with less than 6 % of viable bacteria remaining 24 hours after infection. Similar results were obtained in both male (***Figure 4.14, A/B***) and female (***Figure 4.14, C/D***) BMDM. Collectively, those results support the idea that the phagocytosis process and killing ability of macrophages are not affected by Bscl2 disruption.
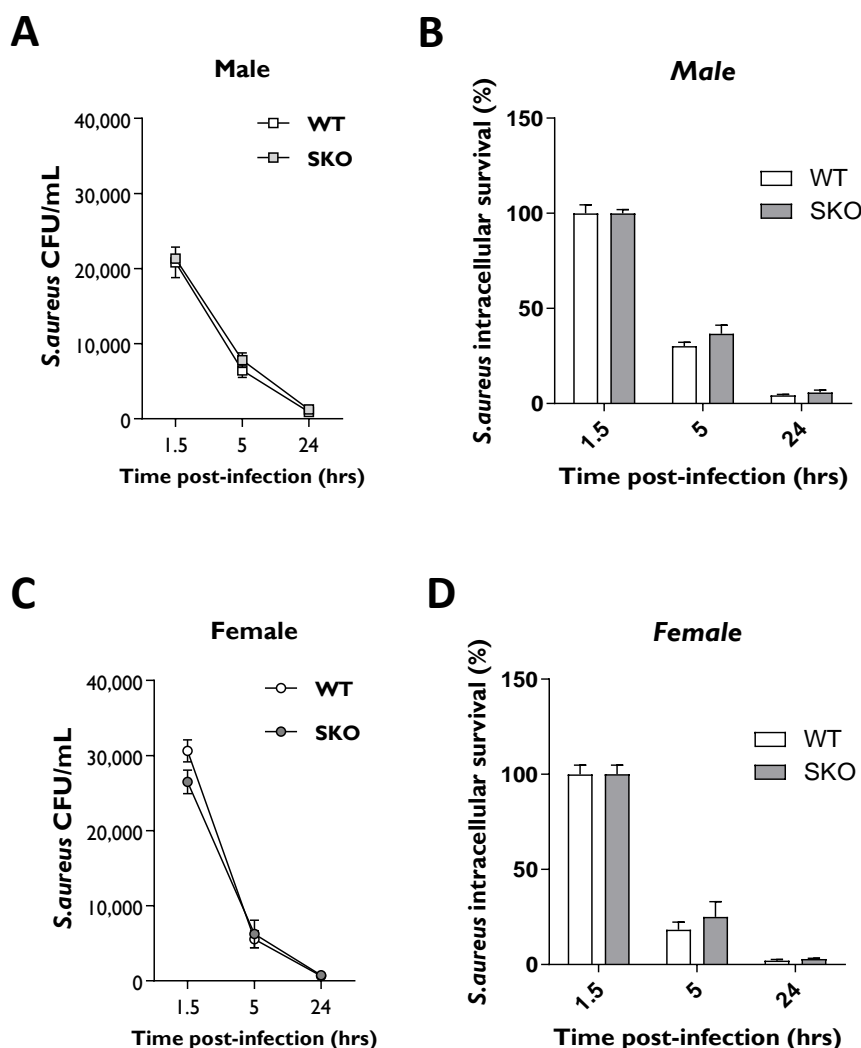
Figure 4.14*: **Staphylococcus aureus clearance in bone marrow derived macrophages from wild-type and SKO mice.** Colony-forming units (CFU) of S. aureus inside male (**A**) and female (**C**) BMDM isolated from wild-type (WT) and sepin-null (SKO) mice. S. aureus intracellular survival inside male (**B**) and female (**D**) BMDM (n=6). Data are presented as mean ± SEM.*

4.3. Discussion

While investigating the causes of death in patients with CGL2, *Jeronimo et al.* found that the majority died of liver disease or infections. Liver diseases can be attributed to the severe metabolic dysfunction that accompanies this disorder. However, it is not clear why infections are linked to *BSCL2* deficiency. This prompted us to examine the role of Bscl2 in the myeloid lineage and to investigate if lacking Bscl2 might lead to higher risks of infection. To date, it is the first study to document consequences of *Bscl2* deficiency in myeloid cells. Bscl2 is widely expressed in the body, and I found that it also appears to be well expressed in bone marrow derived macrophages. To dissect Bscl2 function in macrophages, I utilised the LysMCre-loxP system to delete Bscl2 in the myeloid lineage only. I found that loss of Bscl2 selectively in the myeloid lineage in LysM-B2KO mice does not lead to changes in metabolic health. Therefore, this model is adapted to study the direct role of Bscl2 in the myeloid lineage as mice do not develop metabolic disorders that could indirectly impair immune function. To mimic an acute inflammatory condition *in vivo*, mice were injected with LPS, a potent inducer of inflammatory responses. I found no impairment of the innate immune response in LysM-B2KO mice challenged with endotoxin. Moreover, cultured bone-marrow derived macrophages isolated from LysM-B2KO mice displayed no alteration in LPS-induced inflammatory cytokine responses. Although the LysMCre system has been extensively used in studies of the myeloid lineage, it led to a poor knockdown in our hands. To explain this, we can infer that the lysozyme M promoter was not efficient at targeting all myeloid cells as others have reported before (372). To fully gain an understanding on Bscl2 function in immune response, I pursued my investigation by isolating bone-marrow derived macrophages from seipin knockout mice, ensuring a complete absence of *Bscl2* in macrophages. SKO macrophages showed no impairment in LPS-mediated inflammatory response. Findings in SKO macrophages entirely corroborate data obtained with LysM-B2KO mice and demonstrate that Bscl2 is not involved in LPS-triggered cytokine production in macrophages. Additionally, SKO macrophages were capable of pathogen recognition, engulfment, phagolysosome maturation and clearance when infected with *Staphylococcus aureus*. A lot of the work presented here relies on the use of BMDM and therefore have some limitations. While macrophages are central to the process of inflammation, participating in both innate and adaptative immune responses, they represent a heterogenous population of cells, highly sensitive to the surrounding environment. Only

BMDMs were analysed in this chapter but this study could have benefit from the examination of other macrophages populations.

Overall, our findings provide substantial evidence that *Bscl2* deficiency within macrophages does not directly impair the innate immune response. Therefore, it is unlikely that *BSCL2* deficiency in the myeloid lineage *per se* significantly contributes to increased risk of infection in CGL2 patients. In light of our findings, it would appear that any increased risk of death from infection in CGL2 patients is likely to result secondary to adipose tissue deficiency and the severe metabolic disease observed in this condition. For example, leptin ; whose circulating levels are considerably decreased in SKO mice and CGL2 patients ; is a key regulator of the innate and adaptative immune response (375). BSCL2/seipin deficiency has been shown to induce ER stress (376), a process that has also been implicated in altered innate immunity and myeloid cell dysfunction in type 2 diabetes and atherosclerosis. Moreover, hyperglycaemia and dyslipidaemia have been implicated in impairment of normal innate immune response and macrophage dysfunction in type 2 diabetes (377). Of note, SKO mice are hyperglycaemic but do not display the hypertriglyceridemia observed in BSCL2 patients (see Chapter 5). Seipin has been shown to be involved in lipid droplet biogenesis (164). Similarly, lipid metabolism plays a significant role in macrophages function and infection resolution (378,379). Therefore, I decided to explore the inflammatory response of SKO macrophages to palmitic acid, the most common saturated fatty acid found in the body (380). In the present study, SKO macrophages exposed to palmitic acid displayed various responses with gender differences. Interestingly, the monocyte chemoattractant protein 1 (Mcp1) also known as C-C motif chemokine ligand 2 (CCL2) was more elevated in SKO macrophages challenged with PA in both male and female. As implied by its name, Mcp1 is key chemokine involved in the recruitment of monocytes/macrophages in both immunological surveillance of tissues and in response to inflammatory signals (381). This upregulation in Mcp1 mRNA expression corroborate our observations of macrophages infiltration in pancreatic islets of SKO mice (see Chapter 5). Additionally, Mcp1 has been reported to play a role in the pathogenesis of atherosclerosis, obesity and diabetes (382–384). Taken together, I hypothesise that hyperglycaemia and ectopic fat deposition in SKO mice could lead to the upregulation of Mcp1 and to a chronic low-grade inflammatory state. Therapeutic strategies that could alleviate the chronic inflammatory state might be beneficial to decrease the susceptibility to infection and mortality rate amongst CGL2 patients. Antagonist of Mcp1 receptor (CCR2) might decrease the infiltration of macrophages and lower the inflammation.

In summary, this chapter provides evidence that Bscl2 does not appear to have a critical role in macrophages immune functions. The increased rates of infections among CGL2 patients are likely to be secondary to adipose tissue deficiency and the metabolic disturbances observed in this condition. However, this study does not rule out a role of seipin in macrophages, under certain circumstances in which lipids are highly abundant for example. Defining this would require further work specifically probing these functions.

CHAPTER 5

5. Pancreatic islet adaptation and the metabolic response to adipose insufficiency in a mouse model of severe lipodystrophy

5.1. Introduction

Tight control of insulin release from pancreatic islets and the sensitivity of other tissues to insulin determines overall control condition of circulating glucose in the body. Therefore, the interplay between pancreatic islets, liver and other peripheral organs is a highly controlled process. Pancreatic islets are highly vascularised structures that can sense the environment and respond to external cues including glucose, fatty acids, or amino acids in an appropriate manner. β-cells represent the majority of endocrine cells within the pancreatic islets. They appear as highly adaptative cells able to respond to a wide variety of signals with an adequate insulin secretory response. This plasticity confers them with a remarkable ability to adapt to both physiological and pathological conditions. This is particularly relevant in the case of insulin resistance where β-cells undergo several changes to increase their insulin secretion to maintain normoglycaemia. This process is commonly referred to as compensation. Diabetes usually develops when β-cells no longer cope with that increased insulin demand and fail to compensate further.

To the best of our knowledge, pancreatic islets have never been investigated in congenital generalised lipodystrophy type 2 (CGL2) nor seipin knockout (SKO) mice with the exception of one paper published at the end of 2019 (385). Moreover, most studies were conducted in 12-week-old SKO mice and the comparison with younger or older mice was not performed.

This study was designed to gain a comprehensive understanding of compensatory mechanisms employed by pancreatic islets to counteract hyperglycaemia in SKO mice. To that end, seipin knockout mice were first phenotypically characterised to evaluate the progression of the disease in this model. Morphology, secretory function, and gene expression of SKO mice islets were then analysed to evaluate pancreatic islet adaptation to metabolic requirements in a context of lipodystrophy.

5.2. Results

5.2.1.　　Characterisation of seipin knockout (SKO) mice

Male mice were used to examine the progression of CGL2 in SKO mice in much of the work shown here. However, when possible, female mice were also included in the study (see section 5.2.11). Control and SKO mice were fed a standard chow diet and monitored regularly from 7 to 34 weeks of age. When compared to control mice, male SKO mice had a similar body weight throughout the study (*Figure 5.1, A*). Whole body magnetic resonance imaging revealed significantly reduced fat mass in SKO mice when compared to their littermate controls. This reduction was observed as early as 7 weeks of age, persisted over time, and became more striking in older mice as control mice gain fat mass with age (*Figure 5.1, B/C*). This reduction in fat mass was concomitant with an increase in lean mass (*Figure 5.1, D/E*).
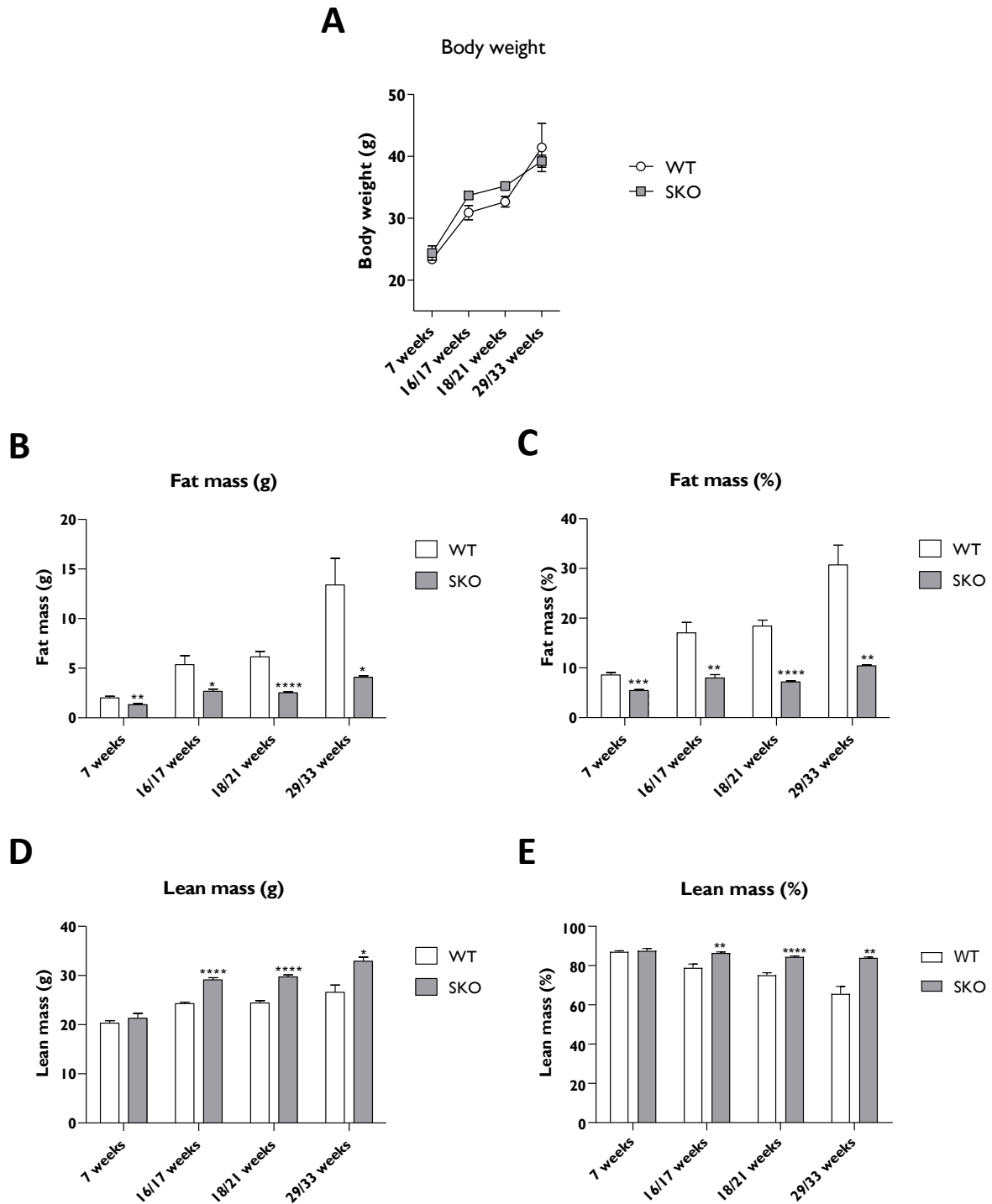
Figure 5.1: Body composition of wild-type and seipin knockout mice. *Body weight in grams (g) (**A**), fat mass in grams (g) (**B**) and as percentage (%) (**C**) and lean mass in grams (g) (**D**) and as percentage (%) (**E**) of male wild-type (WT) and seipin-null (SKO) mice at the ages indicated up to 33 weeks of age. n= 6v5 (7 weeks); 5v5 (16/17 weeks); 17v19 (18/21 weeks); 6v4 (29/33 weeks). Data are expressed as mean ± SEM. *p<0.05, **p<0.01, ***p<0.001, ****p<0.0001.*

I acknowledge Dr. George D. Mcilroy for the echo-MRI imaging of 29/33 weeks of age mice.

To determine if alterations in tissues weight were also present, mice were dissected at the end of the study at 34 weeks of age and organs mass were compared (**Table 5.1**). Fat depots were virtually absent in SKO mice; therefore, the weight of retroperitoneal and gonadal white adipose tissue could not be determined. Brown adipose tissue was almost ten times smaller in SKO mice when compared to littermate controls. The liver was found to be massively enlarged in SKO mice with a 4-fold weight increase when compared to control mice. Additionally, the pancreas was significantly heavier in SKO mice and will be discussed later in section 5.2.4. Liver and pancreas weight gain, together with an increase in heart, kidney (**Table 5.1**) and spleen (data not shown) mass suggested a generalised organomegaly.

***Table 5.12**: Tissues weight comparison between WT and SKO mice at 34 weeks of age*.

Age	30/34 weeks	
Genotype	**WT**	**SKO**
Liver (mg/g)	38,64 ± 7,43	165,31 ± 42,65***
Kidney (mg/g)	8,81 ± 0,91	12,34 ± 0,74***
Heart (mg/g)	4,37 ± 0,60	6,12 ± 0,97*
Testis (mg/g)	5,60 ± 1,47	4,72 ± 0,94
Pancreas (mg/g)	4,97 ± 2,44	10,41 ± 0,89**
BAT (mg/g)	3,92 ± 0,78	0,40 ± 0,16****
rWAT (mg/g)	19,45 ± 5,35	n.d.
gWAT (mg/g)	44,25 ± 14,04	n.d.

*Abbreviations: WT, wild type; SKO, seipin-knockout male mice; BAT, brown adipose tissue; rWAT, retroperitoneal white adipose tissue; gWAT, gonadal white adipose tissue; n.d., not detected. (n=6v4). Tissues weights were normalised to body weight. Values correspond to mean ± S.D. *p<0,05; **p<0,01; ***p<0,001; ****p<0,0001.*

5.2.2.   Hepatic steatosis development in SKO mice

As seen in the previous section, SKO mice exhibit an enlarged liver most likely due to the elevated triglycerides content in this organ (**Table 5.1**). To precisely examine the development of this hepatic steatosis, triglycerides levels were determined in livers collected from 7- to 34-week-old male mice. Triglycerides began to accumulate in the liver of SKO mice

as early as 7 weeks of age although this was not statistically significant. I acknowledge that a low number of mice were used in this 7-week-old group. This low-powered group has a greater chance of not detecting an effect and could have easily missed significant differences. Triglycerides levels markedly escalated at 16 to 17 weeks of age reaching a 15-fold increase when compared to littermate counterparts then plateaued. Despite the lipid accumulation associated with ageing in control mice, triglyceride levels remain more than 2-fold higher in older SKO livers until the end of the study (***Figure 5.2***).
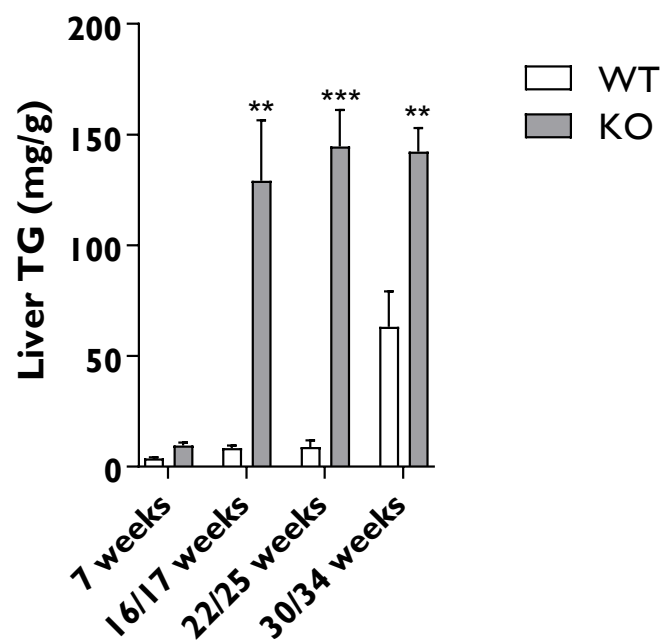
Figure 5.2: ***Hepatic steatosis development in male SKO mice***. *Triglyceride's measurements in livers from male SKO mice up to 34 weeks of age. n= 2v2 (7 weeks); 5v5 (16/17 weeks); 6v5 (22/25 weeks); 6v4 (30/34 weeks). Data are expressed as mean ± SEM, **p<0.01, ***p<0.001.*

To gain more insight into hepatic steatosis progression in SKO mice, I examined liver histologically in young and older mice. To that end, frozen liver sections were stained with Oil red O and hematoxylin to mark lipids in red and nuclei in blue, respectively.

As expected from the triglycerides measurements made in the liver, lipid droplets were clearly visible in SKO mice and at all ages. Large and small vacuoles containing lipids were observed suggesting the presence of both macrovesicular and microvesicular steatosis. However, hepatic steatosis was predominantly macrovesicular in older SKO mice. Extremely small lipid droplets were apparent in WT mice from 22 weeks onwards (***Figure 5.3***).
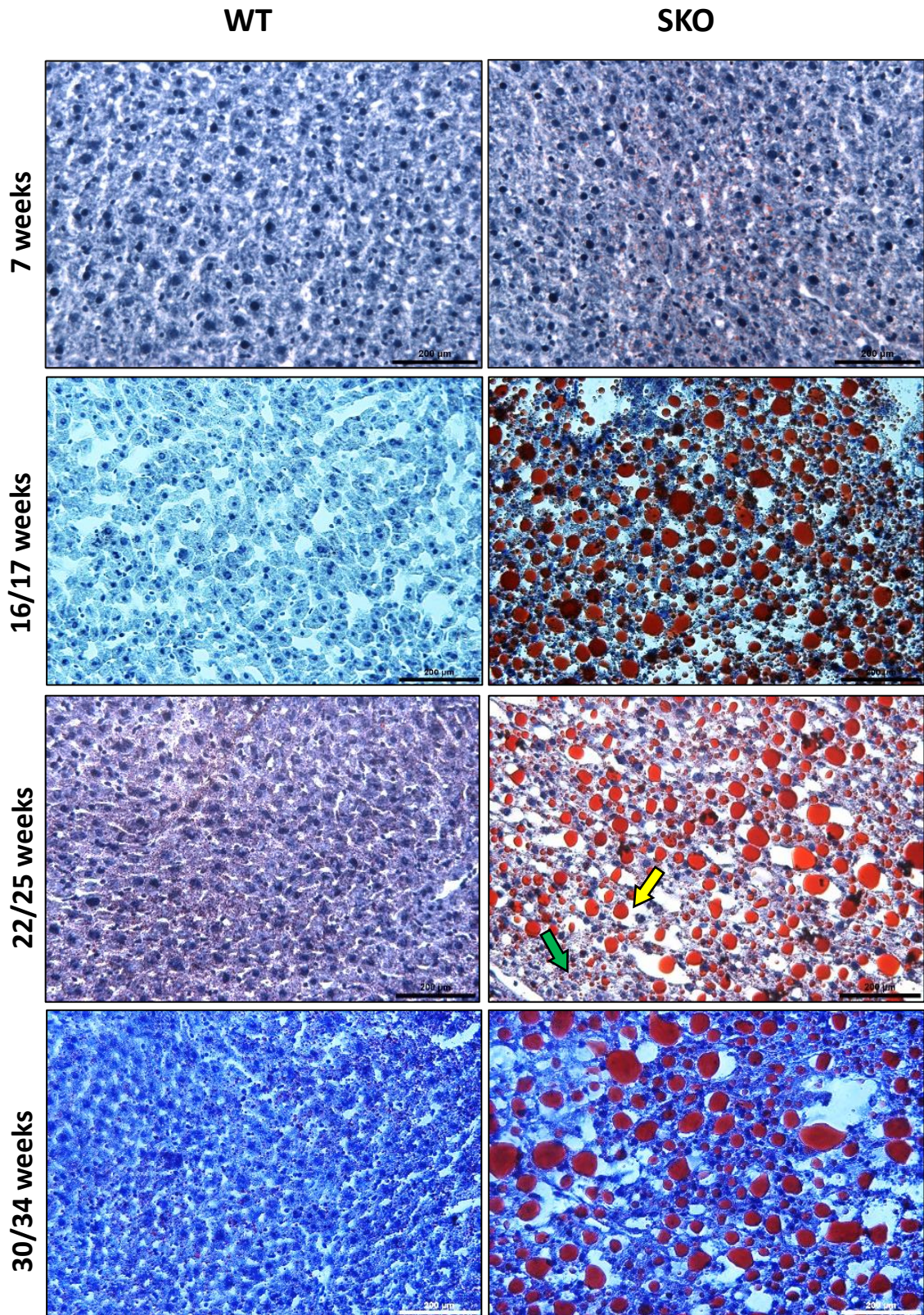
Figure 5.3: Hepatic steatosis development in male SKO mice. *Representative brightfield images of hematoxylin and Oil red O staining of frozen liver tissues from wild-type (WT) and seipin-null (SKO) mice at different ages. N= 6v5 (7 weeks); 5v5 (16/17 weeks); 3v3 (22/25 weeks); 4v4 (30/34 weeks). Bars denote 200 μm. Green and yellow arrows point at micro- and macro-vesicular steatosis, respectively.*

127

Hypertriglyceridemia is a common feature of CGL2 patients (84). However, consistent with observations made by others (386), hypertriglyceridemia was not observed in our SKO model (***Table 5.2***). Fasted triglycerides levels in the serum were found to be significantly decreased in 34-week-old SKO mice (***Table 5.2***). This hypotriglyceridemia most likely results from an increased uptake of triacylglycerol-rich lipoproteins (TRL) and non-esterified fatty acids (NEFA) by the liver. Levels of triglycerides in testis were equivalent in WT and SKO mice and at all ages. Additionally, SKO mice displayed decreased levels of cardiac triglycerides at 16 and 34 weeks of age (***Table 5.2***).

Collectively, our mouse model fully recapitulates previously reported seipin knockout models with a generalised lipoatrophy and hepatic steatosis (117,152,386).

Table 5.13 *: **Triglycerides level comparison between wild-type and SKO mice**.*

Age	7 weeks		16/17 weeks		30/34 weeks	
Genotype	**WT**	**SKO**	**WT**	**SKO**	**WT**	**SKO**
Serum (mg/dL)	102,4 ± 31,32	111,05 ± 52,47	29,87 ± 7,33	37,57 ± 13,54	55,48 ± 13,88	33,28 ± 8,43*
Heart (mg/g)	2,55 ± 0,14	2,22 ± 0,22	3,18 ± 0,27	2,15 ± 0,56**	2,51 ± 0,44	1,54 ± 0,36*
Testis (mg/g)	3,15 ± 0,93	2,68 ± 0,08	2,44 ± 0,69	1,81 ± 0,61	3,51 ± 1,54	1,51 ± 0,37

*Abbreviations: WT, wild type; SKO, seipin-knockout mice; n.d., not detected. n= 2v2 (7 weeks); 5v5 (16/17 weeks); 6v4 (30/34 weeks). Values correspond to mean ± S.D. Asterisks denote significance between WT and SKO mice within the same age group. *p<0,05; **p<0,01.*

5.2.3.   Hyperglycaemia and hyperinsulinemia in SKO mice

Additional features of CGL2 patients include hyperglycaemia and hyperinsulinemia (80). To determine the onset of metabolic disorders in SKO mice, glucose and insulin levels were examined in young and older mice. Fasted glucose levels were maintained at approximately 10 mmol/L in WT mice and did not differ significantly in SKO mice at any of the ages examined (***Figure 5.4, A***). Random-fed glucose levels were equivalent in control and SKO mice at 7 weeks of age. SKO mice displayed elevated glycaemia in the fed state starting from 12 weeks onwards (***Figure 5.4, B***). From previous studies and current observations, hyperglycaemia is believed to have started at around 9 weeks of age (117). Regarding insulinemia, fasted insulin levels were already elevated in 7-week-old SKO mice, and this was statistically significant. In 16/17-week-old SKO mice, insulinemia considerably increased then dropped to levels similar to those seen at 7 weeks of age in 30/34-week-old SKO mice (***Figure***

5.4, C). To assess the extent of insulin resistance, quantitative insulin sensitivity check index (QUICKI) analysis was performed. When compared to littermate controls, QUICKI analysis revealed that SKO mice were already insulin resistant by 7 weeks of age. Measurements made at 16/17 and 30/34 weeks of age indicated that this insulin resistance persisted over time (*Figure 5.4, D*). This was confirmed with the homeostatic model assessment for insulin resistance (HOMA-IR). In accordance with insulin levels, HOMA-IR analysis revealed that insulin resistance peaked at 16/17 weeks and returned to levels seen at 7 weeks of age in 30/34-week-old SKO mice (*Figure 5.4, E*).

In combination with observations made in the preceding section (see 5.2.2), it would appear that livers were less sensitive to insulin in 16/17-week-old SKO mice and that it is most likely due to the lipid deposition in this organ. Hyperglycaemia observed in the fed state, implying impaired glucose uptake by target tissues, occurred in SKO mice from 12 weeks onwards. The observed hyperinsulinemia suggests that in an attempt to lower blood glucose, pancreases released more insulin to counterbalance the decreased glucose elimination. At 30/34 weeks of age, insulin levels drop dramatically but fasting glucose remain within the physiological range. Taken together, these data suggest that SKO mice are still able to secrete enough insulin to correct the circulating glucose levels resulting in an apparent normoglycemia up to 34 weeks of age. However, the dramatic reduction of insulin secretory capacity in 34-week-old SKO mice also implied a progressive loss of the compensatory hyperinsulinemia that is most likely to ultimately lead to diabetes if mice had been aged further.
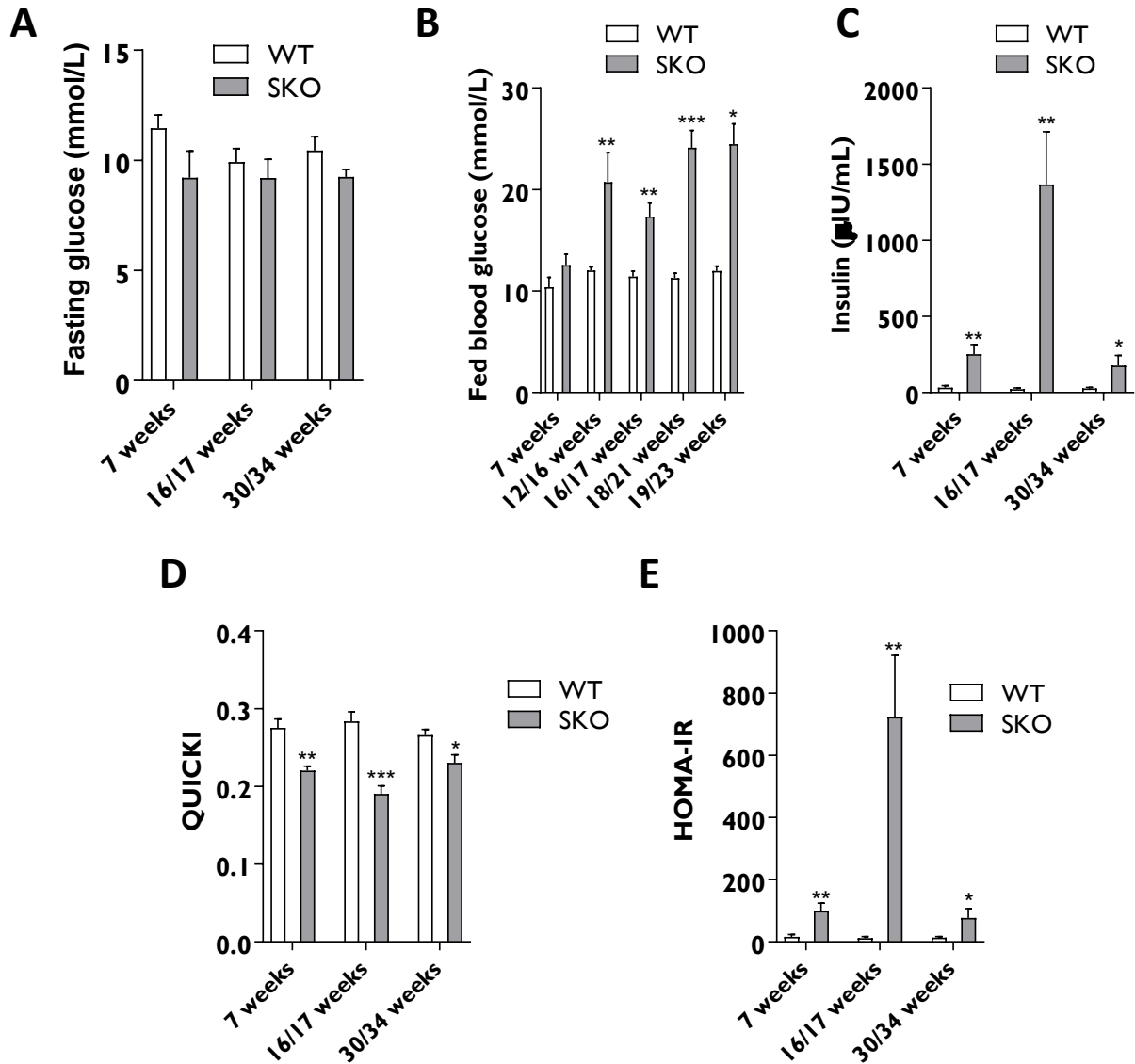
Figure 5.4: Hyperglycaemia and hyperinsulinemia in male SKO mice. *Fasted serum glucose (**A**), fed serum glucose (**B**), fasting insulinemia (**C**), quantitative insulin sensitivity check index (QUICKI) (**D**) and homeostatic model assessment for insulin resistance (HOMA-IR) (**E**) analysis in male wild-type (WT) and seipin-null (SKO) mice at the ages indicated up to 34 weeks of age. n= 6v5 (7 weeks); 7v4 (12/16 weeks); 5v4 (16/17 weeks); 6v10 (18/21 weeks); 7v3 (19/23 weeks); 6v4 (30/34 weeks). Data are expressed as mean ± SEM, *p<0.05, **p<0.01, ***p<0.001.*

To examine whether SKO mice showed any alteration in their ability to respond to an acute glucose challenge, glucose tolerance tests (GTT) were performed at 16/17 weeks of age (***Figure 5.5, A/B***). These did not show any delayed response upon intraperitoneal injection of 1mg/kg glucose in SKO mice compared to wild-type controls. Therefore, despite hyperglycaemia in the fed state, GTTs fail to demonstrate glucose intolerance in male SKO mice. It is possible that

the severe hyperinsulinemia observed in 16/17 weeks of age SKO mice is sufficient to prevent glucose intolerance at that age.

A

B
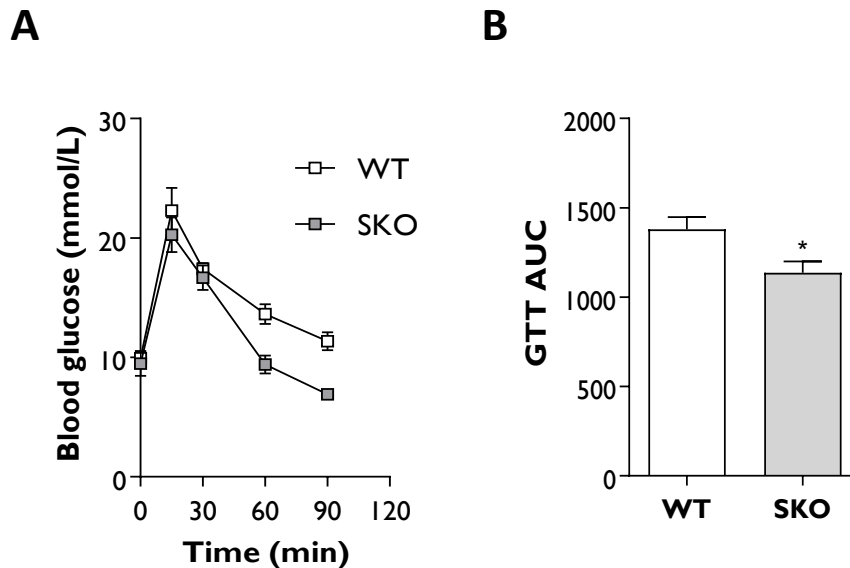
Figure 5.5*: **Male SKO mice are not glucose intolerant at 16/17 weeks of age**. (A) Glucose tolerance test (GTT) performed on 16/17-week-old wild-type (WT) and seipin-null (SKO) mice fasted for 5 hours. (**B**) Area under the curve of the GTT (n=5v4). Data are expressed as mean ± SEM, *p<0.05.*

5.2.4. Pancreas hypertrophy and islets hyperplasia in SKO mice

As seen in ***Table 5.1***, pancreases were significantly heavier in 30/34-week-old male SKO mice when compared to control mice. To assess whether this difference was observed from an earlier time point, I have also examined the pancreas of 7 weeks and 16/17 weeks of age mice. When normalised to body weight, pancreatic tissue weight did not differ between WT controls and SKO mice at 7 weeks of age. Interestingly, pancreas weight significantly increased in 16/17-week-old SKO mice, similar to levels observed at 30/34 weeks of age, when the hyperglycaemia and hyperinsulinemia were clearly evident (***Figure 5.6, A***). Given the difference in lean and fat mass observed in SKO mice (see 5.2.1), pancreases weights were also provided as absolute values and showed similar trends (*Figure 5.6, B*).
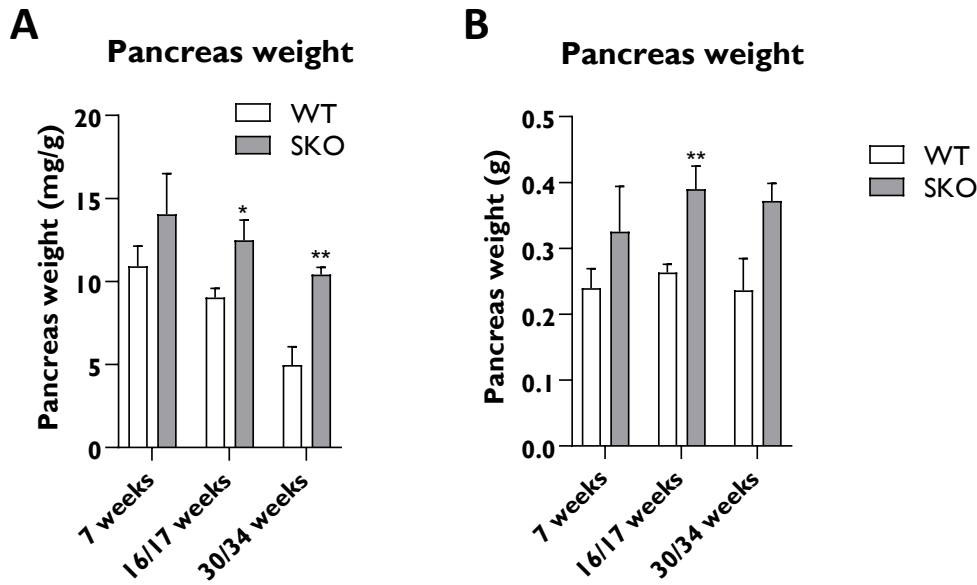
Figure 5.6: Pancreas hypertrophy in male SKO mice. *Pancreatic tissue weight was normalised to body weight (**A**) or provided as absolute values (**B**) in 7 to 34 weeks of age male wild-type (WT) and seipin-null (SKO) mice. n= 4v3 (7 weeks); 5v5 (16/17 weeks); 5v4 (30/34 weeks). Data are expressed as mean ± SEM, *p<0.05, **p<0.01.*

To investigate whether the differences in pancreatic tissue weight and the hyperinsulinemia in SKO mice can be attributed to an alteration in islets distribution, pancreases from 7, 16/17 and 30/34 weeks of age mice were examined histologically. Pancreases were embedded in paraffin and cut in longitudinal sections to obtain an overall view of the head, the body and the tail parts of the pancreas as shown schematically in ***Figure 5.7, A***. The total number of islets per area of pancreas was equivalent between WT controls and SKO mice at 7 weeks of age, although only a limited number of mice were available for this age group and so this should be treated with caution. However, islet number per section was elevated in SKO mice at 16/17 weeks of age when compared to age-matched controls, although this was not significant. Interestingly, there was a constant increase in islets number in SKO mice, with the number of islets approximately doubling for each time-point while the number of islets in control mice only moderately fluctuated (***Figure 5.7, B***).

A Longitudinal section

B Number of islets per pancreatic section
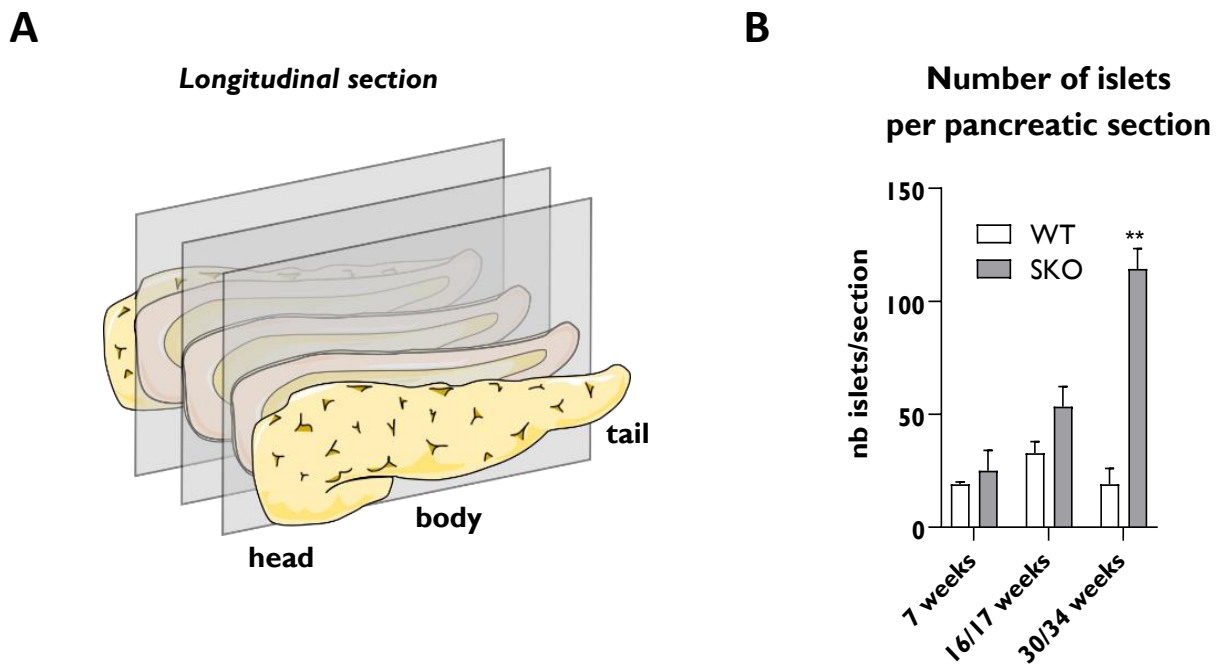
Figure 5.7: Islets are highly abundant in male SKO mice. (A) Schematic diagram of a longitudinal section of the pancreas. (B) Number of islets per pancreatic section in male wild-type (WT) and seipin-null (SKO) mice. n= 2v2 (7 weeks); 5v5 (16/17 weeks); 3v3 (30/34 weeks). Data are expressed as mean ± SEM, **p<0.01.

Hematoxylin and eosin (H&E) staining revealed that islets size and appearance in 7-week-old mice did not differ clearly between SKO and control mice. However, morphometric analysis at 16/17 and 30/34 weeks of age revealed that SKO mice possessed significantly enlarged islets when compared to controls (***Figure 5.8, A***). Additionally, islets isolated from 40-week-old male SKO mice showed similar enlargement (***Figure 5.8, B***).
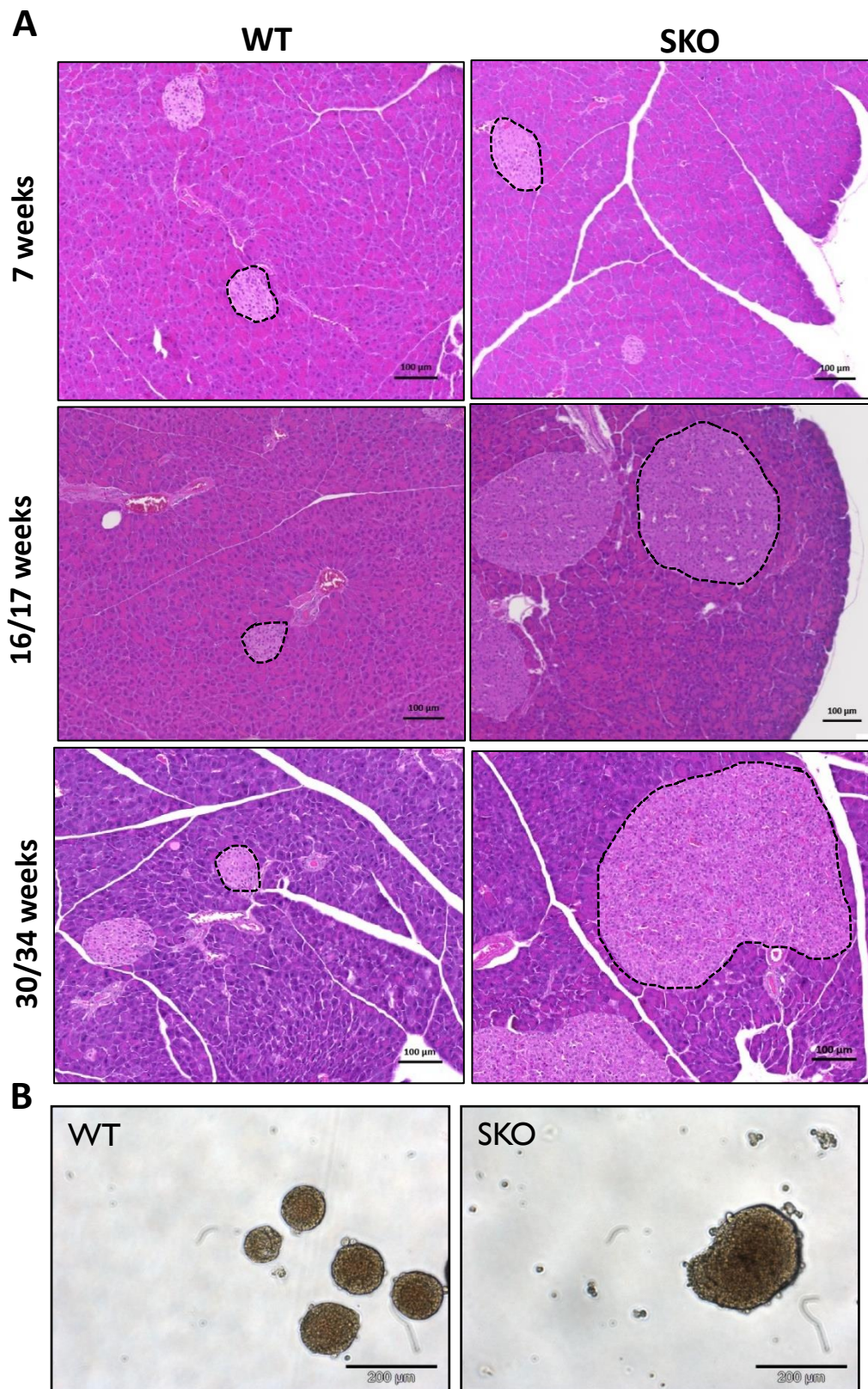
Figure 5.8: ***Pancreatic islets hyperplasia in male SKO mice***. *Representative brightfield images of hematoxylin and eosin staining of pancreatic tissues (**A**) and 40-week-old isolated islets (**B**) from wild-type (WT) and seipin-null (SKO) mice. Dotted lines in (A) delimit an islet of Langerhans. n= 4v3 (7 weeks); 5v5 (16/17 weeks); 3v3 (30/34 weeks). Bars denote 100 µm in (A) and 200 µm in (B).*

Further analysis of islet morphology demonstrated that SKO mice displayed larger islets than WT mice and at all ages, which may be evident even in 7-week-old mice (*Figure 5.9, A*). The analysis of the distribution of islets size showed that small islets (<10 000 μm²) account for the majority of the islets present in both WT and SKO mice, independently of their age. In comparison with WT mice, the proportion of small islets was slightly reduced in SKO mice in favour of larger islets (*Figure 5.9, B; Table 5.3*). Islet morphology was consistent with circulating insulin levels. Large islets (>100 000 μm²) were mainly observed in 16/17-week-old mice explaining the high insulin circulating levels observed at that age. Interestingly, there is a decrease in the population of large islets in 30/34-week-old SKO mice (*Table 5.3*). Together with the increased number of total pancreatic islets, it suggested that islets in older SKO mice most likely result from the fission of large islets rather than neogenesis of new islets.

Collectively, these data revealed that compensatory hyperinsulinemia observed in 16/17-week-old SKO mice was accompanied by an increase in islets number but also by the expansion of existing islets. The decrease in insulin levels in 30/34-week-old mice also suggested that there might be a progressive loss of β-cell insulin secretory capacity in SKO mice as islets remained abundant at that age.
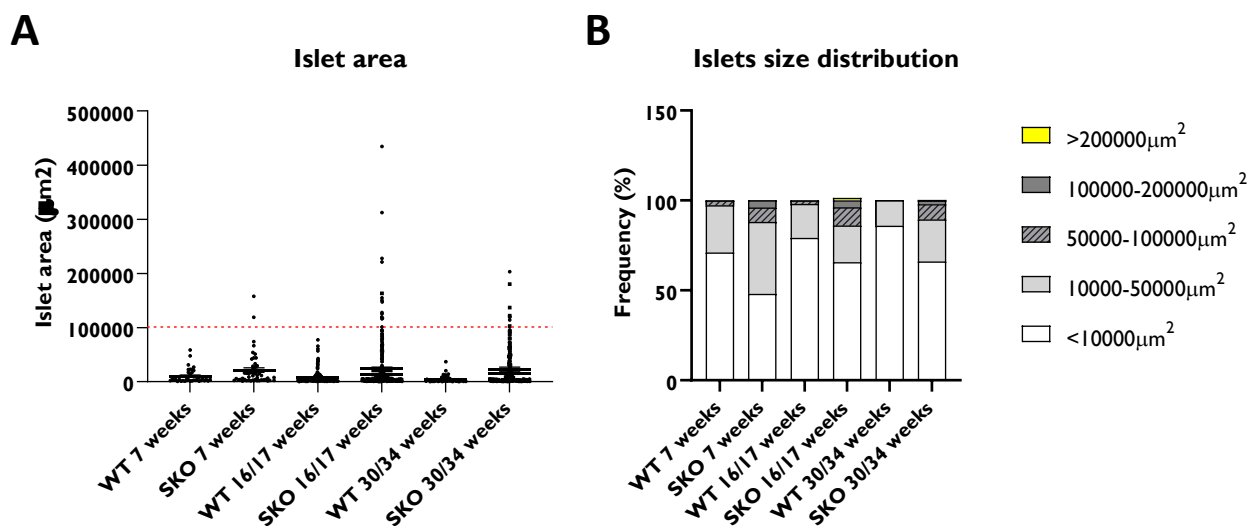
Figure 5.9: Islets size distribution in male SKO mice. Area of individual islets (A) and distribution of islet size in pancreatic sections (B). n= 2v2 (7 weeks); 5v5 (16/17 weeks); 3v3 (30/34 weeks). A total of 38 islets for wild-type (WT) and 50 islets for seipin-null (SKO) mice at 7 weeks; 207 islets for WT and 286 islets for SKO mice at 16/17 weeks; 57 islets for WT and 342 for SKO mice at 30/34 weeks; were analysed.

Table 5.14 : Islets size distribution in male SKO mice.

Age	7 weeks		16/17 weeks		30/34 weeks	
Islet size (µm²)	WT	SKO	WT	SKO	WT	SKO
< 10000	71	48	79	66	86	66
10000-50000	26	40	19	20	14	23
50000-100000	3	8	2	10	0	8
100000-200000	0	4	0	4	0	2
> 500000	0	0	0	1	0	0

Frequency values are expressed in percentage. Abbreviations: WT, wild type; SKO, seipin-knockout mice. n= 2v2 (7 weeks); 5v5 (16/17 weeks); 3v3 (30/34 weeks).

5.2.5. Pancreatic β-cell proliferation in SKO mice

To determine whether islet cell proliferation occurred in SKO mice as part of a compensatory mechanism, pancreatic sections were stained with immunoperoxidase for insulin and for the proliferation marker Ki67. Ki67+ cells were not detected in young mice (data not shown). Ki67+ cells were detected at a very low rate in both WT and SKO pancreases from 30/34-week-old mice (***Figure 5.10***). Interestingly, double positive cells (Ki67+, insulin+) were only observed in SKO pancreatic sections. Those were not present in large but small islets suggesting β-cell proliferation in nascent islets (***Figure 5.10***). This might suggest that neogenesis of new islets is present in 30/34 weeks of age SKO mice.
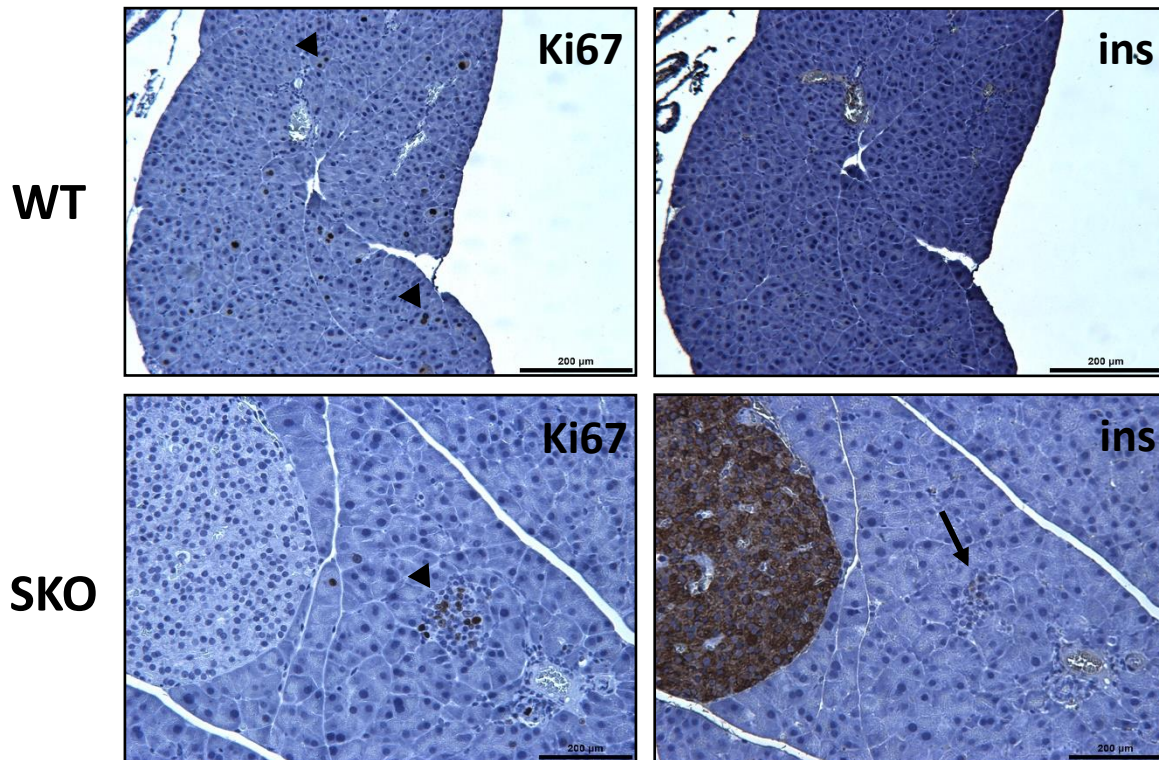
Figure 5.10*: **Pancreatic β-cell proliferation in male SKO mice.** Representative images of pancreatic sections from 30/34-week-old wild-type (WT) and seipin-null (SKO) mice stained in brown with 3,3'-diaminobenzidine (DAB) for Ki67 and insulin (ins). Sections were counterstained with hematoxylin (n= 3v3). Black arrowheads indicate Ki67+ cells. Black arrow points at a nascent islet positive for both Ki67 and insulin staining. Bars denote 200 µm.*

5.2.6.   Effects of long-term hyperglycaemia on islet morphology

To determine if the prolonged hyperglycaemia in SKO mice leads to changes in islet architecture, serial sections of pancreas were stained with immunoperoxidase for insulin, glucagon, and somatostatin, highlighting pancreatic β, α and δ cells, respectively. 3,3'-Diaminobenzidine (DAB) staining intensity for insulin revealed no clear differences between age-matched WT controls and SKO mice (***Figure 5.11, A/B***). An apparent reduction in glucagon and somatostatin-expressing cells in favour of insulin-expressing cells was observed in 16/17- and 30/34-week-old SKO mice (***Figure 5.11, B***). In WT mice, α and δ cells were evenly distributed at the periphery of islets at all ages (***Figure 5.11, A***). Interestingly however, glucagon-positive cells and somatostatin-positive cells from 16/17- and 30/34-week-old SKO mice were no longer restricted to the mantle but populated the core of the islet (***Figure 5.11, B***). These structural changes were similar to the ones observed in mouse models of obesity (177).
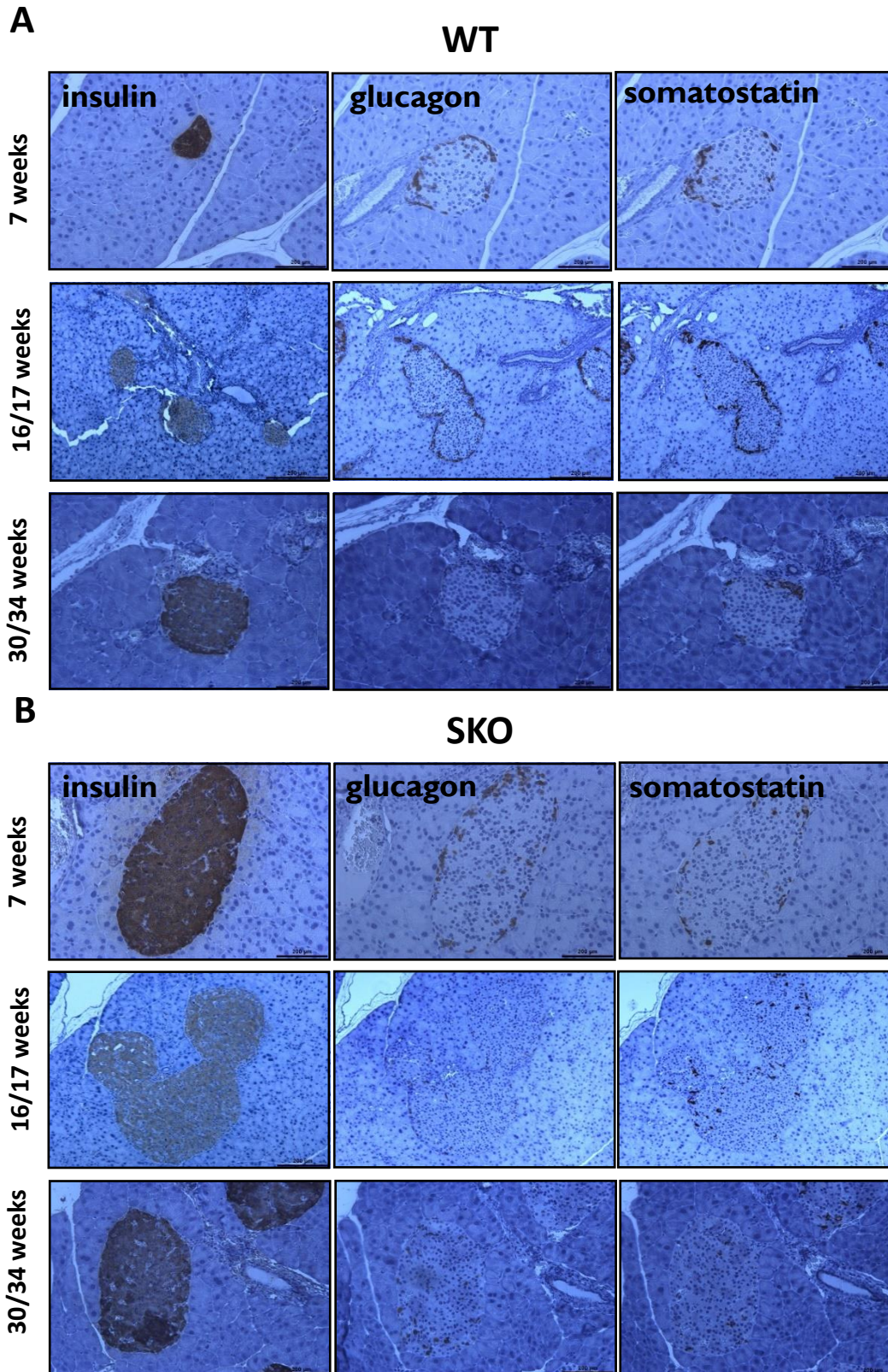
Figure 5.11*: **Effect of long-term hyperglycaemia on organisation of pancreatic α, β and δ
cells.** Representative images of pancreatic sections from wild-type (WT) (**A**) and seipin-null
(SKO) mice (**B**) at different ages stained with 3,3'-diaminobenzidine (DAB) for insulin,
glucagon, and somatostatin. Sections were counterstained with hematoxylin. n= 3v3 (7 weeks);
5v5 (16/17 weeks); 3v3 (30/34 weeks). Bars denote 200 μm.*

5.2.7.　　Hypervascularisation in pancreatic islets from SKO mice

Pancreatic islets are highly vascularised structures and that vascular network is essential for providing endocrine cells with not only oxygen but also nutrients and other metabolic cues (387). To investigate whether changes in vascularisation to accommodate increased insulin demand occurred in SKO mice, islet vasculature was briefly examined with H&E staining. Please note that no endothelial cell staining was performed in this study. When mentioned, the hypervascularisation here relies solely on H&E-stained pancreatic sections and requires further validation.

Islets from SKO mice showed hypervascularisation at both 16/17 (***Figure 5.12, A***) and 30/34 weeks of age (***Figure 5.12, B***). This hypervascularisation was accompanied with a thickening of intra-islet capillaries in SKO mice. I hypothesise that the extensive capillary network was first intended to promote survival of islets and sustain growth to support increased demand of insulin in SKO mice. It is worth noting that similar remodelling of islet vasculature has been described in rodent models of obesity and insulin resistance (388). To evaluate whether that rich capillary network altered glucose sensing in β-cells, pancreatic sections were also stained with immunoperoxidase for glucose transporter 2 (Glut2). I found no striking differences in the expression of Glut2 between WT controls and SKO mice pancreatic islets (***Figure 5.12, A/B***).
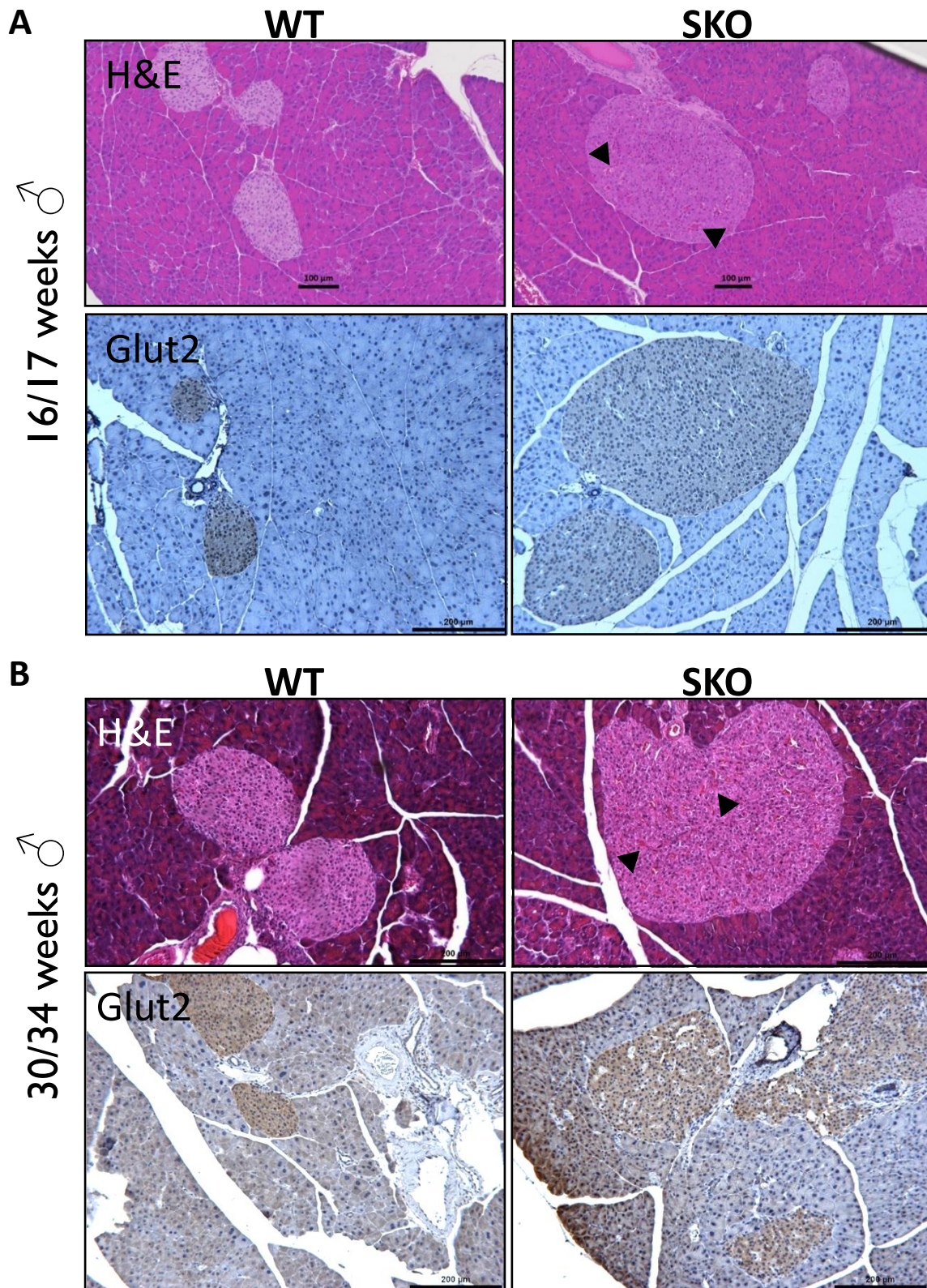
Figure 5.12: ***Hypervascularisation in male SKO pancreatic islets.*** *Representative brightfield images of hematoxylin and eosin staining and 3,3'-diaminobenzidine (DAB) stained pancreatic sections for Glut2 from 16/17-week-old (**A**) and 30/34-week-old (**B**) wild-type (WT) and seipin-null (SKO) mice. Black arrowheads indicate thickening of capillary vessel. n=5v5 (16/17 weeks); 3v3 (30/34 weeks). See annotation on the bars for scale.*

5.2.8.   Identification of macrophages infiltration in SKO mice

It is commonly accepted that islet macrophages accumulate during obesity and type 2 diabetes, with consequences on β-cell function (389–391). However, macrophages have also been shown to be essential for β-cell formation (392,393). Recently, Chittezhath *et al.* reported that islet resident macrophages were associated with islet remodelling and increased insulin secretion during islet compensation in diabetes (394). To investigate whether macrophages participate in pancreatic islet adaptation in our model of SKO mice, I stained pancreatic sections with cluster of differentiation 68 (CD68) to mark macrophages. No macrophages were observed in younger mice (data not shown). Interestingly, the number of intra-islet macrophages was markedly elevated in SKO mice at 30/34 weeks when compared to age-matched controls (***Figure 5.13***). Macrophage accumulation was only observed in aged SKO mice, but it was not dependent on ageing itself as WT mice did not exhibit such accumulation (***Figure 5.13***). Further analysis would be needed to determine if macrophage accumulation results from an invasion of monocytes or the replication of resident macrophages.

In light of our observations, intra-islets macrophages could contribute to islet compensation in the early stages of pre-diabetes as fasting normoglycaemia was still maintained in our model of SKO mice. This does not exclude a potential contribution of macrophages to the inflammation of pancreatic islets *i.e.* insulitis in older SKO mice.
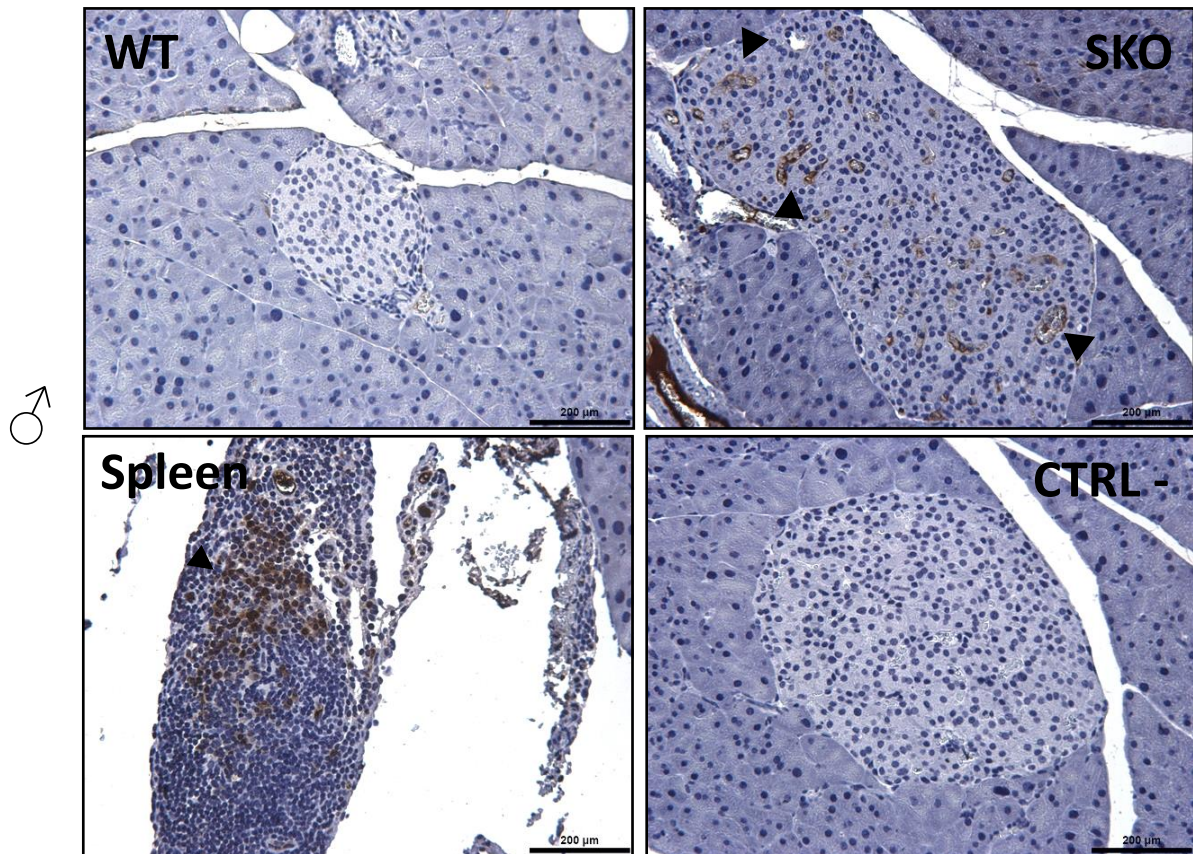
Figure 5.13: Macrophages infiltration in male SKO pancreatic islets. Representative images of pancreatic sections from 30/34 weeks of age male wild-type (WT) and seipin-null (SKO) mice stained with 3,3'-diaminobenzidine (DAB) for CD68 macrophage marker. Sections were counterstained with hematoxylin (n=3v3). Spleen was used as a positive control for CD68. Negative control (CTRL-) corresponds to a pancreatic section from 30/34-week-old SKO mice incubated with the secondary antibody only and stained with DAB. Bars denote 200 μm. Arrowheads point at CD68-positive cells.

5.2.9. Secretory function of SKO islets

To assess whether this disorganised islet composition affects β-cell function, isolated islets were obtained from 40-week-old male mice – the only age available at this time - and their insulin secretion in response to different concentrations of glucose was monitored. To minimise any bias introduced by SKO islets hyperplasia, both large and small islets were picked for the assay and insulin release was normalised to total insulin content. Total insulin content was slightly more elevated in SKO islets although this was not significant (*Figure 5.14, A*). Interestingly, glucose-stimulated insulin secretion was equivalent between control and SKO islets at both low glucose (2,5 mM) and high glucose (25 mM) conditions (*Figure 5.14, B/C*).

That similar response to glucose in WT and SKO mice would suggest that β-cell functionality is preserved in SKO islets at least up to 40 weeks of age.
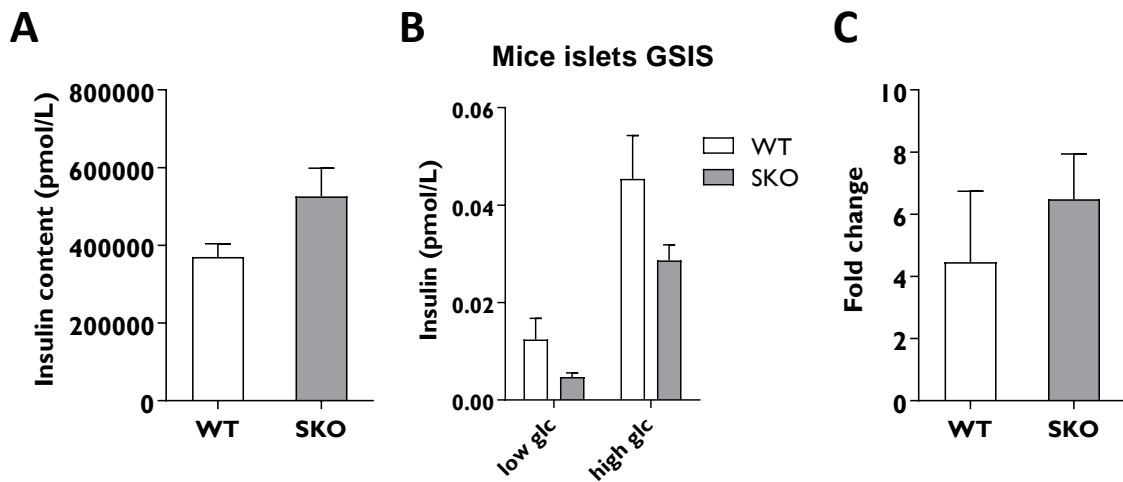
Figure 5.14: Secretory function of male SKO islets. *(A) Total insulin content, (B) Glucose-stimulated insulin secretion (GSIS) in isolated islets from male 40-week-old wild-type (WT) and seipin-null (SKO) mice. Islets were exposed to either low glucose (low glc: 2,5 mM) or high glucose (high glc: 25 mM) as indicated. (C) Fold change between high and low glucose conditions. (n=3, 15 islets/condition). Released insulin was normalised to total insulin content. Data are expressed as mean ± SEM.*

5.2.10.   Glucose metabolism of SKO pancreatic islets

Adaptation of pancreatic β-cells to insulin resistance are believed to be associated with a modulation of the expression of glycolytic genes (317,395,396). To investigate the molecular mechanisms involved in adaptation to hyperglycaemia in SKO mice, I examined the mRNA expression of genes encoding key enzymes of the glycolytic pathway or β-cell signalling in isolated islets (***Figure 5.15, A***). To mimic the *in vivo* environment of SKO mice and chronic hyperglycaemia, isolated islets were maintained in 25 mM glucose. Glucose transporter 2, Glut2 (also known as solute carrier family 2, SLC2A2) permits the passive transport of glucose across plasma membranes in pancreatic β-cells. *Glut2* mRNA expression was equivalent between SKO and control islets. Glucokinase (GCK) expression however, which acts as the rate-controlling enzyme of the glycolysis, was increased in SKO islets when compared to WT islets. Glucose-6-phosphate isomerase (GPI) catalyses the reversible isomerisation of glucose-6-phosphate and fructose-6-phosphate. Interestingly, a 2-fold increase in the mRNA expression of *GPI* was observed in SKO islets in comparison to WT islets. Additionally, the expression of

the platelet isoform of phosphofructokinase (*Pfkp*), which irreversibly converts fructose-6-phosphate to fructose-1,6-bis-phosphate, was also increased by approximately 2,5-fold in SKO islets when compared to WT islets. Similarly, aldolase A (*AldoA*) and lactate dehydrogenase A (*LdhA*), two other key enzymes acting downstream in the glycolytic pathway, were also upregulated in SKO islets (***Figure 5.15, B***).

Taken together, pancreatic islets obtained from SKO mice displayed altered expression of several genes encoding key glycolytic enzymes, suggesting that there could be a higher rate of glycolysis in SKO islets.

Finally, the relative expression of insulin was significantly increased in SKO islets (***Figure 5.15, C***). Psck1 mRNA expression which encodes the prohormone convertase 1/3, involved in the processing of proinsulin and proglucagon (397), was also increased by approximately 2-fold in SKO pancreatic islets (***Figure 5.15, D***). Upregulation of *Psck1* and *Insulin* gene expression is likely to participate to the compensation process in SKO mice.

Collectively, my data indicate that part of β-cell compensation in SKO mice is achieved by the upregulation of several glycolytic enzymes. Whether this translates into higher glycolytic rate remains to be assessed.
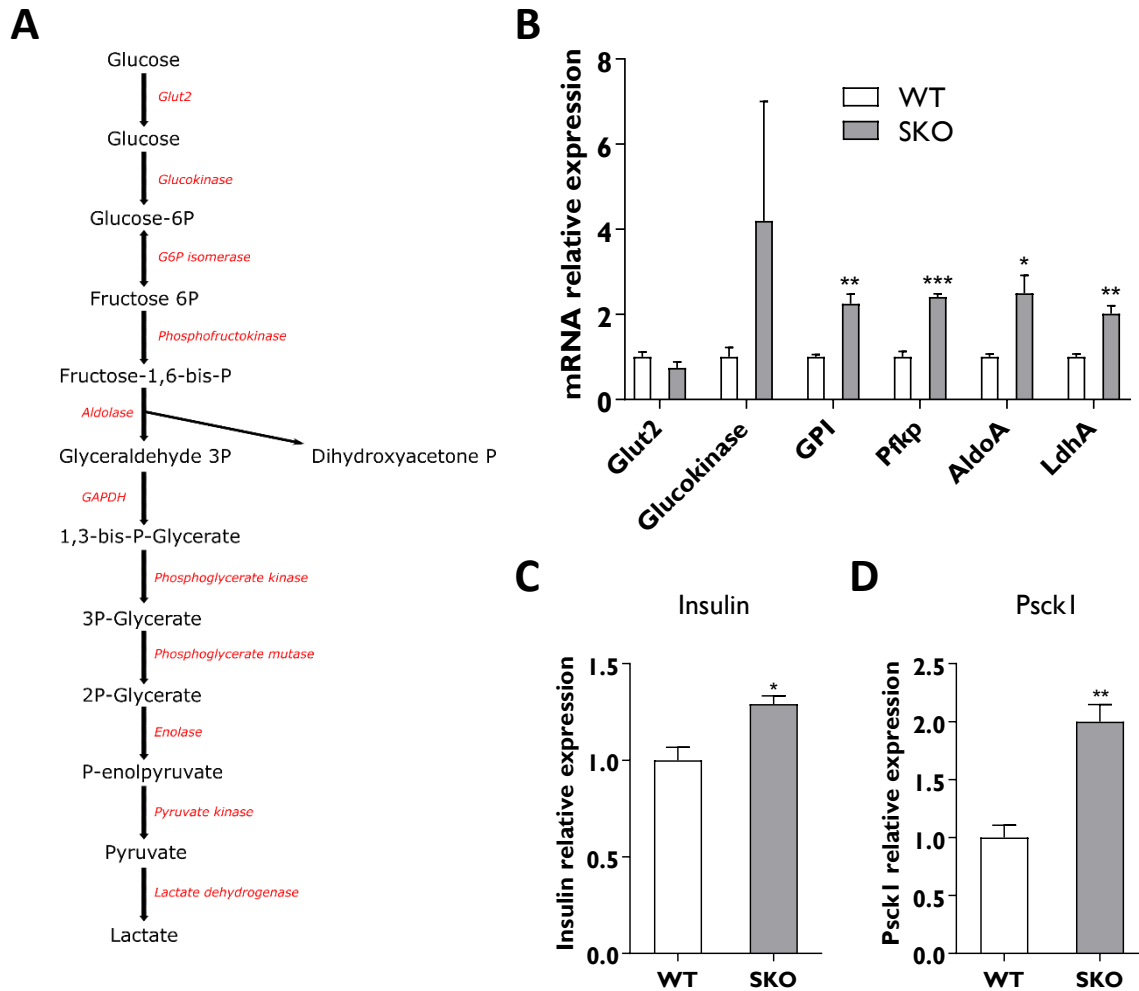
Figure 5.15*: **Glucose metabolism in male SKO pancreatic islets.** (**A**) Schematic representation of the glycolytic pathway in pancreatic islets. (**B**) relative mRNA expression of genes encoding glycolytic enzymes, (**C**) Insulin and (**D**) Prohormone convertase 1/3 (Psck1) relative expression in isolated islets from 40 weeks of age wild-type (WT) and seipin-null (SKO) mice (n=3). Gene expression was normalised to the geometric mean of Hprt, Nono and Yhwaz reference genes. Data are expressed as mean ± SEM, *p<0.05, **p<0.01, ***p<0.001. Abbreviations: Glucose transporter 2 (Glut2), Glucose-6-phosphate isomerase (GPI), Phosphofructokinase (Pfkp), Aldolase A (AldoA) and Lactate dehydrogenase A (LdhA).*

5.2.11.   Sexual dimorphism in SKO mice

Initial studies were carried out with male mice because male cohorts of differing ages were available for use in these studies. However, several studies have reported gender differences regarding glucose and lipid metabolism (Reviewed in (398)). In an attempt to decipher and understand gender differences in SKO mice, both male and female mice were subsequently compared in this study. Glucose tolerance tests were performed at 18/21 weeks

of age on fasted mice. This revealed that male WT and SKO mice responded very similarly to a glucose challenge (***Figure 5.16, A/B***). In contrast, female SKO mice showed impaired glucose tolerance when compared to WT controls (***Figure 5.16, C/D***). These observations suggest that female mice already displayed altered glucose control at 18 weeks of age indicative of a pre-diabetic state. This is consistent with clinical cases reporting a more severe phenotype in CGL2 women (399).
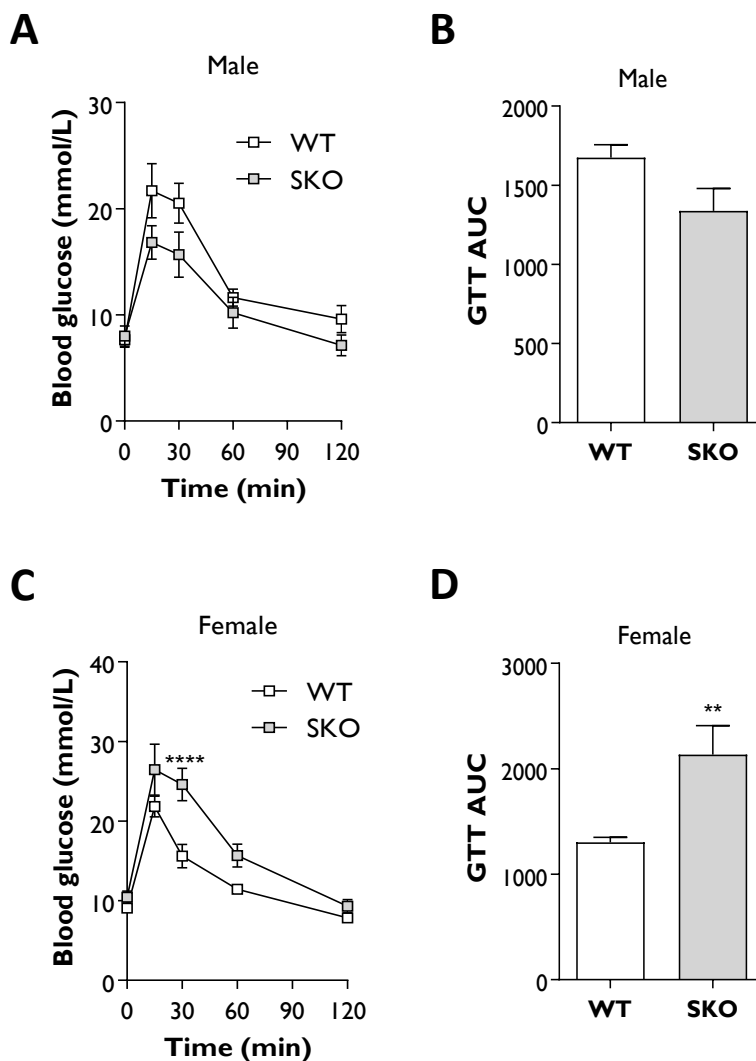
Figure 5.16*: Sexual dimorphism in 18/21-week-old SKO mice. Glucose tolerance test (GTT) performed on male (**A**) and female (**C**) 18/21-week-old wild-type (WT) and seipin-null (SKO) mice fasted for 5 hours. Area under the curve (AUC) of the male (**B**) and female (**D**) GTTs. n=5v5 (male); 10v6 (female). Data are expressed as mean ± SEM, **p<0.01, ****p<0.05.*

Next, gene expression was examined in islets from 25/29-week-old female wild-type and SKO mice. In contrast to the findings in male mice, islets collected from female SKO mice did not exhibit increased expression of genes involved in glycolysis. Expression of mRNA encoding GCK, GPI, Pfkp, AldoA and LdhA did not differ between WT and SKO islets isolated from female mice. Additionally, *Glut2* expression was found to be decreased in female SKO islets (***Figure 5.17***) rather than unchanged as seen in male SKO mice (***Figure 5.15, B***). Taken together, these data highlight a strong sexual dimorphism in SKO mice regarding glucose tolerance and β-cell compensation. Unfortunately, these analyses were limited to a single time point in female mice. Thus, it is unclear whether β-cell compensation occurred in female SKO mice at an earlier age or if they were instead unable to induce this compensation at any stage.
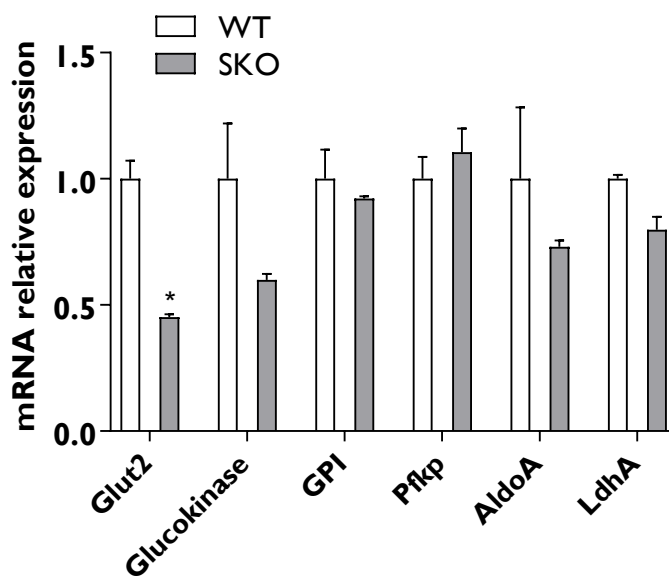
***Figure 5.17**: **Glucose metabolism in female SKO pancreatic islets.** mRNA relative expression of genes encoding glycolytic enzymes in isolated pancreatic islets from 25/29-week-old female wild-type (WT) and seipin-null (SKO) mice (n=3). Gene expression was normalised to the geometric mean of Hprt, Nono and Yhwaz reference genes. Data are expressed as mean ± SEM, *p<0.05.*

Histological analysis demonstrated that female SKO mice displayed large islets by 40/44 weeks of age (***Figure 5.18, A***), similar to male SKO mice. Hypervascularisation of pancreatic islets was also clearly evident at this age in female SKO mice (***Figure 5.18, A***). Moreover, Glut2 protein expression did not appear to differ between female WT and SKO mice when assessed by immunostaining (***Figure 5.18, B***). The preservation of islets in aged-female SKO mice

suggests that glucose intolerance first arise from an impaired metabolism in these SKO mice rather than because of β-cell degeneration.
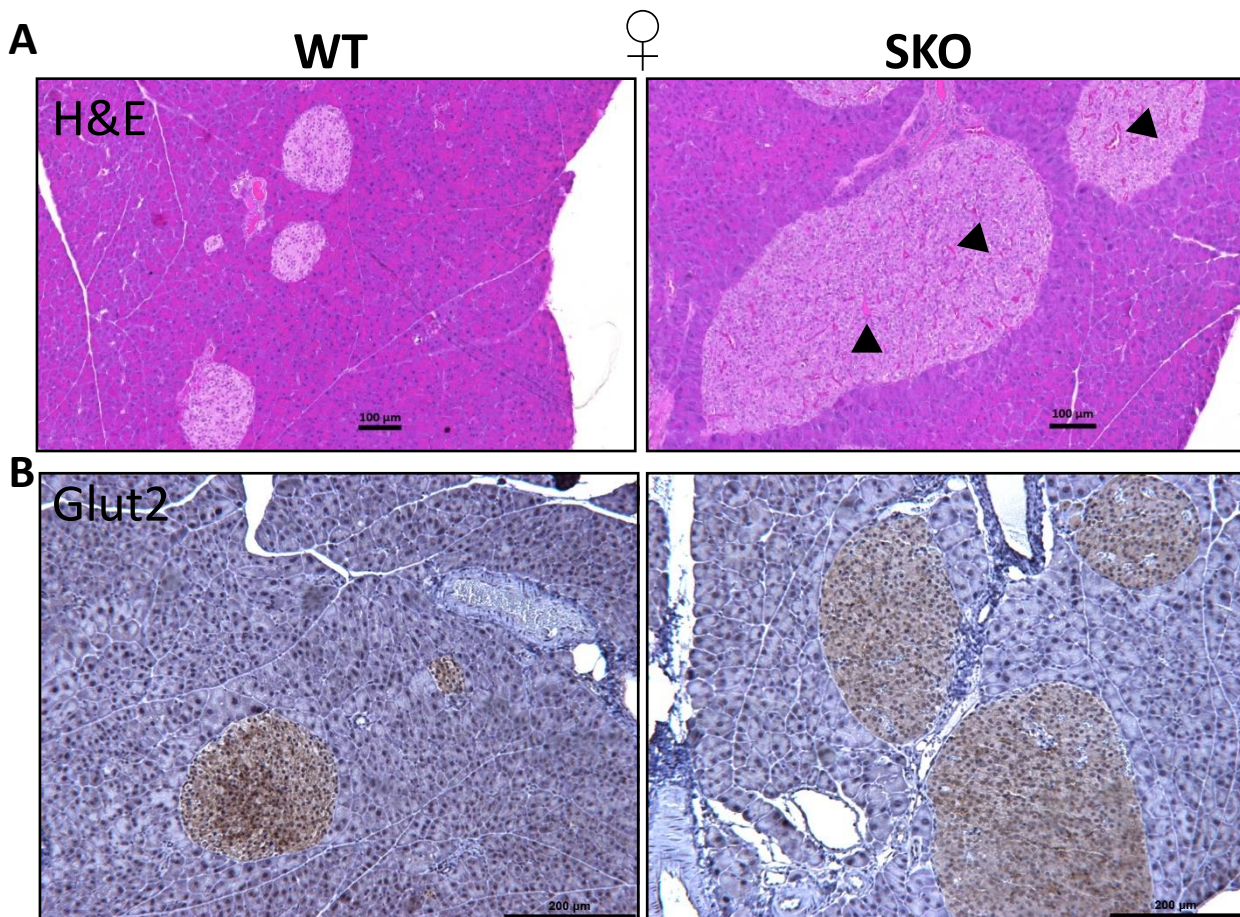
Figure 5.18*: **Hyperplasia and hypervascularisation in female SKO pancreatic islets.** Representative brightfield images of hematoxylin and eosin staining (**A**) and 3,3'-diaminobenzidine (DAB) stained pancreatic sections for Glut2 (**B**) from 40/44-week-old wild-type (WT) and seipin-null (SKO) female mice. Black arrowheads indicate thickening of capillary vessel. (n=3). See bars annotation for scale.*

Similar to male observations, female SKO mice were also characterised by an increase in intra-islet CD68+ macrophages (***Figure 5.19, A/B***). Additionally, an intra-islet fat deposition, not noted in males, was observed in female SKO mice while adipocytes were only found surrounding the islets in WT mice (***Figure 5.19, A***). The close proximity between macrophages and lipids in SKO mice in ***Figure 5.19, A*** might indicate an involvement of lipids in macrophages recruitment to the site of pancreatic fatty infiltration.

Collectively, our observations provide clear evidence that female SKO mice are more affected by metabolic complications than male SKO mice. Despite signs of adaptation with larger pancreatic islets, this appeared not sufficient to maintain normal glucose control in female SKO mice, at least at the specific age tested. On the contrary, male SKO mice displayed a robust adaptation to insulin resistance with no signs of glucose intolerance, apart from the hyperglycaemia in the fed state.
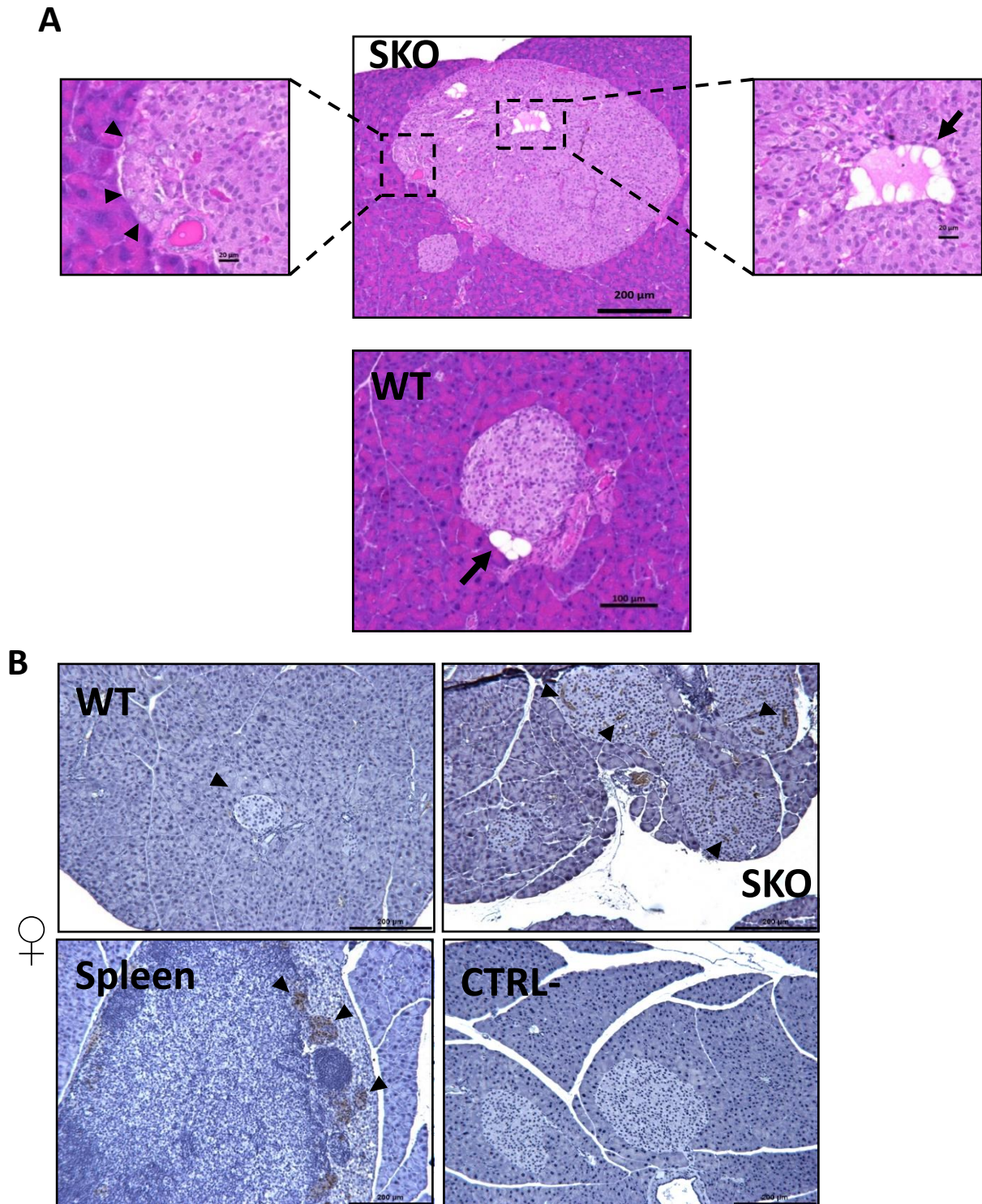
Figure 5.19: ***Macrophages and lipids infiltration in female SKO mice***. (***A***) *Representative brightfield images of hematoxylin and eosin staining of pancreatic tissues from female wild-type (WT) and seipin-null (SKO) mice. (**B**) 3,3'-diaminobenzidine (DAB) stained pancreatic sections for CD68 macrophage marker. Sections were counterstained with hematoxylin (n=3). Spleen was used as a positive control for CD68. Negative control (CTRL-) corresponds to a pancreatic section from 40/44 weeks of age SKO mice incubated with the secondary antibody only and stained with DAB. Black arrowheads and arrows indicate immune cells and lipids, respectively (n=3). Insets show higher magnification images. See bars annotation for scale.*

5.3. Discussion

Congenital Generalised Lipodystrophy type 2 (CGL2) is the most severe form of lipodystrophy and is caused by mutations in the *BSCL2* gene. Affected patients exhibit a near complete loss of adipose tissue and suffer metabolic disorders including insulin resistance, glucose intolerance, hepatic steatosis and hypertriglyceridemia (80). A decade has passed since the first mouse model of CGL2 has been generated (386). In the present study, disruption of *Bscl2* gene in mice recapitulated almost entirely the phenotype observed in CGL2 patients. Seipin knockout (SKO) mice displayed a total absence of white adipose tissue and a clear reduction of brown adipose tissue stores but did not show hypertriglyceridemia. SKO mice developed a generalised organomegaly including hepatomegaly and pancreatomegaly. Lipid accumulation in the liver was observed as early as 7 weeks of age but hepatic steatosis became extremely severe only at around 16 weeks of age. SKO mice were found to be insulin resistant from a very young age but successfully maintained fasting euglycaemia throughout the study. This was achieved by a transient hyperinsulinemia. However, little is known about the mechanisms that drive this compensatory phase in SKO mice.

To date, this study is the first one to provide a description of the steps involved in β-cell adaptation in a model of congenital generalised lipodystrophy. Compensatory hyperinsulinemia in SKO mice included an increase in islets number accompanied by an expansion of islet mass. Stimulating factors responsible for that expansion remain to be identified but we can infer from previous studies that those factors most likely include glucose (400,401), free fatty acids (402) and incretin hormones such as glucagon-like-peptide 1 (GLP-1) (403).

Chronic hyperglycaemia in our model led to structural changes in islet architecture with a redistribution of endocrine cells within the islet. SKO mice displayed an enhanced glucose metabolism as evidenced by the transcriptional upregulation of several genes encoding key glycolytic enzymes. This was independent of the entry of glucose within the islet as Glut2 expression was unchanged.

To accommodate increasing insulin demand, compensation also included a remodelling of islet vasculature associated with an increase in CD68+ macrophages within the islet. From observations made in obese mice, intra-islets macrophages most likely originate from the proliferation of islet resident macrophages rather than monocytic invasion (404). Whether macrophages contribute to islet compensation or participate to a proinflammatory state in SKO

mice remain to be addressed. Their presence in 34-week-old male SKO mice was probably not detrimental as SKO islets were still compensating with larger and more numerous islets, robust insulin expression and increased insulin secretion at that age.

Overall, our data demonstrated that, up to 34 weeks of age, male SKO mice were in a prediabetic state in which β-cells were able to compensate for insulin resistance. That robust adaptation required a thorough regulation at many steps (see *Figure 5.20*). It would have been interesting to have another age-group in the study, in which diabetes was clearly apparent, to clearly define the transition from compensation to decompensation and β-cell dysfunction. This would have occurred probably not long after 34 weeks of age as there were already a dramatic decline in insulin secretion at that age. The chronic hyperglycaemia, along with the prolonged hepatic steatosis and insulitis will eventually lead to β-cell dysfunction and failure of compensation then diabetes. Additional assaults such as lipotoxicity will most likely contribute to the slow deterioration of β-cell function.

Another interesting point that came out from our observations was the necessity to include both male and female in metabolic studies of this type. In our SKO mouse model, female mice were clearly more affected by metabolic complications than males. This highlights the potential for sexual dimorphism, which is clearly evident in human studies of metabolic disease and lipodystrophy in particular. The data presented here indicate that the seipin-null SKO model of CGL type 2 may be a valuable model in which to explore some of the mechanisms underlying differences between the effects of adipose tissue restriction on metabolic health in male versus female subjects.

To further explore CGL2 and seipin functions, several mouse models of tissue-specific deletion of *Bscl2* have been generated. Metabolic disturbances were not observed when *Bscl2* was specifically disrupted in the brain, the liver or in muscle (150,405,406). Despite the evident lack of systemic lipid storage in those mice, metabolic dysfunction was also not reported in mice lacking *Bscl2* specifically in adipose tissue (337,407). Interestingly, work from our lab has shown that simultaneous deletion of *Bscl2* in both adipose tissue and hepatocytes was also not affecting metabolic function. This suggests that seipin does not appear to make an important cell-autonomous contribution to steatosis within the hepatocytes. Given the critical role of the pancreatic β-cells in glucose homeostasis, it might be possible that seipin exerts effects in these cells directly. This is the subject of studies that will be presented in Chapter 6.
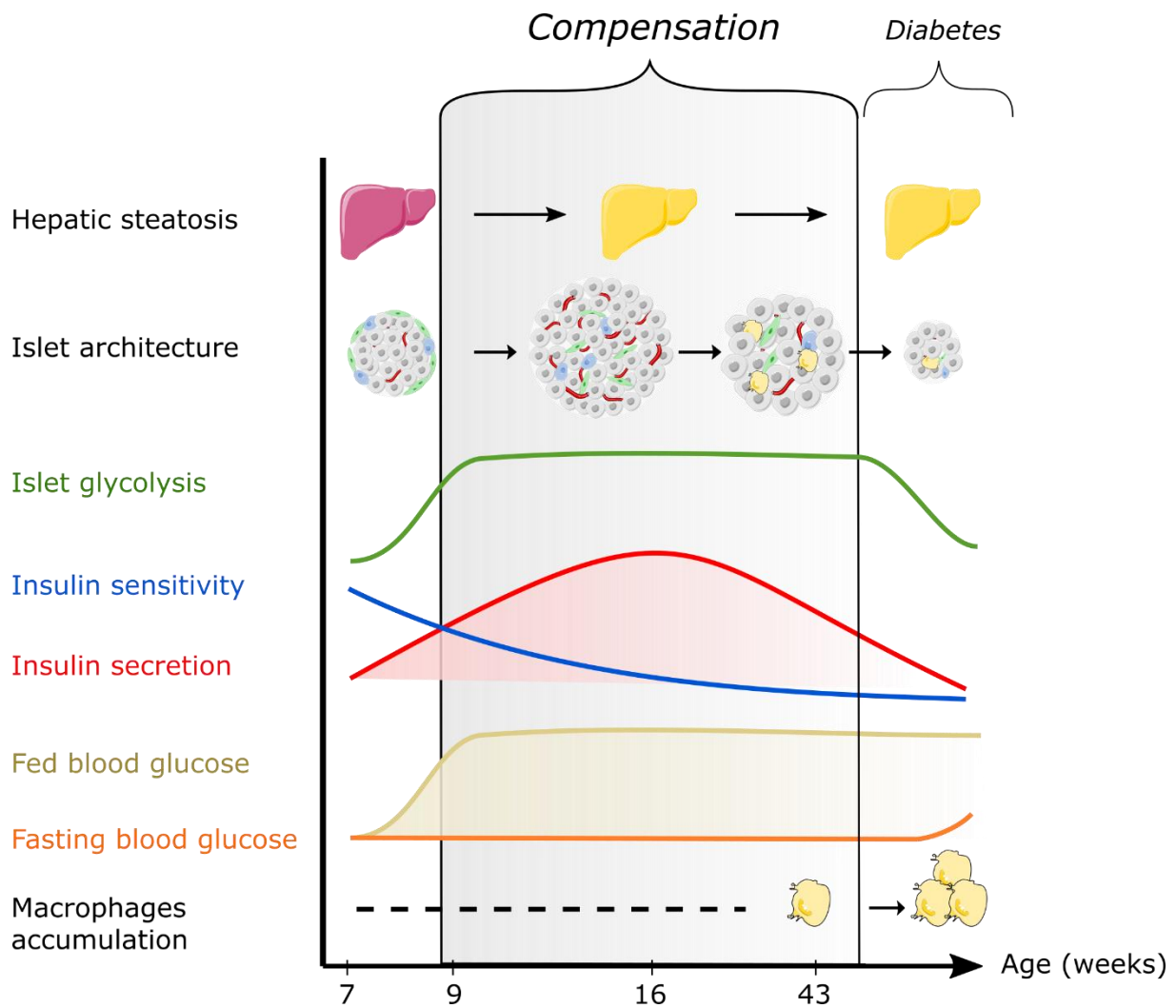
Figure 5.20*: **Proposed compensatory mechanisms in male SKO mice**. The data presented in this chapter are consistent with a model where a primary defect in adipose expansion leads to lipid accumulation in the liver and insulin resistance. This is accompanied with a reduction in insulin sensitivity and glucose regulation by insulin. To accommodate with these changes, remodelling of the pancreatic islets occurs with an initial increase in β-cell mass and function. Hyperinsulinemia is commonly observed at this stage. Over time and as a consequence of prolonged insulin resistance and inflammation, islets fail to compensate appropriately or further resulting in the apparition of fasting hyperglycaemia and the development of diabetes. Changes in islet glycolysis, insulin sensitivity, insulin secretion and blood glucose over the progression from normal glucose tolerance to overt diabetes are provided as line profiles.*

CHAPTER 6

6. Mechanisms underpinning pancreatic islet hyperplasia in SKO mice

6.1. Introduction

It was clear from the work presented in the previous chapter (Chapter 5) that SKO mice displayed significant β-cell compensation, which included a dramatic expansion of islets mass together with an increase in insulin secretion and altered glucose metabolism. Glucose is thought to be the main stimulating factor for β-cell compensation in obesity as evidenced by the inability of haploinsufficient β-cell specific glucokinase mice ($Gck^{+/-}$ mice) to demonstrate an expansion of β-cell mass upon high-fat feeding (323,401). However, the expansion of β-cell mass in lipodystrophy has not been examined. Glucagon-like peptide 1 (GLP-1), an incretin hormone secreted by the L-cells of the intestine, has been shown to promote β-cell proliferation and to protect against apoptosis in pancreatic β-cells (408). This action is achieved through its interaction with GLP-1 Receptor (GLP-1R), a G protein-coupled receptor (GPCR). Exendin-4, a GLP-1R agonist, is approved for the treatment of type 2 diabetes when other antidiabetic drugs have failed to achieve adequate glycaemic control (409). To examine the potential involvement of GLP-1 as a signal for the compensatory hyperinsulinemia observed in SKO mice, GLP-1 levels were examined in the serum and the expression of the GLP-1 receptor determined in tissues isolated from wild-type (WT) and seipin knockout (SKO) mice.

Chronic exposure of pancreatic β cells to nutrient overload, including free fatty acids (FFA), is thought to contribute to β-cell dysfunction and apoptosis and ultimately lead to type 2 diabetes (410). FFA are stored in the form of triglycerides and sterol esters in lipid droplets (LD) (see section 1.1.5.1). By modulating the processes of lipogenesis and lipolysis, LD-associated proteins play a critical role in lipid metabolism (411). However, their involvement in β-cell function is poorly defined with the exception of few studies investigating the role of members of the perilipin (PLIN) family of proteins. Plin2 silencing using both antisense oligonucleotides and siRNA markedly reduced glucose-stimulated insulin secretion (GSIS) in the presence of fatty acids (FA) in a mouse pancreatic β-cell line (412). More recently, specific disruption of Plin2 in β cells has been shown to impair insulin secretion in mice fed a high fat diet (413). Similarly, potentiation of GSIS by FA was further augmented in mouse islets and a β-cell line overexpressing Plin5, another member of PLIN family of proteins (414). Given the role of seipin in lipid droplet biogenesis and its high expression in pancreatic β-cells (164,385), I investigated whether seipin, similarly to Plin2 and 5, plays any cell autonomous role in this cell type using the well characterised INS-1 pancreatic β-cell line (415). Using siRNA directed

against Bscl2, I directly evaluated the effect of seipin loss on glucose stimulated insulin secretion (GSIS) and glucose metabolism through gene expression analysis of key glycolytic enzymes.

Finally, using human embryonic kidney (HEK) 293 cells and immunoprecipitations assays, I also evaluated the potential interaction between seipin and GLP-1R following up on a study of GLP-1R interactors (416).

6.2. Results

6.2.1. GLP-1 levels are increased in SKO mice

To determine if SKO mice have altered GLP-1 production compared to age-matched controls, blood samples were collected from 5 hours fasted male mice and glucose, insulin, glucagon, and total GLP-1 levels were measured (*Figure 6.1*). As shown in the previous chapter, SKO mice displayed normoglycaemia in the fasted state (*Figure 6.1, A*) but hyperinsulinemia at both 16/17 weeks and 30/34 weeks of age when compared to littermate controls (*Figure 6.1, B*). Interestingly, total GLP-1 levels were increased in 16/17-week-old SKO mice (*Figure 6.1, C*) while glucagon levels remain similar between WT and SKO mice (*Figure 6.1, D*). However, total GLP-1 levels were equivalent in older mice (*Figure 6.1, C*). As SKO mice displayed hyperinsulinemia and enlarged islets at 16/17 weeks of age, I hypothesised that the associated increase in GLP-1 levels could represent a compensatory mechanism of SKO mice to counteract hyperglycaemia in this model by stimulating insulin secretion through GLP-1 Receptor (GLP-1R) signalling.
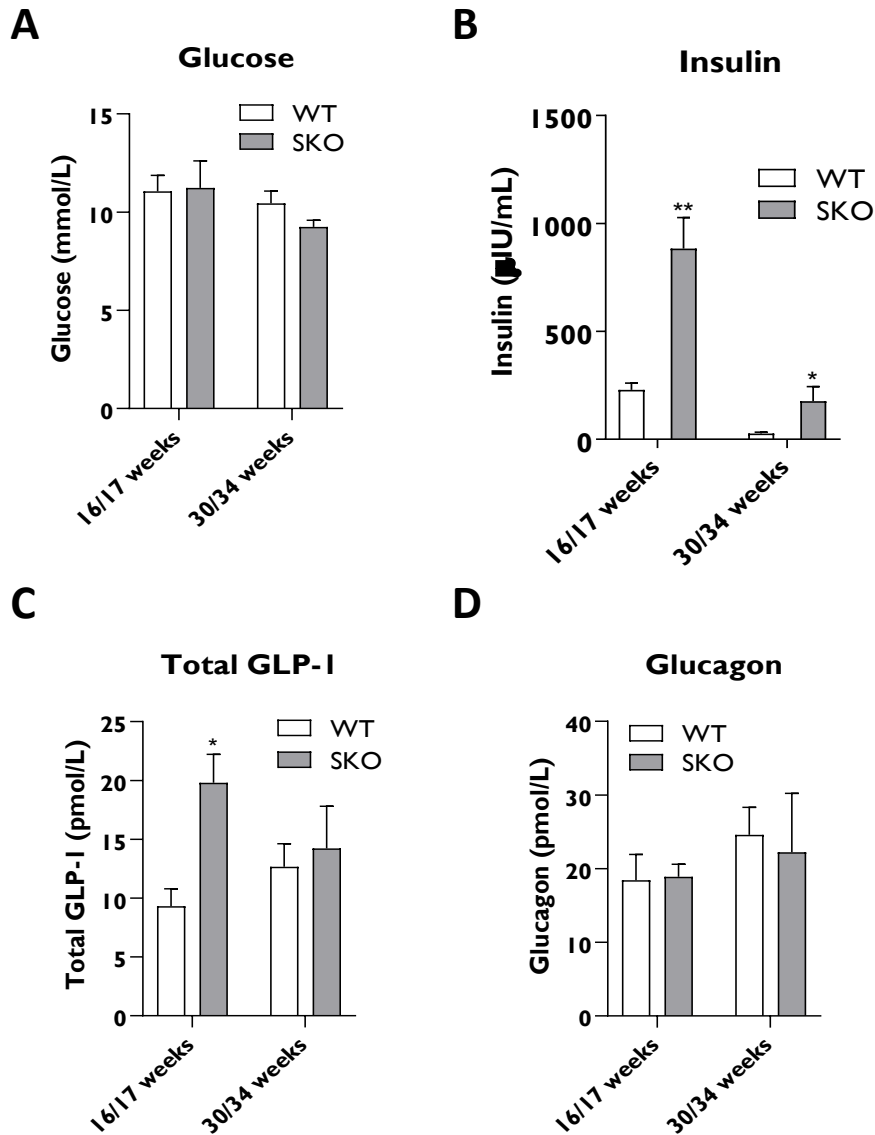
Figure 6.1: GLP-1 levels are increased in male SKO mice. *Serum analysis of glucose (**A**), insulin (**B**), total glucagon-like peptide 1 (GLP-1) (**C**) and glucagon levels (**D**) in 5 hours fasted male wild-type (WT) and seipin-null (SKO) mice at the ages indicated. n= 5v5 (16/17 weeks); 6v4 (30/34 weeks). Data are expressed as mean ± SEM.*p<0.05, **p<0.01. (A/B) reproduced from Figure 5.4 in Chapter 5.*

6.2.2. GLP1 Receptor expression is upregulated in SKO mice

To investigate whether that increase in circulating GLP-1 levels is accompanied by any alteration in the expression of its receptor, I measured the mRNA levels of *Glp-1R* in different tissues. Due to the paucity of residual white adipose tissue in SKO mice, *Glp-1R* mRNA expression could not easily be determined in this tissue. However, *Glp-1R* expression was readily detectable in pancreatic islets. Interestingly, *Glp-1R* mRNA expression was elevated in SKO islets when compared to islets isolated from control mice (***Figure 6.2, A***). *Glp-1R* was expressed at a much lower level in the liver but a two-fold increase in hepatic *Glp-1R* expression was observed in SKO mice at both 16/17 and 30/34 weeks of age when compared to age-matched controls (***Figure 6.2, B***). Thus, increased GLP-1R expression in pancreatic islets might increase β-cell sensitivity to circulating levels of GLP-1 peptide. Together, these data suggest that the increase in both circulating GLP-1 levels and its receptor in pancreatic beta cells and insulin-sensitive tissues may contribute to glucose tolerance and β-cell adaptation in insulin-resistant SKO mice.
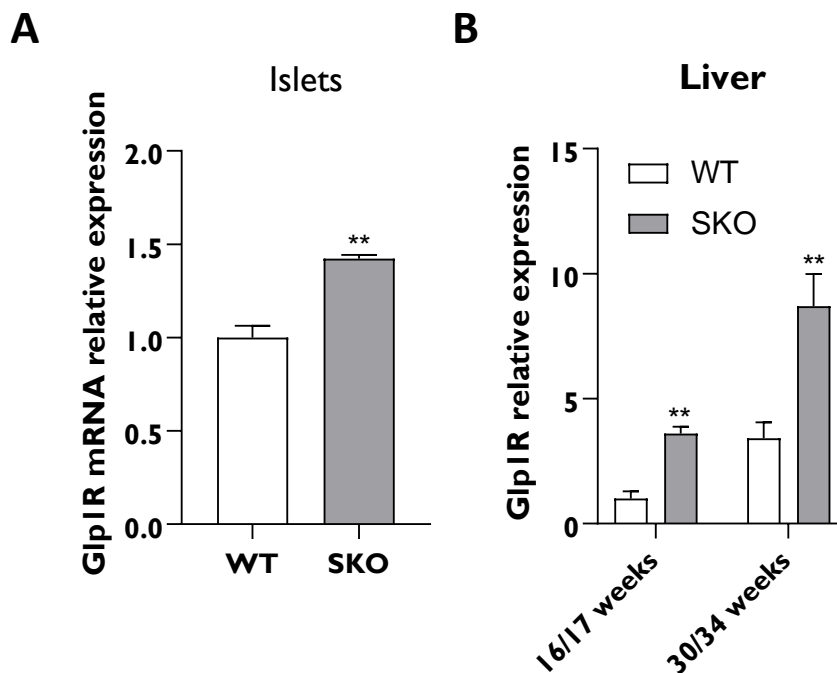
Figure 6.2: GLP-1 Receptor expression is upregulated in male SKO mice. *Glp1R mRNA relative expression in 40 weeks of age islets (**A**) and livers (**B**) from wild-type (WT) and seipin-null (SKO) mice. Gene expression was normalised to the geometric mean of Hprt, Nono and Yhwaz reference genes. Islets: n=3, 15 islets/condition. Livers: n= 3v4 (16/17 weeks); 6v4 (30/34 weeks). Data are expressed as mean ± SEM. **p<0.01.*

6.2.3.   GLP1R agonist promotes insulin secretion in SKO pancreatic islets

The most significant effect of GLP-1 is to promote insulin secretion from pancreatic β-cells in a glucose-dependent manner (255). As seen in the previous sections, SKO mice exhibited increased circulating GLP-1 levels and *Glp-1R* mRNA expression. To investigate whether this was associated with an enhanced insulin secretion in SKO mice, I assessed the insulin secretion profile of SKO islets in response to GLP-1R agonist. GLP-1 peptide is rapidly degraded by dipeptidyl peptidase 4 (DPP-4) resulting in a short half-life of the active form of GLP-1 (417). To circumvent this inactivation, I used a long-acting GLP-1R agonist, exendin-4 (also known as exenatide), which is resistant to DPP-4 proteolysis and displays similar affinity to native GLP-1R and therefore same effects as GLP-1 peptide (418) (***Figure 6.3, A***). Although this was not significant, SKO islets secreted less insulin than WT islets when exposed to low glucose (2.5 mM) (***Figure 6,3, B***). Moreover, exendin-4 did not alter insulin secretion when incubated at low glucose. Incubation with high glucose medium (25 mM) stimulated insulin secretion to a similar extent in islets isolated from both WT and SKO mice (***Figure 6.3, B***). Insulin secretion was further potentiated with 10 nM of exendin-4 in SKO islets (***Figure 6.3, B***). As, unexpectedly, this potentiation was not observed in islets isolated from WT mice, these data should probably be treated with caution and further replication will be important to confirm these results. As such, it is not entirely clear at this stage whether islets isolated from SKO mice displayed an increased sensitivity to exendin-4 or not.
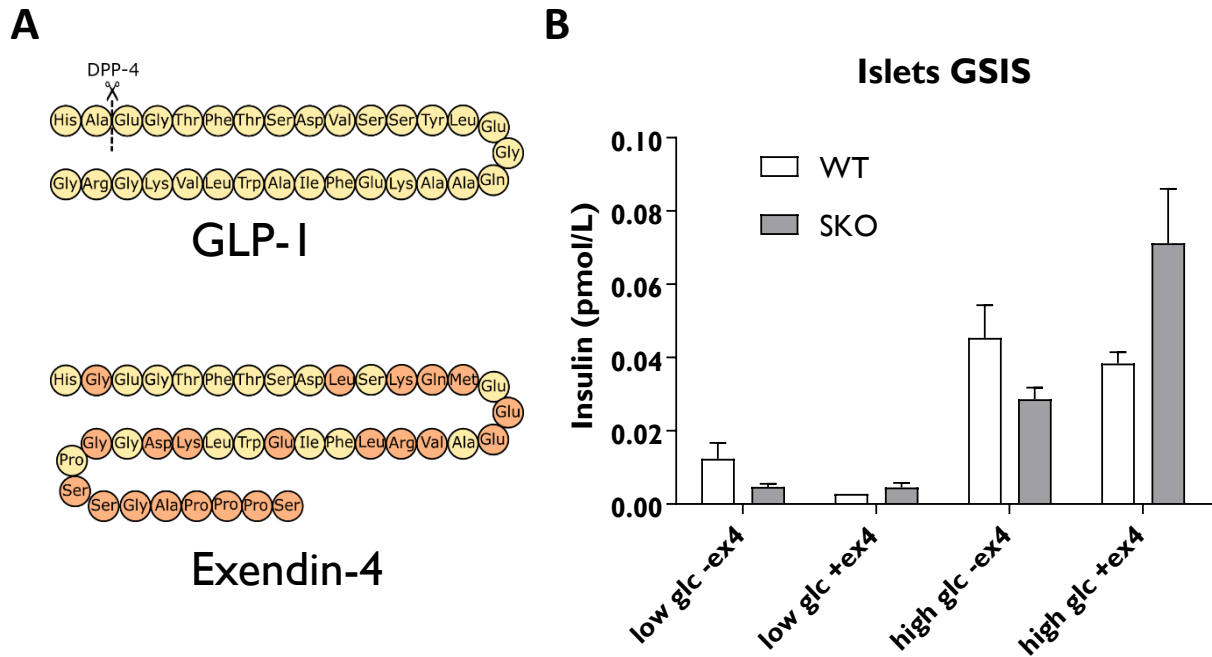
***Figure 6.3: Insulin secretion in response to Glp-1 agonist in male SKO mice.** (A) Schematic representation of Glp-1 and Exendin-4 peptides. (**B**) Glucose-stimulated insulin secretion (GSIS) in isolated islets from 40 weeks of age male wild-type (WT) and seipin-null (SKO) mice. Islets were exposed to either low glucose (low glc: 2,5 mM) or high glucose (high glc: 25 mM) as indicated. Exendin-4 (ex4) was used at a concentration of 10 nM to stimulate insulin secretion (n=3, 15 islets/condition). Released insulin was normalised to total insulin content. Data are expressed as mean ± SEM.*

6.2.4.   Seipin loss increases glucose-stimulated insulin secretion in a pancreatic β-cell line

Given the limitations of obtaining mouse pancreatic islets in sufficient quantities and given the high expression of seipin in β-cells (385), I sought to examine the consequences of seipin loss specifically in pancreatic β cells. To investigate the role of seipin in β-cell function, I used the well-studied INS-1 rat pancreatic β cell line, which retains glucose-stimulated insulin secretion capacity in culture (415). The use of a pancreatic β cell line not only rules out the contribution of the *in vivo* milieu to seipin alterations in pancreas but also permits the direct investigation of cell-autonomous role that seipin might play in these cells. Using RT-PCR, I found that *Bscl2* was readily detectable in INS-1 cells (***Figure 6.4, A***). Using three different short-interfering RNA (siRNA), I knocked down *Bscl2* mRNA expression in INS-1 cells. *Bscl2* mRNA expression was successfully reduced by 75 to 90 % forty-eight hours after the

transfection (***Figure 6.4, A***). The first siRNA, which gave the better knockdown, was used for the following experiments. To evaluate the effect of seipin loss on insulin release, glucose-stimulated insulin secretion was assessed in transfected INS-1 cells. No differences were observed at 2.5 mM of glucose. High glucose medium (25 mM) increased insulin secretion by 2-fold in INS-1 cells transfected with scrambled siRNA (***Figure 6.4, B***). Interestingly, GSIS was significantly elevated by almost 4-fold in cells transfected with an siRNA directed against Bscl2 treated with high glucose medium (***Figure 6.4, B***). This significant increase was not associated with elevated total insulin content within the cells (***Figure 6.4, C***).
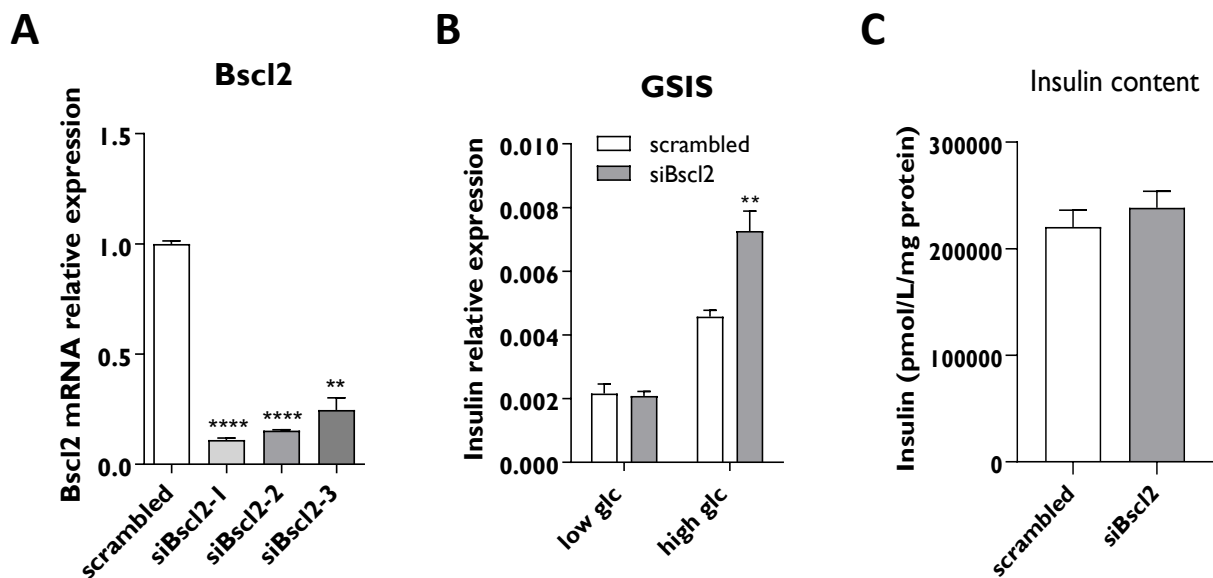
Figure 6.4: Seipin loss increases insulin secretion in INS-1 pancreatic β cells. *INS-1 cells were transfected with a control siRNA (scrambled) or a siRNAs targeted against Bscl2 (siBscl2-1-3). 48 hours after transfection, cells were analysed. (**A**) mRNA relative expression of Bscl2. Gene expression was normalised to the geometric mean of Hprt, Nono and Yhwaz (n=3). (**B**) Glucose-stimulated insulin secretion (GSIS) in INS-11 cells. siBscl2-1 was used to knockdown Bscl2 expression. Cells were exposed to either low glucose (low glc: 2,5 mM) or high glucose (high glc: 25 mM) as indicated. Released insulin was normalised to total insulin content (**C**) (n=9). Data are expressed as mean ± SEM. **p<0.01, ****p<0.0001.*

As expected, the addition of 10 nM of exendin-4 did not affect the insulin secretion when both control and *Bscl2* knockdown cells were incubated with 2.5 mM of glucose (low glucose) as GLP-1 requires glucose to effectively potentiate insulin secretion (***Figure 6.5, A***) (255). As previously observed (***Figure 6.4***), seipin knockdown increased insulin secretion in cells incubated with high glucose medium. Exendin-4 significantly enhances insulin secretion in high glucose conditions (25 mM) (***Figure 6.5, A***). Insulin secretion in response to exendin-

4 in high glucose condition was slightly more elevated in seipin knockdown cells but failed to reach significance (p=0.0507) compared to that in control cells. When expressed as a fold change, exendin-4 induced a similar 4-fold increase in insulin secretion in both control and seipin knockdown cells (***Figure 6.5, B***). Thus, it would appear that loss of seipin may principally increase glucose stimulated insulin release, rather than increasing sensitivity to exendin-4/GLP-1 under these conditions. However, it may also be that this concentration of exendin-4 is saturating and that lower concentrations of exendin-4 are needed to observe changes in GLP-1 sensitivity. Thus, further studies would be valuable to investigate this further, given the increased GLP-1 receptor observed in seipin knockout islets (***Figure 6.2, A***).
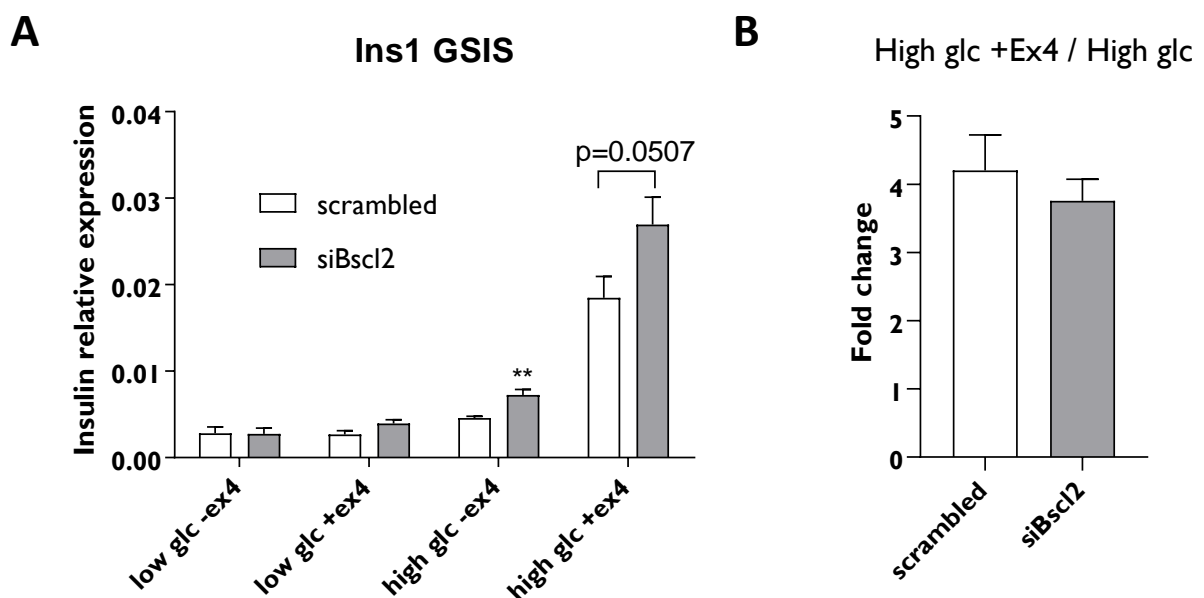
Figure 6.5: Seipin loss does not severely impair insulin secretion response of INS-1 cells to GLP-1R agonist exendin-4. *INS-1 cells were transfected with a control siRNA (scrambled), or a siRNA targeted against Bscl2 (siBscl2). 48 hours after transfection, cells were assessed for glucose-stimulated insulin secretion (GSIS). (**A**) Glucose-stimulated insulin secretion (GSIS) of INS-1 cells in the absence or presence of 10 nM Exendin-4 (ex4). Cells were exposed to either low glucose (low glc: 2,5 mM) or high glucose (high glc: 25 mM) as indicated. Released insulin was normalised to total insulin content. (**B**) Fold change in insulin secretion in response to exendin-4 and high glucose when compared to high glucose condition alone (n=9). Data are expressed as mean ± SEM. **p<0.01*

6.2.5. Seipin deficiency upregulates Glp-1R and Glut2 expression in INS-1 cells

To further probe the possible mechanisms underlying the increased insulin secretion in response to glucose in Bscl2-deficient cells, the expression of key genes involved in glucose metabolism were examined by qPCR. Changes in the expression of these genes might reflect changes in the glycolytic flux. The siRNA used in this experiment almost completely abolished *Bscl2* expression in transfected INS-1 cells (**Figure 6.6, A**). Interestingly, silencing of *Bscl2* significantly increased *Glp-1R* expression in comparison with control cells transfected with a scrambled siRNA (**Figure 6.6, B**). The extent of *Glp-1R* upregulation was similar to the one observed in islets isolated from SKO mice (see section 6.2.2 **Figure 6.2, A**). Loss of seipin also leads to the upregulation of glucose transporter 2 (*Glut2*) expression (**Figure 6.6, C**). This may indicate that seipin-deficient cells have a higher capacity to sense glucose than control cells.
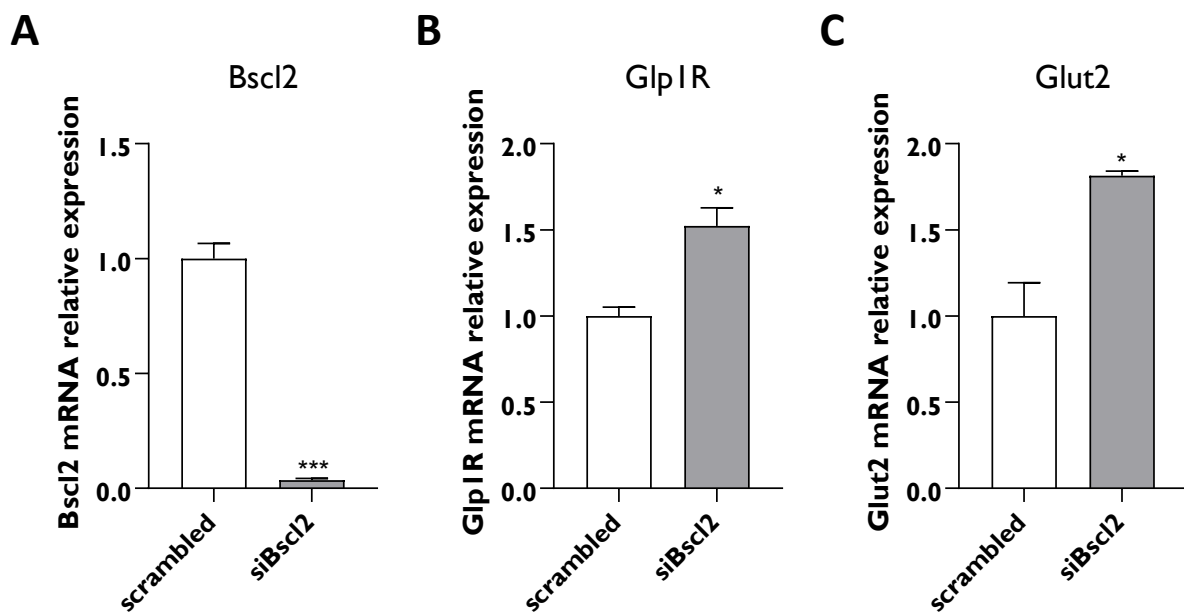
***Figure 6.6**: **Silencing of Bscl2 increases Glp-1R and Glut2 expression in INS-1 cells**. INS-1 cells were transfected with a control siRNA (scrambled), or a siRNA targeted against Bscl2 (siBscl2). 48 hours after transfection, cells were analysed for gene expression. mRNA relative expression of Bscl2 (**A**), Glucagon-like peptide 1 receptor (Glp-1R) (**B**) and Glucose transporter 2 (Glut2) (**C**). Gene expression was normalised to the geometric mean of Hprt, Nono and Yhwaz (n=3). Data are expressed as mean ± SEM.*p<0.05, ***p<0.001.*

The expression of glucokinase (*Gck*), which acts a rate-limiting enzyme of the glycolytic pathway, was equivalent between controls and cells transfected with a siRNA targetting Bscl2 (***Figure 6.7, A***). Two of the 3 genes investigated downstream of Gck were found to be downregulated, namely glucose-6-phosphate isomerase (*Gpi*) and aldolase A (AldoA) (***Figure 6.7, B/D***), while phosphofructokinase P (*Pfkp*, platelet isoform) was significantly upregulated in seipin-deficient INS-1 cells (***Figure 6.7, C***). Taken together, these results indicate that seipin loss upregulates the expression of the nutrient sensors Glut 2 and Glp-1R and alters the expression of glycolytic genes. This suggests that seipin deficiency could enable β-cells to better respond to nutrient signals including glucose and GLP-1. This might then translate into an increase in insulin secretion in those cells.
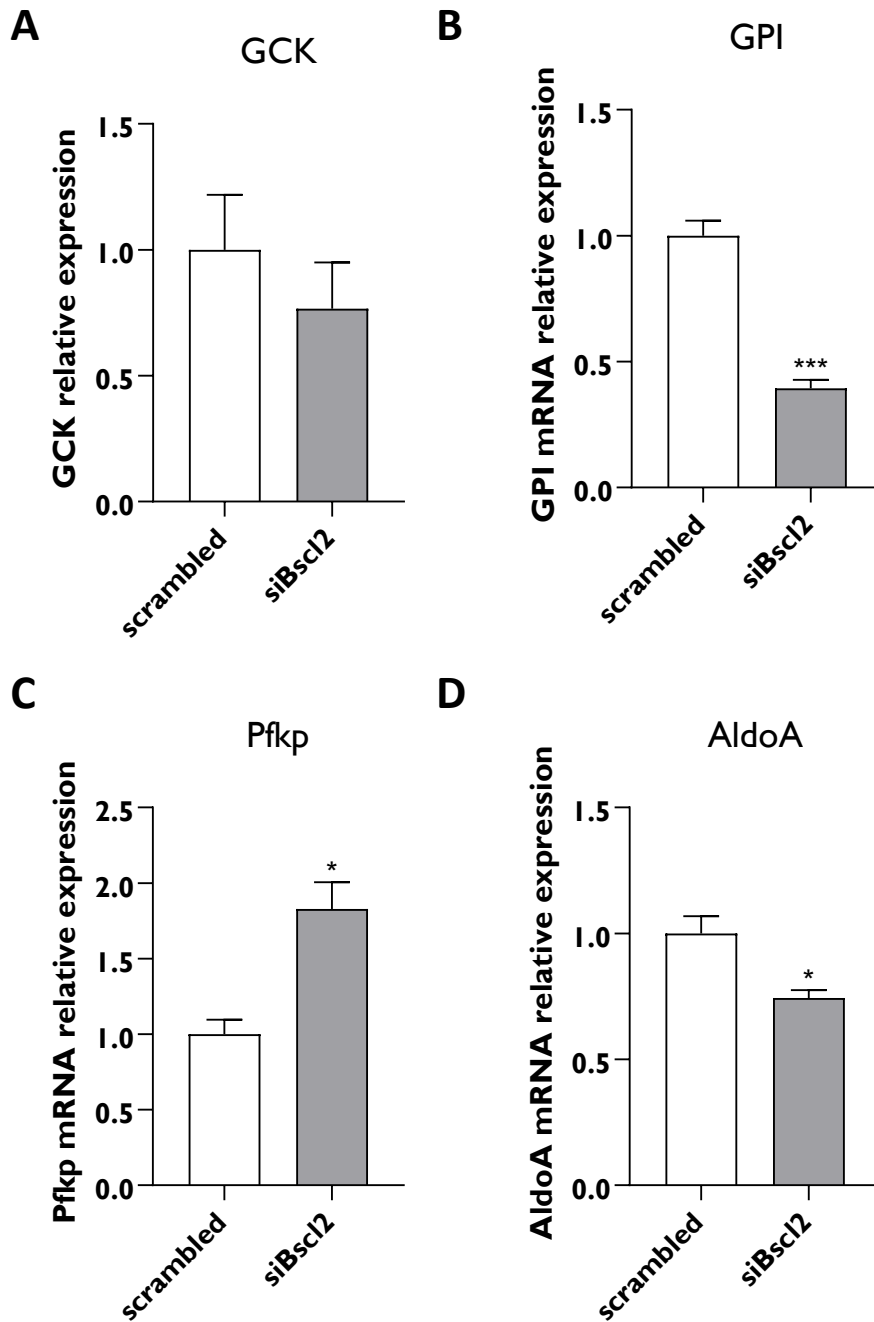
Figure 6.7: **Altered glucose metabolism in seipin-deficient INS-1 cells**. *INS-1 cells were transfected with a control siRNA (scrambled) or a siRNA targetting Bscl2 (siBscl2). 48 hours after transfection, cells were analysed for gene expression. mRNA relative expression of Glucokinase (Gck) (**A**), Glucose 6 phosphate isomerase (Gpi) (**B**), Phosphofructokinase P (Pfkp) (**C**) and Aldolase A (AldoA) (**D**). Gene expression was normalised to the geometric mean of Hprt, Nono and Yhwaz (n=3). Data are expressed as mean ± SEM.*p<0.05 ; ***p<0.001.*

6.2.6.   **GLP1R might interact with seipin protein**

While investigating potential interactors of GLP-1R from mouse islet cDNA libraries, *Dai et al.* identified seipin protein as a putative GLP-1R interactor (416). In light of this, I also wished to investigate whether seipin could indeed bind GLP-1R as this would offer a mechanism *via* which seipin could influence the insulin secretory system. To investigate any association between seipin and GLP-1R, tagged-versions of the proteins were co-expressed in human embryonic kidney (HEK) 293 cells. GLP-1R and seipin were tagged with FLAG and MYC epitopes, respectively as depicted in ***Figure 6.8, A*** and ***6.8, B***. To optimise the transfection efficiency, varying amounts of plasmid DNA were tested in a ratio to one another of 1:1 to 4:1. Cell lysates were harvested 48 hours after transfection and immunoblotted with FLAG and MYC antibodies. This revealed that HEK 293 cells robustly expressed both proteins when transfected with equal amounts of seipin and GLP-1R plasmids (1:1 ratio). The optimal amount of total DNA was estimated at 1 μg for a 12-well tissue culture plate (***Figure 6.8, C***). Increasing the total quantity of DNA to 2 μg did not yield greater expression (***Figure 6.8, C***).
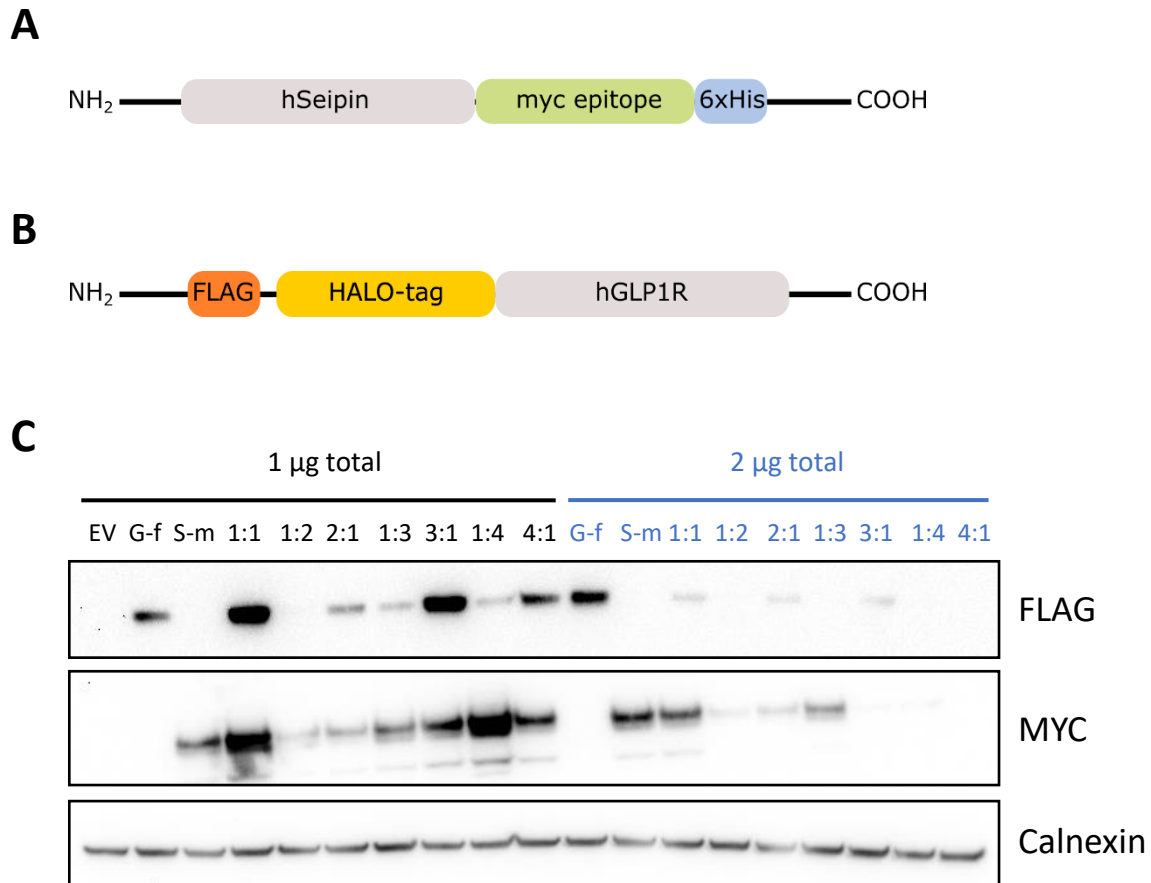
Figure 6.8*: **Optimisation of cotransfection efficiency in HEK 293 cells.** Schematic representation of Seipin- (**A**) and GLP-1R-tagged expression constructs (**B**). MYC and HIS epitopes are present downstream of seipin sequence. A HALO-tag and a FLAG-tag are present upstream of GLP-1R sequence. (**C**) HEK 293 cells were transiently transfected with varying amounts of empty vector (EV), Seipin-MYC (S-m) and GLP-1R-FLAG (G-f) constructs and harvested 48 hours after transfection. Lysates were blotted with FLAG and MYC antibodies. Calnexin was used as a loading control. Ratios correspond to the quantity of GLP-1R-FLAG compared to Seipin-MYC (GLP-1R-FLAG: to Seipin-MYC). Presented blots are representative of at least three independent experiments.*

Next, FLAG-tagged GLP-1R and MYC-tagged Seipin constructs were overexpressed in HEK 293 cells and cell lysates were immunoprecipitated with anti-FLAG M2 beads. MYC-tagged seipin was detected in both lysates and anti-FLAG immunoprecipitates from samples in which FLAG-GLP-1R was co-expressed, suggesting a potential interaction between GLP-1R and seipin proteins (***Figure 6.9***).
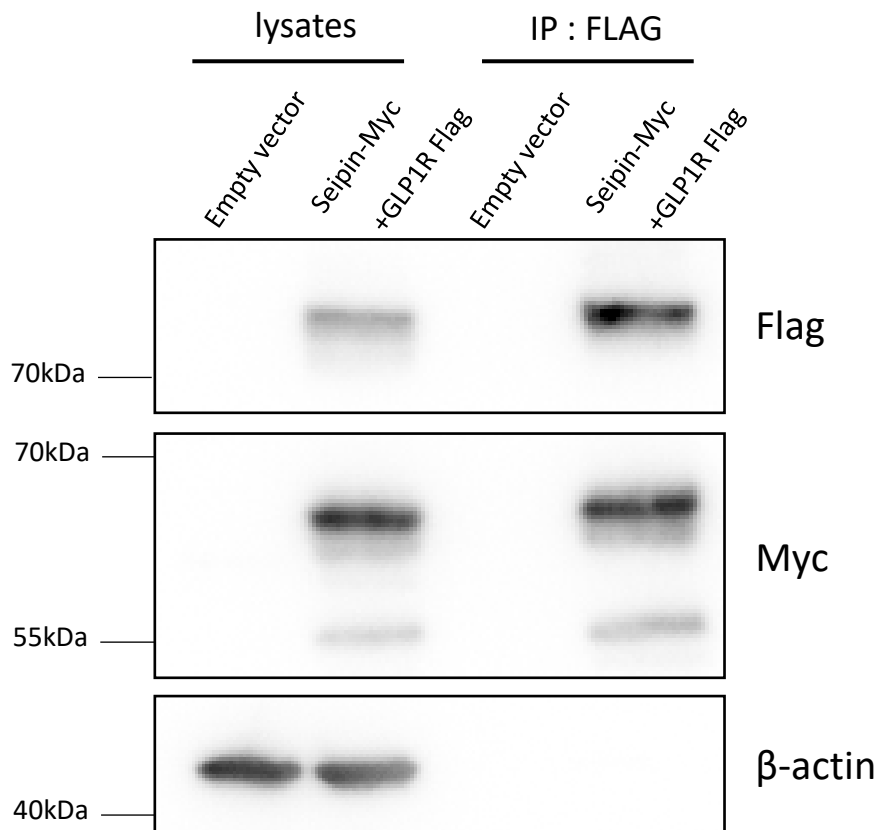
Figure 6.9*: **Overexpression of seipin and GLP-1R in HEK 293 cells reveals an interaction**. HEK 293 cells were transiently transfected with empty vector or Seipin-MYC and GLP-1R-FLAG constructs and harvested 48 hours after transfection. Lysates and anti-FLAG immunoprecipitates were blotted with FLAG and MYC antibodies. β-actin was used as a loading control. Presented blots are representative of at least three independent experiments. Immunoprecipitation (IP).*

The use of two overexpressed tagged proteins in the preceding experiment raises the risk that the association may not be specific, but instead a consequence of substantial overexpression. To mitigate against this, FLAG-tagged GLP-1R construct alone was overexpressed in HEK 293 cells and cell lysates were immunoprecipitated with anti-FLAG M2 beads to isolate the expressed GLP-1R. When immunoprecipitates were probed with anti-human seipin antibody, endogenous seipin protein was clearly detected only in immunoprecipitated samples from GLP-1R expressing cells. This adds further evidence for a specific interaction between GLP-1R and endogenous seipin protein (***Figure 6.10***). However, whether this interaction involves direct contacts or is indirect remains to be assessed.
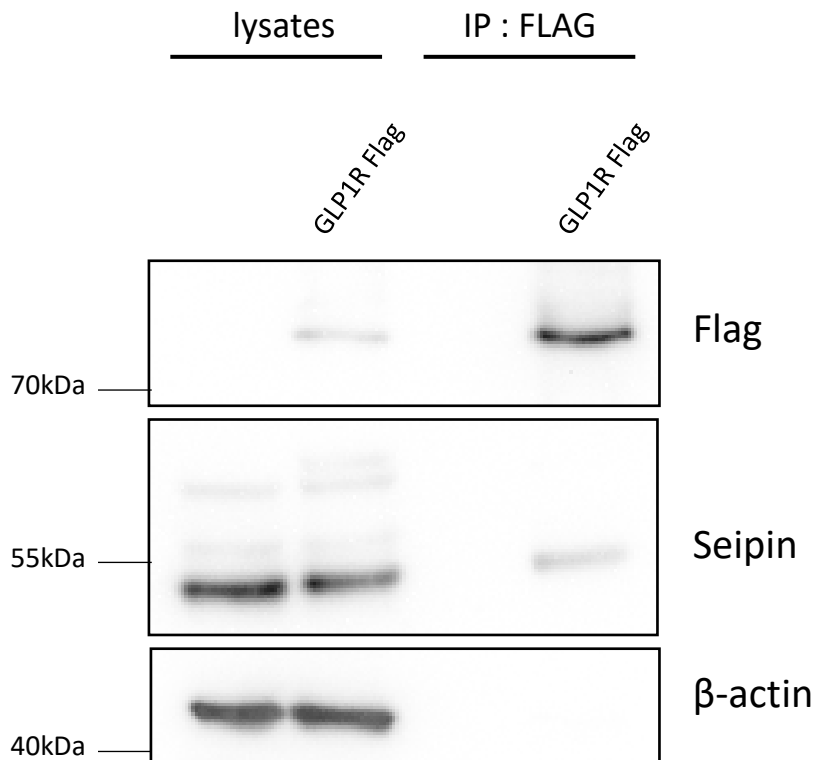
Figure 6.10: The GLP-1 Receptor interacts with endogenous seipin protein. *HEK 293 cells were transiently transfected with empty vector or GLP-1R FLAG constructs. GLP-1R-FLAG was immunoprecipitated with anti-FLAG and precipitates immunoblotted with FLAG and seipin antibodies. β-actin was used as a loading control. Presented blots are representative of at least three independent experiments. Immunoprecipitation (IP).*

6.2.7. C-terminus domain is not required for seipin and GLP1R interaction

As depicted in ***Figure 6.11, A***, seipin is a membrane protein of the endoplasmic reticulum (ER) and is composed of two transmembrane domains and a luminal loop. A short N-terminus and a longer C-terminus are located on the cytosolic side of the ER membrane. In order to identify which regions of seipin may be required for its interaction with GLP-1R, five myc-tagged deletion constructs in which either the N-terminus (ΔNT), the C-terminus (ΔCT), the first transmembrane domain (ΔTm1), the second transmembrane domain (ΔTm2) or the ER luminal loop (ΔLoop) had been deleted were used (***Figure 6.11, B***).

A
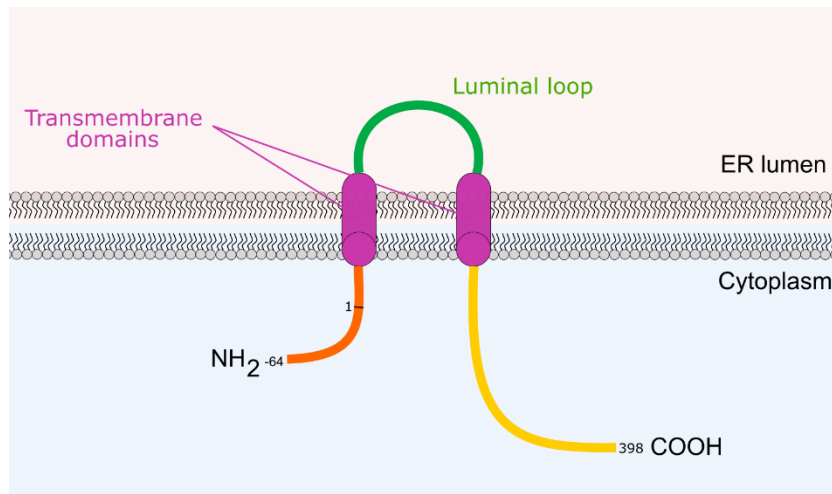
B
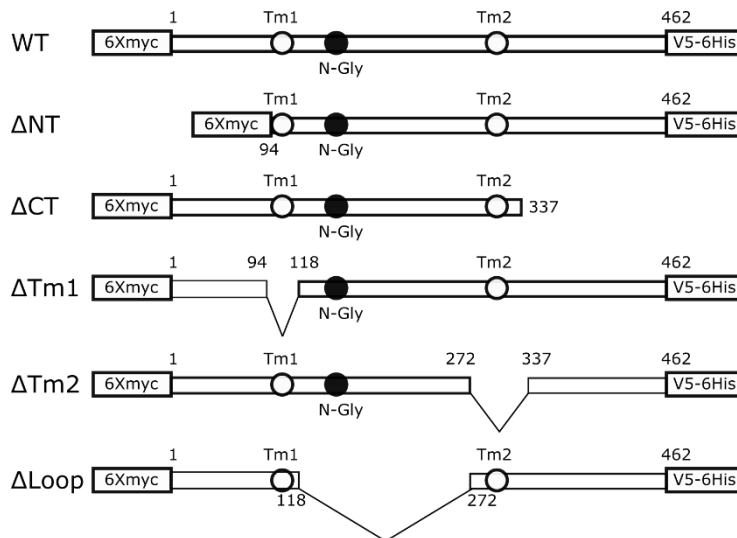
Figure 6.11*: **Seipin domains and contructs mutants used in the study.** (**A**) Schematic structure of seipin within the endoplasmic reticulum (ER) membrane. (**B**) Schematic diagram of seipin wild-type (WT) and deleted domains (Δ) constructs. N-terminus (NT), C-terminus (CT), transmembrane domain 1 (Tm1), transmembrane domain 2 (Tm2), ER luminal loop (loop).*

The ability of wild-type seipin (WT) and deletion mutants to bind co-transfected GLP-1R-FLAG was then determined. All mutants were robustly expressed and immunoprecipitated with anti-flag beads (***Figure 6.12, A***). Overexpression of an empty vector alone, GLP-1R FLAG alone or seipin WT-MYC alone were used as controls (***Figure 6.12, A***). Deletion of C-terminus of seipin did not inhibit its interaction with GLP-1R. Deletion of N-terminus or the ER luminal loop of seipin modestly impaired its interaction with GLP-1R. Deletion of the transmembrane domains 1 (ΔTm1) or 2 (ΔTm2) reduced seipin binding to GLP-1R by more than 50 % (***Figure***

170

6.12, B). These data are preliminary but none of the constructs completely abrogated seipin binding to GLP-1R (***Figure 6.12, B***). Collectively, my observations do not clearly indicate that a specific interaction occurs between GLP-1R and a specific, single domain of the seipin protein. However, the reduced binding to some deletion constructs of seipin may indicate that GLP-1R interacts *via* more than one domain of seipin. It might also result from the presence of endogenous wild type seipin within the cells contributing to oligomers of seipin also containing the transfected mutant seipin and permitting interaction with GLP-1R. Further experiments will clearly be needed to examine this.
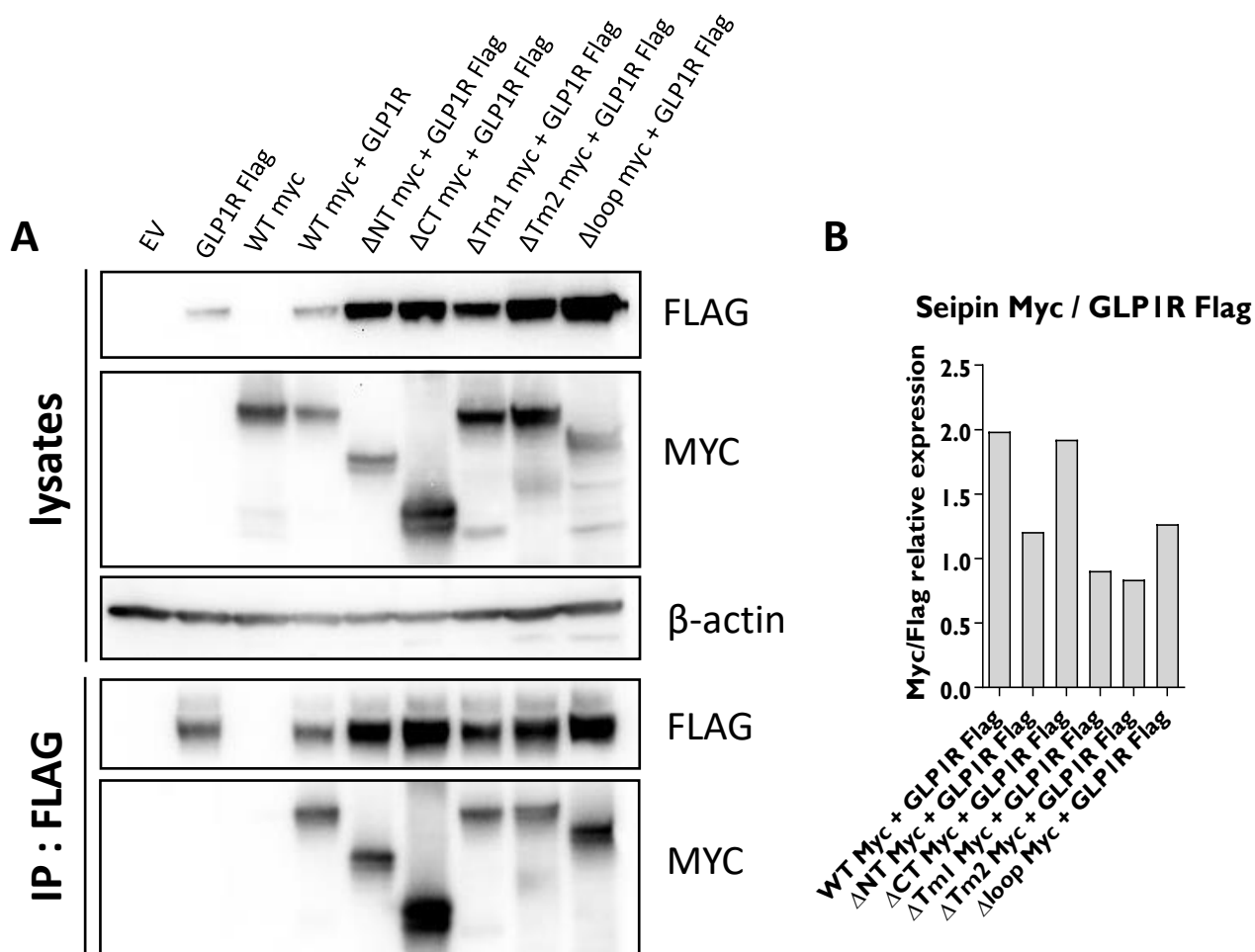
Figure 6.12*: **Seipin domains required for its interaction with GLP-1 Receptor***. *(A) HEK 293 cells were transiently transfected with empty vector (EV) and GLP-1R FLAG constructs in the presence or absence of Seipin.wild-type (WT) and deleted domains (Δ) constructs lacking: N-terminus (NT); C-terminus (CT); transmembrane domain 1 (Tm1); transmembrane domain 2 (Tm2) and the ER luminal loop (loop). Cell lysates and anti-FLAG immunoprecipitates were separated by electrophoresis and blotted with FLAG and MYC antibodies. β-actin was used as a loading control. IP: immunoprecipitation. Presented blots are representative of at least three independent experiments. (**B**) Quantification of binding of deleted forms of seipin (MYC) to GLP-1R (FLAG) presented in A. Data are normalised to FLAG levels in the same samples.*

6.2.8.   Cellular colocalisation of Seipin and GLP-1R

Next, seipin and GLP-1R colocalization was assessed by confocal fluorescence microscopy. Tagged constructs were overexpressed in INS-1 cells (*Figure 6.13, A*) and Min6 cells (*Figure 6.13, B*), a rat and a mouse pancreatic β cell line, respectively. I also evaluated the spatial expression of seipin and GLP-1R in 3T3-L1 cells, a mouse preadipocyte cell line whose large size and defined morphology make it easier to examine subcellular localisation of proteins (*Figure 6.13, C*). Co-transfected cells were immunostained for both FLAG-tagged GLP-1R and MYC-tagged seipin. GLP-1R appears to at least partially colocalise with seipin. GLP-1R was found at both the plasma membrane and intracellular compartments but identification of specific compartments where seipin and GLP-1R colocalise was difficult to determine from these pictures. Other staining might be required to demonstrate whether GLP-1R and seipin indeed localise to the same compartments in the cell.
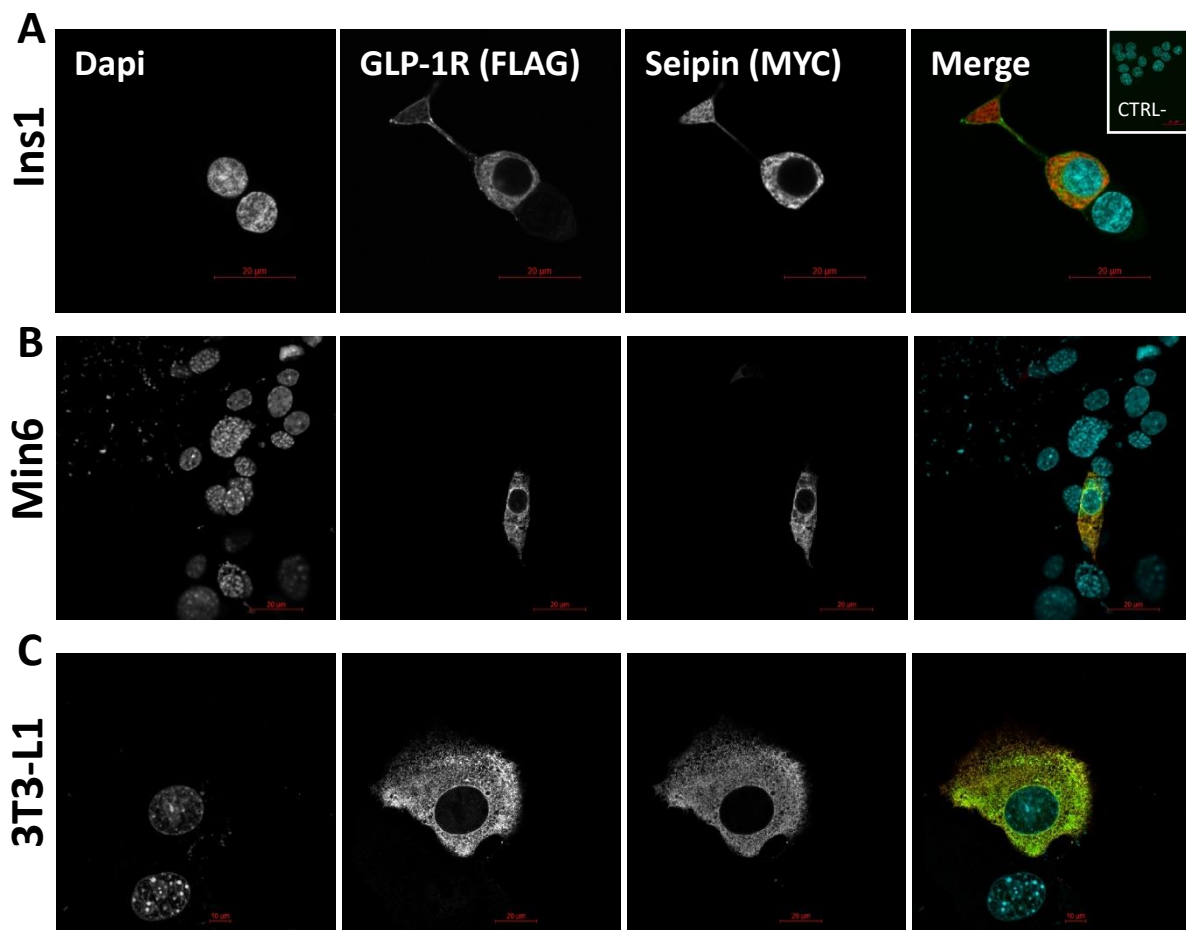
Figure 6.13*: **Seipin colocalises with GLP1R**. Seipin-MYC and GLP1R-FLAG expression constructs were co-transfected in INS-1 (**A**), Min6 (**B**) and 3T3-L1 cells (**C**). 48 hours after transfection, cells were stained with FLAG (green) and MYC (red) antibodies and DAPI to label nuclei (cyan). Bars denote 10 µm. Negative control (CTRL-) was incubated with the*

secondary antibodies for FLAG and MYC, and DAPI. The images presented here are representative of at least three independent experiments.

6.2.9. Liraglutide treatment in SKO mice

The data presented in this chapter so far have shown that male SKO mice exhibit high levels of GLP-1 at 16/17 weeks of age. This age coincides with an extremely high level of insulin in the blood along with a considerable expansion of pancreatic islets in these mice. No glucose intolerance was observed at that age. However, as SKO mice aged further, the levels of insulin markedly dropped as did the GLP-1 levels in the blood. These results could be consistent with a mechanism whereby GLP-1 is the driving signal for the islet expansion and compensation that is observed in SKO mice. If so, maintaining GLP-1 signalling in these mice, beyond 17 weeks of age, might be sufficient to sustain insulin production from pancreatic β-cells and prevent the slow deterioration of glycaemic control. Moreover, as GLP-1R is also more abundant in SKO islets, it is possible they are particularly sensitive to GLP-1 peptide. This could be the case regardless of any interaction between the GLP-1R and seipin directly. To test this, I investigated the therapeutic potential of liraglutide, a long-acting GLP-1R agonist, to treat metabolic disease in our SKO mice. Liraglutide is approved for the treatment of type 2 diabetes since 2010 (419) but its use to treat metabolic disease in lipodystrophy has not been formally investigated.

18/21 weeks of age wild-type (WT) and seipin-knockout (SKO) mice were divided into two groups and treated either with saline (PBS/control) or with 0.2 mg/kg liraglutide administered intraperitoneally. Both male and female mice were examined in this study.

To investigate the effects of liraglutide on glucose control, insulin tolerance tests (ITT) (***Figure 6.14***) and glucose tolerance tests (GTT) (***Figure 6.15***) were performed after a 5-hour fast and a single injection of either PBS or liraglutide.

Consistent with data presented in Chapter 5, both female and male SKO mice were insulin-resistant as shown in ***Figure 6.14, A/B*** and ***6.14, C/D***, respectively. A single administration of liraglutide markedly enhanced glucose disposal in response to insulin stimulation in insulin-resistant SKO female mice (***Figure 6.14, A/B***). A similar effect was observed in the SKO male mice although this failed to reach statistical significance (p=0.057) (***Figure 6.14, C/D***).
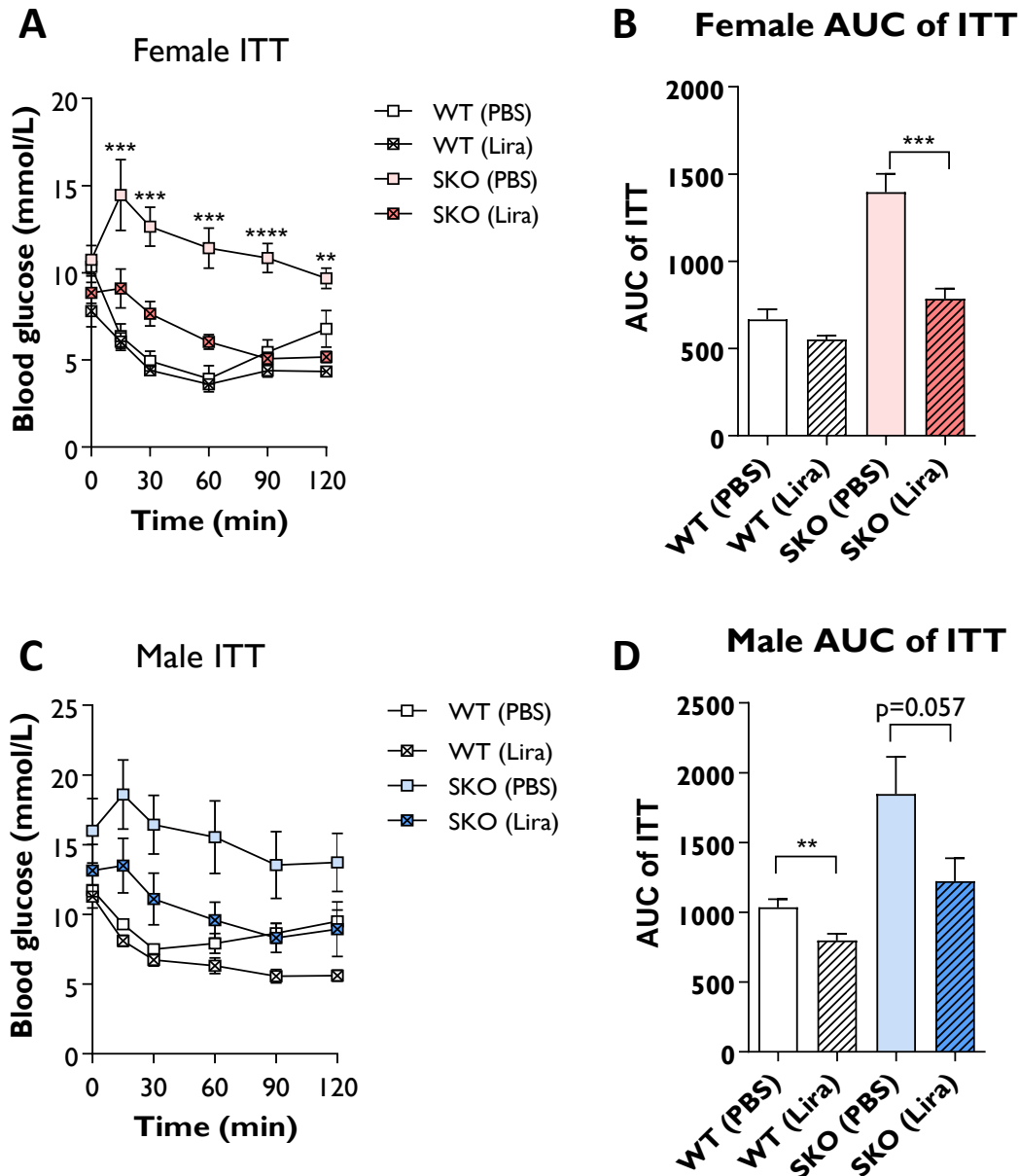
Figure 6.14: Liraglutide improves insulin resistance in SKO mice. *Insulin tolerance tests (ITT) were performed on 18/21-week-old wild-type (WT) and seipin-null (SKO) mice fasted for 5 hours. Mice either received a single injection of phosphate-buffered saline (PBS) or 0.2mg/kg liraglutide (Lira) intraperitoneally 45 min before the assay. (**A**) ITT in female WT and SKO mice. (**B**) Area under the curve (AUC) of the ITT in females (n $_{WT}$=6v6, n $_{SKO}$=6v7). (**C**) ITT in male WT and SKO mice. (**D**) Area under the curve (AUC) of the ITT in males (n $_{WT}$=9v8, n $_{SKO}$=9v10). AUC was calculated from the glucose levels of each time point. Data are expressed as mean ± SEM, **p<0.01, ***p<0.001, ****p<0.0001.*

Treatment with liraglutide also considerably improved blood glucose control in response to a glucose challenge (2 g/kg body weight) in SKO female mice (***Figure 6.15, A/B***). Liraglutide treatment also significantly improved glucose response in SKO male mice although it was less striking than in female SKO mice (***Figure 6.15, C/D***).

174

Together, these results demonstrate that liraglutide improves glucose tolerance in SKO mice. This effect is evident in both sexes but more apparent in female SKO mice.
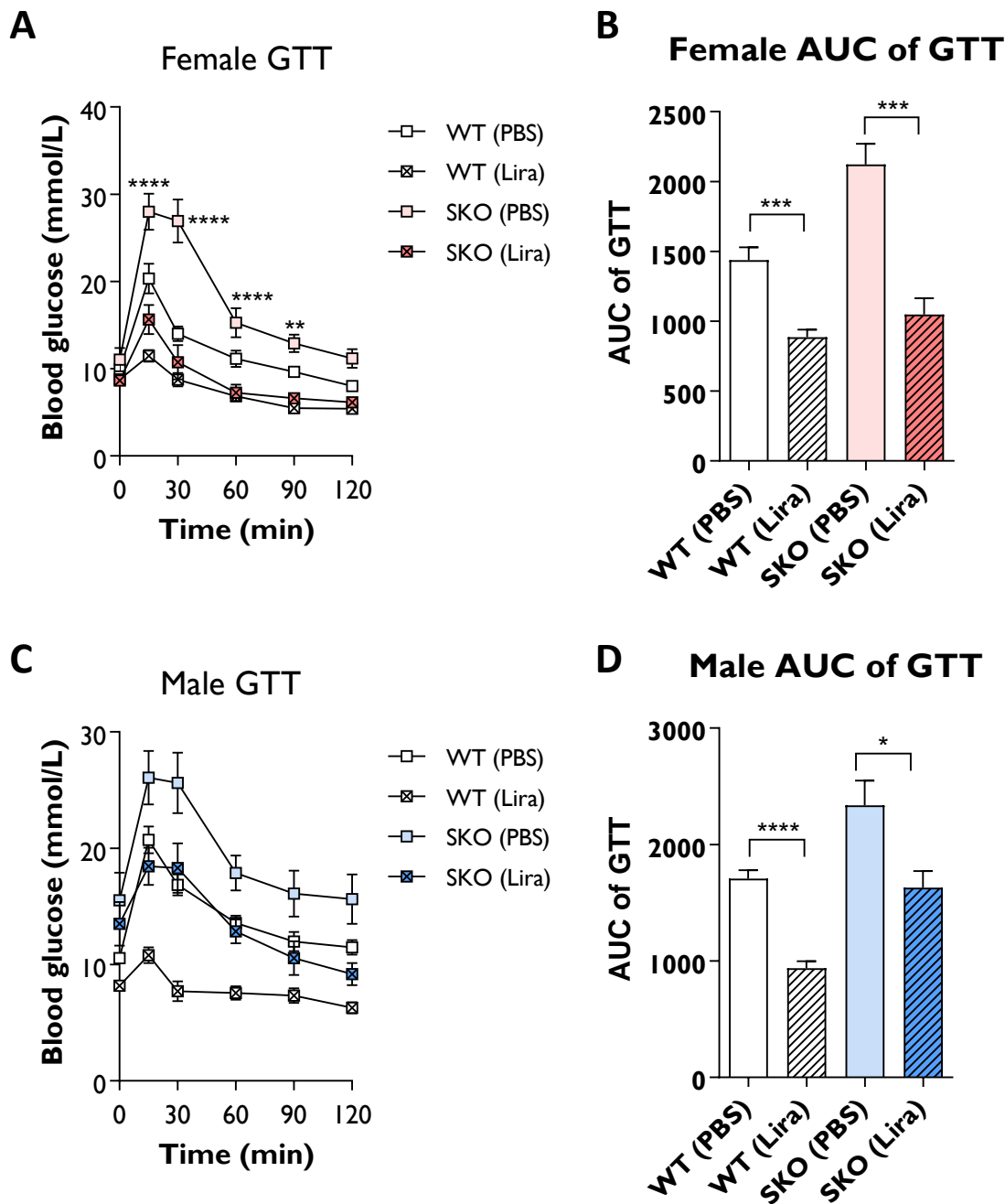
Figure 6.15: Liraglutide improves glucose tolerance in SKO mice. Glucose tolerance tests (GTT) were performed on 18/21-week-old wild-type (WT) and seipin-null (SKO) mice fasted for 5 hours. Mice either received a single injection of phosphate-buffered saline (PBS) or 0.2 mg/kg liraglutide (Lira) intraperitoneally 45 min before the assay. (A) GTT in female WT and SKO mice. (B) Area under the curve (AUC) of the GTT in females (n $_{WT}$ =7v7, n $_{SKO}$ =6v7). (C) GTT in male WT and SKO mice. (D) Area under the curve (AUC) of the GTT in males (n $_{WT}$ =9v8, n $_{SKO}$ =9v10). Data are expressed as mean ± SEM, *p<0.05, **p<0.01, ***p<0.001, ****p<0.0001.

Given the beneficial effects of acute liraglutide treatment on glucose homeostasis observed during the glucose and insulin tolerance tests in SKO mice, I sought to examine the therapeutic potential of a more chronic treatment with liraglutide. For this, mice were treated once daily with liraglutide (0.2 mg/kg body weight) or PBS for two weeks.

Body weight was slightly elevated in SKO mice in comparison with WT mice, but this was not altered by liraglutide treatment (*Figure 6.16, A/B*). Analysis of tissue weight revealed that liraglutide treatment significantly reduced liver mass in both male and female SKO mice (*Figure 6.16, C/D*). There was a trend toward hypertrophy of the pancreas in female SKO mice receiving PBS (*Figure 6.16, E*). Liraglutide treatment further increased pancreas weight in female SKO mice (*Figure 6.16, E*). Male SKO mice displayed enlarged pancreata but this was unaffected by liraglutide treatment (*Figure 6.16, F*). Other tissues analysed, including heart, kidney, spleen, brain, BAT and testis did not differ in weight between PBS- and liraglutide-treated female SKO mice (*Figure 6.16, G*). This was also the case in male SKO mice with the exception of the spleen which displayed a marked reduction in mass after two weeks of treatment with liraglutide (*Figure 6.16, H*).
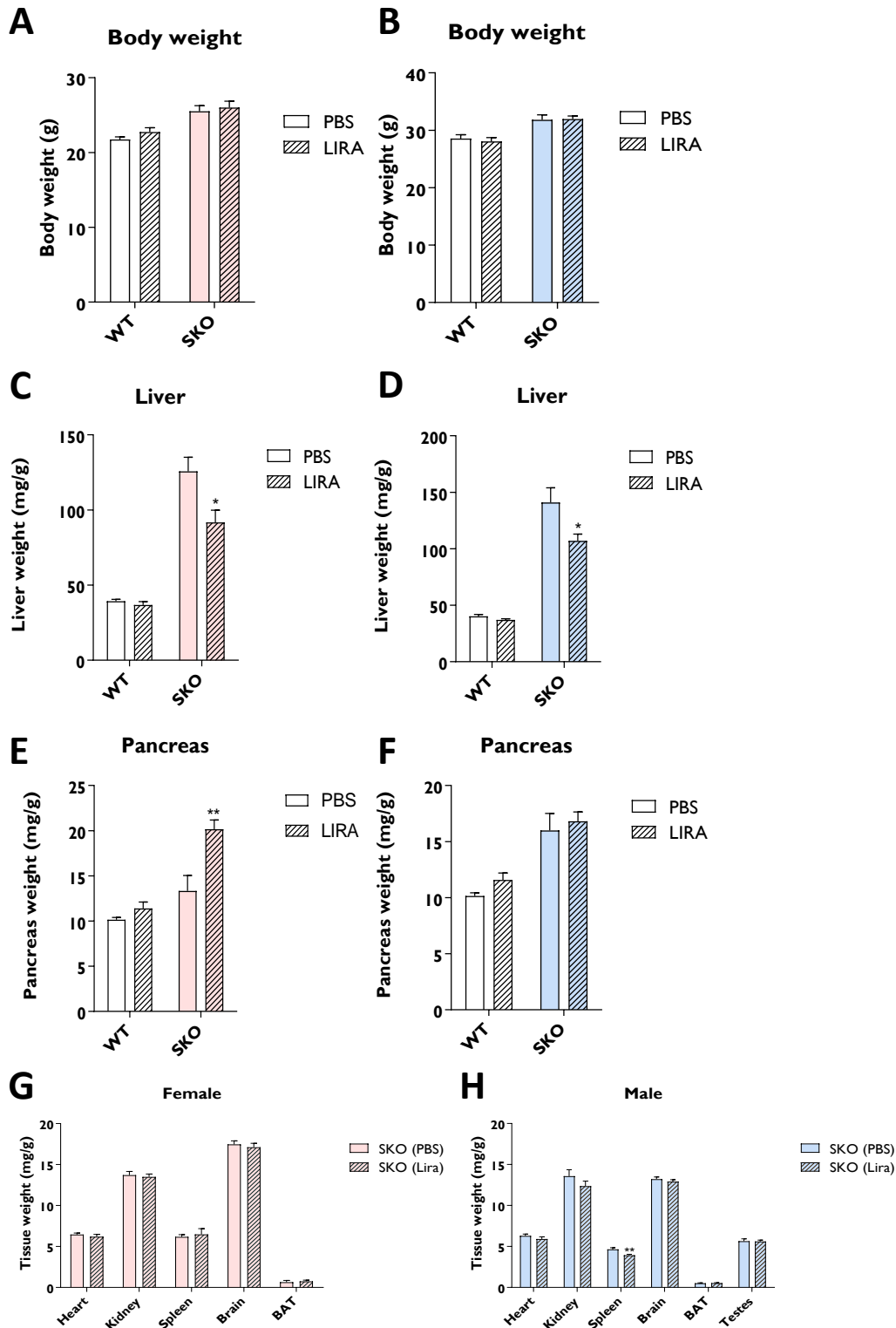
Figure 6.16: Effects of a two-week treatment of liraglutide on body and tissue weights. Mice either received a daily injection of phosphate-buffered saline (PBS) or 0.2 mg/kg liraglutide (Lira) intraperitoneally for 2 weeks, as indicated. Changes in female body (A) and male body weight (B), female liver (C) and male liver weight (D), female pancreas (E) and male pancreas weight (F), female other tissues (G) and male other tissues (H). Tissue weights are normalised to body weight. ($n_{females\ WT}$=7v7, n_{SKO}=6v7), ($n_{males\ WT}$=9v8, n_{SKO}=9v10). Data are expressed as mean ± SEM, *p<0.05, **p<0.01.

The reduction of liver weight observed in both male and female SKO mice upon treatment with liraglutide prompted me to examine liver histology to determine any changes in hepatic steatosis. Interestingly, liraglutide treatment considerably reduced hepatic steatosis in female SKO mice with only a few lipid droplets observed in these mice following 2 weeks of treatment (*Figure 6.17, A*). In contrast, male SKO mice still exhibited numerous lipid droplets after the treatment with liraglutide (*Figure 6.17, B*). Thus, whilst a beneficial effect of liraglutide on hepatic steatosis in male SKO mice cannot be ruled out, it is difficult to assess this from these images alone. Quantification of triglycerides levels in the liver would be valuable to more precisely define potential liraglutide-induced changes in hepatic steatosis in both male and female SKO mice.

As of the time of this writing, serum analyses, triglyceride measurements, further tissue analysis and food/water intake measurements are underway as part of this study. Overall, the preliminary data presented above strongly support the potential value of liraglutide for the management of metabolic disturbances in CGL2.
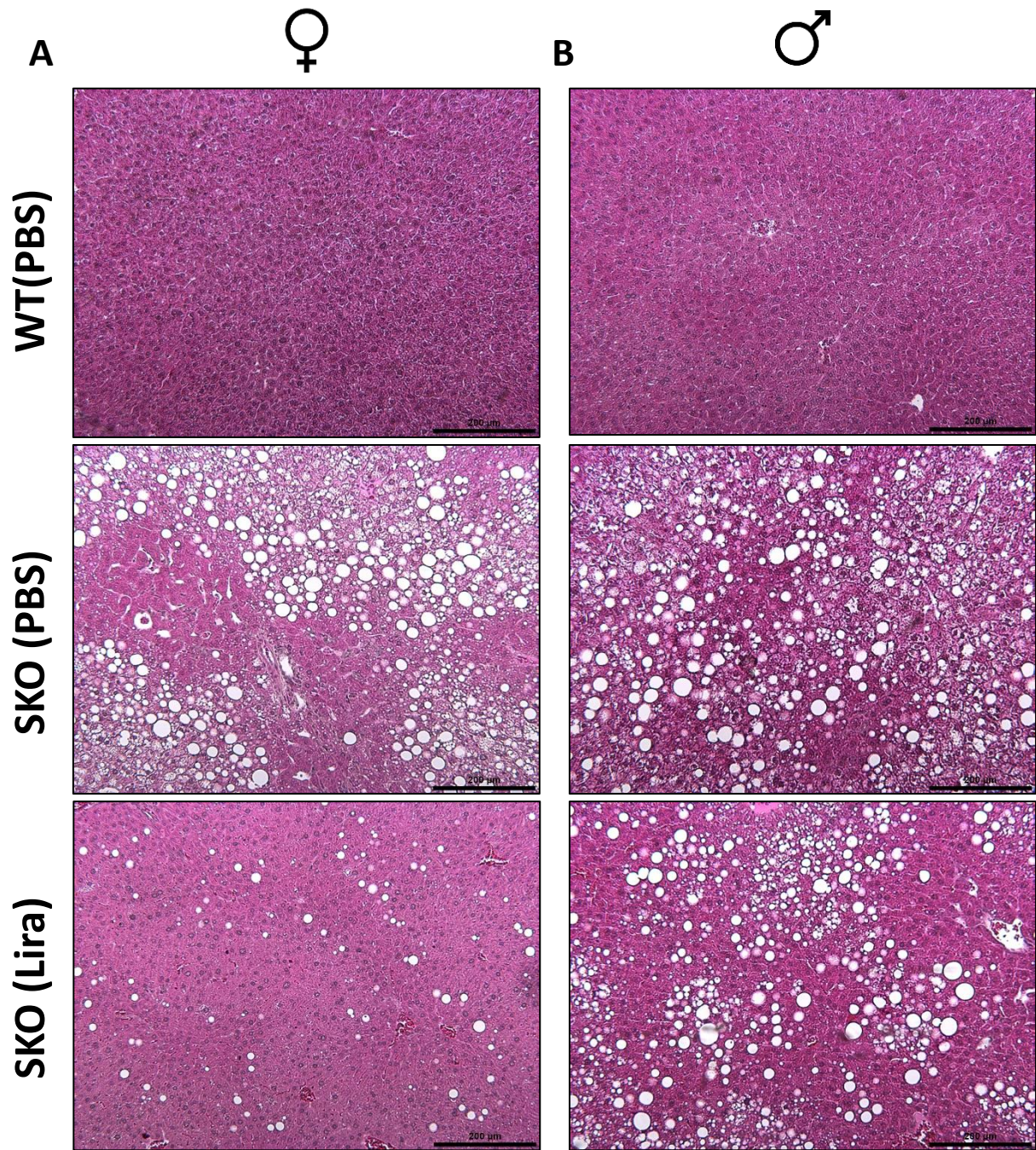
Figure 6.17: Liraglutide improves hepatic steatosis in SKO mice. *Representative images of hematoxylin and eosin (H&E) staining of paraffin-embedded liver sections of wild-type (WT) and seipin-null (SKO) female (**A**) and male (**B**) mice. Mice were either treated with phosphate-buffered saline (PBS) or 0.2 mg/kg liraglutide (Lira) daily for 2 weeks, as indicated. Bars denote 200 μm.*

6.3. Discussion

Progressive loss of β-cell mass and β-cell function are thought to significantly contribute to the pathogenesis of type 2 diabetes (327,420). The data presented in Chapter 5 showed that SKO mice are able to effectively compensate for insulin resistance by increasing pancreatic islet mass and insulin secretion. Several signals have been suggested to drive this compensation in insulin-resistant states, such as nutrients, cytokines and hormones (421). The incretin hormone GLP-1, acting *via* binding to GLP-1 receptor, exerts numerous anti-diabetic effects including, but not limited to, stimulation of β-cell insulin secretion, β-cell survival and β-cell proliferation (422). In this chapter, I investigated whether GLP-1 may provide a key signal for β-cell compensation in SKO mice and a potential mechanism to further enhance this. These studies revealed that GLP-1 plasma levels were elevated in 16-week-old SKO mice, coinciding with the enhancement of insulin secretion at that age. Similarly, GLP-1R mRNA expression was upregulated in islets isolated from SKO mice. It is worth noting that the protein levels of GLP-1R were not evaluated and this will be valuable to include in future experiments. These changes in GLP-1 levels and GLP-1R expression prompted us to examine the incretin effect in our SKO mouse model. The insulin secretory response to the GLP-1R agonist, exendin-4, was preserved in islets isolated from SKO mice when studied *ex vivo*. Unfortunately, the expected response to exendin-4 in the presence of high glucose was not observed in WT islets. This made us cautious about concluding whether the sensitivity to GLP-1R activation was genuinely increased in SKO islets without further replication of these experiments. Potentiation of glucose-stimulated insulin secretion by GLP-1 has been reported to be impaired in type 2 diabetes (423,424). Similarly, a reduced GLP-1 response has been shown to correlate with the slow deterioration of glucose tolerance in a 7 year-longitudinal study (425). However, some studies have also reported increased incretin effect and islet GLP-1R levels in high fat diet-induced insulin resistant states (426,427). Therefore, it will be interesting to perform an oral glucose tolerance test in our mice to analyse to which extent the incretin effect might play a role in altered glycaemic control in our SKO mice.

Several models of tissue-specific deletion of *Bscl2* have been generated (150,337,347,407,428–430). While *Bscl2* is ubiquitously expressed throughout the body, albeit at different levels (85), the lack of adipose tissue was originally thought to be the main driver of metabolic disturbances observed in CGL2. However, adipose tissue-specific *Bscl2* knockout mice failed to recapitulate those (337,407). Given the high expression of *Bscl2* in the pancreas,

in the work presented in this chapter, I sought to examine the potential contribution of seipin to β-cell function. INS-1 cells and siRNA knockdown were used to investigate the effect of seipin deficiency on glucose-stimulated insulin secretion. Interestingly, I found that the knockdown of *Bscl2* resulted in increased insulin secretion, without affecting total insulin content and GLP-1-induced insulin secretion. In addition, the mRNA expression of the glucose transporter Glut2 and GLP-1R was upregulated following *Bscl2* loss and the expression of glycolytic genes was also altered. I believe that this is the first detailed examination of seipin function in pancreatic β cells. Further analysis will be required to elucidate the role of seipin in the regulation of glucose homeostasis but preliminary data point at a cell-autonomous role of seipin in pancreatic islets by influencing insulin release from β cells. In future, it would be intriguing to generate and study pancreas- or β-cell-specific *Bscl2* knockout mice to directly evaluate the influence of pancreatic seipin loss on β-cell function. Similarly, only knockdown experiments have been performed in the experiments presented in this chapter but overexpression of native or mutant forms of seipin in pancreatic β cells might also provide valuable insights into seipin function.

The GLP-1 receptor is a member of the B class G protein-coupled receptor (GPCR) family. Like other GPCRs, GLP-1R activates adenylyl cyclase (AC) through the stimulatory protein G_S and leads to cAMP accumulation (254). Most of GLP-1 actions are mediated by the protein kinase A (PKA) and exchange protein directly activated by cAMP 2 (Epac2) which are triggered by this cAMP accumulation (255). In addition to G protein subunits, the activation and signal transduction of GLP-1R rely on accessory proteins which are largely unknown (431). In an attempt to identify these accessory proteins that interact with GLP-1R, *Dai et al.* performed membrane-based split ubiquitin yeast two-hybrid (MYTH) assays (416). Screening of mouse islet cDNA library revealed 29 novel potential interacting proteins, among which was seipin. In this chapter, I confirmed by immunoprecipitation the interaction between GLP-1R and seipin. However, I failed to identify which specific domain of seipin is crucial for this interaction. This could either indicate that none of the domains deleted in this study are essential for the interaction or that multiple domains contribute. An important caveat is that overexpression of contructs, as performed in this chapter, may promote artificial or non-specific interactions. Therefore, the proposed interaction between GLP-1R and seipin still requires further validation. In this context, immunoprecipitation of endogenous GLP1R or seipin directly would be beneficial although other interaction assays could also be used to investigate this interaction further. Interestingly, the main component of caveolae, caveolin-1 (cav-1), has also been shown to interact with the GLP-1R (432). This interaction was necessary for the

correct localisation and cellular trafficking of GLP-1R to lipid rafts and plasma membrane. Mutations in the caveolin 1 gene cause CGL3, another type of congenital generalised lipodystrophy (433).

As shown in section 6.2.4, siRNA-mediated knockdown of *Bscl2* significantly increased glucose-stimulated insulin secretion and GLP-1R mRNA expression, without affecting GLP-1-induced insulin secretion in rat pancreatic β-cells. If seipin and GLP-1R interaction is confirmed, then this may suggest that seipin could have an inhibitory role in GLP-1R signalling. To fully understand the contribution of seipin to this pathway, additional work is required but relatively simple experiments such as the measurement of cAMP accumulation induced by GLP-1, the main second messenger of GPCRs, could provide us with valuable further information.

In light of this interaction and the cell-autonomous role of seipin in pancreatic β-cells, I have also assessed the therapeutic potential of liraglutide, a long-acting GLP-1R agonist, for the treatment of CGL2. Liraglutide has been shown to increase insulin secretion in a glucose dependent manner, reducing the risk of hypoglycaemia commonly observed with other anti-diabetic agents (103,434). To the best of my knowledge, GLP-1R analogues use has only been reported in patients with partial lipodystrophy and not generalised lipodystrophy (435,436). The study presented here revealed that a single administration of liraglutide improves glucose tolerance and probably insulin sensitivity in SKO mice. Additionally, I observed that once-daily injection of liraglutide for two weeks significantly reduces hepatic steatosis in female SKO mice. Liraglutide treatment appeared to have fewer striking effects in male SKO mice. Sex specific differences in the response to liraglutide also deserve further study. In addition, further work is currently underway in our lab to examine the precise mechanisms by which liraglutide improves glucose homeostasis in SKO mice.

In summary, the work presented in this chapter strongly suggests a cell-autonomous role of seipin in pancreatic β-cells. It would appear that seipin interacts with GLP-1R and may play an inhibitory role in GLP-1R signalling and in the regulation of insulin secretion. This could explain, at least in part, why SKO mice exhibit strikingly enlarged islets by 34 weeks of age, although this requires further investigation. Finally, this study has shown that liraglutide may offer a valuable alternative to other glucose-lowering drugs for the treatment of CGL2.

CHAPTER 7

7. DISCUSSION

7.1. General discussion

Disruption in the BSCL2 gene, which encodes the protein seipin, causes congenital generalised lipodystrophy type 2, the most severe form of lipodystrophy (85). Affected individuals almost entirely lack adipose tissue stores which leads to ectopic fat accumulation in insulin-responsive tissues including liver, pancreas and skeletal muscle (100,101). Lipid deposition in these organs is believed to impair insulin actions and insulin secretion from pancreatic β cells. Type 2 diabetes, hepatic steatosis and hypertriglyceridemia are thus common features associated with CGL2 (100,101). If poorly controlled, these can lead to major complications including hepatic cirrhosis, acute pancreatitis, renal failure and cardiovascular disease (437). While seipin has been shown to play crucial roles in adipocyte differentiation and maintenance (143,151,152,169), it has been detected in multiple tissues including the brain, testes, liver, skeletal muscle, kidney and pancreas (85). Hence, it may also exert cell-autonomous effects in non-adipose tissues relevant to the pathogenesis of CGL2.

The overall aim of this thesis was to understand the molecular mechanisms *via* which *BSCL2* disruption causes metabolic disease in CGL2, to characterise the disease progression in generalised lipodystrophy and to investigate novel therapies that may be of benefit to affected patients.

Given that the primary defect observed in CGL2 patients is the paucity of adipose tissue, my initial experiments focussed on the role of seipin in the adipose tissue itself. *In vitro* experiments using immortalised mouse cell lines have suggested that seipin is not required for stem cell determination toward an adipogenic lineage but does affect subsequent adipocyte differentiation (143,151). The data presented in Chapter 3 examining the effect of *BSCL2* disruption in human SGBS preadipocyte cells did not, however, agree with these observations as only modest defects in adipogenesis were seen in SGBS cells following seipin knockdown. In my view, this discrepancy may most likely be explained by this human cell line having some brown adipocyte phenotype. SGBS cells were derived from a 3-month old infant, an age at which BAT is highly abundant (345). It has been shown previously that seipin is not required for BAT development and brown adipocyte differentiation in mice and so if SGBS cells can differentiate using BAT adipogenic pathways, they may also not require seipin to differentiate. Similarly, adipose tissue composition varies considerably between ages but also within depots. Therefore, SGBS cells may not model human adult WAT preadipocytes of major depots but rather preadipocytes of another, less abundant depot. It has been shown that small depots of

residual adipose tissue can be observed in CGL2 patients, such as in the knee joint, and it is possible that SGBS cells share features with these depots (98). Finally, it may be relevant to mention that SKO mice have been reported to develop some residual WAT depots initially but that these are subsequently lost in early life (170). As SGBS cells are derived from cells isolated from an infant, it may also be that they are similar to these WAT adipocytes which can escape the effects of seipin loss on adipogenesis but are present only for a short period after birth. To investigate further, one could directly examine the effects of seipin disruption in SVF cells isolated from human adipose samples. Additionally, comparing the effects of seipin disruption across multiple adipose tissue depots and at different ages could also be valuable. It might reveal that seipin is required only for the development of certain adipose depots but for the maintenance of others. Regardless of the contribution of seipin to human adipogenesis, the data presented in Chapter 3 does provide evidence of a conserved role of seipin in influencing lipolysis. Exactly how seipin regulates this process is still unclear. Lipolysis is tightly regulated by PLIN1, HSL and ATGL and is under the control of intracellular cyclic AMP (cAMP) concentrations. While seipin might directly modulate cAMP/PKA signalling, it is possible that its interaction with key proteins regulating the lipolytic pathway plays an important role.

Together with other reports, the data presented in Chapter 3 support the observations that unbridled lipolysis could contribute to adipose tissue loss in SKO mice *in vivo* and that this pathway could be a potential therapeutic target for lipodystrophic patients. However, it is not clear to what extent the metabolic dysfunction observed in global seipin knockout mice can be explained solely by the loss of adipose tissue or whether effects of seipin loss in other tissues might contribute to disease. Several mouse models of adipocyte-specific deletion of *Bscl2* have tried to investigate this (169,337,366,407). Our lab has shown previously that adipocyte-specific ablation of seipin leads to early-onset generalised lipodystrophy without metabolic disturbances (337,407). We believe that this is due to the presence of residual adipose tissue in these mice. Supporting this is the observation that re-expression of seipin only in adipose tissue can rescue the metabolic phenotype of seipin-null mice (438). Similarly, adipose tissue transplantation effectively improves metabolic outcomes in seipin-null mice (439). However, it is possible that seipin loss in non-adipose tissues may still contribute to some aspects of the metabolic phenotype observed in SKO mice and CGL2 patients, even if not driving development of the disease. The data presented in Chapter 4 indicate that seipin does not appear to have a critical role in macrophage immune functions. However, seipin might still exert some functions in macrophages under certain circumstances. It is possible that seipin loss in

macrophages combined with hyperglycaemia and hypertriglyceridemia, which is not observed in our model, could be more detrimental to macrophage function than hyperglycaemia and hypertriglyceridemia alone. This may be modelled more accurately in SKO mice crossed to a dyslipidemic apolipoprotein E (ApoE)-null background (440). If so, this could explain why CGL2 patients are more affected by infections than CGL1 patients (86). Another caveat to this investigation is the choice of the infectious agent used. Only bacterial infection was examined in Chapter 4 to assess the contribution of seipin to the immune system. However, it is possible that seipin alters immune response to other infections. As an example, seipin overexpression has been shown to impair hepatitis C virus life cycle, where seipin's contribution to this most likely relies on its role in lipid droplet morphology (441). However, overall, it appears that the increased rates of infection among CGL2 patients are most likely secondary to the adipose tissue loss and the severe metabolic disease in this condition.

Another secondary effect of adipose tissue loss in SKO mice may be the increase in lean mass I have observed (Chapter 5). Using skeletal muscle selective deletion of seipin in mice, *Chen et al.* demonstrated that seipin does not play an important cell-autonomous role in skeletal muscle homeostasis (406). Moreover, increase muscle mass is a feature of other types of lipodystrophy, both CGL and FPLD which further implies that this is not related specifically to the actions of seipin in muscle but to metabolic or endocrine changes common to different forms of lipodystrophy (442). As muscle fatigue is a significant problem for lipodystrophy patients, the mechanisms involved in changes to muscle in these individuals merits further study.

The severe islet expansion observed in our mouse model in Chapter 5, could also be secondary to the adipose tissue loss but there is evidence from the studies presented here that there could be a direct contribution of seipin loss in islets to this effect. Although it is difficult to make the direct comparison, the extent of islet hyperplasia is our SKO mice seems to exceed that observed in mouse models of obesity or in mice fed a high fat diet (443,444). Islet physiology in the context of lipodystrophy is not well characterised but the pancreatic islet expansion observed in Chapter 5 appears more severe than in other lipodystrophic mouse models including the PPARγ knockout mouse model (27,445,446). While it could be driven by systemic changes caused by the lack of adipose tissue in SKO mice, the pancreatic islet expansion in these mice could also reflect a cell-autonomous role of seipin in these cells. The data presented in Chapter 6 reveal that seipin disruption in a rodent pancreatic β cell line significantly increases insulin secretion, GLP-1R and GLUT2 expression in these cells. Whether these are linked mechanistically remains to be determined. Nonetheless, these preliminary data strongly suggest

a cell-autonomous role of seipin in β cells and I believe this is the first time that direct effects of seipin on pancreatic β cell function have been examined. Interestingly, whilst seipin deficiency appears to be detrimental to adipocytes (Chapter 3, (143,151,152,169)), the data presented here suggest that seipin loss in pancreatic β cells may have some positive effects. Loss of seipin in the pancreas does not cause a primary defect in β cells function. Indeed, I observed significant hyperplasia and increased insulin release from seipin deficient islets and from the INS-1 model of β cells with seipin knockdown. This indicates that seipin loss could contribute to adaptative compensatory responses that attempt to maintain glucose regulation. As a consequence, it seems unlikely that seipin loss in β cells participates in the development of metabolic disease seen in CGL2, but instead might mitigate some of the effects of adipose tissue loss by increasing compensatory mechanisms in pancreatic β cells. This makes SKO mice a potentially valuable tool to study mechanisms involved in β cell integrity, islet expansion and adaptations to insulin resistance. Although speculation, it is possible that seipin in pancreatic β cells could play a physiologically relevant role in islets, such as, during their development in early life or in their normal maintenance. It will be interesting to measure the expression of seipin in islets isolated from obese mice and analyse whether their size is negatively correlated with seipin levels. Similarly, one could examine whether the re-expression of seipin specifically in the β cells of SKO mice would prevent or restrict the significant islet expansion I observed here.

Regarding the mechanisms by which seipin might affect islet expansion, a key observation in Chapter 6 is the demonstration that seipin and GLP-1 receptor may directly interact in mammalian cells (see section 6.2.6). While the proposed physical association still requires further validation, it may provide some insight into the role that seipin plays in pancreatic β cells. Future studies will investigate the mechanistic link between seipin and GLP-1R but preliminary data point at an inhibitory role of seipin on GLP-1R signalling. Given that seipin lacks similarity to other known proteins, it is difficult to predict its functions. Interestingly however, a highly conserved, unique CAAX (C: cysteine, A: aliphatic amino acid, X: any amino acid) prenylation motif is present on the C-terminus of seipin, which is reminiscent of G protein subunits (141,447). This posttranslational lipid modification is not only important for protein-membrane interactions but also protein-protein interactions. Therefore, I hypothesise that seipin might influence G protein signalling and modulate GLP-1 signal transduction. In terms of wider clinical relevance, a greater understanding of the role of seipin in pancreatic islets could lead to the identification of novel pathways controlling proliferation, glucose sensitivity and insulin

secretion in this cell type. This could not only provide us with valuable information regarding how insulin secretion is regulated by seipin and disease progression in CGL2 but also new insights regarding the development and function of pancreatic β cells. Ultimately, this may suggest new potential therapeutic targets that may be relevant for both type 1 and type 2 diabetes.

While GLP-1R is mainly expressed in the pancreas and the brain, its expression is also detected in the intestines, lung, kidney and heart in rodents and humans (249–251,448,449). The presence of GLP-1R in adipose tissue has been controversial but there is now a strong body evidence detecting its presence in fat, albeit at a considerably lower level than that found in pancreatic islets (449–451). Both lipogenic and lipolytic activities have been attributed to GLP-1 in adipose tissue. GLP-1 and liraglutide, its synthetic analogue, promoted adipogenesis in the murine 3T3-L1 pre-adipocyte cell line acting *via* GLP-1R and in a dose dependent manner (452,453). Additionally, 100 nM of GLP-1 enhanced lipolysis in differentiated 3T3-L1 adipocytes (450). In human adipocytes, GLP-1 exhibited a lipogenic activity at a low dose but a lipolytic activity when administered at a higher dose (454). GLP-1R was also found to be upregulated in visceral adipose tissue from insulin resistant obese subjects (450). In 2016, Xu *et al.* demonstrated that exendin-4 promoted the "browning" of white adipose tissue in mice in a Sirtuin 1 (SIRT1)-dependent manner (455). Recently, GLP-1 has also been linked to the regulation of brown adipose tissue thermogenesis in rats (456). Given the interaction between seipin and GLP-1R identified in Chapter 6 and the role of seipin in adipogenesis and lipolysis (Chapter 3), it will be interesting to explore further whether GLP-1 and seipin functionally interact to influence adipose development, lipid breakdown and synthesis and adipose browning.

Consistent with the fact that some of the metabolic complications in CGL2 arise from the loss of adipose tissue endocrine function, leptin therapy, in the form of metreleptin, is probably the most effective treatment for CGL2 patients (92,125,126,130,131). However, 30% of patients experience adverse effects including hypoglycaemia when using metreleptin in combination with insulin injections (135). GLP-1 agonists stimulate glucose-dependent insulin secretion, delay gastric emptying, supress glucagon secretion and promote satiety, and are already used in obese insulin-resistant subjects with T2D (457). As the metabolic complications of CGL2 overlap with those reported in obese insulin-resistant subjects, I evaluated the therapeutic potential of the GLP-1 agonist liraglutide for the treatment of the metabolic disorders associated with CGL2 (see section 6.2.9 in Chapter 6). I am not aware of published studies reporting the

use of GLP-1 agonists in CGL2 patients although these agents might already be recommended to patients in practice, on a case-by-case basis. However, several case reports have shown that GLP-1 agonists exenatide or liraglutide significantly improve glycaemic control in patients with familial partial lipodystrophies (435,436). The data presented in Chapter 6 clearly demonstrate the clinical benefits of liraglutide on glycaemic control and insulin-sensitivity in a mouse model of CGL2. In light of these promising results, clinical studies may be valuable to assess the efficacy of GLP-1 agonists in generalised lipodystrophies and understand their effects. While this treatment only addresses the metabolic complications and not the underlying cause of CGL2, it could significantly improve the quality of life of affected individuals. Similarly, DPP-4 inhibitors increase GLP-1 levels by preventing its cleavage by the DPP-4 enzyme. Subject to further study, they may also be used as an alternative treatment for CGL2, therefore broadening the options made available for physicians and patients for managing CGL2.

In summary, this thesis demonstrates that seipin loss promotes lipolysis in a human preadipocyte cell line. In addition to its functions in adipose tissue, unexplored roles of seipin in macrophages and in pancreatic β cells have also been investigated. While seipin does not appear to play a critical role in macrophages function, the data presented strongly imply it may be involved in the regulation of insulin secretion and GLP-1R signalling in pancreatic β cells. This opens a new area of investigation to define how seipin may influence this process. Finally, the data presented in this thesis also indicate that liraglutide could be a promising treatment for CGL2 patients. More broadly, the work presented demonstrates that the pre-clinical model of CGL2 used in this thesis could be of significant value to study multiple aspects of metabolic disease found in lipodystrophy. In addition, it can also provide new insights regarding the compensatory mechanisms that may be invoked to counteract rare and common forms of insulin resistance as well as to investigate potential new therapies that are so clearly needed for treating patients suffering from lipodystrophy syndromes.

The major findings of my thesis are recapitulated in *Figure 7*.
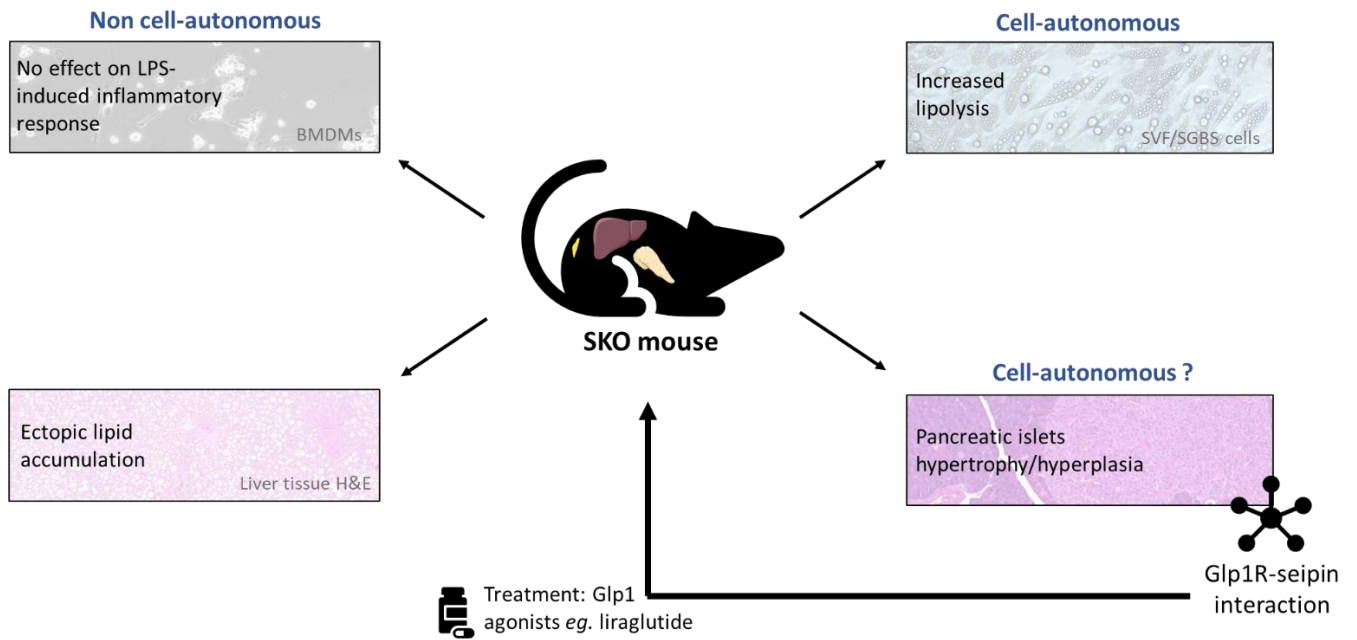
Figure 7: Effects of seipin loss in adipocytes and non-adipose tissues.
Data presented in this thesis demonstrate that seipin does not appear to exert a direct role in macrophages function when BMDMs are challenged with LPS. Seipin plays a cell autonomous role in SGBS human preadipocytes by increasing lipolysis. Seipin might also exert a cell autonomous role in pancreatic β cells although this requires further investigation. A potential interaction between seipin and Glp1R might provide insight into the role that seipin plays in pancreatic β cells. Glp1 agonist, such as liraglutide, has proven itself to be effective in alleviating the metabolic dysfunction of SKO mice. (LPS: Lipopolysaccharides; SVF: Stromal vascular fraction; SGBS: Simpson Golabi Behmel Syndrome; H&E: Hematoxylin & Eosin; SKO: Seipin knockout; BMDMs: Bone marrow-derived macrophages; Glp1: Glucagon-like peptide 1; Glp1R: Glucagon-like peptide 1 receptor).

REFERENCES

1. Chait A, den Hartigh LJ. Adipose Tissue Distribution, Inflammation and Its Metabolic Consequences, Including Diabetes and Cardiovascular Disease. Front Cardiovasc Med [Internet]. 2020 [cited 2021 Aug 8];0. Available from: https://www.frontiersin.org/articles/10.3389/fcvm.2020.00022/full

2. Christiaens V, Lijnen HR. Angiogenesis and development of adipose tissue. Mol Cell Endocrinol. 2010 Apr 29;318(1–2):2–9.

3. Kahn CR, Wang G, Lee KY. Altered adipose tissue and adipocyte function in the pathogenesis of metabolic syndrome. J Clin Invest. 129(10):3990–4000.

4. Spalding KL, Arner E, Westermark PO, Bernard S, Buchholz BA, Bergmann O, et al. Dynamics of fat cell turnover in humans. Nature. 2008 Jun 5;453(7196):783–7.

5. Chen H-J, Meng T, Gao P-J, Ruan C-C. The Role of Brown Adipose Tissue Dysfunction in the Development of Cardiovascular Disease. Front Endocrinol [Internet]. 2021 [cited 2021 Aug 8];0. Available from: https://www.frontiersin.org/articles/10.3389/fendo.2021.652246/full

6. Wu J, Boström P, Sparks LM, Ye L, Choi JH, Giang A-H, et al. Beige adipocytes are a distinct type of thermogenic fat cell in mouse and human. Cell. 2012 Jul 20;150(2):366–76.

7. Giralt M, Villarroya F. White, Brown, Beige/Brite: Different Adipose Cells for Different Functions? Endocrinology. 2013 Sep 1;154(9):2992–3000.

8. Kwok KHM, Lam KSL, Xu A. Heterogeneity of white adipose tissue: molecular basis and clinical implications. Exp Mol Med. 2016 Mar;48(3):e215–e215.

9. Nedergaard J, Bengtsson T, Cannon B. Unexpected evidence for active brown adipose tissue in adult humans. Am J Physiol Endocrinol Metab. 2007 Aug;293(2):E444-452.

10. Zingaretti MC, Crosta F, Vitali A, Guerrieri M, Frontini A, Cannon B, et al. The presence of UCP1 demonstrates that metabolically active adipose tissue in the neck of adult humans truly represents brown adipose tissue. FASEB J Off Publ Fed Am Soc Exp Biol. 2009 Sep;23(9):3113–20.

11. Cypess AM, Lehman S, Williams G, Tal I, Rodman D, Goldfine AB, et al. Identification and importance of brown adipose tissue in adult humans. N Engl J Med. 2009 Apr 9;360(15):1509–17.

12. Yokokawa H, Fukuda H, Saita M, Goto K, Kaku T, Miyagami T, et al. An association between visceral or subcutaneous fat accumulation and diabetes mellitus among Japanese subjects. Diabetol Metab Syndr. 2021 Apr 14;13(1):44.

13. Kwon H, Kim D, Kim JS. Body Fat Distribution and the Risk of Incident Metabolic Syndrome: A Longitudinal Cohort Study. Sci Rep. 2017 Sep 8;7(1):10955.

14. Karpe F, Pinnick KE. Biology of upper-body and lower-body adipose tissue--link to whole-body phenotypes. Nat Rev Endocrinol. 2015 Feb;11(2):90–100.

15. Ruiz-Ojeda FJ, Rupérez AI, Gomez-Llorente C, Gil A, Aguilera CM. Cell Models and Their Application for Studying Adipogenic Differentiation in Relation to Obesity: A Review. Int J Mol Sci. 2016 Jun 30;17(7):1040.

16. Pittenger MF, Mackay AM, Beck SC, Jaiswal RK, Douglas R, Mosca JD, et al. Multilineage potential of adult human mesenchymal stem cells. Science. 1999 Apr 2;284(5411):143–7.

17. Blázquez-Medela AM, Jumabay M, Boström KI. Beyond the Bone: Bone Morphogenetic Protein (BMP) Signaling in Adipose Tissue. Obes Rev Off J Int Assoc Study Obes. 2019 May;20(5):648–58.

18. Qian S, Tang Y, Tang Q-Q. Adipose tissue plasticity and the pleiotropic roles of BMP signaling. J Biol Chem [Internet]. 2021 Jan 1 [cited 2021 Dec 4];296. Available from: https://www.jbc.org/article/S0021-9258(21)00467-1/abstract

19. Bowers RR, Lane MD. Wnt signaling and adipocyte lineage commitment. Cell Cycle Georget Tex. 2008 May 1;7(9):1191–6.

20. Ramji DP, Foka P. CCAAT/enhancer-binding proteins: structure, function and regulation. Biochem J. 2002 Aug 1;365(Pt 3):561–75.

21. Guo L, Li X, Tang Q-Q. Transcriptional regulation of adipocyte differentiation: a central role for CCAAT/enhancer-binding protein (C/EBP) β. J Biol Chem. 2015 Jan 9;290(2):755–61.

22. PAYNE VA, AU W-S, LOWE CE, RAHMAN SM, FRIEDMAN JE, O'RAHILLY S, et al. C/EBP transcription factors regulate SREBP1c gene expression during adipogenesis. Biochem J. 2009 Dec 14;425(1):215–23.

23. Hamm JK, Park BH, Farmer SR. A role for C/EBPbeta in regulating peroxisome proliferator-activated receptor gamma activity during adipogenesis in 3T3-L1 preadipocytes. J Biol Chem. 2001 May 25;276(21):18464–71.

24. Rosen ED, Sarraf P, Troy AE, Bradwin G, Moore K, Milstone DS, et al. PPAR gamma is required for the differentiation of adipose tissue in vivo and in vitro. Mol Cell. 1999 Oct;4(4):611–7.

25. Shao X, Wang M, Wei X, Deng S, Fu N, Peng Q, et al. Peroxisome Proliferator-Activated Receptor-γ: Master Regulator of Adipogenesis and Obesity. Curr Stem Cell Res Ther. 2016;11(3):282–9.

26. He W, Barak Y, Hevener A, Olson P, Liao D, Le J, et al. Adipose-specific peroxisome proliferator-activated receptor gamma knockout causes insulin resistance in fat and liver but not in muscle. Proc Natl Acad Sci U S A. 2003 Dec 23;100(26):15712–7.

27. Wang F, Mullican SE, DiSpirito JR, Peed LC, Lazar MA. Lipoatrophy and severe metabolic disturbance in mice with fat-specific deletion of PPARγ. Proc Natl Acad Sci U S A. 2013 Nov 12;110(46):18656–61.

28.	Imai T, Takakuwa R, Marchand S, Dentz E, Bornert J-M, Messaddeq N, et al. Peroxisome proliferator-activated receptor gamma is required in mature white and brown adipocytes for their survival in the mouse. Proc Natl Acad Sci U S A. 2004 Mar 30;101(13):4543–7.

29.	Semple RK, Chatterjee VKK, O'Rahilly S. PPAR gamma and human metabolic disease. J Clin Invest. 2006 Mar;116(3):581–9.

30.	Eberlé D, Hegarty B, Bossard P, Ferré P, Foufelle F. SREBP transcription factors: master regulators of lipid homeostasis. Biochimie. 2004 Nov;86(11):839–48.

31.	Lefterova MI, Zhang Y, Steger DJ, Schupp M, Schug J, Cristancho A, et al. PPARgamma and C/EBP factors orchestrate adipocyte biology via adjacent binding on a genome-wide scale. Genes Dev. 2008 Nov 1;22(21):2941–52.

32.	Gluchowski NL, Becuwe M, Walther TC, Farese RV. Lipid droplets and liver disease: from basic biology to clinical implications. Nat Rev Gastroenterol Hepatol. 2017 Jun;14(6):343–55.

33.	Barbosa AD, Siniossoglou S. New kid on the block: lipid droplets in the nucleus. FEBS J. 2020;287(22):4838–43.

34.	Giampietri C, Petrungaro S, Conti S, Facchiano A, Filippini A, Ziparo E. c-Flip KO fibroblasts display lipid accumulation associated with endoplasmic reticulum stress. Biochim Biophys Acta BBA - Mol Cell Biol Lipids. 2015 Jul 1;1851(7):929–36.

35.	Velázquez AP, Tatsuta T, Ghillebert R, Drescher I, Graef M. Lipid droplet–mediated ER homeostasis regulates autophagy and cell survival during starvation. J Cell Biol. 2016 Mar 7;212(6):621–31.

36.	Olzmann JA, Carvalho P. Dynamics and functions of lipid droplets. Nat Rev Mol Cell Biol. 2019 Mar;20(3):137–55.

37.	Suzuki M, Otsuka T, Ohsaki Y, Cheng J, Taniguchi T, Hashimoto H, et al. Derlin-1 and UBXD8 are engaged in dislocation and degradation of lipidated ApoB-100 at lipid droplets. Mol Biol Cell. 2012 Mar;23(5):800–10.

38.	Monson EA, Trenerry AM, Laws JL, Mackenzie JM, Helbig KJ. Lipid droplets and lipid mediators in viral infection and immunity. FEMS Microbiol Rev. 2021 Jul 1;45(4):fuaa066.

39.	Hu J, Zhang Z, Shen W-J, Azhar S. Cellular cholesterol delivery, intracellular processing and utilization for biosynthesis of steroid hormones. Nutr Metab. 2010 Jun 1;7:47.

40.	Gao Q, Goodman J. The lipid droplet—a well-connected organelle. Front Cell Dev Biol. 2015;3:49.

41.	Bersuker K, Olzmann JA. Establishing the lipid droplet proteome: Mechanisms of lipid droplet protein targeting and degradation. Biochim Biophys Acta BBA - Mol Cell Biol Lipids. 2017 Oct 1;1862(10, Part B):1166–77.

42. Guo Y, Cordes KR, Farese RV, Walther TC. Lipid droplets at a glance. J Cell Sci. 2009 Mar 15;122(6):749–52.

43. Choudhary V, Ojha N, Golden A, Prinz WA. A conserved family of proteins facilitates nascent lipid droplet budding from the ER. J Cell Biol. 2015 Oct 26;211(2):261–71.

44. Walther TC, Chung J, Farese RV. Lipid Droplet Biogenesis. Annu Rev Cell Dev Biol. 2017 Oct 6;33:491–510.

45. Salo VT, Belevich I, Li S, Karhinen L, Vihinen H, Vigouroux C, et al. Seipin regulates ER-lipid droplet contacts and cargo delivery. EMBO J. 2016 15;35(24):2699–716.

46. Yang H, Galea A, Sytnyk V, Crossley M. Controlling the size of lipid droplets: lipid and protein factors. Curr Opin Cell Biol. 2012 Aug;24(4):509–16.

47. Nielsen TS, Jessen N, Jørgensen JOL, Møller N, Lund S. Dissecting adipose tissue lipolysis: molecular regulation and implications for metabolic disease. J Mol Endocrinol. 2014 Jun 1;52(3):R199–222.

48. Braun K, Oeckl J, Westermeier J, Li Y, Klingenspor M. Non-adrenergic control of lipolysis and thermogenesis in adipose tissues. J Exp Biol. 2018 Mar 7;221(Pt Suppl 1):jeb165381.

49. Zeng W, Pirzgalska RM, Pereira MMA, Kubasova N, Barateiro A, Seixas E, et al. Sympathetic neuro-adipose connections mediate leptin-driven lipolysis. Cell. 2015 Sep 24;163(1):84–94.

50. Thiam AR, Beller M. The why, when and how of lipid droplet diversity. J Cell Sci. 2017 Jan 15;130(2):315–24.

51. Adeva-Andany MM, Carneiro-Freire N, Seco-Filgueira M, Fernández-Fernández C, Mouriño-Bayolo D. Mitochondrial β-oxidation of saturated fatty acids in humans. Mitochondrion. 2019 May;46:73–90.

52. Lee JH, Park A, Oh K-J, Lee SC, Kim WK, Bae K-H. The Role of Adipose Tissue Mitochondria: Regulation of Mitochondrial Function for the Treatment of Metabolic Diseases. Int J Mol Sci. 2019 Oct 4;20(19):E4924.

53. Saito M, Matsushita M, Yoneshiro T, Okamatsu-Ogura Y. Brown Adipose Tissue, Diet-Induced Thermogenesis, and Thermogenic Food Ingredients: From Mice to Men. Front Endocrinol. 2020;11:222.

54. Nedergaard J, Golozoubova V, Matthias A, Asadi A, Jacobsson A, Cannon B. UCP1: the only protein able to mediate adaptive non-shivering thermogenesis and metabolic inefficiency. Biochim Biophys Acta. 2001 Mar 1;1504(1):82–106.

55. Pan R, Zhu X, Maretich P, Chen Y. Combating Obesity With Thermogenic Fat: Current Challenges and Advancements. Front Endocrinol. 2020;11:185.

56. Fasshauer M, Blüher M. Adipokines in health and disease. Trends Pharmacol Sci. 2015 Jul;36(7):461–70.

57.	Scheja L, Heeren J. The endocrine function of adipose tissues in health and cardiometabolic disease. Nat Rev Endocrinol. 2019 Sep;15(9):507–24.

58.	Zhang Y, Proenca R, Maffei M, Barone M, Leopold L, Friedman JM. Positional cloning of the mouse obese gene and its human homologue. Nature. 1994 Dec 1;372(6505):425–32.

59.	Tartaglia LA, Dembski M, Weng X, Deng N, Culpepper J, Devos R, et al. Identification and expression cloning of a leptin receptor, OB-R. Cell. 1995 Dec 29;83(7):1263–71.

60.	Shimizu H, Shimomura Y, Hayashi R, Ohtani K, Sato N, Futawatari T, et al. Serum leptin concentration is associated with total body fat mass, but not abdominal fat distribution. Int J Obes Relat Metab Disord J Int Assoc Study Obes. 1997 Jul;21(7):536–41.

61.	Münzberg H, Morrison CD. Structure, production and signaling of leptin. Metabolism. 2015 Jan;64(1):13–23.

62.	Denroche HC, Huynh FK, Kieffer TJ. The role of leptin in glucose homeostasis. J Diabetes Investig. 2012 Mar 28;3(2):115–29.

63.	Abella V, Scotece M, Conde J, Pino J, Gonzalez-Gay MA, Gómez-Reino JJ, et al. Leptin in the interplay of inflammation, metabolism and immune system disorders. Nat Rev Rheumatol. 2017 Feb;13(2):100–9.

64.	Upadhyay J, Farr OM, Mantzoros CS. The role of leptin in regulating bone metabolism. Metabolism. 2015 Jan;64(1):105–13.

65.	Tahergorabi Z, Khazaei M. Leptin and its cardiovascular effects: Focus on angiogenesis. Adv Biomed Res. 2015 May 6;4:79.

66.	Gariballa S, Alkaabi J, Yasin J, Al Essa A. Total adiponectin in overweight and obese subjects and its response to visceral fat loss. BMC Endocr Disord. 2019 Jun 3;19(1):55.

67.	Ruan H, Dong LQ. Adiponectin signaling and function in insulin target tissues. J Mol Cell Biol. 2016 Apr;8(2):101–9.

68.	Roda C, Charreire H, Feuillet T, Mackenbach JD, Compernolle S, Glonti K, et al. Lifestyle correlates of overweight in adults: a hierarchical approach (the SPOTLIGHT project). Int J Behav Nutr Phys Act. 2016 Nov 3;13(1):114.

69.	Mehrzad R. Chapter 4 - Etiology of obesity. In: Mehrzad R, editor. Obesity [Internet]. Elsevier; 2020 [cited 2021 Dec 5]. p. 43–54. Available from: https://www.sciencedirect.com/science/article/pii/B9780128188392000041

70.	Longo M, Zatterale F, Naderi J, Parrillo L, Formisano P, Raciti GA, et al. Adipose Tissue Dysfunction as Determinant of Obesity-Associated Metabolic Complications. Int J Mol Sci. 2019 May 13;20(9):2358.

71.	Rasouli N. Adipose tissue hypoxia and insulin resistance. J Investig Med Off Publ Am Fed Clin Res. 2016 Apr;64(4):830–2.

72. Lee YS, Kim J-W, Osborne O, Oh DY, Sasik R, Schenk S, et al. Increased adipocyte O2 consumption triggers HIF-1α, causing inflammation and insulin resistance in obesity. Cell. 2014 Jun 5;157(6):1339–52.

73. Kern L, Mittenbühler MJ, Vesting AJ, Ostermann AL, Wunderlich CM, Wunderlich FT. Obesity-Induced TNFα and IL-6 Signaling: The Missing Link between Obesity and Inflammation—Driven Liver and Colorectal Cancers. Cancers. 2018 Dec 27;11(1):24.

74. Crewe C, An YA, Scherer PE. The ominous triad of adipose tissue dysfunction: inflammation, fibrosis, and impaired angiogenesis. J Clin Invest. 2017 Jan 3;127(1):74–82.

75. Russo L, Lumeng CN. Properties and functions of adipose tissue macrophages in obesity. Immunology. 2018;155(4):407–17.

76. Zatterale F, Longo M, Naderi J, Raciti GA, Desiderio A, Miele C, et al. Chronic Adipose Tissue Inflammation Linking Obesity to Insulin Resistance and Type 2 Diabetes. Front Physiol. 2020;10:1607.

77. Zhao J, Wu Y, Rong X, Zheng C, Guo J. Anti-Lipolysis Induced by Insulin in Diverse Pathophysiologic Conditions of Adipose Tissue. Diabetes Metab Syndr Obes Targets Ther. 2020 May 11;13:1575–85.

78. Yazıcı D, Sezer H. Insulin Resistance, Obesity and Lipotoxicity. Adv Exp Med Biol. 2017;960:277–304.

79. Chan JL, Oral EA. Clinical classification and treatment of congenital and acquired lipodystrophy. Endocr Pract Off J Am Coll Endocrinol Am Assoc Clin Endocrinol. 2010 Apr;16(2):310–23.

80. Garg A. Clinical review#: Lipodystrophies: genetic and acquired body fat disorders. J Clin Endocrinol Metab. 2011 Nov;96(11):3313–25.

81. Garg A, Agarwal AK. Lipodystrophies: disorders of adipose tissue biology. Biochim Biophys Acta. 2009 Jun;1791(6):507–13.

82. BERARDINELLI W. AN UNDIAGNOSED ENDOCRINOMETABOLIC SYNDROME: REPORT OF 2 CASES*. J Clin Endocrinol Metab. 1954 Feb 1;14(2):193–204.

83. Seip M. Lipodystrophy and gigantism with associated endocrine manifestations. A new diencephalic syndrome? Acta Paediatr. 1959 Nov;48:555–74.

84. Garg A. Lipodystrophies. Am J Med. 2000 Feb 1;108(2):143–52.

85. Magré J, Delépine M, Khallouf E, Gedde-Dahl T, Van Maldergem L, Sobel E, et al. Identification of the gene altered in Berardinelli-Seip congenital lipodystrophy on chromosome 11q13. Nat Genet. 2001 Aug;28(4):365–70.

86. Lima JG, Nobrega LHC, Lima NN, Dos Santos MCF, Silva PHD, Baracho M de FP, et al. Causes of death in patients with Berardinelli-Seip congenital generalized lipodystrophy. PloS One. 2018;13(6):e0199052.

87. Simha V, Garg A. Phenotypic heterogeneity in body fat distribution in patients with congenital generalized lipodystrophy caused by mutations in the AGPAT2 or seipin genes. J Clin Endocrinol Metab. 2003 Nov;88(11):5433–7.

88. Agarwal AK, Arioglu E, De Almeida S, Akkoc N, Taylor SI, Bowcock AM, et al. AGPAT2 is mutated in congenital generalized lipodystrophy linked to chromosome 9q34. Nat Genet. 2002 May;31(1):21–3.

89. Van Maldergem L, Magré J, Khallouf TE, Gedde-Dahl T, Delépine M, Trygstad O, et al. Genotype-phenotype relationships in Berardinelli-Seip congenital lipodystrophy. J Med Genet. 2002 Oct;39(10):722–33.

90. Haque WA, Shimomura I, Matsuzawa Y, Garg A. Serum adiponectin and leptin levels in patients with lipodystrophies. J Clin Endocrinol Metab. 2002 May;87(5):2395.

91. Bindlish S, Presswala LS, Schwartz F. Lipodystrophy: Syndrome of severe insulin resistance. Postgrad Med. 2015 Jun;127(5):511–6.

92. Garg A, Wilson R, Barnes R, Arioglu E, Zaidi Z, Gurakan F, et al. A gene for congenital generalized lipodystrophy maps to human chromosome 9q34. J Clin Endocrinol Metab. 1999 Sep;84(9):3390–4.

93. Ceccarini G, Magno S, Pelosini C, Ferrari F, Sessa MR, Scabia G, et al. Congenital Generalized Lipoatrophy (Berardinelli-Seip Syndrome) Type 1: Description of Novel AGPAT2 Homozygous Variants Showing the Highly Heterogeneous Presentation of the Disease. Front Endocrinol [Internet]. 2020 [cited 2021 Apr 20];11. Available from: https://www.frontiersin.org/articles/10.3389/fendo.2020.00039/full

94. Kim CA, Delépine M, Boutet E, El Mourabit H, Le Lay S, Meier M, et al. Association of a homozygous nonsense caveolin-1 mutation with Berardinelli-Seip congenital lipodystrophy. J Clin Endocrinol Metab. 2008 Apr;93(4):1129–34.

95. Hayashi YK, Matsuda C, Ogawa M, Goto K, Tominaga K, Mitsuhashi S, et al. Human PTRF mutations cause secondary deficiency of caveolins resulting in muscular dystrophy with generalized lipodystrophy. J Clin Invest. 2009 Sep;119(9):2623–33.

96. Agarwal AK, Simha V, Oral EA, Moran SA, Gorden P, O'Rahilly S, et al. Phenotypic and genetic heterogeneity in congenital generalized lipodystrophy. J Clin Endocrinol Metab. 2003 Oct;88(10):4840–7.

97. Agarwal AK, Garg A. Seipin: a mysterious protein. Trends Mol Med. 2004 Sep;10(9):440–4.

98. Altay C, Seçil M, Demir T, Atik T, Akıncı G, Özdemir Kutbay N, et al. Determining residual adipose tissue characteristics with MRI in patients with various subtypes of lipodystrophy. Diagn Interv Radiol Ank Turk. 2017 Dec;23(6):428–34.

99. Antuna-Puente B, Boutet E, Vigouroux C, Lascols O, Slama L, Caron-Debarle M, et al. Higher adiponectin levels in patients with Berardinelli-Seip congenital lipodystrophy due to seipin as compared with 1-acylglycerol-3-phosphate-o-acyltransferase-2 deficiency. J Clin Endocrinol Metab. 2010 Mar;95(3):1463–8.

100. Akinci B, Onay H, Demir T, Ozen S, Kayserili H, Akinci G, et al. Natural History of Congenital Generalized Lipodystrophy: A Nationwide Study From Turkey. J Clin Endocrinol Metab. 2016 Jul;101(7):2759–67.

101. Lima JG, Nobrega LHC, de Lima NN, do Nascimento Santos MG, Baracho MFP, Jeronimo SMB. Clinical and laboratory data of a large series of patients with congenital generalized lipodystrophy. Diabetol Metab Syndr [Internet]. 2016 Mar 15 [cited 2021 Apr 20];8. Available from: https://www.ncbi.nlm.nih.gov/pmc/articles/PMC4793761/

102. Maeda M, Maeda T, Ebihara K, Ihara K. The long-term management of congenital generalized lipodystrophy (Berardinelli-Seip syndrome): the clinical manifestations of Japanese siblings for approximately 20 years. Clin Pediatr Endocrinol. 2019;28(4):139–45.

103. Brown RJ, Araujo-Vilar D, Cheung PT, Dunger D, Garg A, Jack M, et al. The Diagnosis and Management of Lipodystrophy Syndromes: A Multi-Society Practice Guideline. J Clin Endocrinol Metab. 2016 Dec 1;101(12):4500–11.

104. Diker-Cohen T, Cochran E, Gorden P, Brown RJ. Partial and generalized lipodystrophy: comparison of baseline characteristics and response to metreleptin. J Clin Endocrinol Metab. 2015 May;100(5):1802–10.

105. Araújo-Vilar D, Santini F. Diagnosis and treatment of lipodystrophy: a step-by-step approach. J Endocrinol Invest. 2019 Jan 1;42(1):61–73.

106. Garg A. Acquired and inherited lipodystrophies. N Engl J Med. 2004 Mar 18;350(12):1220–34.

107. Meehan CA, Cochran E, Kassai A, Brown RJ, Gorden P. Metreleptin for injection to treat the complications of leptin deficiency in patients with congenital or acquired generalized lipodystrophy. Expert Rev Clin Pharmacol. 2016;9(1):59–68.

108. Rojas LBA, Gomes MB. Metformin: an old but still the best treatment for type 2 diabetes. Diabetol Metab Syndr. 2013 Feb 15;5:6.

109. Shaw RJ, Lamia KA, Vasquez D, Koo S-H, Bardeesy N, Depinho RA, et al. The kinase LKB1 mediates glucose homeostasis in liver and therapeutic effects of metformin. Science. 2005 Dec 9;310(5754):1642–6.

110. Stears A, Hames C. Diagnosis and management of lipodystrophy: A practical update. Clin Lipidol. 2014 Apr 1;9:235–59.

111. Josivan G L, Natalia N L, Ricardo LM L, Maria FP B, Lucia HC N. Glargine U300 Insulin as a Better Option than Degludec U100 to Treat a Congenital Generalized Lipodystrophy Patient. Clin Diabetes Res [Internet]. 2017 Aug 3 [cited 2021 Apr 24];1(1). Available from: https://scholars.direct/Articles/diabetology/cdr-1-004.php?jid=diabetology

112. Moskowitz H, Sadeghi-Nejad A. Exogenous Insulin Ameliorates Acanthosis Nigricans in Congenital Generalized Lipodystrophy. Pediatr Res. 1999 Apr;45(7):94–94.

113. Bolli GB, Owens DR. Insulin glargine. The Lancet. 2000 Aug 5;356(9228):443–5.

114. Karges B, Boehm BO, Karges W. Early hypoglycaemia after accidental intramuscular injection of insulin glargine. Diabet Med J Br Diabet Assoc. 2005 Oct;22(10):1444–5.

115. Lane WS, Cochran EK, Jackson JA, Scism-Bacon JL, Corey IB, Hirsch IB, et al. High-dose insulin therapy: is it time for U-500 insulin? Endocr Pract Off J Am Coll Endocrinol Am Assoc Clin Endocrinol. 2009 Feb;15(1):71–9.

116. Cochran E, Musso C, Gorden P. The Use of U-500 in Patients With Extreme Insulin Resistance. Diabetes Care. 2005 May 1;28(5):1240–4.

117. Prieur X, Dollet L, Takahashi M, Nemani M, Pillot B, Le May C, et al. Thiazolidinediones partially reverse the metabolic disturbances observed in Bscl2/seipin-deficient mice. Diabetologia. 2013 Aug 1;56(8):1813–25.

118. Prieur X, Le May C, Magré J, Cariou B. Congenital Lipodystrophies and Dyslipidemias. Curr Atheroscler Rep. 2014 Jul 22;16(9):437.

119. Hsu R-H, Lin W-D, Chao M-C, Hsiao H-P, Wong S-L, Chiu P-C, et al. Congenital generalized lipodystrophy in Taiwan. J Formos Med Assoc Taiwan Yi Zhi. 2019 Jan;118(1 Pt 1):142–7.

120. Browne D, Arundel F, Meeking D. Failure of metformin and pioglitazone in the treatment of congenital generalised lipodystrophy. Endocr Abstr [Internet]. 2003 Mar 1 [cited 2021 Apr 21];5. Available from: https://www.endocrine-abstracts.org/ea/0005/ea0005p30

121. Chaves C, Chaves M, Anselmo J, César R. Successful long-term use of pioglitazone in Berardinelli–Seip lipodystrophy-associated diabetes. Endocrinol Diabetes Metab Case Rep [Internet]. 2021 Apr 1 [cited 2021 May 1];2021(1). Available from: https://edm.bioscientifica.com/view/journals/edm/2021/1/EDM20-0183.xml

122. Chou K, Perry CM. Metreleptin: first global approval. Drugs. 2013 Jun;73(9):989–97.

123. Rodriguez AJ, Mastronardi CA, Paz-Filho GJ. New advances in the treatment of generalized lipodystrophy: role of metreleptin. Ther Clin Risk Manag. 2015;11:1391–400.

124. Brown RJ, Meehan CA, Cochran E, Rother KI, Kleiner DE, Walter M, et al. Effects of Metreleptin in Pediatric Patients With Lipodystrophy. J Clin Endocrinol Metab. 2017 01;102(5):1511–9.

125. Oral EA, Simha V, Ruiz E, Andewelt A, Premkumar A, Snell P, et al. Leptin-replacement therapy for lipodystrophy. N Engl J Med. 2002 Feb 21;346(8):570–8.

126. Ebihara K, Kusakabe T, Hirata M, Masuzaki H, Miyanaga F, Kobayashi N, et al. Efficacy and safety of leptin-replacement therapy and possible mechanisms of leptin actions in patients with generalized lipodystrophy. J Clin Endocrinol Metab. 2007 Feb;92(2):532–41.

127. Moran SA, Patten N, Young JR, Cochran E, Sebring N, Reynolds J, et al. Changes in body composition in patients with severe lipodystrophy after leptin replacement therapy. Metabolism. 2004 Apr;53(4):513–9.

128. McDuffie JR, Riggs PA, Calis KA, Freedman RJ, Oral EA, DePaoli AM, et al. Effects of exogenous leptin on satiety and satiation in patients with lipodystrophy and leptin insufficiency. J Clin Endocrinol Metab. 2004 Sep;89(9):4258–63.

129. Musso C, Cochran E, Javor E, Young J, Depaoli AM, Gorden P. The long-term effect of recombinant methionyl human leptin therapy on hyperandrogenism and menstrual function in female and pituitary function in male and female hypoleptinemic lipodystrophic patients. Metabolism. 2005 Feb;54(2):255–63.

130. Beltrand J, Beregszaszi M, Chevenne D, Sebag G, De Kerdanet M, Huet F, et al. Metabolic correction induced by leptin replacement treatment in young children with Berardinelli-Seip congenital lipoatrophy. Pediatrics. 2007 Aug;120(2):e291-296.

131. Lima JG, Santos MCF dos, Campos JTA de M. Congenital Generalized Lipodystrophy. J Rare Dis Res Treat [Internet]. 2018 May 11 [cited 2021 Apr 20];3(2). Available from: https://www.rarediseasesjournal.com/articles/congenital-generalized-lipodystrophy.html

132. Petersen KF, Oral EA, Dufour S, Befroy D, Ariyan C, Yu C, et al. Leptin reverses insulin resistance and hepatic steatosis in patients with severe lipodystrophy. J Clin Invest. 2002 May 15;109(10):1345–50.

133. Javor ED, Ghany MG, Cochran EK, Oral EA, DePaoli AM, Premkumar A, et al. Leptin reverses nonalcoholic steatohepatitis in patients with severe lipodystrophy. Hepatology. 2005;41(4):753–60.

134. Simha V, Szczepaniak LS, Wagner AJ, DePaoli AM, Garg A. Effect of Leptin Replacement on Intrahepatic and Intramyocellular Lipid Content in Patients With Generalized Lipodystrophy. Diabetes Care. 2003 Jan 1;26(1):30–5.

135. Chan JL, Lutz K, Cochran E, Huang W, Peters Y, Weyer C, et al. Clinical effects of long-term metreleptin treatment in patients with lipodystrophy. Endocr Pract Off J Am Coll Endocrinol Am Assoc Clin Endocrinol. 2011;17(6):922–32.

136. Beltrand J, Lahlou N, Charpentier TL, Sebag G, Leka S, Polak M, et al. Resistance to leptin-replacement therapy in Berardinelli–Seip congenital lipodystrophy: an immunological origin. Eur J Endocrinol. 2010 Jun 1;162(6):1083–91.

137. Chan JL, Koda J, Heilig JS, Cochran EK, Gorden P, Oral EA, et al. Immunogenicity associated with metreleptin treatment in patients with obesity or lipodystrophy. Clin Endocrinol (Oxf). 2016 Jul;85(1):137–49.

138. Tsoukas MA, Mantzoros CS. Chapter 37 - Lipodystrophy Syndromes. In: Jameson JL, De Groot LJ, de Kretser DM, Giudice LC, Grossman AB, Melmed S, et al., editors. Endocrinology: Adult and Pediatric (Seventh Edition) [Internet]. Philadelphia: W.B. Saunders; 2016 [cited 2021 Apr 21]. p. 648-661.e5. Available from: https://www.sciencedirect.com/science/article/pii/B9780323189071000378

139. Rheuban KS, Blizzard RM, Parker MA, Carter T, Wilson T, Gutgesell HP. Hypertrophic cardiomyopathy in total lipodystrophy. J Pediatr. 1986 Aug;109(2):301–2.

140. Gupta N, Asi N, Farah W, Almasri J, Barrionuevo P, Alsawas M, et al. Clinical Features and Management of Non-HIV–Related Lipodystrophy in Children: A Systematic Review. J Clin Endocrinol Metab. 2016 Dec 14;102(2):363–74.

141. Cartwright BR, Goodman JM. Seipin: from human disease to molecular mechanism. J Lipid Res. 2012 Jun;53(6):1042–55.

142. Windpassinger C, Auer-Grumbach M, Irobi J, Patel H, Petek E, Hörl G, et al. Heterozygous missense mutations in BSCL2 are associated with distal hereditary motor neuropathy and Silver syndrome. Nat Genet. 2004 Mar;36(3):271–6.

143. Payne VA, Grimsey N, Tuthill A, Virtue S, Gray SL, Dalla Nora E, et al. The human lipodystrophy gene BSCL2/seipin may be essential for normal adipocyte differentiation. Diabetes. 2008 Aug;57(8):2055–60.

144. Lundin C, Nordström R, Wagner K, Windpassinger C, Andersson H, von Heijne G, et al. Membrane topology of the human seipin protein. FEBS Lett. 2006 Apr 17;580(9):2281–4.

145. Rahman OU, Khawar N, Khan MA, Ahmed J, Khattak K, Al-Aama JY, et al. Deletion mutation in BSCL2 gene underlies congenital generalized lipodystrophy in a Pakistani family. Diagn Pathol. 2013 May 9;8:78.

146. Jin J, Cao L, Zhao Z, Shen S, Kiess W, Zhi D, et al. Novel BSCL2 gene mutation E189X in Chinese congenital generalized lipodystrophy child with early onset diabetes mellitus. Eur J Endocrinol. 2007 Dec;157(6):783–7.

147. Windpassinger C, Wagner K, Petek E, Fischer R, Auer-Grumbach M. Refinement of the Silver syndrome locus on chromosome 11q12-q14 in four families and exclusion of eight candidate genes. Hum Genet. 2003 Dec;114(1):99–109.

148. Ito D, Suzuki N. Seipinopathy: a novel endoplasmic reticulum stress-associated disease. Brain J Neurol. 2009 Jan;132(Pt 1):8–15.

149. Jiang M, Gao M, Wu C, He H, Guo X, Zhou Z, et al. Lack of testicular seipin causes teratozoospermia syndrome in men. Proc Natl Acad Sci. 2014 May 13;111(19):7054–9.

150. Zhou L, Yin J, Wang C, Liao J, Liu G, Chen L. Lack of seipin in neurons results in anxiety- and depression-like behaviors via down regulation of PPARγ. Hum Mol Genet. 2014 Aug 1;23(15):4094–102.

151. Chen W, Yechoor VK, Chang BH-J, Li MV, March KL, Chan L. The human lipodystrophy gene product Berardinelli-Seip congenital lipodystrophy 2/seipin plays a key role in adipocyte differentiation. Endocrinology. 2009 Oct;150(10):4552–61.

152. Chen W, Chang B, Saha P, Hartig SM, Li L, Reddy VT, et al. Berardinelli-Seip Congenital Lipodystrophy 2/Seipin Is a Cell-Autonomous Regulator of Lipolysis Essential for Adipocyte Differentiation. Mol Cell Biol. 2012 Mar;32(6):1099–111.

153. Wang H, Becuwe M, Housden BE, Chitraju C, Porras AJ, Graham MM, et al. Seipin is required for converting nascent to mature lipid droplets. eLife [Internet]. [cited 2021 May 13];5. Available from: https://www.ncbi.nlm.nih.gov/pmc/articles/PMC5035145/

154. Fei W, Shui G, Gaeta B, Du X, Kuerschner L, Li P, et al. Fld1p, a functional homologue of human seipin, regulates the size of lipid droplets in yeast. J Cell Biol. 2008 Feb 11;180(3):473–82.

155. Szymanski KM, Binns D, Bartz R, Grishin NV, Li W-P, Agarwal AK, et al. The lipodystrophy protein seipin is found at endoplasmic reticulum lipid droplet junctions and is important for droplet morphology. Proc Natl Acad Sci U S A. 2007 Dec 26;104(52):20890–5.

156. Cao Z, Hao Y, Fung CW, Lee YY, Wang P, Li X, et al. Dietary fatty acids promote lipid droplet diversity through seipin enrichment in an ER subdomain. Nat Commun. 2019 Jul 1;10(1):2902.

157. Taurino M, Costantini S, Domenico SD, Stefanelli F, Ruano G, Delgadillo MO, et al. SEIPIN Proteins Mediate Lipid Droplet Biogenesis to Promote Pollen Transmission and Reduce Seed Dormancy. Plant Physiol. 2018 Feb 1;176(2):1531–46.

158. Boutet E, El Mourabit H, Prot M, Nemani M, Khallouf E, Colard O, et al. Seipin deficiency alters fatty acid Δ9 desaturation and lipid droplet formation in Berardinelli-Seip congenital lipodystrophy. Biochimie. 2009 Jun 1;91(6):796–803.

159. Tian Y, Bi J, Shui G, Liu Z, Xiang Y, Liu Y, et al. Tissue-autonomous function of Drosophila seipin in preventing ectopic lipid droplet formation. PLoS Genet. 2011 Apr;7(4):e1001364.

160. Sim MFM, Dennis RJ, Aubry EM, Ramanathan N, Sembongi H, Saudek V, et al. The human lipodystrophy protein seipin is an ER membrane adaptor for the adipogenic PA phosphatase lipin 1. Mol Metab. 2012;2(1):38–46.

161. Han S, Binns DD, Chang Y-F, Goodman JM. Dissecting seipin function: the localized accumulation of phosphatidic acid at ER/LD junctions in the absence of seipin is suppressed by Sei1p(ΔNterm) only in combination with Ldb16p. BMC Cell Biol. 2015 Dec 4;16:29.

162. Talukder MMU, Sim MFM, O'Rahilly S, Edwardson JM, Rochford JJ. Seipin oligomers can interact directly with AGPAT2 and lipin 1, physically scaffolding critical regulators of adipogenesis. Mol Metab. 2015 Mar;4(3):199–209.

163. Wolinski H, Hofbauer HF, Hellauer K, Cristobal-Sarramian A, Kolb D, Radulovic M, et al. Seipin is involved in the regulation of phosphatidic acid metabolism at a subdomain of the nuclear envelope in yeast. Biochim Biophys Acta. 2015 Nov;1851(11):1450–64.

164. Pagac M, Cooper DE, Qi Y, Lukmantara IE, Mak HY, Wu Z, et al. SEIPIN Regulates Lipid Droplet Expansion and Adipocyte Development by Modulating the Activity of Glycerol-3-phosphate Acyltransferase. Cell Rep. 2016 01;17(6):1546–59.

165. Wee K, Yang W, Sugii S, Han W. Towards a mechanistic understanding of lipodystrophy and seipin functions. Biosci Rep [Internet]. 2014 Oct 2 [cited 2021 May 15];34(e00141). Available from: https://doi.org/10.1042/BSR20140114

166. Cai Y, Goodman JM, Pyc M, Mullen RT, Dyer JM, Chapman KD. Arabidopsis SEIPIN Proteins Modulate Triacylglycerol Accumulation and Influence Lipid Droplet Proliferation. Plant Cell. 2015 Sep;27(9):2616–36.

167. Grippa A, Buxó L, Mora G, Funaya C, Idrissi F-Z, Mancuso F, et al. The seipin complex Fld1/Ldb16 stabilizes ER–lipid droplet contact sites. J Cell Biol. 2015 Nov 23;211(4):829–44.

168. Chung J, Wu X, Lambert TJ, Lai ZW, Walther TC, Farese RV. LDAF1 and Seipin Form a Lipid Droplet Assembly Complex. Dev Cell. 2019 Dec 2;51(5):551-563.e7.

169. Zhou H, Lei X, Benson T, Mintz J, Xu X, Harris RB, et al. Berardinelli-Seip congenital lipodystrophy 2 regulates adipocyte lipolysis, browning, and energy balance in adult animals. J Lipid Res. 2015 Oct;56(10):1912–25.

170. Dollet L, Levrel C, Coskun T, Lay SL, May CL, Ayer A, et al. FGF21 Improves the Adipocyte Dysfunction Related to Seipin Deficiency. Diabetes. 2016 Nov 1;65(11):3410–7.

171. A-Kader HH, Ghishan FK. The Pancreas. Textb Clin Pediatr. 2012;1925–36.

172. Longnecker DS. Anatomy and Histology of the Pancreas. Pancreapedia Exocrine Pancreas Knowl Base [Internet]. 2021 Jan 18 [cited 2021 Apr 10]; Available from: /reviews/anatomy-and-histology-of-pancreas

173. Pandol SJ. Anatomy [Internet]. Morgan & Claypool Life Sciences; 2010 [cited 2021 Apr 10]. Available from: https://www.ncbi.nlm.nih.gov/books/NBK54134/

174. Röder PV, Wu B, Liu Y, Han W. Pancreatic regulation of glucose homeostasis. Exp Mol Med. 2016 Mar;48(3):e219.

175. Wierup N, Svensson H, Mulder H, Sundler F. The ghrelin cell: a novel developmentally regulated islet cell in the human pancreas. Regul Pept. 2002 Jul 15;107(1–3):63–9.

176. Güemes M, Rahman SA, Hussain K. What is a normal blood glucose? Arch Dis Child. 2016 Jun;101(6):569–74.

177. Kim A, Miller K, Jo J, Kilimnik G, Wojcik P, Hara M. Islet architecture. Islets. 2009 Sep;1(2):129–36.

178. Arrojo e Drigo R, Ali Y, Diez J, Srinivasan DK, Berggren P-O, Boehm BO. New insights into the architecture of the islet of Langerhans: a focused cross-species assessment. Diabetologia. 2015 Oct 1;58(10):2218–28.

179. Brissova M, Fowler MJ, Nicholson WE, Chu A, Hirshberg B, Harlan DM, et al. Assessment of Human Pancreatic Islet Architecture and Composition by Laser Scanning Confocal Microscopy. J Histochem Cytochem. 2005 Sep 1;53(9):1087–97.

180. Orci L, Unger RH. Functional subdivision of islets of Langerhans and possible role of D cells. Lancet Lond Engl. 1975 Dec 20;2(7947):1243–4.

181. Steiner DJ, Kim A, Miller K, Hara M. Pancreatic islet plasticity: Interspecies comparison of islet architecture and composition. Islets. 2010 May;2(3):135–45.

182. Gerich JE. Physiology of glucose homeostasis. Diabetes Obes Metab. 2000;2(6):345–50.

183. Aronoff SL, Berkowitz K, Shreiner B, Want L. Glucose Metabolism and Regulation: Beyond Insulin and Glucagon. Diabetes Spectr. 2004 Jul 1;17(3):183–90.

184. Pessin JE, Saltiel AR. Signaling pathways in insulin action: molecular targets of insulin resistance. J Clin Invest. 2000 Jul 15;106(2):165–9.

185. Thorens B, Mueckler M. Glucose transporters in the 21st Century. Am J Physiol - Endocrinol Metab. 2010 Feb;298(2):E141–5.

186. Rorsman P, Renström E. Insulin granule dynamics in pancreatic beta cells. Diabetologia. 2003 Aug;46(8):1029–45.

187. Newsholme P, Bender K, Kiely A, Brennan L. Amino acid metabolism, insulin secretion and diabetes. Biochem Soc Trans. 2007 Nov;35(Pt 5):1180–6.

188. Krause MS, McClenaghan NH, Flatt PR, de Bittencourt PIH, Murphy C, Newsholme P. L-arginine is essential for pancreatic β-cell functional integrity, metabolism and defense from inflammatory challenge. J Endocrinol. 2011 Oct;211(1):87–97.

189. Newsholme P, Keane D, Welters HJ, Morgan NG. Life and death decisions of the pancreatic beta-cell: the role of fatty acids. Clin Sci Lond Engl 1979. 2007 Jan;112(1):27–42.

190. Newsholme P, Gaudel C, McClenaghan NH. Nutrient Regulation of Insulin Secretion and β-Cell Functional Integrity. In: Islam MdS, editor. The Islets of Langerhans [Internet]. Dordrecht: Springer Netherlands; 2010 [cited 2021 Apr 13]. p. 91–114. (Advances in Experimental Medicine and Biology). Available from: https://doi.org/10.1007/978-90-481-3271-3_6

191. Grodsky GM, Batts AA, Bennett LL, Vcella C, Mcwilliams NB, Smith DF. EFFECTS OF CARBOHYDRATES ON SECRETION OF INSULIN FROM ISOLATED RAT PANCREAS. Am J Physiol. 1963 Oct;205:638–44.

192. Coore HG, Randle PJ. Regulation of insulin secretion studied with pieces of rabbit pancreas incubated in vitro. Biochem J. 1964 Oct;93(1):66–78.

193. Mueckler M, Thorens B. The SLC2 (GLUT) family of membrane transporters. Mol Aspects Med. 2013 Jun;34(2–3):121–38.

194. Thorens B. GLUT2, glucose sensing and glucose homeostasis. Diabetologia. 2015 Feb 1;58(2):221–32.

195. German MS. Glucose sensing in pancreatic islet beta cells: the key role of glucokinase and the glycolytic intermediates. Proc Natl Acad Sci U S A. 1993 Mar 1;90(5):1781–5.

196. Matschinsky FM. A Lesson in Metabolic Regulation Inspired by the Glucokinase Glucose Sensor Paradigm. Diabetes. 1996 Feb 1;45(2):223–41.

197. Ferre T, Riu E, Bosch F, Valera A. Evidence from transgenic mice that glucokinase is rate limiting for glucose utilization in the liver. FASEB J Off Publ Fed Am Soc Exp Biol. 1996 Aug;10(10):1213–8.

198. MacDonald MJ, Kaysen JH, Moran SM, Pomije CE. Pyruvate dehydrogenase and pyruvate carboxylase. Sites of pretranslational regulation by glucose of glucose-induced insulin release in pancreatic islets. J Biol Chem. 1991 Nov 25;266(33):22392–7.

199. Komatsu M, Takei M, Ishii H, Sato Y. Glucose-stimulated insulin secretion: A newer perspective. J Diabetes Investig. 2013 Nov 27;4(6):511–6.

200. Newsholme P, Krause M. Nutritional Regulation of Insulin Secretion: Implications for Diabetes. Clin Biochem Rev. 2012 May;33(2):35–47.

201. Aguilar-Bryan L, Bryan J. Molecular biology of adenosine triphosphate-sensitive potassium channels. Endocr Rev. 1999 Apr;20(2):101–35.

202. Ashcroft FM, Gribble FM. ATP-sensitive K+ channels and insulin secretion: their role in health and disease. Diabetologia. 1999 Aug;42(8):903–19.

203. Ashcroft FM, Harrison DE, Ashcroft SJ. Glucose induces closure of single potassium channels in isolated rat pancreatic beta-cells. Nature. 1984 Dec 29;312(5993):446–8.

204. Cook DL, Ikeuchi M, Fujimoto WY. Lowering of pHi inhibits Ca2+-activated K+ channels in pancreatic B-cells. Nature. 1984 Sep 20;311(5983):269–71.

205. Rorsman P, Ashcroft FM, Trube G. Single Ca channel currents in mouse pancreatic B-cells. Pflugers Arch. 1988 Oct;412(6):597–603.

206. Satin LS, Cook DL. Voltage-gated Ca2+ current in pancreatic B-cells. Pflugers Arch. 1985 Aug;404(4):385–7.

207. Henquin JC. Triggering and amplifying pathways of regulation of insulin secretion by glucose. Diabetes. 2000 Nov 1;49(11):1751–60.

208. Daniel S, Noda M, Straub SG, Sharp GW. Identification of the docked granule pool responsible for the first phase of glucose-stimulated insulin secretion. Diabetes. 1999 Sep;48(9):1686–90.

209. Chan CB, MacPhail RM. KATP channel-dependent and -independent pathways of insulin secretion in isolated islets from fa/fa Zucker rats. Biochem Cell Biol Biochim Biol Cell. 1996;74(3):403–10.

210. Straub SG, James RF, Dunne MJ, Sharp GW. Glucose activates both K(ATP) channel-dependent and K(ATP) channel-independent signaling pathways in human islets. Diabetes. 1998 May;47(5):758–63.

211. Abdel-Halim SM, Guenifi A, Khan A, Larsson O, Berggren PO, Ostenson CG, et al. Impaired coupling of glucose signal to the exocytotic machinery in diabetic GK rats: a defect ameliorated by cAMP. Diabetes. 1996 Jul;45(7):934–40.

212. Hohmeier HE, Mulder H, Chen G, Henkel-Rieger R, Prentki M, Newgard CB. Isolation of INS-1-derived cell lines with robust ATP-sensitive K+ channel-dependent and -independent glucose-stimulated insulin secretion. Diabetes. 2000 Mar;49(3):424–30.

213. Gembal M, Gilon P, Henquin JC. Evidence that glucose can control insulin release independently from its action on ATP-sensitive K+ channels in mouse B cells. J Clin Invest. 1992 Apr;89(4):1288–95.

214. Sato Y, Aizawa T, Komatsu M, Okada N, Yamada T. Dual functional role of membrane depolarization/Ca2+ influx in rat pancreatic B-cell. Diabetes. 1992 Apr;41(4):438–43.

215. Henquin J-C. The dual control of insulin secretion by glucose involves triggering and amplifying pathways in β-cells. Diabetes Res Clin Pract. 2011 Aug 1;93:S27–31.

216. Curi R, Lagranha CJ, Doi SQ, Sellitti DF, Procopio J, Pithon-Curi TC, et al. Molecular mechanisms of glutamine action. J Cell Physiol. 2005 Aug;204(2):392–401.

217. Prentki M, Matschinsky FM, Madiraju SRM. Metabolic signaling in fuel-induced insulin secretion. Cell Metab. 2013 Aug 6;18(2):162–85.

218. Anello M, Ucciardello V, Piro S, Patané G, Frittitta L, Calabrese V, et al. Chronic exposure to high leucine impairs glucose-induced insulin release by lowering the ATP-to-ADP ratio. Am J Physiol Endocrinol Metab. 2001 Nov;281(5):E1082-1087.

219. Gembal M, Detimary P, Gilon P, Gao ZY, Henquin JC. Mechanisms by which glucose can control insulin release independently from its action on adenosine triphosphate-sensitive K+ channels in mouse B cells. J Clin Invest. 1993 Mar;91(3):871–80.

220. Urban KA, Panten U. Selective loss of glucose-induced amplification of insulin secretion in mouse pancreatic islets pretreated with sulfonylurea in the absence of fuels. Diabetologia. 2005 Dec;48(12):2563–6.

221. Detimary P, Van den Berghe G, Henquin JC. Concentration dependence and time course of the effects of glucose on adenine and guanine nucleotides in mouse pancreatic islets. J Biol Chem. 1996 Aug 23;271(34):20559–65.

222. Komatsu M, Noda M, Sharp GW. Nutrient augmentation of Ca2+-dependent and Ca2+-independent pathways in stimulus-coupling to insulin secretion can be distinguished by their guanosine triphosphate requirements: studies on rat pancreatic islets. Endocrinology. 1998 Mar;139(3):1172–83.

223. Gheni G, Ogura M, Iwasaki M, Yokoi N, Minami K, Nakayama Y, et al. Glutamate acts as a key signal linking glucose metabolism to incretin/cAMP action to amplify insulin secretion. Cell Rep. 2014 Oct 23;9(2):661–73.

224. Sprague JE, Arbeláez AM. Glucose Counterregulatory Responses to Hypoglycemia. Pediatr Endocrinol Rev PER. 2011 Sep;9(1):463–75.

225. Schwartz NS, Clutter WE, Shah SD, Cryer PE. Glycemic thresholds for activation of glucose counterregulatory systems are higher than the threshold for symptoms. J Clin Invest. 1987 Mar;79(3):777–81.

226. Cooperberg BA, Cryer PE. Insulin reciprocally regulates glucagon secretion in humans. Diabetes. 2010 Nov;59(11):2936–40.

227. Ramnanan CJ, Edgerton DS, Kraft G, Cherrington AD. Physiologic action of glucagon on liver glucose metabolism. Diabetes Obes Metab. 2011 Oct;13(Suppl 1):118–25.

228. Sherwin RS, Saccà L. Effect of epinephrine on glucose metabolism in humans: contribution of the liver. Am J Physiol. 1984 Aug;247(2 Pt 1):E157-165.

229. Dufour S, Lebon V, Shulman GI, Petersen KF. Regulation of net hepatic glycogenolysis and gluconeogenesis by epinephrine in humans. Am J Physiol-Endocrinol Metab. 2009 Jul 1;297(1):E231–5.

230. Mitrakou A, Ryan C, Veneman T, Mokan M, Jenssen T, Kiss I, et al. Hierarchy of glycemic thresholds for counterregulatory hormone secretion, symptoms, and cerebral dysfunction. Am J Physiol. 1991 Jan;260(1 Pt 1):E67-74.

231. Tesfaye N, Seaquist ER. Neuroendocrine Responses to Hypoglycemia. Ann N Y Acad Sci. 2010 Nov;1212:12–28.

232. Rhyu YA, Jang J-Y, Park S, An JH, Kim D-L, Kim SK, et al. Impaired Cortisol and Growth Hormone Counterregulatory Responses among Severe Hypoglycemic Patients with Type 2 Diabetes Mellitus. Endocrinol Metab. 2019 Jun;34(2):187–94.

233. Muscelli E, Mari A, Natali A, Astiarraga BD, Camastra S, Frascerra S, et al. Impact of incretin hormones on beta-cell function in subjects with normal or impaired glucose tolerance. Am J Physiol Endocrinol Metab. 2006 Dec;291(6):E1144-1150.

234. Nauck MA, Homberger E, Siegel EG, Allen RC, Eaton RP, Ebert R, et al. Incretin effects of increasing glucose loads in man calculated from venous insulin and C-peptide responses. J Clin Endocrinol Metab. 1986 Aug;63(2):492–8.

235. Holst JJ, Gromada J. Role of incretin hormones in the regulation of insulin secretion in diabetic and nondiabetic humans. Am J Physiol Endocrinol Metab. 2004 Aug;287(2):E199-206.

236. Williams JA. GLP-1 (Version 1.0). Pancreapedia Exocrine Pancreas Knowl Base [Internet]. 2014 May 15 [cited 2021 May 20]; Available from: /molecules/glp-1-version-10

237. Bell GI, Sanchez-Pescador R, Laybourn PJ, Najarian RC. Exon duplication and divergence in the human preproglucagon gene. Nature. 1983 Jul;304(5924):368–71.

238. Holt MK, Richards JE, Cook DR, Brierley DI, Williams DL, Reimann F, et al. Preproglucagon Neurons in the Nucleus of the Solitary Tract Are the Main Source of Brain GLP-1, Mediate Stress-Induced Hypophagia, and Limit Unusually Large Intakes of Food. Diabetes. 2019 Jan;68(1):21–33.

239. Marchetti P, Lupi R, Bugliani M, Kirkpatrick CL, Sebastiani G, Grieco FA, et al. A local glucagon-like peptide 1 (GLP-1) system in human pancreatic islets. Diabetologia. 2012 Dec;55(12):3262–72.

240. Fava GE, Dong EW, Wu H. Intra-islet glucagon-like peptide 1. J Diabetes Complications. 2016 Dec;30(8):1651–8.

241. Müller TD, Finan B, Bloom SR, D'Alessio D, Drucker DJ, Flatt PR, et al. Glucagon-like peptide 1 (GLP-1). Mol Metab. 2019 Dec 1;30:72–130.

242. Kuhre RE, Gribble FM, Hartmann B, Reimann F, Windeløv JA, Rehfeld JF, et al. Fructose stimulates GLP-1 but not GIP secretion in mice, rats, and humans. Am J Physiol Gastrointest Liver Physiol. 2014 Apr 1;306(7):G622-630.

243. Higuchi N, Hira T, Yamada N, Hara H. Oral administration of corn zein hydrolysate stimulates GLP-1 and GIP secretion and improves glucose tolerance in male normal rats and Goto-Kakizaki rats. Endocrinology. 2013 Sep;154(9):3089–98.

244. Hirasawa A, Tsumaya K, Awaji T, Katsuma S, Adachi T, Yamada M, et al. Free fatty acids regulate gut incretin glucagon-like peptide-1 secretion through GPR120. Nat Med. 2005 Jan;11(1):90–4.

245. Hui H, Farilla L, Merkel P, Perfetti R. The short half-life of glucagon-like peptide-1 in plasma does not reflect its long-lasting beneficial effects. Eur J Endocrinol. 2002 Jun;146(6):863–9.

246. Meier JJ, Nauck MA, Kranz D, Holst JJ, Deacon CF, Gaeckler D, et al. Secretion, degradation, and elimination of glucagon-like peptide 1 and gastric inhibitory polypeptide in patients with chronic renal insufficiency and healthy control subjects. Diabetes. 2004 Mar;53(3):654–62.

247. Gilbert MP, Pratley RE. GLP-1 Analogs and DPP-4 Inhibitors in Type 2 Diabetes Therapy: Review of Head-to-Head Clinical Trials. Front Endocrinol. 2020 Apr 3;11:178.

248. Thorens B. Expression cloning of the pancreatic beta cell receptor for the gluco-incretin hormone glucagon-like peptide 1. Proc Natl Acad Sci U S A. 1992 Sep 15;89(18):8641–5.

249. Bullock BP, Heller RS, Habener JF. Tissue distribution of messenger ribonucleic acid encoding the rat glucagon-like peptide-1 receptor. Endocrinology. 1996 Jul;137(7):2968–78.

250. Campos RV, Lee YC, Drucker DJ. Divergent tissue-specific and developmental expression of receptors for glucagon and glucagon-like peptide-1 in the mouse. Endocrinology. 1994 May 1;134(5):2156–64.

251. Wei Y, Mojsov S. Tissue-specific expression of the human receptor for glucagon-like peptide-I: brain, heart and pancreatic forms have the same deduced amino acid sequences. FEBS Lett. 1995 Jan 30;358(3):219–24.

252. Gupta NA, Mells J, Dunham RM, Grakoui A, Handy J, Saxena NK, et al. Glucagon-like peptide-1 receptor is present on human hepatocytes and has a direct role in decreasing hepatic steatosis in vitro by modulating elements of the insulin signaling pathway. Hepatol Baltim Md. 2010 May;51(5):1584–92.

253. Yokomori H, Ando W. Spatial expression of glucagon-like peptide 1 receptor and caveolin-1 in hepatocytes with macrovesicular steatosis in non-alcoholic steatohepatitis. BMJ Open Gastroenterol. 2020 May 1;7(1):e000370.

254. Doyle ME, Egan JM. Mechanisms of action of glucagon-like peptide 1 in the pancreas. Pharmacol Ther. 2007 Mar;113(3):546–93.

255. Meloni AR, DeYoung MB, Lowe C, Parkes DG. GLP-1 receptor activated insulin secretion from pancreatic β-cells: mechanism and glucose dependence. Diabetes Obes Metab. 2013 Jan;15(1):15–27.

256. Béguin P, Nagashima K, Nishimura M, Gonoi T, Seino S. PKA-mediated phosphorylation of the human K(ATP) channel: separate roles of Kir6.2 and SUR1 subunit phosphorylation. EMBO J. 1999 Sep 1;18(17):4722–32.

257. Light PE, Manning Fox JE, Riedel MJ, Wheeler MB. Glucagon-like peptide-1 inhibits pancreatic ATP-sensitive potassium channels via a protein kinase A- and ADP-dependent mechanism. Mol Endocrinol Baltim Md. 2002 Sep;16(9):2135–44.

258. Drucker DJ, Philippe J, Mojsov S, Chick WL, Habener JF. Glucagon-like peptide I stimulates insulin gene expression and increases cyclic AMP levels in a rat islet cell line. Proc Natl Acad Sci U S A. 1987 May;84(10):3434–8.

259. Fehmann HC, Habener JF. Insulinotropic hormone glucagon-like peptide-I(7-37) stimulation of proinsulin gene expression and proinsulin biosynthesis in insulinoma beta TC-1 cells. Endocrinology. 1992 Jan;130(1):159–66.

260. Wang Y, Egan JM, Raygada M, Nadiv O, Roth J, Montrose-Rafizadeh C. Glucagon-like peptide-1 affects gene transcription and messenger ribonucleic acid stability of components of the insulin secretory system in RIN 1046-38 cells. Endocrinology. 1995 Nov;136(11):4910–7.

261. Buteau J, Foisy S, Joly E, Prentki M. Glucagon-like peptide 1 induces pancreatic beta-cell proliferation via transactivation of the epidermal growth factor receptor. Diabetes. 2003 Jan;52(1):124–32.

262. Buteau J, Roduit R, Susini S, Prentki M. Glucagon-like peptide-1 promotes DNA synthesis, activates phosphatidylinositol 3-kinase and increases transcription factor pancreatic and duodenal homeobox gene 1 (PDX-1) DNA binding activity in beta (INS-1)-cells. Diabetologia. 1999 Jul;42(7):856–64.

263. Buteau J, Foisy S, Rhodes CJ, Carpenter L, Biden TJ, Prentki M. Protein kinase Czeta activation mediates glucagon-like peptide-1-induced pancreatic beta-cell proliferation. Diabetes. 2001 Oct;50(10):2237–43.

264. Hui H, Nourparvar A, Zhao X, Perfetti R. Glucagon-like peptide-1 inhibits apoptosis of insulin-secreting cells via a cyclic 5'-adenosine monophosphate-dependent protein

kinase A- and a phosphatidylinositol 3-kinase-dependent pathway. Endocrinology. 2003 Apr;144(4):1444–55.

265. Wang Q, Li L, Xu E, Wong V, Rhodes C, Brubaker PL. Glucagon-like peptide-1 regulates proliferation and apoptosis via activation of protein kinase B in pancreatic INS-1 beta cells. Diabetologia. 2004 Mar;47(3):478–87.

266. Fridolf T, Böttcher G, Sundler F, Ahrén B. GLP-1 and GLP-1(7-36) amide: influences on basal and stimulated insulin and glucagon secretion in the mouse. Pancreas. 1991 Mar;6(2):208–15.

267. Hare KJ, Vilsbøll T, Asmar M, Deacon CF, Knop FK, Holst JJ. The glucagonostatic and insulinotropic effects of glucagon-like peptide 1 contribute equally to its glucose-lowering action. Diabetes. 2010 Jul;59(7):1765–70.

268. Junker AE, Gluud LL, van Hall G, Holst JJ, Knop FK, Vilsbøll T. Effects of glucagon-like peptide-1 on glucagon secretion in patients with non-alcoholic fatty liver disease. J Hepatol. 2016 Apr;64(4):908–15.

269. Plamboeck A, Veedfald S, Deacon CF, Hartmann B, Vilsbøll T, Knop FK, et al. The role of efferent cholinergic transmission for the insulinotropic and glucagonostatic effects of GLP-1. Am J Physiol Regul Integr Comp Physiol. 2015 Sep;309(5):R544-551.

270. De Marinis YZ, Salehi A, Ward CE, Zhang Q, Abdulkader F, Bengtsson M, et al. GLP-1 inhibits and adrenaline stimulates glucagon release by differential modulation of N- and L-type Ca2+ channel-dependent exocytosis. Cell Metab. 2010 Jun 9;11(6):543–53.

271. Henderson SJ, Konkar A, Hornigold DC, Trevaskis JL, Jackson R, Fritsch Fredin M, et al. Robust anti-obesity and metabolic effects of a dual GLP-1/glucagon receptor peptide agonist in rodents and non-human primates. Diabetes Obes Metab. 2016 Dec;18(12):1176–90.

272. Beiroa D, Imbernon M, Gallego R, Senra A, Herranz D, Villarroya F, et al. GLP-1 agonism stimulates brown adipose tissue thermogenesis and browning through hypothalamic AMPK. Diabetes. 2014 Oct;63(10):3346–58.

273. Gutzwiller JP, Drewe J, Göke B, Schmidt H, Rohrer B, Lareida J, et al. Glucagon-like peptide-1 promotes satiety and reduces food intake in patients with diabetes mellitus type 2. Am J Physiol. 1999 May;276(5):R1541-1544.

274. Linnebjerg H, Park S, Kothare PA, Trautmann ME, Mace K, Fineman M, et al. Effect of exenatide on gastric emptying and relationship to postprandial glycemia in type 2 diabetes. Regul Pept. 2008 Nov 29;151(1–3):123–9.

275. Nakatani Y, Maeda M, Matsumura M, Shimizu R, Banba N, Aso Y, et al. Effect of GLP-1 receptor agonist on gastrointestinal tract motility and residue rates as evaluated by capsule endoscopy. Diabetes Metab. 2017 Oct;43(5):430–7.

276. Haeusler RA, McGraw TE, Accili D. Biochemical and cellular properties of insulin receptor signalling. Nat Rev Mol Cell Biol. 2018 Jan;19(1):31–44.

277. Hubbard SR. The insulin receptor: both a prototypical and atypical receptor tyrosine kinase. Cold Spring Harb Perspect Biol. 2013 Mar 1;5(3):a008946.

278. Hubbard SR, Wei L, Ellis L, Hendrickson WA. Crystal structure of the tyrosine kinase domain of the human insulin receptor. Nature. 1994 Dec 22;372(6508):746–54.

279. Wei L, Hubbard SR, Hendrickson WA, Ellis L. Expression, characterization, and crystallization of the catalytic core of the human insulin receptor protein-tyrosine kinase domain. J Biol Chem. 1995 Apr 7;270(14):8122–30.

280. Youngren JF. Regulation of insulin receptor function. Cell Mol Life Sci CMLS. 2007 Apr;64(7–8):873–91.

281. Taniguchi CM, Emanuelli B, Kahn CR. Critical nodes in signalling pathways: insights into insulin action. Nat Rev Mol Cell Biol. 2006 Feb;7(2):85–96.

282. White MF. The IRS-signalling system: a network of docking proteins that mediate insulin action. Mol Cell Biochem. 1998 May;182(1–2):3–11.

283. White MF, White MF. Mechanisms of Insulin Action. In: Skyler J, editor. Atlas of Diabetes: Fourth Edition [Internet]. Boston, MA: Springer US; 2012 [cited 2021 Apr 18]. p. 19–38. Available from: https://doi.org/10.1007/978-1-4614-1028-7_2

284. Copps KD, White MF. Regulation of insulin sensitivity by serine/threonine phosphorylation of insulin receptor substrate proteins IRS1 and IRS2. Diabetologia. 2012 Oct;55(10):2565–82.

285. Cherrington AD, Edgerton D, Sindelar DK. The direct and indirect effects of insulin on hepatic glucose production in vivo. Diabetologia. 1998 Sep;41(9):987–96.

286. Moore MC, Coate KC, Winnick JJ, An Z, Cherrington AD. Regulation of Hepatic Glucose Uptake and Storage In Vivo12. Adv Nutr. 2012 May 4;3(3):286–94.

287. Iynedjian PB. Molecular physiology of mammalian glucokinase. Cell Mol Life Sci CMLS. 2009 Jan;66(1):27–42.

288. Agius L. Glucokinase and molecular aspects of liver glycogen metabolism. Biochem J. 2008 Aug 15;414(1):1–18.

289. Iynedjian PB, Jotterand D, Nouspikel T, Asfari M, Pilot PR. Transcriptional induction of glucokinase gene by insulin in cultured liver cells and its repression by the glucagon-cAMP system. J Biol Chem. 1989 Dec 25;264(36):21824–9.

290. Ausina P, Da Silva D, Majerowicz D, Zancan P, Sola-Penna M. Insulin specifically regulates expression of liver and muscle phosphofructokinase isoforms. Biomed Pharmacother Biomedecine Pharmacother. 2018 Jul;103:228–33.

291. Buschiazzo H, Exton JH, Park CR. Effects of glucose on glycogen synthetase, phosphorylase, and glycogen deposition in the perfused rat liver. Proc Natl Acad Sci U S A. 1970 Feb;65(2):383–7.

292. Kruszynska YT, Home PD, Alberti KG. In vivo regulation of liver and skeletal muscle glycogen synthase activity by glucose and insulin. Diabetes. 1986 Jun;35(6):662–7.

293. Petersen KF, Laurent D, Rothman DL, Cline GW, Shulman GI. Mechanism by which glucose and insulin inhibit net hepatic glycogenolysis in humans. J Clin Invest. 1998 Mar 15;101(6):1203–9.

294. Edgerton DS, Johnson KMS, Cherrington AD. Current strategies for the inhibition of hepatic glucose production in type 2 diabetes. Front Biosci Landmark Ed. 2009 Jan 1;14:1169–81.

295. Han H-S, Kang G, Kim JS, Choi BH, Koo S-H. Regulation of glucose metabolism from a liver-centric perspective. Exp Mol Med. 2016 Mar;48(3):e218–e218.

296. Shepherd PR, Kahn BB. Glucose transporters and insulin action--implications for insulin resistance and diabetes mellitus. N Engl J Med. 1999 Jul 22;341(4):248–57.

297. Leto D, Saltiel AR. Regulation of glucose transport by insulin: traffic control of GLUT4. Nat Rev Mol Cell Biol. 2012 May 23;13(6):383–96.

298. Stöckli J, Fazakerley DJ, James DE. GLUT4 exocytosis. J Cell Sci. 2011 Dec 15;124(24):4147–59.

299. Alves-Bezerra M, Cohen DE. Triglyceride metabolism in the liver. Compr Physiol. 2017 Dec 12;8(1):1–8.

300. Petersen MC, Shulman GI. Mechanisms of Insulin Action and Insulin Resistance. Physiol Rev. 2018 Oct 1;98(4):2133–223.

301. Horton JD, Goldstein JL, Brown MS. SREBPs: activators of the complete program of cholesterol and fatty acid synthesis in the liver. J Clin Invest. 2002 May;109(9):1125–31.

302. Kawano Y, Cohen DE. Mechanisms of hepatic triglyceride accumulation in non-alcoholic fatty liver disease. J Gastroenterol. 2013 Apr;48(4):434–41.

303. Jaworski K, Sarkadi-Nagy E, Duncan RE, Ahmadian M, Sul HS. Regulation of triglyceride metabolism. IV. Hormonal regulation of lipolysis in adipose tissue. Am J Physiol Gastrointest Liver Physiol. 2007 Jul;293(1):G1-4.

304. Duncan RE, Ahmadian M, Jaworski K, Sarkadi-Nagy E, Sul HS. Regulation of Lipolysis in Adipocytes. Annu Rev Nutr. 2007;27:79–101.

305. Freeman AM, Pennings N. Insulin Resistance. In: StatPearls [Internet]. Treasure Island (FL): StatPearls Publishing; 2021 [cited 2021 Jun 20]. Available from: http://www.ncbi.nlm.nih.gov/books/NBK507839/

306. Romao I, Roth J. Genetic and environmental interactions in obesity and type 2 diabetes. J Am Diet Assoc. 2008 Apr;108(4 Suppl 1):S24-28.

307. Kahn BB, Flier JS. Obesity and insulin resistance. J Clin Invest. 2000 Aug;106(4):473–81.

308. Kahn SE, Hull RL, Utzschneider KM. Mechanisms linking obesity to insulin resistance and type 2 diabetes. Nature. 2006 Dec 14;444(7121):840–6.

309. Boden G, Shulman GI. Free fatty acids in obesity and type 2 diabetes: defining their role in the development of insulin resistance and beta-cell dysfunction. Eur J Clin Invest. 2002 Jun;32 Suppl 3:14–23.

310. Yaribeygi H, Farrokhi FR, Butler AE, Sahebkar A. Insulin resistance: Review of the underlying molecular mechanisms. J Cell Physiol. 2019;234(6):8152–61.

311. Lingohr MK, Buettner R, Rhodes CJ. Pancreatic beta-cell growth and survival--a role in obesity-linked type 2 diabetes? Trends Mol Med. 2002 Aug;8(8):375–84.

312. Karaca M, Magnan C, Kargar C. Functional pancreatic beta-cell mass: involvement in type 2 diabetes and therapeutic intervention. Diabetes Metab. 2009 Apr;35(2):77–84.

313. Bonner-Weir S. Islet growth and development in the adult. J Mol Endocrinol. 2000 Jun;24(3):297–302.

314. Topp BG, Atkinson LL, Finegood DT. Dynamics of insulin sensitivity, -cell function, and -cell mass during the development of diabetes in fa/fa rats. Am J Physiol Endocrinol Metab. 2007 Dec;293(6):E1730-1735.

315. Buettner R, Newgard CB, Rhodes CJ, O'Doherty RM. Correction of diet-induced hyperglycemia, hyperinsulinemia, and skeletal muscle insulin resistance by moderate hyperleptinemia. Am J Physiol Endocrinol Metab. 2000 Mar;278(3):E563-569.

316. Gonzalez A, Merino B, Marroquí L, Ñeco P, Alonso-Magdalena P, Caballero-Garrido E, et al. Insulin hypersecretion in islets from diet-induced hyperinsulinemic obese female mice is associated with several functional adaptations in individual β-cells. Endocrinology. 2013 Oct;154(10):3515–24.

317. Liu YQ, Jetton TL, Leahy JL. beta-Cell adaptation to insulin resistance. Increased pyruvate carboxylase and malate-pyruvate shuttle activity in islets of nondiabetic Zucker fatty rats. J Biol Chem. 2002 Oct 18;277(42):39163–8.

318. Weir GC, Laybutt DR, Kaneto H, Bonner-Weir S, Sharma A. Beta-cell adaptation and decompensation during the progression of diabetes. Diabetes. 2001 Feb;50 Suppl 1:S154-159.

319. Cockburn BN, Ostrega DM, Sturis J, Kubstrup C, Polonsky KS, Bell GI. Changes in pancreatic islet glucokinase and hexokinase activities with increasing age, obesity, and the onset of diabetes. Diabetes. 1997 Sep;46(9):1434–9.

320. Hosokawa H, Hosokawa YA, Leahy JL. Upregulated hexokinase activity in isolated islets from diabetic 90% pancreatectomized rats. Diabetes. 1995 Nov;44(11):1328–33.

321. Liu YQ, Moibi JA, Leahy JL. Chronic high glucose lowers pyruvate dehydrogenase activity in islets through enhanced production of long chain acyl-CoA: prevention of impaired glucose oxidation by enhanced pyruvate recycling through the malate-pyruvate shuttle. J Biol Chem. 2004 Feb 27;279(9):7470–5.

322. Liu YQ, Nevin PW, Leahy JL. beta-cell adaptation in 60% pancreatectomy rats that preserves normoinsulinemia and normoglycemia. Am J Physiol Endocrinol Metab. 2000 Jul;279(1):E68-73.

323. Weir GC, Bonner-Weir S. A dominant role for glucose in β cell compensation of insulin resistance. J Clin Invest. 2007 Jan 2;117(1):81–3.

324. Cnop M, Vidal J, Hull RL, Utzschneider KM, Carr DB, Schraw T, et al. Progressive loss of beta-cell function leads to worsening glucose tolerance in first-degree relatives of subjects with type 2 diabetes. Diabetes Care. 2007 Mar;30(3):677–82.

325. Weyer C, Bogardus C, Mott DM, Pratley RE. The natural history of insulin secretory dysfunction and insulin resistance in the pathogenesis of type 2 diabetes mellitus. J Clin Invest. 1999 Sep;104(6):787–94.

326. Leahy JL. Pathogenesis of Type 2 Diabetes Mellitus. Arch Med Res. 2005 May 1;36(3):197–209.

327. Hudish LI, Reusch JEB, Sussel L. **β** Cell dysfunction during progression of metabolic syndrome to type 2 diabetes. J Clin Invest. 2019 Oct 1;129(10):4001–8.

328. Rabhi N, Salas E, Froguel P, Annicotte J-S. Role of the unfolded protein response in β cell compensation and failure during diabetes. J Diabetes Res. 2014;2014:795171.

329. Eizirik DL, Cardozo AK, Cnop M. The role for endoplasmic reticulum stress in diabetes mellitus. Endocr Rev. 2008 Feb;29(1):42–61.

330. Marchetti P, Bugliani M, De Tata V, Suleiman M, Marselli L. Pancreatic Beta Cell Identity in Humans and the Role of Type 2 Diabetes. Front Cell Dev Biol. 2017;5:55.

331. Supale S, Li N, Brun T, Maechler P. Mitochondrial dysfunction in pancreatic β cells. Trends Endocrinol Metab. 2012 Sep 1;23(9):477–87.

332. Gerber PA, Rutter GA. The Role of Oxidative Stress and Hypoxia in Pancreatic Beta-Cell Dysfunction in Diabetes Mellitus. Antioxid Redox Signal. 2017 Apr 1;26(10):501–18.

333. Gilbert ER, Liu D. Epigenetics: the missing link to understanding β-cell dysfunction in the pathogenesis of type 2 diabetes. Epigenetics. 2012 Aug;7(8):841–52.

334. Kahn SE. The relative contributions of insulin resistance and beta-cell dysfunction to the pathophysiology of Type 2 diabetes. Diabetologia. 2003 Jan;46(1):3–19.

335. Kasuga M. Insulin resistance and pancreatic β cell failure. J Clin Invest. 2006 Jul 3;116(7):1756–60.

336. Kahn BB. Type 2 Diabetes: When Insulin Secretion Fails to Compensate for Insulin Resistance. Cell. 1998 Mar 6;92(5):593–6.

337. Mcilroy GD, Suchacki K, Roelofs AJ, Yang W, Fu Y, Bai B, et al. Adipose specific disruption of seipin causes early-onset generalised lipodystrophy and altered fuel utilisation without severe metabolic disease. Mol Metab. 2018;10:55–65.

338. Kim K, Kim H, Lee D. Site-specific modification of genome with cell-permeable Cre fusion protein in preimplantation mouse embryo. Biochem Biophys Res Commun. 2009 Oct 9;388(1):122–6.

339. Katz A, Nambi SS, Mather K, Baron AD, Follmann DA, Sullivan G, et al. Quantitative insulin sensitivity check index: a simple, accurate method for assessing insulin sensitivity in humans. J Clin Endocrinol Metab. 2000 Jul;85(7):2402–10.

340. Matthews DR, Hosker JP, Rudenski AS, Naylor BA, Treacher DF, Turner RC. Homeostasis model assessment: insulin resistance and beta-cell function from fasting plasma glucose and insulin concentrations in man. Diabetologia. 1985 Jul;28(7):412–9.

341. Fischer-Posovszky P, Newell FS, Wabitsch M, Tornqvist HE. Human SGBS cells - a unique tool for studies of human fat cell biology. Obes Facts. 2008;1(4):184–9.

342. Pfaffl MW. A new mathematical model for relative quantification in real-time RT-PCR. Nucleic Acids Res. 2001 May 1;29(9):e45.

343. NIH Image to ImageJ: 25 years of image analysis | Nature Methods [Internet]. [cited 2021 Mar 15]. Available from: https://www.nature.com/articles/nmeth.2089

344. Yang W, Thein S, Guo X, Xu F, Venkatesh B, Sugii S, et al. Seipin differentially regulates lipogenesis and adipogenesis through a conserved core sequence and an evolutionarily acquired C-terminus. Biochem J. 2013 May 15;452(1):37–44.

345. Wabitsch M, Brenner RE, Melzner I, Braun M, Möller P, Heinze E, et al. Characterization of a human preadipocyte cell strain with high capacity for adipose differentiation. Int J Obes Relat Metab Disord J Int Assoc Study Obes. 2001 Jan;25(1):8–15.

346. Tenorio J, Arias P, Martínez-Glez V, Santos F, García-Miñaur S, Nevado J, et al. Simpson-Golabi-Behmel syndrome types I and II. Orphanet J Rare Dis. 2014 Sep 20;9(1):138.

347. Mcilroy GD, Mitchell SE, Han W, Delibegović M, Rochford JJ. Ablation of Bscl2/seipin in hepatocytes does not cause metabolic dysfunction in congenital generalised lipodystrophy. Dis Model Mech [Internet]. 2020 Jan 13 [cited 2021 Apr 9];13(1). Available from: https://www.ncbi.nlm.nih.gov/pmc/articles/PMC6994952/

348. Jiao Y, Ahmed U, Sim MFM, Bejar A, Zhang X, Talukder MMU, et al. Discovering metabolic disease gene interactions by correlated effects on cellular morphology. Mol Metab. 2019 Jun;24:108–19.

349. Green H, Meuth M. An established pre-adipose cell line and its differentiation in culture. Cell. 1974 Oct 1;3(2):127–33.

350. Farmer SR. Transcriptional control of adipocyte formation. Cell Metab. 2006 Oct;4(4):263–73.

351. Rosen ED, Walkey CJ, Puigserver P, Spiegelman BM. Transcriptional regulation of adipogenesis. Genes Dev. 2000 Jun 1;14(11):1293–307.

352. Rosen ED, Hsu C-H, Wang X, Sakai S, Freeman MW, Gonzalez FJ, et al. C/EBPalpha induces adipogenesis through PPARgamma: a unified pathway. Genes Dev. 2002 Jan 1;16(1):22–6.

353. Ntambi JM, Young-Cheul K. Adipocyte Differentiation and Gene Expression. J Nutr. 2000 Dec 1;130(12):3122S-3126S.

354. Lowe CE, O'Rahilly S, Rochford JJ. Adipogenesis at a glance. J Cell Sci. 2011 Aug 15;124(16):2681–6.

355. Christy RJ, Yang VW, Ntambi JM, Geiman DE, Landschulz WH, Friedman AD, et al. Differentiation-induced gene expression in 3T3-L1 preadipocytes: CCAAT/enhancer binding protein interacts with and activates the promoters of two adipocyte-specific genes. Genes Dev. 1989 Jan 9;3(9):1323–35.

356. Tontonoz P, Hu E, Graves RA, Budavari AI, Spiegelman BM. mPPAR gamma 2: tissue-specific regulator of an adipocyte enhancer. Genes Dev. 1994 May 15;8(10):1224–34.

357. Zimmermann R, Strauss JG, Haemmerle G, Schoiswohl G, Birner-Gruenberger R, Riederer M, et al. Fat mobilization in adipose tissue is promoted by adipose triglyceride lipase. Science. 2004 Nov 19;306(5700):1383–6.

358. Haemmerle G, Lass A, Zimmermann R, Gorkiewicz G, Meyer C, Rozman J, et al. Defective lipolysis and altered energy metabolism in mice lacking adipose triglyceride lipase. Science. 2006 May 5;312(5774):734–7.

359. Garton AJ, Yeaman SJ. Identification and role of the basal phosphorylation site on hormone-sensitive lipase. Eur J Biochem. 1990 Jul 20;191(1):245–50.

360. Schlottmann I, Ehrhart-Bornstein M, Wabitsch M, Bornstein SR, Lamounier-Zepter V. Calcium-dependent release of adipocyte fatty acid binding protein from human adipocytes. Int J Obes. 2014 Sep;38(9):1221–7.

361. Allott EH, Oliver E, Lysaght J, Gray SG, Reynolds JV, Roche HM, et al. The SGBS cell strain as a model for the in vitro study of obesity and cancer. Clin Transl Oncol. 2012 Oct 1;14(10):774–82.

362. Brasaemle DL, Barber T, Wolins NE, Serrero G, Blanchette-Mackie EJ, Londos C. Adipose differentiation-related protein is an ubiquitously expressed lipid storage droplet-associated protein. J Lipid Res. 1997 Nov;38(11):2249–63.

363. Guennoun A, Kazantzis M, Thomas R, Wabitsch M, Tews D, Seetharama Sastry K, et al. Comprehensive molecular characterization of human adipocytes reveals a transient brown phenotype. J Transl Med. 2015 Apr 30;13(1):135.

364. Yeo CR, Agrawal M, Hoon S, Shabbir A, Shrivastava MK, Huang S, et al. SGBS cells as a model of human adipocyte browning: A comprehensive comparative study with primary human white subcutaneous adipocytes. Sci Rep. 2017 Jun 22;7(1):4031.

365. Dollet L, Magré J, Joubert M, Le May C, Ayer A, Arnaud L, et al. Seipin deficiency alters brown adipose tissue thermogenesis and insulin sensitivity in a non-cell autonomous mode. Sci Rep. 2016 Oct 17;6(1):35487.

366. Liu L, Jiang Q, Wang X, Zhang Y, Lin RCY, Lam SM, et al. Adipose-Specific Knockout of Seipin/Bscl2 Results in Progressive Lipodystrophy. Diabetes. 2014 Jul 1;63(7):2320–31.

367. Bohnert M. New friends for seipin - Implications of seipin partner proteins in the life cycle of lipid droplets. Semin Cell Dev Biol. 2020 Dec;108:24–32.

368. Dichlberger A, Kovanen PT, Schneider WJ. Mast cells: from lipid droplets to lipid mediators. Clin Sci Lond Engl 1979. 2013 Aug;125(3):121–30.

369. Melo RCN, Dvorak AM. Lipid body-phagosome interaction in macrophages during infectious diseases: host defense or pathogen survival strategy? PLoS Pathog. 2012;8(7):e1002729.

370. Akira S, Takeda K. Toll-like receptor signalling. Nat Rev Immunol. 2004 Jul;4(7):499–511.

371. Bronte V, Pittet MJ. The spleen in local and systemic regulation of immunity. Immunity. 2013 Nov 14;39(5):806–18.

372. Vannella KM, Barron L, Borthwick LA, Kindrachuk KN, Narasimhan PB, Hart KM, et al. Incomplete deletion of IL-4Rα by LysM(Cre) reveals distinct subsets of M2 macrophages controlling inflammation and fibrosis in chronic schistosomiasis. PLoS Pathog. 2014 Sep;10(9):e1004372.

373. Shi H, Kokoeva MV, Inouye K, Tzameli I, Yin H, Flier JS. TLR4 links innate immunity and fatty acid–induced insulin resistance. J Clin Invest. 2006 Nov 1;116(11):3015–25.

374. Lowy FD. Staphylococcus aureus Infections. N Engl J Med. 1998;13.

375. Maurya R, Bhattacharya P, Dey R, Nakhasi HL. Leptin Functions in Infectious Diseases. Front Immunol [Internet]. 2018 Nov 26 [cited 2021 Mar 11];9. Available from: https://www.ncbi.nlm.nih.gov/pmc/articles/PMC6275238/

376. Craveiro Sarmento AS, de Azevedo Medeiros LB, Agnez-Lima LF, Lima JG, de Melo Campos JTA. Exploring Seipin: From Biochemistry to Bioinformatics Predictions. Int J Cell Biol [Internet]. 2018 Sep 19 [cited 2021 Mar 9];2018. Available from: https://www.ncbi.nlm.nih.gov/pmc/articles/PMC6192094/

377. Ratter JM, Tack CJ, Netea MG, Stienstra R. Environmental Signals Influencing Myeloid Cell Metabolism and Function in Diabetes. Trends Endocrinol Metab. 2018 Jul 1;29(7):468–80.

378. Teng O, Ang CKE, Guan XL. Macrophage–Bacteria Interactions—A Lipid-Centric Relationship. Front Immunol [Internet]. 2017 Dec 20 [cited 2021 Mar 11];8. Available from: https://www.ncbi.nlm.nih.gov/pmc/articles/PMC5742358/

379. Remmerie A, Scott CL. Macrophages and lipid metabolism. Cell Immunol. 2018 Aug;330:27–42.

380. Carta G, Murru E, Banni S, Manca C. Palmitic Acid: Physiological Role, Metabolism and Nutritional Implications. Front Physiol [Internet]. 2017 Nov 8 [cited 2021 Mar 9];8. Available from: https://www.ncbi.nlm.nih.gov/pmc/articles/PMC5682332/

381. Baggiolini M. Chemokines and leukocyte traffic. Nature. 1998 Apr;392(6676):565–8.

382. Leach N, Vesa SC, Alexescu T, Dronca E, Negrean V, P SD. Association between serum monocyte chemoattractant protein-1(MCP-1) levels, insulin resistance and subclinical atherosclerosis in patients with nonalcoholic steatohepatitis. Atherosclerosis. 2016 Sep 1;252:e153–4.

383. Kanda H, Tateya S, Tamori Y, Kotani K, Hiasa K, Kitazawa R, et al. MCP-1 contributes to macrophage infiltration into adipose tissue, insulin resistance, and hepatic steatosis in obesity. J Clin Invest. 2006 Jun 1;116(6):1494–505.

384. Panee J. Monocyte Chemoattractant Protein 1 (MCP-1) in Obesity and Diabetes. Cytokine. 2012 Oct;60(1):1–12.

385. Xiong J, Sun P, Wang Y, Hua X, Song W, Wang Y, et al. Heterozygous deletion of Seipin in islet beta cells of male mice has an impact on insulin synthesis and secretion through reduced PPARγ expression. Diabetologia. 2020 Feb 1;63(2):338–50.

386. Cui X, Wang Y, Tang Y, Liu Y, Zhao L, Deng J, et al. Seipin ablation in mice results in severe generalized lipodystrophy. Hum Mol Genet. 2011 Aug 1;20(15):3022–30.

387. Bonner-Weir S, Orci L. New perspectives on the microvasculature of the islets of Langerhans in the rat. Diabetes. 1982 Oct;31(10):883–9.

388. Dai C, Brissova M, Reinert RB, Nyman L, Liu EH, Thompson C, et al. Pancreatic Islet Vasculature Adapts to Insulin Resistance Through Dilation and Not Angiogenesis. Diabetes. 2013 Dec;62(12):4144–53.

389. Ehses JA, Perren A, Eppler E, Ribaux P, Pospisilik JA, Maor-Cahn R, et al. Increased Number of Islet-Associated Macrophages in Type 2 Diabetes. Diabetes. 2007 Sep 1;56(9):2356–70.

390. Richardson SJ, Willcox A, Bone AJ, Foulis AK, Morgan NG. Islet-associated macrophages in type 2 diabetes. Diabetologia. 2009 Aug;52(8):1686–8.

391. Butcher MJ, Hallinger D, Garcia E, Machida Y, Chakrabarti S, Nadler J, et al. Association of proinflammatory cytokines and islet resident leucocytes with islet dysfunction in type 2 diabetes. Diabetologia. 2014 Mar;57(3):491–501.

392. Banaei-Bouchareb L, Gouon-Evans V, Samara-Boustani D, Castellotti MC, Czernichow P, Pollard JW, et al. Insulin cell mass is altered in Csf1op/Csf1op macrophage-deficient mice. J Leukoc Biol. 2004 Aug;76(2):359–67.

393. Xiao X, Gaffar I, Guo P, Wiersch J, Fischbach S, Peirish L, et al. M2 macrophages promote beta-cell proliferation by up-regulation of SMAD7. Proc Natl Acad Sci U S A. 2014 Apr 1;111(13):E1211-1220.

394. Chittezhath M, Gunaseelan D, Zheng X, Hasan R, Tay VSY, Lim ST, et al. Islet macrophages are associated with islet vascular remodeling and compensatory hyperinsulinemia during diabetes. Am J Physiol Endocrinol Metab. 2019 Dec 1;317(6):E1108–20.

395. Chen C, Hosokawa H, Bumbalo LM, Leahy JL. Mechanism of compensatory hyperinsulinemia in normoglycemic insulin-resistant spontaneously hypertensive rats. Augmented enzymatic activity of glucokinase in beta-cells. J Clin Invest. 1994 Jul;94(1):399–404.

396. Chen C, Bumbalo L, Leahy JL. Increased catalytic activity of glucokinase in isolated islets from hyperinsulinemic rats. Diabetes. 1994 May;43(5):684–9.

397. Stijnen P, Ramos-Molina B, O'Rahilly S, Creemers JWM. PCSK1 Mutations and Human Endocrinopathies: From Obesity to Gastrointestinal Disorders. Endocr Rev. 2016 Aug 1;37(4):347–71.

398. Tramunt B, Smati S, Grandgeorge N, Lenfant F, Arnal J-F, Montagner A, et al. Sex differences in metabolic regulation and diabetes susceptibility. Diabetologia. 2020 Mar 1;63(3):453–61.

399. Raygada M, Rennert O. Congenital generalized lipodystrophy: profile of the disease and gender differences in two siblings. Clin Genet. 2005;67(1):98–101.

400. Srinivasan S, Bernal-Mizrachi E, Ohsugi M, Permutt MA. Glucose promotes pancreatic islet beta-cell survival through a PI 3-kinase/Akt-signaling pathway. Am J Physiol Endocrinol Metab. 2002 Oct;283(4):E784-793.

401. Terauchi Y, Takamoto I, Kubota N, Matsui J, Suzuki R, Komeda K, et al. Glucokinase and IRS-2 are required for compensatory β cell hyperplasia in response to high-fat diet–induced insulin resistance. J Clin Invest. 2007 Jan 2;117(1):246–57.

402. Steil GM, Trivedi N, Jonas JC, Hasenkamp WM, Sharma A, Bonner-Weir S, et al. Adaptation of beta-cell mass to substrate oversupply: enhanced function with normal gene expression. Am J Physiol Endocrinol Metab. 2001 May;280(5):E788-796.

403. Van Citters GW, Kabir M, Kim SP, Mittelman SD, Dea MK, Brubaker PL, et al. Elevated Glucagon-Like Peptide-1-(7–36)-Amide, but Not Glucose, Associated with Hyperinsulinemic Compensation for Fat Feeding. J Clin Endocrinol Metab. 2002 Nov 1;87(11):5191–8.

404. Ying W, Lee YS, Dong Y, Seidman JS, Yang M, Isaac R, et al. Expansion of Islet-Resident Macrophages Leads to Inflammation Affecting β Cell Proliferation and Function in Obesity. Cell Metab. 2019 Feb 5;29(2):457-474.e5.

405. Chen W, Zhou H, Saha P, Li L, Chan L. Molecular mechanisms underlying fasting modulated liver insulin sensitivity and metabolism in male lipodystrophic Bscl2/Seipin-deficient mice. Endocrinology. 2014 Nov;155(11):4215–25.

406. Xu W, Zhou H, Xuan H, Saha P, Wang G, Chen W. Novel metabolic disorders in skeletal muscle of Lipodystrophic Bscl2/Seipin deficient mice. Mol Cell Endocrinol. 2019 Feb 15;482:1–10.

407. Mcilroy GD, Mitchell SE, Han W, Delibegović M, Rochford JJ. Female adipose tissue-specific Bscl2 knockout mice develop only moderate metabolic dysfunction when housed at thermoneutrality and fed a high-fat diet. Sci Rep. 2018 Dec 14;8(1):17863.

408. Drucker DJ. Glucagon-like peptide-1 and the islet beta-cell: augmentation of cell proliferation and inhibition of apoptosis. Endocrinology. 2003 Dec;144(12):5145–8.

409. DeFronzo RA, Ratner RE, Han J, Kim DD, Fineman MS, Baron AD. Effects of exenatide (exendin-4) on glycemic control and weight over 30 weeks in metformin-treated patients with type 2 diabetes. Diabetes Care. 2005 May;28(5):1092–100.

410. Oh YS, Bae GD, Baek DJ, Park E-Y, Jun H-S. Fatty Acid-Induced Lipotoxicity in Pancreatic Beta-Cells During Development of Type 2 Diabetes. Front Endocrinol. 2018;9:384.

411. Itabe H, Yamaguchi T, Nimura S, Sasabe N. Perilipins: a diversity of intracellular lipid droplet proteins. Lipids Health Dis. 2017 Apr 28;16(1):83.

412. Faleck DM, Ali K, Roat R, Graham MJ, Crooke RM, Battisti R, et al. Adipose differentiation-related protein regulates lipids and insulin in pancreatic islets. Am J Physiol - Endocrinol Metab. 2010 Aug;299(2):E249–57.

413. Mishra A, Liu S, Promes J, Harata M, Sivitz W, Fink B, et al. Perilipin 2 downregulation in β cells impairs insulin secretion under nutritional stress and damages mitochondria. JCI Insight. 2021 May 10;6(9):144341.

414. Trevino MB, Machida Y, Hallinger DR, Garcia E, Christensen A, Dutta S, et al. Perilipin 5 Regulates Islet Lipid Metabolism and Insulin Secretion in a cAMP-Dependent Manner: Implication of Its Role in the Postprandial Insulin Secretion. Diabetes. 2015 Apr 1;64(4):1299–310.

415. Asfari M, Janjic D, Meda P, Li G, Halban PA, Wollheim CB. Establishment of 2-mercaptoethanol-dependent differentiated insulin-secreting cell lines. Endocrinology. 1992 Jan 1;130(1):167–78.

416. Dai FF, Bhattacharjee A, Liu Y, Batchuluun B, Zhang M, Wang XS, et al. A Novel GLP1 Receptor Interacting Protein ATP6ap2 Regulates Insulin Secretion in Pancreatic Beta Cells. J Biol Chem. 2015 Oct 9;290(41):25045–61.

417. Deacon CF, Nauck MA, Toft-Nielsen M, Pridal L, Willms B, Holst JJ. Both subcutaneously and intravenously administered glucagon-like peptide I are rapidly degraded from the NH2-terminus in type II diabetic patients and in healthy subjects. Diabetes. 1995 Sep;44(9):1126–31.

418. Reedtz-Runge S, Schimmer S, Oschmann J, Bruun C, Knudsen S, Jeppesen C, et al. Differential Structural Properties of GLP-1 and Exendin-4 Determine Their Relative Affinity for the GLP-1 Receptor N-Terminal Extracellular Domain †. Biochemistry. 2007 Jun 1;46:5830–40.

419. Wajcberg E, Amarah A. Liraglutide in the management of type 2 diabetes. Drug Des Devel Ther. 2010 Oct 22;4:279–90.

420. Inaishi J, Saisho Y. Beta-Cell Mass in Obesity and Type 2 Diabetes, and Its Relation to Pancreas Fat: A Mini-Review. Nutrients. 2020 Dec 16;12(12):3846.

421. Ahrén B, Pacini G. Islet adaptation to insulin resistance: mechanisms and implications for intervention. Diabetes Obes Metab. 2005 Jan;7(1):2–8.

422. Rowlands J, Heng J, Newsholme P, Carlessi R. Pleiotropic Effects of GLP-1 and Analogs on Cell Signaling, Metabolism, and Function. Front Endocrinol. 2018;9:672.

423. Holst JJ, Knop FK, Vilsbøll T, Krarup T, Madsbad S. Loss of Incretin Effect Is a Specific, Important, and Early Characteristic of Type 2 Diabetes. Diabetes Care. 2011 May 1;34(Supplement 2):S251–7.

424. Bagger JI, Knop FK, Lund A, Vestergaard H, Holst JJ, Vilsbøll T. Impaired regulation of the incretin effect in patients with type 2 diabetes. J Clin Endocrinol Metab. 2011 Mar;96(3):737–45.

425. Koopman ADM, Rutters F, Rauh SP, Nijpels G, Holst JJ, Beulens JW, et al. Incretin responses to oral glucose and mixed meal tests and changes in fasting glucose levels during 7 years of follow-up: The Hoorn Meal Study. PLoS ONE. 2018 Jan 11;13(1):e0191114.

426. Winzell MS, Ahrén B. Durable islet effects on insulin secretion and protein kinase A expression following exendin-4 treatment of high-fat diet-fed mice. J Mol Endocrinol. 2008 Feb;40(2):93–100.

427. Ahlkvist L, Brown K, Ahrén B. Upregulated insulin secretion in insulin-resistant mice: evidence of increased islet GLP1 receptor levels and GPR119-activated GLP1 secretion. Endocr Connect. 2013 Jun 1;2(2):69–78.

428. Liu L, Jiang Q, Wang X, Zhang Y, Lin RCY, Lam SM, et al. Adipose-specific knockout of SEIPIN/BSCL2 results in progressive lipodystrophy. Diabetes. 2014 Jul;63(7):2320–31.

429. Zhou H, Black SM, Benson TW, Weintraub NL, Chen W. Berardinelli-Seip Congenital Lipodystrophy 2/Seipin Is Not Required for Brown Adipogenesis but Regulates Brown Adipose Tissue Development and Function. Mol Cell Biol. 2016 Jul 14;36(15):2027–38.

430. Chen W, Zhou H, Saha P, Li L, Chan L. Molecular Mechanisms Underlying Fasting Modulated Liver Insulin Sensitivity and Metabolism in Male Lipodystrophic Bscl2/Seipin-Deficient Mice. Endocrinology. 2014 Nov 1;155(11):4215–25.

431. Thompson MD, Cole DEC, Jose PA, Chidiac P. G protein-coupled receptor accessory proteins and signaling: pharmacogenomic insights. Methods Mol Biol Clifton NJ. 2014;1175:121–52.

432. Syme CA, Zhang L, Bisello A. Caveolin-1 Regulates Cellular Trafficking and Function of the Glucagon-Like Peptide 1 Receptor. Mol Endocrinol. 2006 Dec 1;20(12):3400–11.

433. Garg A, Agarwal AK. Caveolin-1: A New Locus for Human Lipodystrophy. J Clin Endocrinol Metab. 2008 Apr;93(4):1183–5.

434. Iepsen EW, Torekov SS, Holst JJ. Liraglutide for Type 2 diabetes and obesity: a 2015 update. Expert Rev Cardiovasc Ther. 2015;13(7):753–67.

435. Oliveira J, Lau E, Carvalho D, Freitas P. Glucagon-like peptide-1 analogues - an efficient therapeutic option for the severe insulin resistance of lipodystrophic syndromes: two case reports. J Med Case Reports. 2017 Jan 13;11(1):12.

436. Banning F, Rottenkolber M, Freibothe I, Seissler J, Lechner A. Insulin secretory defect in familial partial lipodystrophy Type 2 and successful long-term treatment with a glucagon-like peptide 1 receptor agonist. Diabet Med. 2017;34(12):1792–4.

437. Maldergem LV, Magré J, Khallouf TE, Gedde-Dahl T, Delépine M, Trygstad O, et al. Genotype-phenotype relationships in Berardinelli-Seip congenital lipodystrophy. J Med Genet. 2002 Oct 1;39(10):722–33.

438. Gao M, Wang M, Guo X, Qiu X, Liu L, Liao J, et al. Expression of seipin in adipose tissue rescues lipodystrophy, hepatic steatosis and insulin resistance in seipin null mice. Biochem Biophys Res Commun. 2015 May 1;460(2):143–50.

439. Wang H, Xu P-F, Li J-Y, Liu X-J, Wu X-Y, Xu F, et al. Adipose tissue transplantation ameliorates lipodystrophy-associated metabolic disorders in seipin-deficient mice. Am J Physiol Endocrinol Metab. 2019 Jan 1;316(1):E54–62.

440. Liao J, Liu X, Gao M, Wang M, Wang Y, Wang F, et al. Dyslipidemia, steatohepatitis and atherogenesis in lipodystrophic apoE deficient mice with Seipin deletion. Gene. 2018 Mar 30;648:82–8.

441. Clément S, Fauvelle C, Branche E, Kaddai V, Conzelmann S, Boldanova T, et al. Role of seipin in lipid droplet morphology and hepatitis C virus life cycle. J Gen Virol. 2013 Oct;94(Pt 10):2208–14.

442. Akinci B, Sahinoz M, Oral E. Lipodystrophy Syndromes: Presentation and Treatment. In: Feingold KR, Anawalt B, Boyce A, Chrousos G, de Herder WW, Dhatariya K, et al., editors. Endotext [Internet]. South Dartmouth (MA): MDText.com, Inc.; 2000 [cited 2021 Apr 19]. Available from: http://www.ncbi.nlm.nih.gov/books/NBK513130/

443. Parween S, Kostromina E, Nord C, Eriksson M, Lindström P, Ahlgren U. Intra-islet lesions and lobular variations in β-cell mass expansion in ob/ob mice revealed by 3D imaging of intact pancreas. Sci Rep. 2016 Oct 7;6(1):34885.

444. Singhal G, Fisher FM, Chee MJ, Tan TG, El Ouaamari A, Adams AC, et al. Fibroblast Growth Factor 21 (FGF21) Protects against High Fat Diet Induced Inflammation and Islet Hyperplasia in Pancreas. PloS One. 2016;11(2):e0148252.

445. Duan SZ, Ivashchenko CY, Whitesall SE, D'Alecy LG, Duquaine DC, Brosius FC, et al. Hypotension, lipodystrophy, and insulin resistance in generalized PPARγ-deficient mice rescued from embryonic lethality. J Clin Invest. 2007 Mar 1;117(3):812–22.

446. Kim S, Huang L-W, Snow KJ, Ablamunits V, Hasham MG, Young TH, et al. A mouse model of conditional lipodystrophy. Proc Natl Acad Sci U S A. 2007 Oct 16;104(42):16627–32.

447. Patni N, Garg A. Congenital generalized lipodystrophies—new insights into metabolic dysfunction. Nat Rev Endocrinol. 2015 Sep;11(9):522–34.

448. Dunphy JL, Taylor RG, Fuller PJ. Tissue distribution of rat glucagon receptor and GLP-1 receptor gene expression. Mol Cell Endocrinol. 1998 Jun 25;141(1–2):179–86.

449. Zhu L, Zhou J, Pan Y, Lv J, Liu Y, Yu S, et al. Glucagon-like peptide-1 receptor expression and its functions are regulated by androgen. Biomed Pharmacother. 2019 Dec 1;120:109555.

450. Vendrell J, El Bekay R, Peral B, García-Fuentes E, Megia A, Macias-Gonzalez M, et al. Study of the potential association of adipose tissue GLP-1 receptor with obesity and insulin resistance. Endocrinology. 2011 Nov;152(11):4072–9.

451. Ejarque M, Guerrero-Pérez F, de la Morena N, Casajoana A, Virgili N, López-Urdiales R, et al. Role of adipose tissue GLP-1R expression in metabolic improvement after bariatric surgery in patients with type 2 diabetes. Sci Rep [Internet]. 2019 Apr 18 [cited 2021 Apr 3];9. Available from: https://www.ncbi.nlm.nih.gov/pmc/articles/PMC6472499/

452. Challa TD, Beaton N, Arnold M, Rudofsky G, Langhans W, Wolfrum C. Regulation of adipocyte formation by GLP-1/GLP-1R signaling. J Biol Chem. 2012 Feb 24;287(9):6421–30.

453. Chen J, Zhao H, Ma X, Zhang Y, Lu S, Wang Y, et al. GLP-1/GLP-1R Signaling in Regulation of Adipocyte Differentiation and Lipogenesis. Cell Physiol Biochem. 2017;42(3):1165–76.

454. Villanueva-Peñacarrillo ML, Márquez L, González N, Díaz-Miguel M, Valverde I. Effect of GLP-1 on Lipid Metabolism in Human Adipocytes. Horm Metab Res. 2001 Feb;33(2):73–7.

455. Xu F, Lin B, Zheng X, Chen Z, Cao H, Xu H, et al. GLP-1 receptor agonist promotes brown remodelling in mouse white adipose tissue through SIRT1. Diabetologia. 2016 May 1;59(5):1059–69.

456. Krieger J-P, Santos da Conceição EP, Sanchez-Watts G, Arnold M, Pettersen KG, Mohammed M, et al. Glucagon-like peptide-1 regulates brown adipose tissue thermogenesis via the gut-brain axis in rats. Am J Physiol Regul Integr Comp Physiol. 2018 Oct 1;315(4):R708–20.

457. Drucker DJ, Nauck MA. The incretin system: glucagon-like peptide-1 receptor agonists and dipeptidyl peptidase-4 inhibitors in type 2 diabetes. Lancet Lond Engl. 2006 Nov 11;368(9548):1696–705.